UNIVERSITAT DE BARCELONA

Study of the role of cell-matrix force transmission in naive to primed pluripotency transition in mouse embryonic stem cells

Srivatsava Viswandha Venkata Naga Sai

Study of the role of cell-matrix force transmission in naive to primed pluripotency transition in mouse embryonic stem cells

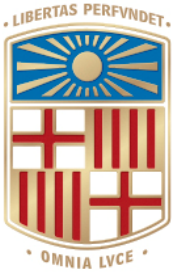

UNIVERSITAT DE BARCELONA

Memòria per optar al grau de Doctor per la Universitat de Barcelona
Programa de Doctorat en Biomedicina

Realitzada a l'Institut de Bioenginyeria de Catalunya

Presentada per:

Srivatsava
Viswandha Venkata Naga Sai

Dirigida per:

Dr. Pere
Roca-Cusachs Soulere

Dr. Zanetta
Kechagia

Acknowledgements

Just like the pluripotent epiblast which possess the lineage induction ability but require the assistance of the molecular and cellular players in its niche, my five-year long journey during this PhD is one highlighted by support from people here and far.

I would first like to thank Dr. Pere Roca-Cusachs for hosting my doctoral study in his laboratory. I am forever grateful to you Pere for not being hasty with my progress and offering the solidarity during the emotional distress, be it in the pandemic period or when the experiments weren't working. I am also thankful for your support during my preparation for postdoc interviews and for helping me in securing one. I still wonder if it was a mere coincidence that you selected a candidate with no prior cell-culture experience and thrust him into the work that deals with pluripotency. Intentional or not, you did believe in the potential of a scientifically 'naive' individual and let me work on this project that has opened several doors and taught me how to approach a research problem. For all these, I forever remain grateful to you Pere.

My second vote of thanks goes to the other supervisor Dr. Zanetta Kechagia (Jenny). From butchering your name to Kenny on our very first encounter to ruining plenty of initial experiments, you were very accommodative of my mistakes Jenny. You were also quick to realize the flaws in the way I work and offered constructive criticism. In looking out for these little things you ensured the progress of the project and my maturation as a scientist. You have always subjected my data presentation and idea conception to a scientific rigour of higher standards and in doing so 'primed' me for success in my every endeavour. Any number of words will be insufficient to express my gratitude towards your role during this journey. All I could say is: Ευχαριστώ για κάθε μικρό πράγμα μεγάλη αδελφή.

I would also to thanks Dr. Xavier Trepat and Dr. Nuria Montserrat for offering valuable advice and testing my scientific temper as part of yearly evaluation.

This could have turned out to be a case of road not taken if not for the support of four individuals during my PhD applications: Varun Tej Raviprolu, Prathyusha Konda, Srinivas Allanki and Srikiran Chandrasekaran. The confidence you guys have provided me during the graduate school application be it with SOP edits and mock interview preparation, has helped me to come this far. By constantly checking on me, you made sure that I was not compromising on my mental well being while being obsessed with research work.

Varun, *manam kalisi ippatiki pushkaram daatindhi. Naa quirks ni ardam chesukoni enterntain chese nee lanti snehithudu dorakadam aprayatnapu adrustam gaa eppudu bhaavisthanu. Ee prayanam lo vennu dannu gaa nilichav, dani koraku nenu neeku sada kruthagnudni. Next time kalise sariki iddaram Doctors aipoyuntam* !!!

Pratyusha, thanks for the emotional solidarity you have always offered. Your perseverance and scientific temper are the two traits I would like to match. Every time I doubted myself, you always assured me to swim away from the turbulence of mind to the safe waters of *Stitha pragnatha* (Equanimity). The words of wisdom hold it dearly to my heart as they helped me a ton during several testing times and for that I am immensely thankful to you.

Srinivas*, baa, nenu emani cheppedhi. Asalu M.S ke apply cheyakapovachu ani anukuntune, naaloni prathibhani gurtinchi motivate chesindhi nuvvu. Canada lo okkadine struggle avthunte, nee panulu kooda aapukoni every weekend matladuthu naa SOPs ni edit chesav. Nee lab lone join avdham anukunna but ala avvakapovadam kooda manchidhe aindhi. Mana friendship withstood the test of times and separation.* Prathyusha *tho patu nuvvu offer chesina emotional support nenu eppatiki gurthunchukunta*. I really hope one day we get to collaborate and push the limits of our understanding on several of the elusive topics. *Ee stage ki nenu reach avvagaliganu ante danlo nee paathra anirvachaneeyam*.

I would also like to thank my two other best friends from my pre-doctoral times Yaswanth Dontu and Milind Pukale.

Dontu *baa, teliso teliyako prathi seminal moment lo you interacted with me. Matladina prathi sari nenu progressively happy avthunnanu ani point out chesav. Nuvvu ichina perspective was also very helpful to look at life in an optimistic way. Thanks for that baa*.

Milind, *Bro nim'ma vārāntyadalli yāvāgalū nannondige mātanāḍalu samaya tegedukoṇḍiddakkāgi dhan'yavādagaḷu. Nāvu sākaṣṭu baud'dhika carcegaḷannu naḍesiddēve ādare kaḷeda ondu varṣadalli nīvu nanage nīḍida bhāvanātmaka bembalavannu nānu gauravisuttēne. Viśēṣavāgi sāṅkrāmika samayadalli nīvu prati vārāntyadalli nannondige mātanāḍuvudannu khacitapaḍisikoṇḍiddīri mattu adakkāgi nānu yāvāgalū kṛtajñanāgiddēne*.

I want to take this opportunity to thank my fellow Indian bro Nimesh Chahare. From the long walks on Gran via discussing the fine details of certain economic structure to arranging movie nights in your house, I have always cherished every moment that I have spent with you Nimesh. I was always impressed by the intellect you possess not just in science but in the range of social topics. I hope we could collaborate in future and pay homage, through our work, to a famous quote: “Let’s be realistic. Let’s do the impossible”.

Leone Rossetti, firstly thanks for helping me to get the pronunciation of Versailles right without a second thought as to why two Indians were discussing a post-world war treaty. Thanks for teaching me to segment phase contrast images through Weka plugin in ImageJ. Despite of not using it, that experience broke the barriers for me to approach you and every time I did, the interaction was always helpful be it regarding statistics, scientific communication, or life in general. You are one of the erudite individuals I have ever come across and every interaction with you has always offered me tit bits of wisdom. I know I owe you the recipe for tomato rice, with the thesis done, I will be sending it soon.

Ignasi Granero-Moya*,* I have always confided in you and every time I spoke to you it, tranquillity was restored. Also, thanks for reassuring and reminding me of my candidature when I was doubting myself for postdoc applications. Thanks, in particular for navigating me during the all-important thesis submission process.

Ion, you have guided me to perform the first immunostaining protocol during my doctoral work. Your magnanimity of taking it upon yourself to teach a first year PhD student whom you are not guiding is something I have always had a huge respect for. Also, the first lunch we had in the cafeteria after the pandemic you reassured me how my project was not easy and what seemed like a little progress up until then is in fact significant. Thanks for all this support.

Amy, thanks for offering valuable advice with respect to data analysis especially for the DN-KASH experiments. Although our research topics are not similar, I have always had huge admiration for your work ethic and clarity of thought. Also, thanks very much for helping me with my postdoc application.

Anabel-lise, although the interactions we had are minimal, I have always admired your perseverance and hard work. The significance of these two virtuous traits can never be overstated. These are two traits I have tried to inculcate during my journey and thanks for standing as the example for these traits.

I would like to thank Sefora for help during the initial stages of the project, for teaching me primo patterning and to the valuable interactions both within and away from the workspace. Sefora, I am amazed by your tenacity and given our similar research interests, would be following your work closely. I also wish we could collaborate and set new frontiers in mechanobiology.

I would like to thank Agata Nyga who was constantly sharing relevant research work corresponding to my thesis. Agata, you suggested to me apply for preLighter position at The Node to work on my scientific communication skills and for improving networking. I am incredibly grateful for all the help and suggestions.

I would like to thank Isabela for offering emotional solidarity, for helping me in improving primo patterning, and for attending my stand-up comedy show to laugh at my stupid jokes. Isabela, your work efficiency and troubleshooting skills are two traits I would like to inculcate. Outside work, thanks for the amazing happy memories we shared.

I would like to thank Juanfra for offering valuable inputs on treatment with drugs such as blebbistatin and also for helping me with my application for postdoc.

I would like to thank Ozge for sharing relevant research work pertaining to pluripotency, for critical insights into mechanobiology of stem cells in general and for helping me with my postdoc application process.

I would like to thank Elena, for helping me trouble shoot experiments in mic 2 and, Manu for helping me with the script-based imaging in mic 3 and in the segmentation of edge and interior regions in live imaging.

I would like to thank the frequent users of mic 3 for turning a blind eye when I booked over weekend live images sessions in a predatory fashion. Among them additional thanks to Alice, Clement, Meng, Miquel, and Marija for starting their experiments 30 minutes to 1 hour late as I was still waiting for my last time point of imaging to finish.

I would like to thank Laura, Victor, Xarxa, Aina, Ona, Miguel, Jorge, Mamatha, Susana, Melissa, Nacho, Yudish, Marilena, Ariadna, Ernest Latorre, Macia, Raimon, Pau, Rohit, Guillermo, Natalia and Monica, for helping me conduct this research and offering valuable insights during the interactions as part of lab meetings.

Finally, I would like to thank my family members: my mother Srikanta Krishnaveni, my father Viswanadha Kameswara Rao and my dearest sister Viswanadha Srivagdevi. *Amma, Nanna, vagu, meeru ee 5 years lo entha sahanam tho naa attitude ni bharincharu. Mee understanding lekapothe ee PhD complete cheyadam kastam ayyedi. Ee PhD naa okkadidhe*

kaadhu, mana andaridhi. Mee support lekapoyunte ee vijayam anithara saadhyam. Meeru ichina emotional support naa homesick ni koddo goppo dhooram chesay. Vagu nuvvu especially nenu arichina kopadina baga ardham cheskunnav. Amma Nanna naa visugu ni kooda meeru bharincharu. Inka nundi ee paatalatho eppatiki mimmalni kasurukonu. Andhuke mee paatra lenidhe Viswanadha Srivatsava ki doctor patta andadhu.

I would also like to thank my cousins Kavya Piduri, her husband Naveen Maddali for lending emotional support during the times of distress and in lifting the spirits prior to PhD applications. I would also like to thank my other set of cousins Hima Sailaja, Ashok Vardhan, Sarvani and Lalitha for their constant support.

Resum de la tesi en llengua catalana

"Fer el correcte, en el moment adequat, en la mesura correcta, de la manera correcta i amb el propòsit correcte". No es tracta d'un intent de mala virtut invocant Aristòtil. Més aviat és la meva comprensió filosòfica del desenvolupament embrionari. Durant els meus anys de formació, ser ensenyat per puristes biològics em va portar a adoptar un enfocament reduccionista de buscar un efector bioquímic i entendre la seva transducció a través de vies de senyalització. Tot i que m'ha informat molt sobre els detalls de la bioquímica darrere de la morfogènesi embrionària, encara em quedaven preguntes persistents. Com dóna lloc un embrió simètric i esfèric a un organisme el desenvolupament i supervivència del qual necessita asimetria, ja sigui en la col·locació d'òrgans o en la funció corporal general? És el flux d'informació genètica l'única manera de materialitzar els canvis necessaris per al desenvolupament embrionari? Hi ha fonts alternatives de senyals de senyalització diferents dels factors solubles? Impulsada per aquesta curiositat, vaig fer revisió bibliogràfica durant el màster i em vaig introduir en el món de la mecanobiologia. Em va intrigar com les forces físiques regulen el moment, la col·locació i l'extensió del flux d'informació genètica i confereixen robustesa al desenvolupament embrionari fent-lo virtuós!! És important destacar que va canviar la meva percepció de la matriu extracel·lular (ECM) que fins aleshores considerava que tenia un paper passiu com un mer suport estructural. La deposició ECM que constitueix un senyal mecànic i la transmissió de força a ECM impulsant la morfogènesi tissular va evocar un interès per dilucidar el seu paper funcional en les primeres etapes del desenvolupament embrionari.

Com que l'epiblast pluripotent estableix les bases per a tots els òrgans i teixits, volia entendre com la interacció amb ECM regula la dissolució de pluripotència i es prepara per a futures etapes del desenvolupament embrionari. Pere Roca-Cusachs i, sota la cosupervisió de la doctora Zanetta Kechagia, vaig realitzar el treball de tesi actual, que consisteix a estudiar el paper de la transmissió de forces cèl·lula-ECM en la transició de pluripotència en cèl·lules mare embrionàries de ratolí.

La tesi està dividida en set capítols. En el primer capítol s'esmenta una introducció a la pluripotència i la seva dissolució, i l'statu quo sobre la nostra comprensió de la dissolució de la pluripotència. Un cop identificades les llacunes clau de coneixement, en el segon capítol s'enumeren l'objectiu principal de l'estudi i els objectius específics a través dels quals s'aconsegueix.

El tercer capítol tracta de les tècniques experimentals i dels materials emprats en l'obra. En el quart, s'enumeren els resultats que suggereixen per què es requereix la transmissió de força a ECM per a la dissolució de pluripotència. La discussió detallada de cada intervenció experimental i el que signifiquen a la llum del coneixement actual, juntament amb possibles futures direccions de recerca a seguir, es donen al capítol cinquè. En el sisè capítol s'enumeren les conclusions clau de l'estudi seguit del capítol setè, que és la bibliografia.

Els resultats d'aquesta tesi estan recollits en un manuscrit del qual sóc primer autor, i el manuscrit està a punt de ser enviat.

Preface

"Doing the right thing, at the right time, to the right extent, in the right manner, and for the right purpose". This isn't a shoddy attempt at virtue signalling by invoking Aristotle. It rather is my philosophical understanding of embryonic development. During my formative years, being taught by biological purists led to me adopting a reductionist approach of looking for a biochemical effector and understanding its transduction through signalling pathways. While it has informed me greatly on the fine details of the biochemistry behind embryo morphogenesis, I was still left with lingering questions. How does a symmetrical and spherical embryo give rise to an organism whose development and survival needs asymmetry, be it in organ placement or overall bodily function? Is the genetic information flow the only mode of materializing the changes needed for embryonic development? Are there alternative sources of signalling cues other than soluble factors? Driven by this curiosity, I performed literature review during my masters and got introduced to the world of mechanobiology. I was intrigued by how physical forces regulate the timing, placement and extent of genetic information flow and confer robustness to embryonic development making it virtuous!! Importantly, it changed my perception of extracellular matrix (ECM) which until then I considered to play a passive role as a mere structural support. ECM deposition constituting a mechanical cue and the force transmission to ECM driving tissue morphogenesis evoked an interest to elucidate its functional role in early stages of embryonic development.

As the foundation for all organs and tissues are laid by pluripotent epiblast, I wanted to understand how interaction with ECM regulates pluripotency dissolution and prepares for further stages of embryonic development. To achieve this, I joined Dr.Pere Roca-Cusachs' lab and under the co-supervision of Dr. Zanetta Kechagia, I performed the current thesis work which is to study the role of cell-ECM force transmission in pluripotency transition in mouse embryonic stem cells.

The thesis is divided into seven chapters. In the first chapter, an introduction to pluripotency and its dissolution, and the status quo on our understanding of pluripotency dissolution is mentioned. Having identified the key knowledge gaps, in the second chapter, the main objective of the study and the specific aims through which it is achieved are listed out.

The third chapter deals with the experimental techniques and materials employed in the work. In the fourth, the results are listed out which suggest why force transmission to ECM is required for pluripotency dissolution. The detailed discussion of each experimental intervention and what they mean in light of the current knowledge along with potential future research directions to pursue are given in chapter five. In the sixth chapter, the key conclusions of the study are listed followed by chapter seven which is the bibliography.

The results of this thesis are included in a manuscript for which I am a first author, and the manuscript is about to be submitted.

To borrow the message of Martin A Schwart's essay "The importance of stupidity in scientific research", scientific pursuit is the process of being productive while confronting our ignorance. The end result is to garner wisdom and to acknowledge one's absolute stupidity about research problems of higher difficulty. While performing this thesis work, I have always abided by this motto. With that being said, I wish you therefore enjoy reading the work by a "stupid of the highest orda".

Table of contents

Chapter 1: Introduction

Section 1: Pluripotency and its dissolution in the mouse embryonic context

1.1.1 Onset of pluripotency *in vivo*

Embryonic development is a series of cell fate decisions accompanied by gradual decline in differentiation potential. In mammals, the first fate specification yields a hollow ball of cells called blastocyst or blastula. It is composed of polarized outer cell layer surrounding a fluid filled cavity and non-polar inner cell mass (ICM) [1] marked by the expression of transcription factor Oct3/4. In the model organism mouse, the outer cells referred to as trophoblasts, characterized by Cdx2 expression, and facilitate blastocyst adherence to maternal uterine wall [2,3]. This process known as Implantation establishes an interface for the maternal supply of nutrients to the embryo. Trophoblasts assemble into Trophectoderm (TE), the single cell layer transporting epithelium that surrounds ICM [4] (as shown in Fig.1). This circumferential wall is the precursor for foetal part of placenta, the organ that aids in nutrient exchange and waste removal.

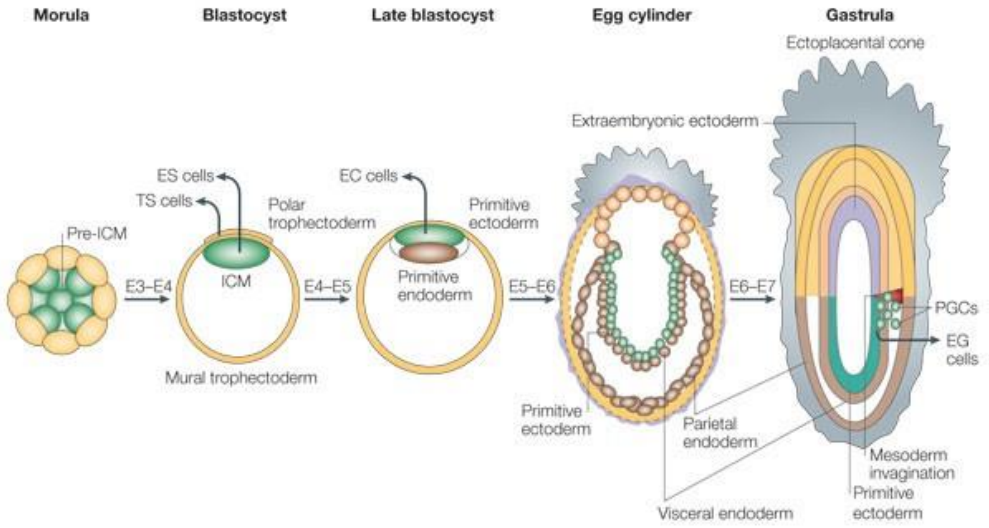

Figure.1: Schematic representation of mouse embryonic development adapted from Bioani M and Scholer HR *et al*., 2005 *Nat Rev Mol Cell Biol*.

Besides its nourishing role, implantation represents a critical juncture in embryogenesis. Blastocyst, post its implantation, is dynamically reorganized to be compatible for ensuing developmental programs and morphogenetic events [5] to form all organs and tissues. To catch up with these future demands, embryo undergoes its second round of fate specification shortly before implantation, when the ICM segregates to form Gata6 positive Primitive endoderm (PrE) and Nanog positive Epiblast [6,7]. PrE cell derivates become major constituents of yolk sacs [8]. The epiblast is entrusted with laying the foundation for all soma

and germ cells of an adult organism [9,10]. To be able to do so, the epiblast is endowed with pluripotency, the ability to generate the three primary germ layers: ectoderm, mesoderm, and endoderm [11,12].

Since ICM's developmental potential, prior to epiblast and PrE distinction, is not confined to the three germ layers [13,14], the exclusive appearance of pluripotency occurs only with epiblast segregation.

During the two segregation events, the apportion of cell population was considered to stochastic with a mere correlation to the mutually exclusive expression patterns of transcription factors: Cdx2 and Oct3/4 for the first specification [14,15] and, Nanog and Gata6 for the second with initial predisposition through sensitivity to Fibroblast growth factor (FGF) signalling [16,17]. However, recent studies have established the central role of mechanical signalling in allocating lineages. For the first, positional information ends up being a binary switch to switch on/off the YAP-TEAD pathway in outside/inside cells to respectively generate TE and ICM lineages [18]. In the second instance, two mechanical parameters, one cell-intrinsic and the other from the niche, are at play to robustly partition Epi and PrE populations. Briefly, the work by Yanagida et al 2022 elucidated the mechanism of phase separation based on differences in cell membrane fluctuations [19], while Ryan and colleagues showed increased hydrostatic pressure due to lumen expansion guiding Epi/PrE lineages' position and fate [20].

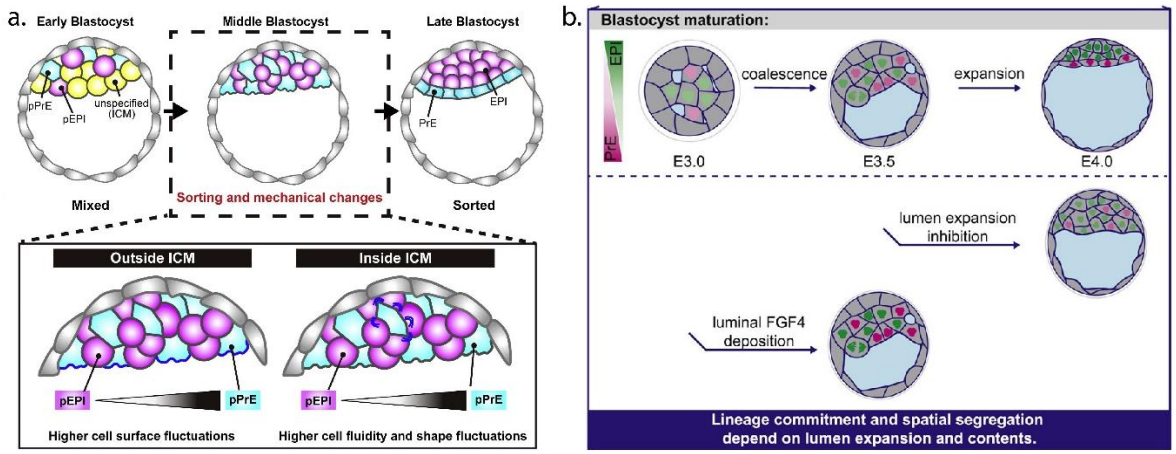

Figure.2: Schematic representation of epiblast (EPI) and primitive endoderm (PrE) segregation being driven by a.) membrane tension differences and b.) luminal pressure. Pictures adapted from Yanagida A *et al*., 2022 *Cell* and Ryan AQ *et al*., 2019 *Dev Cell*.

1.1.2 Pluripotency *in vivo* – a fleeting entity

Established at second fate decision, pluripotency is sustained for a brief period during embryogenesis. It exhausts at the initiation of an event termed gastrulation in which blastula folds on itself to specify germ layers [21,22]. In mouse, this corresponds to a time period of 72 hours (E3.5 to E6.5) with the landmark event for initiation of pluripotency dissolution being implantation. In the wake of implantation, the embryo undergoes a plethora of morphogenetic changes guided and aided by secretion of soluble signalling cues and deposition of extracellular matrix (ECM). The initially symmetrical (and spherical) embryo is progressively shaped into an elongated cylinder with the establishment of embryonic and abembryonic poles, with the former region fated to give rise to whole body and the latter setting a reference point towards which the Epiblast expands.

Focusing solely on the epiblast, what starts as a collection of loosely adherent cells undergoes a mesenchymal to epithelial transition (MET) around implantation [22] followed by polarization into a rosette structure (Figure.3).

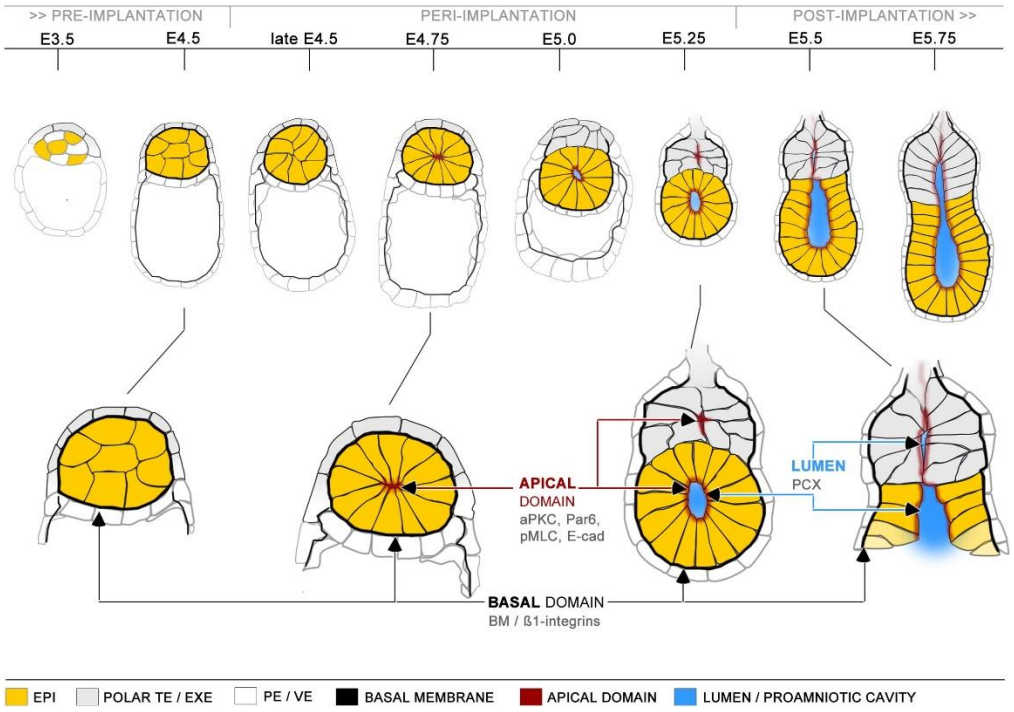

Figure.3: Schematic representation of the morphological transformation of epiblast from cell mass to lumen formed polarized epithelia through a rosette intermediate. Tisue marked in yellow is epiblast, apical domain is marked in red and basement membrane is marked in black. Picture adapted from Bedzhov I and Zernicka-Goetz M *et al*., 2014 *Cell*.

These two morphological changes function as quality control to ensure developmental progression is keeping up with time, besides guiding changes in transcriptional profiles, which further translate to gene expression differences. Another critical milestone is the de novo formation of lumen initiated by the repulsion of apical cell surfaces in the polarized rosette. This is mediated through the surface expression of anti-adhesive sialomucin protein podocalyxin [23,24]. It is to be noted that commitment to irreversible loss of pluripotency is an obligatory first step for the tissue to polarize and set the stage for lumen formation [15].

As mentioned earlier, these morphogenetic events are driven by the secretion of soluble morphogens whose identity and regulatory role have been well characterized. A prominent example is the secretion of FGF signalling components as a single burst concomitant with implantation [25]. However, for the embryo to be malleable for ongoing morphogenetic events, a notable contribution from the ECM is warranted. Two major events stand out in this regard. First, the deposition of Laminin-rich ECM, which serves as a polarizing cue for rosette formation [23,24]. Second, the perforations in Laminin-rich ECM occurring towards the early stages of gastrulation facilitating the migration of differentiation ready pluripotent cells and establishment of body axis plan. [26].

Another key milestone during the procession to gastrulation is the maturation of both Epiblast's and Extraembryonic-endoderm (ExE) lumen. This is initiated by an osmotic imbalance of soluble cues resulting in water influx and build-up of hydrostatic pressure [27]. The increasing luminal pressure, perceived as elevated cortical tension [28,29], leads to the elongation of ExE and epiblast tissues, eventually fusing their lumens. Such tissue arrangement, coupled with the establishment of morphogen gradients, compartmentalizes epiblast tissue in terms of predisposition (or priming) to germ layer fate during gastrulation. The functional consequence of such tissue structure and its impact on pluripotency will be dealt with in the next sub-section.

Besides these intra-embryonic forces, pluripotent epiblast is subjected to mechanical cues emanating from surrounding tissues. The pre-implantation embryo which floats in intraluminal fluid, is subjected to nominal shear stress [30] and, upon implantation, experiences the periodic contractile forces from decidual tissues [31], eventually leading to luminal closure to house the embryo. The fact that the three body axes are aligned with the

three symmetry axes of the uterine tissue underscores the instructive role of mechanical signalling in post-implantation embryonic and pluripotency changes [32].

All the above phenomenon substantiates that mechanical signalling lies at the heart of shaping post-implantation embryo. Concomitant to shape changes, cellular molecular signature is constantly reconfigured to permit pluripotency dissolution. As cellular state lays the foundation for tissue shape whose changes, in turn rewire the transcriptional networks of constituent cells, form and fate exist in a dialectical relationship in post-implantation mouse embryos, with the common denominator being mechanical signalling perceived as forces. Therefore, tissue shape serves as a proxy for pluripotent state.

The deposition of ECM and its later remodelling, the morphogenetic changes of tissues, the lumen formation and its enlargement, and other critical features of embryo occur incrementally. Mirroring these changes, pluripotency as well progresses gradually in vivo.

1.1.3 Pluripotency *in vivo* – a spectrum of substates

Between the two extremities of its regime, epiblast segregation and gastrulation, the attributes of pluripotent cells are markedly different. These include molecular signatures, metabolic profiles, morphological features and adhesive properties besides developmental potential [33-37]. If pluripotency were a binary property, the acquisition of these changes happens via a single step state transition, which is both overwhelming and prone to error propagation. Instead of this fallible one-step process, as evidenced by shape changes, epiblasts adopt a sequential approach. It accumulates the changes by traversing through several intermediate stages, all pluripotent, each with subtle difference of every feature [38-40]. Hence, in vivo, pluripotency is consistent with multiple molecular designs and spans a continuum whose functional relevance will be discussed later. The term pluripotency substate represents a variant of pluripotency with its unique molecular configuration.

1.1.4 Nomenclature of *in vivo* pluripotency

Pluripotency at its two extremities can be differentiated by the developmental scope of individual epiblast cells. This is the basis of assigning pluripotency labels to the two ends of the spectrum. These naming tags are best understood when the change in differentiation ability is studied with the post-implantation morphological transformations (shown in Figure.4) of the epiblast.

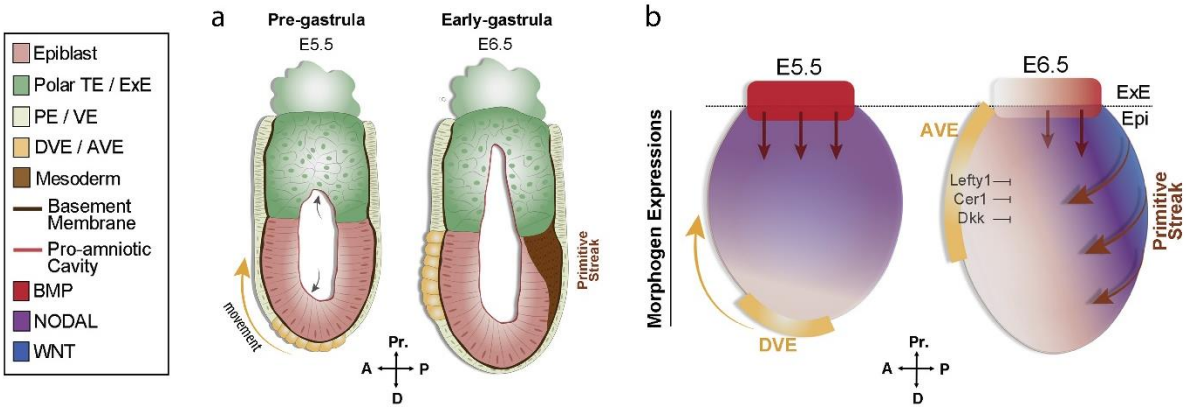

Figure.4: **Morphogenetic transitions prime lineage induction in mouse embryo. Schematic representation of morphogenetic changes in embryonic tissues around gastrulation in mouse embryo (a) and accompanying morphogen gradients (b). The distal and anterior visceral endoderm (DVE and AVE) secrete morphogen inhibitors Cer1 (for NODAL), Lefty1 (for BMP) along with Wnt agonist Dkk1. DVE and AVE movement establishes morphogen gradients later translated to body plan axis along anterior – posterior (A-P) and Proximal-Distal (Pr-D) body axes. Pictured adapted from Sozen B, Cornwall-Scoones J, Zernicka-Goetz M *et al.,* 2021 *Dev Biol*.**

In addition to the morphological changes and its drivers explained earlier, upon implantation, the enlargement of embryo size is accounted for by the increase in epiblast cell count through rapid proliferation [24]. Simultaneously, to shape the blastocyst, PrE and TE assemble the basement membrane and, secrete signalling factors contributing to luminal pressure build-up due to osmotic imbalances. Cumulatively, these upscaling and sculpting efforts, stimulate cell polarization [24,26,41] and instruct epiblast to eventually become pseudo-stratified columnar epithelium [42]. Around the same time, biomolecular gradients orchestrate the formation of spatialized lineage-specific gene expression (Figure.5) [43,44]. As alluded in the earlier paragraphs, the functional consequence of such tissue organization is that epiblast cells at late post-implantation stage are arranged into fate-restricted regions with each region expressing specific differentiation associated markers [45]. Simply stated,

even before gastrulation occurs, cells are primed to certain lineages according to their location [38]. Such pluripotent ability is hence named **Primed state pluripotency** [46].

Despite being expressed in primed state, the lineage specific markers are not permitted to execute their fate specification role until late gastrulation. So, primed state cells are only poised to differentiate but not actively differentiating. Once supplemented with specifying cues, cells can differentiate. Thus, pluripotent ability at primed state is ready for putting to use or executable.

In contrast, the amorphous epiblast cells of pre-implantation blastocyst are free from signalling gradients due to their tight packing. This leads to homogeneous gene expression ruling out inter-cell variability. Moreover, each epiblast cell is equipped with transcriptional circuitry and epigenetic marks, which render the lineage specifying genes inactive. Therefore, when pluripotency is newly established, the full developmental potential is preserved by preventing premature differentiation [47]. As a result of such regulation cells are unable to respond to differentiation cues. This apparent unpreparedness prevents cells from realizing their capabilities. To signify such developmentally competent but functionally immature status, pre-implantation epiblast cells are labelled as **Naive state pluripotent** [36]. Unlike in their primed counterparts, naïve state cells' differentiation capacity is unrestricted.

Their cell cycle dynamics strongly reflect the naïve state's aversion and the primed state's propensity to differentiate. The G1 phase of the cycle is the period when cells decide whether to continue proliferating or arrest cell division to proceed with differentiation [48]. The longer the G1 phase, the higher the probability of differentiation. This G1 phase is shorter for the naïve epiblast cells, and they advance rapidly into further stages of cell cycle [49]. Such truncated G1 phase impedes spontaneous differentiation in naïve cells. Whereas the G1 gap is extended for primed state cells, making them eligible to apply for differentiation. These cell cycle differences, however, only juxtapose naïve and primed states offering no further insights into the origins of their divergent traits and pluripotency continuum. Therefore, to fully grasp the biology of pluripotency, it is of relevance to understand the benchmark for categorizing pluripotent substates.

1.1.5 The molecular framework of classifying pluripotency substates

The foundations of pluripotency and its various facets are laid as gene regulatory networks (GRNs) [12,50], which are predominantly driven by transcription factors. The disparities between pluripotent substates are no different as they manifest the differences in the expression and usage of transcription factors. Hence, the gold standard for sorting pluripotency substates is built on transcriptional profiling and the aforementioned variations in lineage predisposition, pluripotency maturity and cell cycle duration only serve as adjuncts.

The transcription factors probed to verify substate identity are arranged into the following four categories: (i) General pluripotency factors, (ii) Naïve state specifiers, (iii) lineage primers and (iv) Early post-implantation markers. The general pluripotency factors are indispensable for pluripotency maintenance be it in any substate. The set is comprised of two players, *Oct4* and *Sox2*. Until gastrulation, their function is to safeguard pluripotency and repress differentiation. *Oct4* and *Sox2* serve as rival lineage specifiers during gastrulation: Neuroectoderm induction by *Sox2* and Meso-/Endoderm by *Oct4* [51]. However, *Oct4* and *Sox2* mutually promote the other transcription factor expression [52]. Because of this transcriptionally promoting but functionally repressive interaction *Oct4* and *Sox2* stoichiometry is finely tuned and any perturbance leads to irreversible loss of pluripotency. Since, their presence is obligatory for maintaining pluripotency irrespective of substate identity, Oct4 and Sox2 cannot distinguish naïve and primed states. Instead, the cells are earmarked based on the expression of the other three categories of transcription factors.

The transcription factor set that delineates naïve state are called naïve specifiers. In that list, the hallmark ones are *Nanog*, *Rex1 (*Zfp42*), Esrrb*, *Klf-2/4/5* [45]. Except for Nanog, the rest of the naïve specifiers have binary expression patterns. That is to say, they are highly expressed in naïve state and absent from primed state, making them qualitative classifiers. However, the rate of decline differs for each protein [68]. On the other hand, *Nanog* expression is strong and homogenous in the naïve state and fluctuates in the post-implantation embryo [53-55]. Its expression levels inversely correlate with the odds of spontaneous differentiation making *Nanog* a differentiation rheostat [56].

The pronounced G1 phase duration when synchronized with the troughs of *Nanog*'s oscillations, increases the likelihood of differentiation in the primed state. In other words, its

weak expression pattern in the primed state impairs *Nanog* from preventing spontaneous differentiation as effectively as it is done in naïve state. Compared to *Oct4* and *Sox2*, the differentiation inhibition of Nanog is neither uniform nor continuous. Rather it is a function of its concentration. This expression coupled differentiation withholding skill is what excludes Nanog from general pluripotency factor set despite it being present throughout pluripotency. Finally, Nanog is naïve state-specific because the extent of its differentiation suppression is greatest when pluripotency is newly launched.

On the other hand, primed state cells are characterized by regionalized expression of lineage specifiers *Foxa2, Brachyruy (T)* and *Cer* [36,39]. The expression of these three factors is initiated only during the late post-implantation stage. Between implantation and gastrulation onset, epiblast passes through a stage devoid of lineage specifiers with low/no expression of naïve specifiers. At this stage cells, are mainly identified by the expression of *Fgf5, Otx2* and *Oct6* (*Pou3f1*) [36,39]. These are key early post-implantation markers whose constantly increasing expression attests to the intermediate shades of pluripotency.

In addition to these transcription factor expression profiles, naïve and primed states are distinguished by several other factors, including but not limited to epigenetic markers, metabolism, signalling pathway(s) dependence and chromosomal organization. These are detailed in **Table.1**

Due to their differentiation repression, *Oct4*, *Sox2* and *Nanog*, form the core of pluripotency GRN [12,50]. Together they are referred to as OSN triad [134]. Upon implantation, the network is constantly reshuffled with the inclusion of lineage specifiers and post-implantation factor, and the downregulation of naïve markers. The molecular logic behind how such dynamic reorganization capacitates epiblast to shed pluripotency and assume differentiation capability is briefly explained in the next sub-section.

Table1: Salient differences in the characteristics of Naïve and Primed pluripotent states.

Property	Naïve state	Primed state
Pluripotency	Is of each individual cell	Collectivised
Global DNA hypomethylation	High [34,35]	Low [34,35]
Metabolism	Oxidative phosphorylation, Glycolysis [57]	Glycolysis [57]
Germ line induction potential	High [11]	No [11]
Developmental potential	Unrestricted [36]	Predisposed as per spatial localization in embryo [36,39]
Contribution to chimeras	Yes [11]	No [11]
X-chromosome inactivation	No [58-60]	Yes (for females) [58-60]
Pluripotency factors expressed	*Oct4, Sox2, Nanog, Esrrb, Rex1, Klf*-family proteins, *Tbx3. Tfcp21l*	*Oct4, Sox2, Foxa2, Fgf5 Brachyruy (T)* and *Cer*
Tissue organization	More mesenchymal like [61,62]	Strictly epithelial [61,62]
Cadherin orientation	Circumferential [27]	Basolateral [27]
***Oct4* enhancer usage**	Proximal [63]	Distal [63]
Matrix protein expression	Laminin-111 and at cell-cell contacts [23,24,64]	Laminin-111, Collagen and Fibronectin, at the basal surface [26,68]
***Oct4* primary biniding partner**	*Sox2* (pluripotency gatekeeper) [65]	*Sox17* (endoderm specifier) [65]
***Sox2* function**	Pluripotency maintenance	Neuroectoderm specification [51]
OSN triad role	Pluripotency preservation	Lineage induction
***Oct4-Sox2* interaction**	Mutually promoting (transcriptional and functional wise) [12,50]	Functionally antagonizing [51]
Surface marker expression	SSEA1 [66]	CD24 [67]
Mitochondrial activity	High [38]	Low [38]

1.1.6 Pluripotency dissolution: Tilting the balance towards differentiation

As discussed above, when it is first established, pluripotency is protected by shielding cells from differentiation. The transcriptional circuit at work is further potentiated by cooperative cross-regulation and self-reinforcing mechanisms [69-71]. On top of this, pluripotency repressors that commit cells to differentiation, are silenced by non-transcriptional mechanisms [40]. All this tips the scales unanimously in favour of pluripotency preservation over lineage induction, thereby conferring robustness to naïve state. At this stage, the active players of the transcriptional network constitute naïve state specifiers and general pluripotency factors.

Once embryo implants, epiblast cells are subjected to inductive cues which instruct the rapid downregulation of naïve markers [72]. This leads to the dismantling of naïve state transcriptional network. Concomitantly there is a reciprocal gain in the expression of a new suite of transcription factors, the early post-implantation markers [53,72-74]. They function to predispose epiblast cells for transitioning to primed state [75,76]. Additionally, the silencing of pluripotency repressors is lifted, which unlocks multi-lineage differentiation capability. Immediately prior to gastrulation, the core pluripotency factors are relinquished from guarding pluripotency, which promotes the expression of the canonical lineage specifiers, *Foxa2, Brachyury (T),* and *Cer*. Once freed from pluripotency surveillance, *Oct4* and *Sox2*, which were previously mutually cooperating are repurposed as rival lineage instructors [51]. This way, as epiblast gradually attains a primed state, pluripotency becomes increasingly frail and, the tendency to differentiate strengthens. In other words, epiblast maturation is a process where cells tread a fine line between conserving and utilizing pluripotency.

Another offshoot effect of naïve to primed state transition is the change in the mode of pluripotent identity. In the primed state, due to the lineage predisposition, a single cell is incapable of engendering all three germ layers. Instead, it becomes the ability of entire epiblast population. Whereas, the absence of lineage priming means each naïve state cell is equally proficient in giving rise to all tissues and organs. Thus, considering the strength of the trait, in the naïve state, pluripotency is strong and is the asset of every single cell while at primed state it is collectively owned. So, whether the focus of attention is on single cell, or a collection is determined by the substate of pluripotency being studied.

1.1.7 Functional relevance of pluripotency continuum

As mentioned earlier, pluripotency is constantly reconfigured to serve two key purposes. First, the pluripotent substate transitions coordinate morphogenesis such that the eventual organism complies with the rules of body-plan axis [23]. Simply put, these intermediate steps ensure that all the organs are appropriately placed with their formation timed to perfection.

Second and most importantly, the myriad of substates let the cells efficiently walk the tightrope between pluripotency maintenance and differentiation onset. This is thought to enable the steady accumulation of changes required to establish differentiation competence in epiblast cells [38]. In simpler terms, such sequential transition ensures that multi-lineage differentiation potential is unwrapped bit by bit to be made completely ready to use only by the time of gastrulation. The gamut of intermediates between naïve and primed states are broadly classified as "**Formative pluripotency**" as they serve to develop pluripotency. Formative pluripotency is profiled by the expression of the three early post-implantation markers, *Oct6* (*Pou3f1*), *Otx2*, and *Fgf5*.

Another plausibility for such orderly progression is the facility of better evaluating pluripotency status to check whether it matches the demands of ongoing morphogenetic and developmental programs [77]. For example, lumen formation, the necessary intermediate step for pluripotency priming and epiblast epithelialization, begins with naïve state exit, the first step in pluripotency dissolution. Cell symmetry breaking on which lumenogenesis is built, necessitates the complete loss of naïve transcriptional activity and if any precocious cell polarization occurs, it is only initiated reversibly and not stabilized [23] (Figure.5). In this way, uninterrupted pairing of pluripotent substate identity with cell morphology offers a tighter regulatory control over correcting any incoherence that arises during ontogeny.

Additionally, when further embryo developmental is deemed risky, for example, in harsh climate, blastocyst implantation is deferred. But the embryo remains alive and despite the temporary suspension, its development can resume later. This phenomenon of delayed implantation is referred to as diapause and is primarily seen in rodents, among placental animals, to prevent termination of pregnancy [78]. The lag in embryogenesis is subverted due to naive epiblast's metastability, the essential quality for pluripotency to transit fluidly.

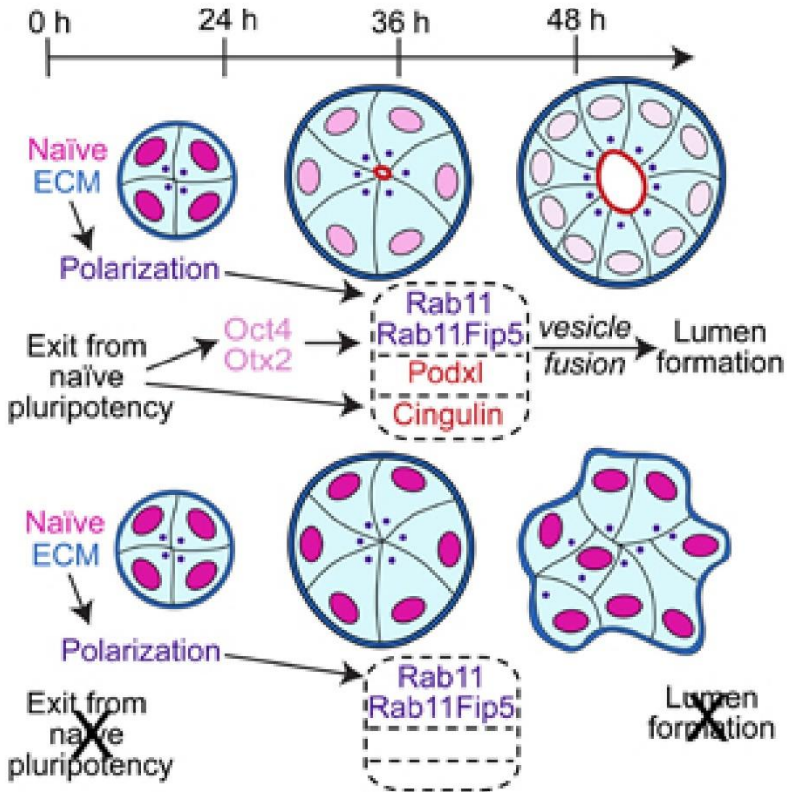

Figure.5: **Naïve state exit is required for lumenogenesis. Picture scheme representing the impaired lumen formation for pluripotent epiblast compromised in naïve state exit. Picture adapted from Shahbazi MN *et al*., 2018 *Nature***.

Hence, pluripotency progression as a continuum determines embryo's viability, its developmental rate and ontogeny success. Studying it offers unprecedented means to understand early organism development and related disorders. Moreover, a detailed analysis of pluripotency maturation would elucidate the predisposition to individual germ layers. This knowledge can be exploited to control differentiation trajectories *in vitro* to improve the success of the application of pluripotent cells in regenerative therapies. Therefore, investigating pluripotency progression is a valued addition to the progress of pluripotency research be it fundamental or applied.

As it sets the precedent for investigating pluripotency dissolution, realizing how substate identity is regulated is of utmost importance.

1.1.8 Microenvironment regulates Epiblast cell's substate identity

The alterations in gene regulatory network underlying pluripotent substate transition are not cell inherent. Instead they are the calibrated efforts of milieu, also referred to as niche. To orchestrate pluripotency substate transition, the microenvironment guides each epiblast cell with biochemical and mechanical instructions, which emerge from the respective derivatives of TE and PrE, and from the neighbouring epiblast cell(s). Once sensed, these cues are relayed as a cascade of molecular and biophysical events that go on to trigger multiple signalling pathways. Said signal transduction mechanism terminates by meddling with the effective concentration and/or sub-cellular localization of transcription factors. The eventual transcriptional signature is the net outcome of all the signalling inputs received by the cell. Thus, the pluripotent identity of an epiblast cell is governed by the prevailing conditions in its niche. Such extrinsic regulation is more evident when pluripotency is surveyed *in vitro* and the need for pluripotency cultures is realized when the hurdles of *in vivo* study are considered.

1.1.9 Bottlenecks for investigating pluripotency *in vivo*

Pluripotency progression should be ideally studied in the embryonic context. However, the fleeting existence of pluripotency in embryos makes it difficult to track and perform comprehensive studies. Other limitations include the restricted access to pre- and post-implantation embryos, the sub-optimal development of embryo *ex vivo*, and the lack of tools to probe the desired changes. Thus, studying pluripotency in its authentic environment is hindered by its transient nature, technical inconveniences, research costs, limited starting material and undesired effects of experimental intervention.

These limitations were averted by the in vitro adaptation of pluripotency, which will be discussed extensively in the next section covering aspects ranging from the sources of pluripotent tissue to the media recipes employed and how near perfectly the in vitro system mimics changes associated with naïve state exit and further pluripotency dissolution. Before moving on to those details, a short summary of this section is presented below.

Section summary:

- Pluripotency originates in mouse embryo with epiblast tissue specification.
- Pluripotency when established has unrestricted developmental potential but differentiation incompetence, hence termed Naïve pluripotency.
- Pluripotent epiblast prior to gastrulation is arranged as regions of predisposed lineage bias, hence this state is referred to as Primed pluripotency.
- Naïve to primed transition occurs as a continuum and all the intermediate states are collectively referred to as Formative pluripotency.
- Changes in transcriptional signature lays the foundation for pluripotency state transition.
- Naïve to primed transition is accompanied by dynamic morphogenetic changes driven by molecular and mechanical cues.
- Pluripotent epiblast fate and form exist in a dialectical relationship mediated by force.
- Pluripotency is short lived *in vivo* and therefore warrants an *in vitro* alternative.

Section 2: *In vitro* maintenance of murine pluripotency

1.2.1 Sources of pluripotent cell lines

The research field overcame the constraints of studying pluripotency in the embryonic context by employing cell lines. The key reasons that support their candidature and make them viable proposition are threefold. First, the pluripotent phase of murine embryonic development is well characterized, molecularly and morphologically. Second, mouse epiblast cells are relatively easy to derive. And finally, defined growth media offered the means to immortalize pluripotent stem cells with a fixed substate identity. The resultant cell lines when cultured in optimized conditions possess uncompromised developmental transition and a differentiation potential similar to the respective in vivo states [79,80].

Besides epiblast tissue, alternative sources, of pluripotent cell lines, both natural and engineered, exist. Their similarities with epiblast-derived lines and on what basis they are side-lined are worth discussing.

Pluripotent cells of non-epiblast origin can also be harvested and expanded into cultures. These include the Embryonic germ cells (EGCs) derived from germline primordium and Embryonic carcinoma cells (ECCs) derived from germline tumors. In either case, the endogenous expression of core pluripotency factors lends them their functional similarities to the epiblast- derived cells. As evidenced by how pluripotency boils down to transcriptional contents in nuclear space, besides the above-mentioned tissue-/tumor-based derivations, pluripotent cells can be engineered by forging the transcriptional signature of the embryos into somatic cells. The earliest attempt, in mammals, to materialize this theoretical concept is the somatic nuclear transfer, wherein an isolated nucleus from somatic cell is placed in denucleated oocyte [81]. Owing to this technique, these cells are named nuclear transfer embryonic stem cells (NT-ESCs). Nearly 4 decades later, such transcriptional reprogramming was achieved with molecular precision by Yamanaka and colleagues yielding a version of pluripotency termed induced pluripotency. Those cells are therefore termed induced pluripotent stem cells (iPSCs) [82]. The standout advantage of iPSC generation is bypassing the need for oocytes or embryos.

These alternate resources, however, are at a disadvantage due to their source of origin and/or generation technique. These include but not limited to, not retaining the pre-X inactivation state, restricted commitment to specific fate, higher mitotic rate giving rise to

low cytogenic stability, greater degree of nuclear irregularity, high tumorigenic potential, obscure epigenetic signatures, low pluripotent cell throughput (for iPSCs and NT-ESCs) and incomplete understanding of the molecular basis of their pluripotency [83, 84], GSCs [85, 86]. More importantly, although the core pluripotency factors are simultaneously expressed, their levels in comparison with epiblast derived cell lines are relatively low, and hence long-term and stable pluripotency maintenance is a significant challenge. Owing to all the above reasons, mouse epiblast explants represent reliable adaptations to adequately study pluripotent progression.

1.2.2 Pluripotency nomenclature *in vitro*

Pluripotent cell types are annotated based on their tissue source and with a lowercase prefix denoting the species, 'm' for mouse. Cultures of pre-implantation blastocyst are called Embryonic stem cells (ESCs) [45,46]. Cell lines derived from late post-implantation epiblast with embryo on the verge of gastrulation are named Epiblast stem cells (EpiSCs) [22,26]. Plenty of standardized mESC (mouse ESC) and mEpiSC lines exist currently. As mentioned before, a multitude of intermediate pluripotent states exist between implantation and gastrulation. Cell lines with these in-between characteristics fall under the broad umbrella of Epiblast like cells (EpiLCs) [39].

As their pluripotency is in a partway transition, generating stable cultures of mEpiLCs has remained elusive. Also, the existing protocols give rise to a highly heterogeneous starting population [74] raising questions about the veracity of the model. The latest effort by Berge and colleagues solved these issues. They unravelled the molecular mechanism driving the sequential transition of mouse embryonic pluripotency. Using this knowledge, the media composition was tweaked to halt mESC maturation which enabled the capture and perpetuation of a highly homogeneous intermediate state with discrete transcription profile and peculiar morphology [77]. Special attention should be given to how ESCs, the extracts of naïve pre-implantation epiblast, produced formative cultures. This hints that the pluripotent substate identity of cell lines is not commissioned by the developmental stage of the embryo.

1.2.3 Growth media dictates *in vitro* pluripotent substate

The pre-implantation, pre-gastrulation, and early post-implantation phases respectively stand for naïve, primed, and formative pluripotency *in vivo*. Yet, the substate identity *in vitro* is not determined by the developmental time at which epiblast is harvested. Rather it is dictated by culture conditions as evidenced by mESCs inculcating formative characteristics when grown in modified media [77]. This notion is confirmed by studies reporting chemically induced naïve (ESC-like) state reversion in EpiSCs and vice-versa, and acquisition naïve/primed identity for EpiLCs cultured in respective growth medium [87-92].

The causative role of growth media in substate identity determination is attributed to its composition. The media is crafted, besides growth factors, with those cytokines, hormones, and pharmacological compounds identified from screening approaches as agents endorsing the transcriptional network of a chosen substate. In this manner, the influence of the developmental origins the epiblast source is overridden. Furthermore, enriched media stimulates unlimited self-renewal. Together, the gene regulatory network boosting and indefinite self-renewal allow the selected substate identity to be stably propagated over several cell generations.

With this information, the key question to be addressed next is, "Among ESC and EpiSC cultures, which is preferable?". The cell type employed is primarily decided by the purpose of investigation, which in our case is to understand pluripotency priming starting with naïve state. Even though EpiSCs can be imparted with naïve characteristics, why ESCs trump them to be the cellular raw material for studying pluripotency progression is explained below.

1.2.4 Growth media makes ESCs the ideal source for *in vitro* naïve pluripotency

The perfect starting point for investigating pluripotent maturation is the naïve state. The corresponding pre-implantation epiblast characteristics can either come straight out-of-the box, like in ESCs, or as add-on features when EpiSCs regress to naïve state with biochemical induction. Despite their naïve identities being practically the same, using ESC lines over EpiSCs is advantageous. This is mainly because chemically baptizing EpiSCs to a naïve state is time consuming with low returns [93] and attenuated pluripotency [87]. Due to the poor yield, EpiSCs must be first expanded before being exposed to naïve state culture

conditions. Such protocol insists using two different media compositions, one for naïve induction and propagation, and another for primed cell-line culturing, which is not cost-effective. On the contrary, initiating pluripotency maturation in ESCs is accomplished by withdrawing the naïve state supporting ingredients in their growth media.

Over the years, multiple growth medium formulations have been worked out for culturing ESCs. They vary in the strength of promoting naïve transcriptional networks. Also, the mode of cultivating cells impacts the efficiency of preserving naïve identity in the long run. So, to identify the appropriate cell-culture technique for our study, it is relevant to review in detail the existing blends of nutrient media and the means of stably propagating ESCs.

1.2.5 Culturing conditions for naïve state perpetuation

Originally, mESCs were cultured as adherent colonies on mitotically inactivated feeder layers in a medium conditioned with foetal bovine serum (FBS) [94]. Conventionally used feeders are produced from primary mouse embryonic fibroblasts (MEFs), although other immortalised lines or cell sources of human or mouse origin exist. MEFs anchor mESCs and nurture them by releasing paracrine factors that allow pluripotent cell expansion in undefined media [95]. The differentiation suppression and self-renewal activation effects of feeders were found to be due to the secretion of cytokine LIF.

However, the use of feeders poses certain limitations. Barring LIF, the biochemical cues emanating from MEFs are ill-defined, with the bulk suspected of undermining pluripotency. Also, feeder cells can be maintained only for limited passages [94], which demands the frequent preparation of new batch of feeders. The consequence of batch-to-batch variation, differential LIF secretion, which, in conjunction with rest of the destabilizing signals, might wither pluripotency. This can be mitigated by the provision of recombinant LIF.

mESCs attach to the extra cellular matrix (ECM) assembled by feeders [96]. Moreover, functionally substituting MEFs with LIF-replenished media alleviates pluripotency decline. These helped in realizing that feeders are dispensable and paved the way for feeder-free maintenance of mESC cultures in minimal media added with FBS and LIF, colloquially referred to as Serum-LIF (Ser+LIF). The pros and cons of traditionally employed techniques and the brief description of protocol to propagate mESCs in '**Ser+LIF**' are compiled in **Table.2**

Culture technique	Cell propagation	Strengths	Limitations
Suspension	Free-floating spherical aggregates	• Low hands-on time for culture maintenance [96] • Established platform, but for trilineage differentiation. • Scale up is convenient. • Cell clumping into Embryoid bodies (EB) mimics 3D *in vivo* growth [98]	• Limited diffusion of O_2 and growth factors lead to necrotic core [99] • Interior cells are highly susceptible to differentiation. • Low sample throughput due to long division time [100] • Starting sample for experiments are highly heterogeneous. Mixture of differentiated and pluripotent cells [101] • Clonal infidelity as clusters with different clonal origins fuse [102] • Efficient use of media and growth factors need stirring [103] • Requires cell-strainer to start the culture as single-cell suspension
Adherent	In decellularized organ/tissue scaffolds	• Replicates physiological dimensionality. • Growth factors that need to be supplemented in media are harboured in natural scaffolds [104] • Natural ECM scaffolds are bioactive: interact with cells	• Metabolic wastes pile up to toxic levels [105] • Short shelf-life of matrices [106] • Lot-to-lot variation in physical, mechanical, and bio-chemical features of natural scaffolds [107] • Lack of control over cell seeding density [108] • ESC might be skewed to differentiate towards the organ from which natural scaffolds are derived. • Difficult to control the degree of decellularization and, to retain the surface composition and structure of ECM [109,110]
	On synthetic polymers (Biodegradable)	• Simple fabrication procedure • Mechanical and biochemical properties can be fine-tuned [111] • Polymer matrices are typically hydrophobic and resist non-specific cell-attachment [106] • Scale up potential	• Require protein tethering as polymers offer no cell-attachment motif • Stable and specific protein conjugation with even distribution on synthetic polymers involve complex chemistry [112] • Lack of consensus on the starting material and design of synthetic scaffolds • Cells detach after short time in culture on most polymers [112]
	On feeders	• More number of potential experimental samples due to quicker proliferation [101] • Feeders secrete nutrients to support ESC self-renewal [95]	• Cross-transfer of pathogens from feeders [101] • Feeders contaminate experimental stem cell sample [96] • ESC attachment declines with feeder passage number [113] • High frequency of passaging to prevent unwanted differentiation

Culture technique	Cell propagation	Strengths	Limitations
Adherent	On feeders	• Feeders synthesize ECM to promote cell adhesion [96] • Feeders detoxify media by sequestering oxygen radicals and metabolic wastes [114]	• Feeder cells' maintenance is expensive and tedious • Batch-to-batch variation of feeders [115] • Feeders' secretion is chemically undefined [96] • Mitotic blocking procedures are costly [116] and incur high cell death [113]
	On Laminin coated tissue culture plastic	• Simplicity of cell passaging protocol • Laminin coating procedure is standardized, and the in-house stock preparation is time- and cost-saving. • ESCs retain *in vivo* structure and organization [117] • Cultures are free from allogenic and xenogenic cell types, and zoonotic pathogens • Laminin, one of the ECM components of epiblast basement membrane. • Control over plating density and colony size [79] • Suitable for long-term maintenance of culture without compromising pluripotency • High viability and cloning efficiency with single cell seeding • Little colony detachment as ESC interaction with Laminin is specific: mediated by β1 integrin [24] • High frequency of obtaining potential experimental samples [101] • Optimized seeding density for regular passaging [79] • Refractive colony growth in defined media minimizes colony merge and preserves clonal fidelity	• Cells must be split every 2-3 days to preserve pluripotency [79] • Passaging is labour intensive and time consuming • Not all cell-lines adapt to coated surfaces [101] • Genetic aberrations accumulate over prolonged culture • Multiple pluripotency substates co-exist in the same colony [118] • Non-physiological stiffness of tissue culture plastic as possible mechanical input to accentuate inter-colony heterogeneity

As seen, the mESC culture protocol on Laminin-coated dishes stacks up better against the rest of the methods. Importantly, except for the regular laborious cell-splitting, the other shortcomings of this procedure can be undone. An unwritten rule in the research community is that a safe passage number to preserve genomic integrity is less than 50. As a safety measure the maximum threshold for this work is set to 40. The rest of the constraints are linked to the undefined nature of culture media whose pluripotency compromising effects are primarily traced to LIF with contribution from FBS. It is imperative to comprehend how these two components instigate cells to forgo pluripotency as it puts in perspective how defined media secures and homogenizes naïve identity.

1.2.6 Serum – A double-edged sword

FBS is used as an additive to ESC culture media as it has a high content of embryonic growth factors that stimulate cell replication. However, it is not a trustworthy pluripotency defender as it also includes differentiation inducers [119]. Notably, the relative proportion of these two constituents varies between different lots. This means certain stocks of serum might not be conducive to fostering the undifferentiated growth of ESCs. Though this can be circumvented by batch testing, the inconsistency in serum's molecular make-up supposedly leads to confounding experimental results. Furthermore, using FBS risks the introduction of adventitious agents as it is a biological product originating from different species.

While replacements such as knockout serum and ESC-grade FBS exist, they are expensive and importantly, since they are commercial products, their composition remains unknown. Factoring in these concerns, N2B27 is the best-suited alternative. The salient features authorizing its use as growth media base are as follows:

(i) N2B27 is empirically formulated to provide optimum cell viability [120].
(ii) Recipe for in-house N2B27 preparation and guidelines for assessing batch quality along with troubleshooting tips are publicly available [79].
(iii) N2B27 lacks lineage specifying cues and only permits naïve to primed transition [79].
(iv) The kinetics of naïve state exit in N2B27 at population level is reported. This helps to inform if any mechanical or chemical perturbation alters the rate of pluripotency priming.

(v) The expression patterns of the key naïve and early post-implantation factors, *Nanog* and *Otx2* respectively, during pluripotency progression in N2B27 mirrors the dynamics in embryo [74].

Clearing the media from differentiation signals by substituting N2B27 for serum is only half the job. For sustained maintenance of pluripotency, epiblast explants must be granted with unlimited self-renewal. This is achieved by including LIF, albeit at the cost of transcription factor heterogeneity, which translates to the co-existence of multiple cell substates [45,121]. To selectively conserve naïve identity, two small molecule inhibitors PD0325901 or **PD,** and CHIR99021 or **Chiron**, are incorporated. This concoction, N2B27 with two 'i'nhibitors, is referred to as '2i' media and culturing ESCs in it with the provision of LIF homogenizes the otherwise wavering expression of naïve factors, seen in Ser+LIF [122-126]. The need for supressing the molecular targets of **PD** and **Chiron** to obtain uniformity in substate identity becomes clear when studied with the non-purist effects of LIF signalling.

1.2.7 Paradoxical yet pivotal role of LIF for naïve pluripotency

Upon binding to its cognate receptor, LIF deploys three main signalling arms of pluripotency regulation. They are: JAK/STAT3, PI3/AKT, and MEK/ERK pathways [121,127]. The first two pathways are pluripotency affirming as they promote the individual expression of *Oct4*, *Sox2*, and *Nanog* (OSN triad). Additionally, they upregulate *Klf4* and *Esrrb* [121,127,128], which favours the establishment of naïve identity. Alongside this transcriptional activation, PI3/AKT pathway silences Gsk3β to prevent the degradation of *c-Myc* and β-catenin [127,128].

The elevated levels of *Nanog* and *c-Myc* result in enhanced ESC self-renewal [121,130]. Also, cells might be locked down in the naïve state as *Nanog* induced self-renewal is functionally antagonizing *Otx2* [130], the early post-implantation factor crucial to begin primed state transition [131]. To further strengthen naïve transcriptional network, the OSN triad and *Klf4* engage in a mutually cooperative interaction [132]. Besides, *Klf4* drives E-cadherin expression to facilitate cell-cell adhesion, which is essential for recruiting, stabilizing, and activating LIF receptor [121, 133]. As this re-initiates LIF signal transduction, the interplay between cadherin and LIF receptor encompasses a positive feedback loop. Finally, β-catenin

features in the list of molecular components advocating naïve identity, in both the forms (1) Transcriptionally active nuclear fraction and (2) Cadherin bound cytoplasmic form. While in the nuclear space it binds to *Tcf3* thereby inhibiting the repressive action of the same on OSN triad [134], the cytoplasmic fraction strengthens E-cadherin membrane stability and sequesters the core pluripotency factors, *Oct4* and *Nanog* [135].

On the other hand, MEK/ERK pathway prepares ESCs for differentiation [136]. Since, naïve state must be relinquished for differentiation program to take over, this pathway breaks down the transcriptional circuit by targeting *Klf4* [132]. To explain briefly, following its phosphorylation, ERK translocates to nucleus and interacts with *Klf4* to transfer its phospho-moiety. Consequently, *Klf4* is removed from the transcription initiation complex, which is composed of RNA polymerase II and the OSN triad. In this unbound state, *Klf4* is labelled by the phospho-tag for exportin-1 (XPO1) mediated nuclear exit. Once relocated to the cytoplasm, poly-ubiquitination directs *Klf4* for proteasomal degradation [132]. Blocking *Klf4* phosphorylation or disabling XPO1 is shown to suspend pluripotency maturation which justifies that *Klf4* nuclear exclusion initiates naïve state exit. This mechanism of ceding naïve pluripotency holds true for cultured ESCs and in intact mouse embryos.

Klf4 integrates thereby strengthening the pluripotency triumvirate of *Oct4*, *Sox2*, and *Nanog*. Its eviction causes *Nanog* downregulation [132], which deteriorates the strength of the OSN trio over time. The drop in *Nanog* level also lifts the restraint on *Otx2.* The increase in *Otx2* expression not only displaces *Oct4* from the enhancers of naïve genes but also lends access to the enhancers of primed state and differentiation genes [88]. In this way, MEK/ERK pathway abets pluripotency priming. As an ancillary, the canonical inhibition of GSK3β is only partial as functionally redundant homologs that are PI3/AKT-proof exist [137]. This compromises *c-Myc* mediated self-renewal and β-catenin's censorship of *Tcf3*, the OSN triad repressor, which further complements MEK/ERK pathway for suspending naïve state.

As such, LIF concurrently provokes pluripotency disapproving and naïve state asserting events. The dominant one between these two contrasting signals is decided by stoichiometry. When the ratio favours of MEK/ERK pathway and/or GSK3β, pluripotency priming kicks off by instructing ESCs to reduce the levels of naïve state specifiers. This, when coupled with the cell-to-cell varying transcriptional noise, gives rise to the mosaic protein expression pattern typical of Ser+LIF cultures.

1.2.8 Culture conditions are optimized by two 'i's

All the above-mentioned defects of LIF are negated by the addition of **PD**, which blocks ERK phosphorylation [138] and **Chiron**, which silences GSK3α/β [139]. By abolishing the pluripotency deterring influence of GSK3 and MEK/ERK pathway, the two inhibitors make sure that only the naïve state certifying inputs of LIF are fed into the gene regulatory network. This sends the naïve transcriptional circuit into a hyperdrive. Simultaneously, **PD** and **Chiron** also do their part in equilibrating naïve factor levels across cells by reducing gene expression noise. All in all, mESCs in 2i+LIF media have consolidated naïve identity and perpetuate with near-perfect uniformity in their transcriptome that resembles pre-implantation epiblast [10].

Apart from modulating the biochemical signalling of LIF, the presence of **PD** and **Chiron** takes care of the key limitation of tissue culture plastic. As ERK and GSK3β are sensitive to mechanical stimulation [140,141], the high non-physiological stiffness of the culture dishes is a prominent differentiation signal. If left unchecked, it leads to the same old problem of distinct pluripotent identities in the culture. The addition of two inhibitors successfully tackles this issue as the downstream activation of ERK and GSK3β, necessary for rigidity sensing, is vetoed. In essence the mESCs are insulated from the mechanical inputs when cultured in 2i media. Thus, addition of these two small molecule inhibitors to the defined N2B27 base media with additional supplementation of cytokine LIF make the growth conditions conducive for maintaining mESCs in naïve state with a high degree of transcriptional homogeneity. The LIF induced pathways and stabilizing effect of 2i compared to Serum are summarized in Figure.6

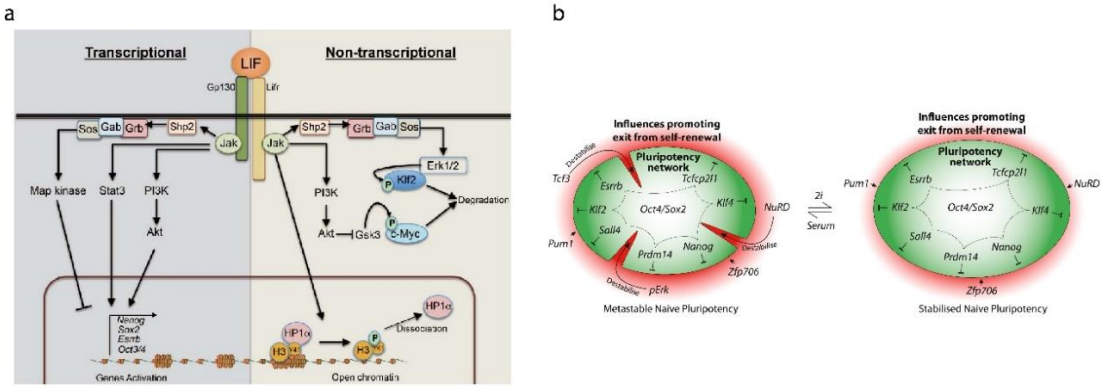

Figure.6: 2i media counteracts pluripotency destabilizing signalling of LIF. a. Schematic depiction of LIF induced intracellular signalling pathways in mESCs adapted from Ohtsuka S, Nakai Futatsugi Y and Niwa H *et al*., 2015 *JAKSTAT* and b. Schematic representation of pluripotency stabilization in 2i by counteracting the differentiation promoting actions of Serum-LIF, adapted from Hackett JA and Surani MA *et al*., 2014 *Cell Stem Cell*

Besides the two inhibitors, Insulin is another key component of the defined N2B27 media to neutralize the pluripotency destabilizing signals. At the concentrations used for cell culture, LIF and **Chiron** (as an indirect Wnt agonist) are reported to promote primitive endoderm specification [142, 143]. Insulin counteracts such lineage induction by fine-tuning self-renewal pathways of TGFβ, PI3/AKT and MAPK [143].

Such duality of LIF and Chiron; to simultaneously promote both pluripotency stabilization and lineage induction is the characteristic trait of the major naïve pluripotency regulators discussed above. For example, Nuclear β-catenin, besides *Tcf3* repression, is shown to induce mesodermal genes through *LEF* and its co-effectors [144], Insulin aids in neural differentiation [79, 145]. The final media composition is carefully crafted with precise concentrations for each component such that the net outcome is the boost of naïve signature. While alternative cost-effective media compositions with the supplementation of additional small molecule inhibitors and/or morphogens were formulated, the propensity of spontaneous differentiation in those is comparatively higher [146-149], besides a host of other shortcomings. All these are summarized with a comparative analysis of the alternative standardized media formulations presented in **Table 3**.

Hence, any media composition does not necessarily insulate cells from differentiation signals but rather, at best, subdues them. Among the concoctions available, the defined N2B27 media with a low concentration of Insulin, along with the supplementation of **PD** and **Chiron**, and cytokine LIF is the one that outweighs the induction cues to safeguard the naïve identity long-term [150,151].

While culturing in N2B27 media, among PD, Chiron and LIF, the provision of any two, particularly the two-inhibitor combination, is reported to be minimally sufficient to homogeneously maintain a naïve state [79]. However, LIF confers additional stability by promoting the expression of the naïve state specifier *Klf4* and E-cadherin. While *Klf4*'s transcriptional role and positive feedback regulation of naïve program by E-cadherin have been summarized earlier, increased E-cadherin offers a characteristic morphological advantage. The increased E-cadherin expression translates to high surface tension, and as a consequence when seeded as single cells in media with LIF, mESCs grow as refractive 3D colonies, with minimal merging, thereby presenting high clonal fidelity. Moreover, any deviation from this morphology serves as an indicator for suboptimal batches of media.

Media name	Pluripotency promoting signals	Pluripotency destabilizing cues	Evaluation
BMP4+LIF	• BMP4 reverts primed population to naïve state [152] • BMP operates through MEK-ERK pathway to drive Kruppel like factor (Klf) family transcription factors [153]. • BMP activates β-catenin based Wnt pathway [154,155].	• BMP4 treatment reverts cell population to early developmental stage with significant TrE population [147,156] • Increased propensity of primordial germ cell fate primed pluripotent population [148, 149] • Reversion of primed cells to naïve state is through primordial germ cell fate [152]. increasing tumorigenic potential due to retaining only male imprint [86] • BMP4 based Wnt signalling poises mesoderm fate specification [157]	• Requires serum to negate the differentiation effects of BMP4 [149]. • Recombinant versions of BMP4 are available but are expensive hence media not cost-effective. • BMP4 doesn't counterbalance but rather augments the differentiation capabilities of LIF. • Starting population is a mixture of ESCs predisposed to distinct germ layer fates. • Not ideal for non-permissive strains of mESCs. • Pluripotency exit kinetics not characterized.
PD+VitaminC (Ascorbic acid – AA)	• PD inhibits MEK/ERK pathway counteracting its differentiation effects. • Ascorbic acid prevents reactive oxygen species mediated senescence and death [158] • Ascorbic acid upregulates the expression of core pluripotency factors through epigenetic mechanisms [159]	• Self-renewal action of MEK/ERK pathway is lost. • Promotion of cardiac lineage through upregulation of phosphorylated SMAD [160] • β-catenin based repression of Tcf3 is compromised. • Ascorbic acid attenuates p53 pathway leading to clonal heterogeneity [161]. • Base medium contains serum.	• Starting population is a mixture of ESCs predisposed to distinct germ layer fates. • Not ideal for non-permissive strains of mESCs. • Expression of transcription factors upon initiating naïve state exit are not characterized. • Self-renewal capacity is compromised leading to suboptimal expansion and long-term maintenance of the culture.
Alternative 2i (Src inhibition + Gsk3β inhibition)	• Bypasses the requirement of MEK/ERK signalling inhibtion without compromising self-renewal [162]	• Src inhibition reduces inclination to ectoderm and endoderm, priming cells to mesoderm fate [163,164] • Src inhibition downregulates YAP possibly compromising the differentiation capability of mESCs. • Retains most of the features of naïve state but not all plausibly owing to downregulation of Myc [165,166]	• Compromised differentiation capability towards 2 of the 3 founder lineages, affecting the fundamental trait of pluripotency. • No added advantage over replacing MEK/ERK inhibition with inhibition of down stream target Src. • Transcriptional changes occurring post naïve state exit induction are not characterized.

5i + LIF + Activin or 6i media	• Addition of small molecule inhibitors for BRAF, SRC and ROCK. • ROCK inhibition permits human ESCs splitting and seeding as single cells. Therefore, might enable clonal expansion of mESCs from non-permissive strains [167]. • Efficient reversion of iPSCs of porcine origin to naïve like state [168]	• Activin initiates the transcriptional program of intermediate stages (formative) pluripotency. • Increased risk of genomic instability [93,169] • Increased propensity to cross differentiate into trophoblast cells [170, 171] • Short media shelf life, a major hindrance to long term culturing without incurring batch variations [172]	• Media composition tailored to be species specific (5i for human and 6i for porcine cell lines). Hasn't been tested for mouse lines. • Serum requirement for long term usage and improved shelf life. • Increased tumorigenic potential. • Starting population adulterated by cells reverted to either earlier differentiation stage or have extra embryonic tissue fate.
N2B27+2i + (LIF)	• PD inhibits MEK/ERK pathway counteracting its differentiation effects. • Chiron inhibits Gsk3β. • LIF activates JAK/STAT, PI3K/Akt and MEK/ERK pathway. • PI3K/AKT pathway stabilizes *c-Myc* and β-catenin. • Differentiation induction is minimal due to low doses of the molecular cues and is countered by other components.	• Self-renewal action of MEK/ERK pathway is lost. • LIF and Chiron promote endoderm specification. • β-catenin primes to mesodermal lineages. • Low shelf-life, to be used within 1 week of preparation. • Increased DNA damage observed in cultures with high passage numbers. • Requires frequent passage.	• Permits expansion of non-permissive strains. • Homogeneous starting population. • Well characterized pluripotency dissolution kinetics. • Self-renewal capacity is maintained. • Media composition is based on murine biology.

Given the molecular framework with which the **2i** media operates, it is understood that the withdrawal of two inhibitors is biochemically permissive to naïve state exit. With additional removal of LIF, the pluripotency dissolution kinetics were reported to occur 12 hours earlier [79]. Since insulin is the only other exogenous signalling cue capable of lineage specification, at the concentration used, ESCs are committed to the neural ectoderm [79]. As mentioned earlier, the molecular changes associated with naïve state exit and ensuing fate specification are well characterized in N2B27 and are briefly summarized in next sub-section.

1.2.9 Culturing in N2B27 recapitulates transcriptional changes of naïve state exit

Loss of ground state identity is signified by the downregulation of naïve state specifiers; *Nanog*, *Klf4* and *Esrrb* [53, 132, 172, 173] with characteristic kinetics. A concomitant increase in the expression of post-implantation markers is observed and of them *Otx2* is indispensable in terms of irreversibly committing the cells to pluripotency dissolution and further lineage specification to neural fate [75,174]. These expression patterns observed in cultured intact embryos, were also replicated in vitro ESC population subjected to naïve state exit by culturing in N2B27 (withdrawal of 2i and LIF). The pluripotency exit protocol was performed for both single cells seeding and mESCs grown as colonies for 48 hours (to reflect the typical ICM population count prior to embryo implantation). Although the rate at which a given transcription factor is upregulated/downregulated varies between single cells and colonies, the series of events are broadly conserved and are listed below.

1. *Klf4* is exhausted the earliest, by 16 hours in single cells and 24 hours in colonies, without further expression [45,79]
2. *Nanog* is transiently downregulated with heterogeneous expression patterns in colonies 24 hours post **2i** withdrawal, with later surge around 72 hours; a developmental time coinciding with gastrulation. [87, 175, 176].
3. *Esrrb*, being a transcriptional target of Nanog is monotonically depleted to undetectable levels by 24 hours in both single cells and colonies. [45]

4. A basal expression of *Otx2* is elevated close to 8-fold during the 16-24hr period in single cells and between 24-48 hour in colonies, followed by a slight decline to 4-fold expression [45, 73, 179].

It must be pointed out that in case of colonies, except for Nanog, the above-mentioned expression patterns were acquired from experimental techniques such as western blotting and RT-PCR, which offer whole population averages without informing the spatial variation / intra-colony heterogeneity.

The transcriptional annotation at discrete time points mentioned above could only confirm the irreversible progression towards pluripotency exit. However, if one were to study the effect on any perturbation on the spatio-temporal dynamics of pluripotency exit in single cells or colonies, there is a need for a cell line which recapitulates the gradual pluripotency dissolution.

1.2.10 Rex1::GFPd2, a designer cell line to track pluripotency continuum

To faithfully reflect the seamless progression of pluripotency, it is imperative that the mESC line should perpetuate with absolute naïve identity without compromising the attainment of later states' identity and tri-lineage differentiation potential. If one were to engineer a cell line, the second constraint rules out the altering or deletion of any of the formative (*Otx2*, *Oct6*, *Fgf5*) and primed factors (*T, Cer*, and *Foxa2*). By selecting a naïve state specifier, while the progression is not sacrificed, the challenge is to maintain the ground state identity long term. To arrive at the ideal candidate, it is important to revisit the pre-implantation markers to try and identify their regulatory role and requirement status.

The bonafide naïve state specifiers are *Nanog*, *Rex1 (Zfp42), Esrrb, Klf-2/4/5*. Since the generation of cell line, compatible with real time monitoring, requires the replacement of protein coding sequence with a luminescent or fluorescent reporter, it is necessary to be informed on the dispensability of each of the four proteins. mESCs are reported to not simultaneously withstand the deletion of either *Esrrb* or *Klf-2/4/5* and maintain ground state identity [132, 178]. *Nanog* is essential for both the establishment of naïve state and for the transition to intermediate stages [179]. Hence, these three factors cannot be meddled with.

The only other factor *Rex1 (Zfp42)* is shown to be downregulated upon implantation [10, 177-179]. Moreover, homozygous deletion of Rex1 coding sequence is reported to have no phenotypic consequence either for the mESC lines or intact embryos [180, 181]. Importantly Rex1 upstream promoter indicates the level of transcriptional activity by the core pluripotency factors as it is the putative binding sequence of OSN triad. Taking advantage of these properties, a mESC cell line where one of the alleles of Rex1 coding sequences was replaced with destabilized GFP (GFPd2) was engineered [182]. The GFPd2 was obtained by fusing the degradation domain of mouse ornithine decarboxylase to the c-terminus region of enhanced GFP (EGFP) conferring the protein a half-life of 2 hours [183]. A schematic representation of the cell line is given below.

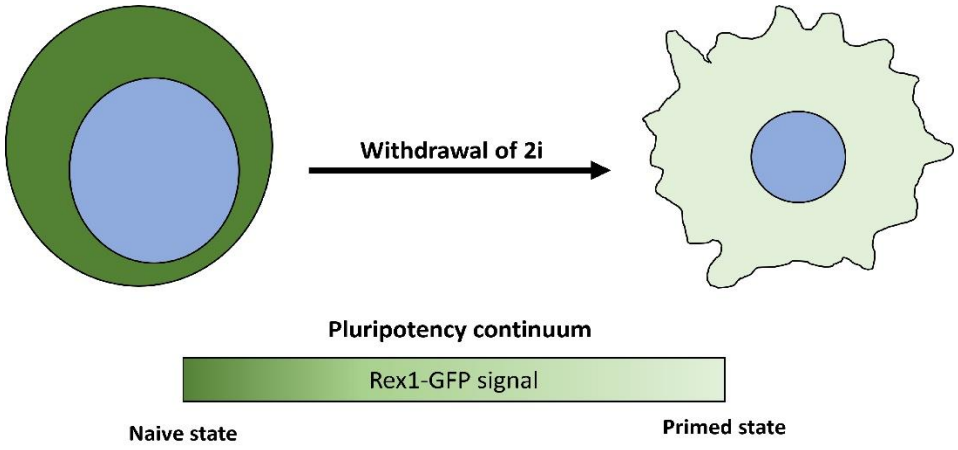

Figure.7: Schematic representation of fluorescent signal intensity marking the distinct states of pluripotency for Rex1::GFPd2 mESCs

To place it in the context of naïve state genetic program, when cultured in 2i (+/-LIF), every 2 hours the existing pool of EGFP is directed to proteasomal degradation and is replenished by the ones produced in the current cycle of transcriptional activity on Rex1 promoter. Thus, high and homogeneous GFP signal indicates the maintenance of naïve state identity in the culture. Upon removal of the two inhibitors, with the transcriptional activity progressively reducing and eventually shutting down on Rex1 promoter, a gradual decline of fluorescence intensity ensues. Since, the last batch of EGFP produced is degraded 2 hours post its transcription, the earliest time point at which the fluorescence intensity of the cell line resembles that of background should be 2 hours after the exit from naïve state.

Another important detail to be considered and look forward to when *Rex1* is taken into conversation is the transcriptional logic between the formative factor *Otx2* and the naïve marker *Nanog*. In mESCs, a basal level of Otx2 expression exists to drive self-renewal [75]. Importantly, *Otx2* expression confers the metastability to naïve state to respond to external cues rather than being insulated and locked in ground state pluripotency. It executes these functions by antagonizing *Nanog* [184]. As *Otx2* inhibition of *Nanog* compromises the OSN triad transcriptional activity, one of the consequences of its knockout is an expected upregulation of *Rex1* expression and so is the case as reported [184]. Therefore, the inverse holds true, i.e. *Rex1* downregulated with *Otx2* expression.

The transcriptional annotation of the discrete time points upon naïve pluripotency exit is the one aspect missing from the comprehensive molecular characterization of Rex1::GFPd2 cell line. Besides this information gap, this cell line has been extensively used and considered to be a reliable model in the community to study the effect of signalling cues of any nature, be it molecular, chemical, or mechanical, on the kinetics or dynamics of the progression from naïve state pluripotency. Below are the key characteristic traits of this cell line when cultured in 2i media and later subjected to N2B27 media for pluripotency dissolution. These details, albeit at the population level, are necessary to evaluate the culture and serve as references to be compared with the results of any perturbation.

(1) Culturing in 2i for 48 hours yields a GFP+ve population with tight unimodal expression.
(2) Change of media to N2B27 leads to bimodal expression around 24 hours with close to half the population being GFP-ve.
(3) The entirety of population is expected to exit naïve state with GFP-ve status post 40 hours of culturing in N2B27.
(4) Day 3 post media change is marked by the emergence of Sox1+ve cells and Day 6 by the expression of class 3 beta tubulin marker Tuj1.

The transcriptional logic summarized in earlier and, the fine details of media recipe and culturing conditions dealt here are borne out of the studies focusing on the genetic and epigenetic regulation of pluripotency progression. However, when considered in context of embryonic development, as suggested earlier, the transition from naïve pluripotency is intimately linked with post-implantation morphogenesis which in turn is driven by mechanical signals of varied nature. Among the mechanical cues at play in the post-implantation embryo,

the prominent ones and their regulation of the form and fate dialectic were briefly outlined in previous sections. Additionally, the body of work dealing with the mechano-regulation of pluripotency progression in vitro and the key knowledge gaps that exist within the field, is yet to be viewed. All of these will therefore be dealt with in the next section, and before moving on, as is customary, the takeaways of this section are listed below.

Section summary:

- Pluripotency can be maintained *in vitro* by harvesting epiblast explants.
- mESC is the shorthand notation of murine pluripotent cells.
- Naïve identity is not commissioned by tissue of origin but by growth media.
- mESC maintenance as adherent cultures on laminin coated plates is advantageous.
- mESC cultures are heterogeneous when grown in **Serum+LIF**.
- Defined **2i** media overcomes **Serum+LIF** issues and propagates homogeneous naïve state.
- Removal of two inhibitors, recapitulates molecular changes associated with naïve exit.
- A designer cell line, Rex1-GFP, allows the real time tracking of pluripotency continuum.

Section 3: Mechanical regulation of murine pluripotency

From blastocyst floating in the intraluminal fluid to the egg cylinder housed in the decidual tissue, pluripotent epiblast is no stranger to mechanical signals. Even for *in vitro* cultures every fine detail ranging from the cytoskeletal organization within an individual cell to the propagation of mESC colonies as compact 3D colonies is at the dispense of mechanical signalling. A detailed review of the literature is presented in this section about such mechanical regulation of pluripotency establishment and progression, in single cells and in colonies, in vitro and in vivo. By being acquainted with the status quo, the goal is to identify the key knowledge gaps that require immediate attention.

An important technical definition before proceeding to the next topic. The cellular responses upon subjecting to mechanical cues are collectively referred to as mechano-responses and manifest at any of the subcellular regions/ components ranging from the plasma membrane to actin cytoskeleton and nucleus.

1.3.1 Mechanics at the forefront of *in vivo* pluripotency establishment

As mentioned briefly in the first section, the first segregation event is driven by the mechanosensitive HIPPO-YAP pathway, where it's on/off status is determined by positional information. Outside cells switch off HIPPO pathway leading to YAP nuclear localization and are eventually directed to Trophectoderm fate while inside cells with HIPPO on, are assigned to ICM lineage.

Fate specification in the second segregation event was attributed to the build-up of luminal pressure. Two recent studies employing optical tweezer measurements highlighted how the predisposition of ICM cells to either fate is determined by the membrane mechanical properties [19, 185]. The cells poised for PrE fate were reported to exhibit higher membrane elasticity / in-plane (apparent) tension. Through a computational model the robust segregation of two fates was recapitulated in both the studies. Delving into molecular details the first work showed that the PrE fated cells presented spatial heterogeneity in the ERM (Ezrin-Radixin-Moesin) protein levels increasing surface and shape fluctuations [19]. Moreover, these results were validated in cultured embryos.

While the above two are examples of *in vivo* setting, several studies point out the deterministic role of mechanics in (re)establishing and maintaining pluripotency *in vitro*. The relevant ones are present in the next sub-section, dealing with single cells first and later proceeding to colonies. The works presented include the ones performed with Serum+LIF and the ones in 2i media and hence, wherever necessary, the media details are provided.

1.3.2 Cell-intrinsic determinants of *in vitro* pluripotency state

Single mESCs maintained in the naïve state exhibit weak adhesion with the underlying substrate and present high contact angle. This is found to be mediated by their peculiar actin organization. Unlike in spread cells, be it primed mEpiSCs or other differentiated cell type, which present prominent actin stress fibres oriented radially towards nucleus [186-188], naïve mESCs were found to have short and inward curving actin filaments organized as interconnected mesh lacking any directionality [188] as shown in Figure below.

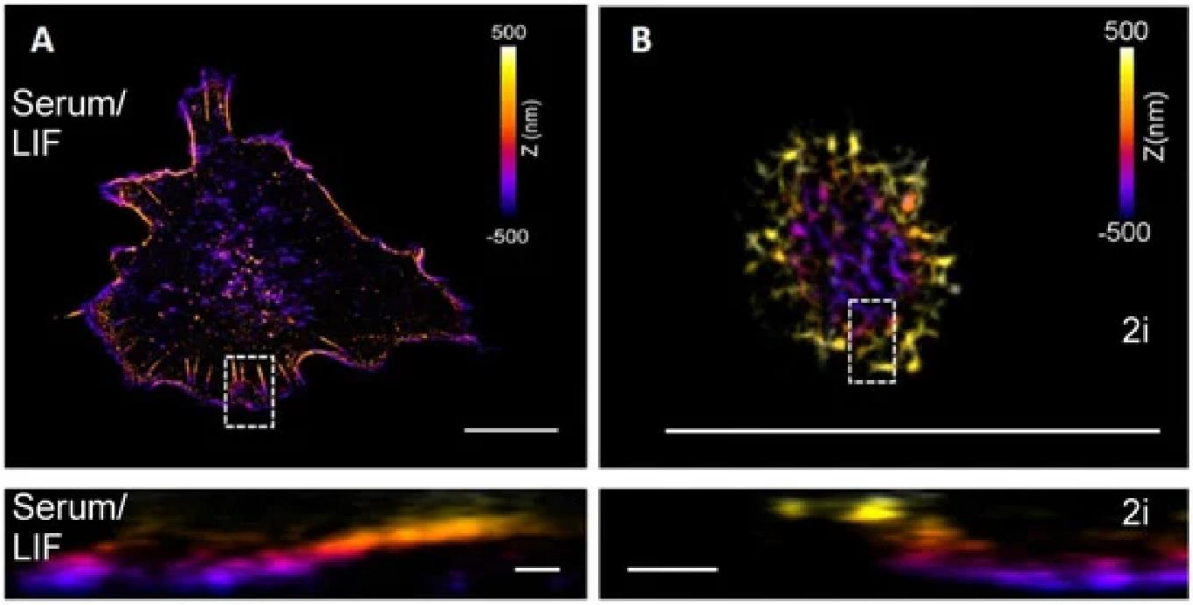

Figure.8: Representative 3D STORM images resolving actin organization for mESCs gorwin in Serum+LIF (A) or 2i media (B) with the lower panels showing orthogonal projections of boxed regions. Scaled bars in upper panels 10 µm and in lower panels 500 nm. Picture adapted from Barooji YF *et al*., 2021 *Cells*

Such cytoskeletal network arrangement is the result of strong actin cortex tethering to plasma membrane mediated by the linker protein, Ezrin [189]. This was shown to confer high in plane membrane tension in the same work, as measured by static tether-pulling assays using AFM. The functional consequence of this high membrane tension is the attenuated membrane signalling activity as was reported in De Belly et al [190].

While both the above-mentioned works have identified membrane tension decrease to be an obligatory first step for naïve state exit to begin, De Belly et al. 2021 laid out the roadmap of the molecular signalling that follows. Briefly summarizing the events to take place, with the withdrawal of two inhibitors, β-catenin degradation by GSK3β downregulates RhoA activity/phosphorylation which lowers the levels of phosphorylated Ezrin, compromising its membrane tethering function. The resultant decrease in membrane tension permits the internalization of FGF ligands, which activate MEK/ERK signalling, leading to a reduction in the expression of naïve pluripotency factors and, as a result, consolidating pluripotency priming. Upon restoring membrane tension through the expression of constitutively active (phosphorylated) RhoA or Ezrin, mESCs maintained naïve identity despite not being provided the two inhibitors (culturing only in N2B27 media) for 48 hours.

These findings highlight the mechanical gatekeeping role of cell membrane tension to preserve naïve state in individual cells. They have adequately informed us on the molecular intricacies of the earliest signalling events directing pluripotency dissolution. However, *in vivo*, naïve pluripotency exit occurs in a collective setting which has also been attempted *in vitro*. While mESCs express the adhesion molecule E-cadherin (E-cad) in both the single cell and colony contexts, only in the latter are E-cads ligated to neighbouring cells. E-cad is a prominent mechanosensitive protein reported to participate in the initiation and regulation of force transduction in other cell types. Due to this added feature of E-cad coupling and with it being implicated in mechanical signalling, naïve mESC colonies exhibit emergent properties in the aspects of both organizational and mechano-responses. The molecular signalling network and transcriptional logic, however, remains conserved between the single cells and colonies. Hence, the knowledge from single-cells studies should, therefore, be used as reference points rather than being extrapolated. With this prudence the following sub-sections gleans the works pertaining to colonies, invoking single-cell data whenever necessary.

Vindicating that force mediates the form-fate interdependency, the work by Du J and colleagues [191] highlighted the transcriptional implication of mESCs growing as 3D colonies. Their characteristic dome morphology is the result of cytoskeleton organized as a supracellular actin cortex (SAC) spanning the outer cell layer. Through such organization, 3D SAC, with the concerted action of myosin motors, generates compressive forces that drive the expression of naïve state specifier *Nanog* and general pluripotency factor *Oct4*. When the force exertion was compromised through azido-blebbistatin treatment to selectively inhibit myosin in outer cells, the expression levels of both *Nanog* and *Oct4* were downregulated. When mESC colonies morphology was patterned into refractive colonies by agarose encapsulation, the effect blebbistatin treatment was lowered. Higher the agarose concentration, more the compactness of the colony and lesser the blebbistatin effect. These results are summarized in Figure.9 below.

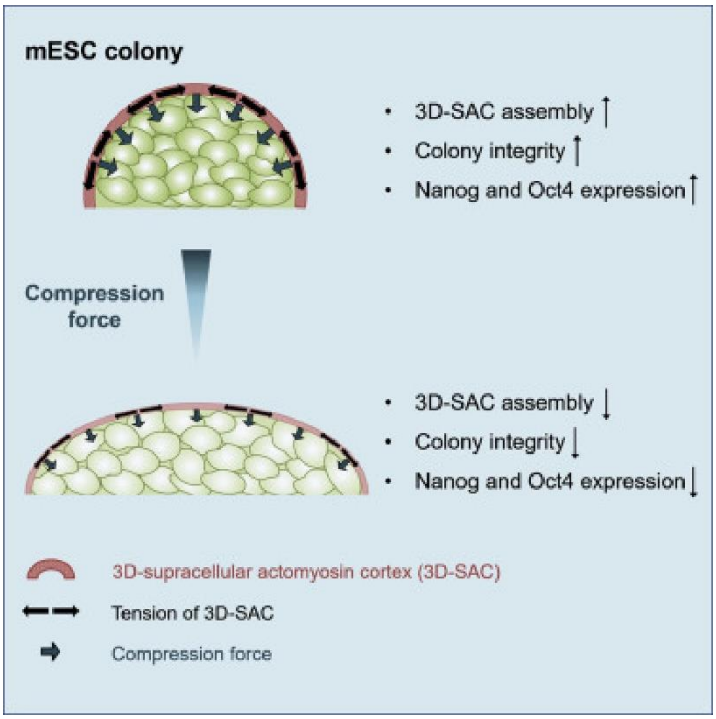

Figure.9: Schematic representation of 3D SAC mediated compressive force driving expression of *Oct4* and *Nanog*. Picture adapted from Du J *et al*., 2019 *Cell Systems*

Here lies the first emergent property for mESCs growing in colonies with actin filaments organizing into a network that spans multiple cells while maintaining high cortical actin expression and tethering. Moreover, both single cells and colonies exhibit refractive morphology, only in latter was it found to be dependent on the contractile activity of myosin.

Interestingly, *Nanog* expression is not maternally inherited but is shown to appear only during blastocyst compaction [192]. Therefore, the physiological luminal pressure can be thought to be replaced in vitro by compressive forces of 3D-SAC. Such supracellular cytoskeletal arrangement is not unique to murine cell lines, as a contractile actin fence was also reported in human iPSCs and is shown to exert compaction forces and enforce colony morphology in a myosin dependent manner [193].

The second contributing factor for the distinctive 3D organization of mESC colonies can be attributed to the strong cell-cell adhesion, as it is reported to induce tissue dewetting in other epithelial systems [194]. In this direction, the study by Ohtsuka and colleagues [195] suggests the gatekeeping of naïve pluripotency by E-cadherin. In this work, mEpiSCs, a stage corresponding to primed state, were induced with cadherin expression. This granted them the developmental potential of naïve state as cadherin high mEpiSCs successfully integrated into pre-implantation embryos and contributed to chimeras.

Reversion of mEpiSCs to naïve state without altering membrane tension might appear to be in direct contradiction to the works referred to earlier [189,190]. Since, E-cadherin localizes to membranes, viewing its role in this sub-cellular context will clear the air.

A key detail of E-cadherin expression in mESC naïve state is it being punctuated by β-catenin [135]. This physical association ensures β-catenin to be membrane sequestered, enabling it to activate RhoA with the downstream effect of Ezrin phosphorylation and high membrane cortex attachment. Therefore, the high membrane tension observed for each single cell might not be compromised and in fact be regained when existing as colonies. This could be one plausible explanation for mEpiSC reversion to naïve state in Ohtsuka S et al 2012 [195].

Hence, the compact dome morphology might be bestowed on the mESC colonies by the cooperative action of Ezrin mediated membrane cortex attachment of each cell, 3D-SAC and E-cadherin acting through β-catenin. Therefore, the actin cytoskeletal organization and E-cad – β-catenin complex are additional regulatory elements to be concentrated when dealing with naïve pluripotency dissolution in mESC colonies.

The studies mentioned so far focused exclusively on cell-intrinsic regulators of naïve state maintenance and its relinquishment, briefly dealing with the effect on extrinsic signal

reception. However, as has been pointed out, pluripotent epiblast is subjected to a wide range of mechanical cues during the peri-implantation period. These originate from both within the embryo and from the surrounding decidual tissue. The latter category of signals has been identified and the deterministic outcomes of the prominent ones on embryo development were mentioned in the first section. To briefly reiterate, the endometrium is receptive to implantation through smooth muscle generated contractile forces [31, 196], following which it houses embryo through luminal closure [32], eventually guiding the three axes of body plan to be aligned with the three symmetry axes of the uterus [30].

The intra-embryonic mechanical cues during embryonic development can be broadly divided into two categories (i) Osmosis driven hydrostatic forces (ii) Fluid flow based hydrodynamic forces and (iii) Insoluble molecules deposited as extra cellular matrix (ECM). The contributions of the first set of cues were described earlier citing the examples of lumen expansion driven segregation of EPI and PrE lineages, and luminal pressure build up coordinating post-implantation epiblast morphogenesis. The second genre of forces are more relevant during post-gastrulation stages of development [197] and even when they exist are only experienced nominally, as in when the embryo floats in the intraluminal fluid [30]. The third category deserves greater attention as the body of work encompassing both the *in vivo* and *in vitro* studies is slim with the understanding of matrix contributions to pluripotency regulation still being in the nascent stages. To better comprehend the literature review in this direction, revisiting the events of matrix deposition during early embryonic development would be of help.

1.3.3 The composition of extracellular matrix in early mouse embryo

The extra cellular matrix (ECM) is a structurally and compositionally complex network of glycosylated and non-glycosylated proteins, and polysaccharides [198]. Among the two major forms in which ECM exists [199], basement membrane (BM) is the most relevant to early embryonic development in mouse owing to its constituents. This flat laminar ECM organized into interconnected sheets is predominantly composed of Collagen IV and Laminin, the two proteins expressed in the embryo around implantation stages [200]. Between them, Collagen IV is apparently dispensable for early morphogenetic events as embryos were

reported to develop without any defect way past the gastrulation stages [201 - 203]. Whereas depletion of Laminin subunits compromised pre-gastrulation viability and displayed defects in the organization of TrE, EPI and PrE lineages. [204, 205]. Moreover, Laminin, specifically Laminin-111 (laminin chains alpha1, beta1, and gamma1), is involved in all the landmark developmental events ranging from its assistance in EPI specification [64] to EPI polarization post-implantation to initiate lumenogenesis [23,24] and finally in facilitating the migration of differentiation ready pluripotent cells [26]. In fact, in one of these studies, the necessity of adhesion to laminin as the cue for driving pluripotency exit was underscored when cells grown on laminin-free matrices such as agarose, maintained naïve state even in N2B27. Hence, when investigating the regulation of ECM on naïve pluripotency maintenance and/or dissolution, it is suggested to fabricate matrices with Laminin-111.

With this information, the seminal works aimed at delineating the matrix regulation of pluripotency along with their critical analysis are presented in the subsequent paragraphs.

1.3.4 Extrinsic regulation of *in vitro* pluripotency

The earliest work on the mechanical regulation of pluripotency in colonies was by Murray et al [229] where they investigated the effects of cell-matrix adhesion and cell spreading. The study was performed employing Ser+LIF media. Briefly, when mESCs spreading was restricted either by culturing on weakly adherent substrates or by the cytoskeletal manipulation through ROCK inhibitor (Y27632) treatment, higher expression of *Nanog* was maintained. Weak adhesion and low cell spreading was shown to functionally replace LIF for long term maintenance of mESC pluripotency in serum media. It must be pointed out that the adhesion strength was determined by the concentration of fetal bovine serum (FBS) adsorbed onto the culture dishes (2.5% for weak and 10% for strong). In addition to Laminin, FBS is comprised of Fibronectin, the ECM protein primarily restricted to TrE tissue and encountered by the pluripotent epiblast post implantation [207, 208]. Moreover, the experiments were performed with the colonies cultured on tissue culture plastic dishes, whose stiffness (Gigapascal range) is orders of magnitude higher than both the endometrium (between 0.1 to 0.7 MPa) [209, 210] and intact embryos (~0.2kPa to 0.6kPa) [211,212].

Substrate stiffness is an important mechanical parameter sensed by cells and has been shown in several studies to regulate differentiation fate and self-renewal in other stem cell systems [213,214]. The need for employing substrates of physiologically relevant stiffness, in case of ESCs, is made clear in the summary of two studies presented below.

In the work by Chowdhury and colleagues [215], soft substrates were shown to maintain, long-term, the undifferentiated status of mESCs when cultured in serum media alone. Nanog expression expected to be extinguished within 48 hours of LIF removal was maintained at high levels for 5 days and was comparable to LIF-provided cultures. The downregulation of cell-matrix interactions was found to be the causative factor. The second corresponds to the work by Labouesse and colleagues [112] where they reported high efficiency of reversion to naïve state on soft polyacrylamide gels compared to stiffer gels and tissue culture plastic for both mouse and human pluripotent cells. Incidentally, in both the studies the elastic modulus of the soft substrates was below 1kPa, falling in the range of pre-implantation embryo's and ESC stiffness [211, 212]. While these studies have furthered our understanding of stiffness mediated pluripotency regulation, they employed a different approach in terms of the choice of matrix protein. Chowdhury et al used Collagen IV which was found to be dispensable during pluripotent stages of embryonic development [201-203]. In Labouesse et al, cells adhered to the hydrogel through fibronectin, which is shown to be necessary for mESC self-renewal [167]. Therefore, fibronectin might also be contributing to reverting the primed state to naïve pluripotency and is not purely based on matrix stiffness. Moreover, mechano-responses have been reported to be specific to protein identity [216]. Therefore, the effect of laminin coating in combination with substrate stiffness needs to be investigated in mESC system.

The usage of polyacrylamide gels as a platform is worthy of short discussion. Various materials are employed in the hydrogel form to investigate the effects of ECM stiffness and subsequent cellular responses. Few examples include Collagen, Matrigel, Polyethylene glycol (PEG) and polyacrylamide (PAA) gels [217-220]. Among them PAA gels stand out due to their tunable stiffness, biocompatibility, resistance to cellular enzyme-based degradation, long-term stability and standardized protein functionalization techniques [220-226].

Cells gauge matrix mechanical properties through surface receptors that mediate adhesion. Among the ones at disposal, integrins' capability as mechano-sensors and -transducers is appreciated for the following reasons [227,228]:

1. Integrins host several adaptor proteins through which they physically engage with cytoskeletal elements such as Actin and Intermediate filaments. Through this association they are capable of transmitting forces to nuclear space and bring about epigenetic changes of gene regulation such as chromatin organization, transcription factor localization *etc*.
2. Since the adaptor proteins once activated initiate downstream molecular cascades, integrins function as biochemical signalling hubs which terminates in the nucleus with changes in transcriptional activity.
3. The confirmational state and thereby the functional activity of integrins and the adaptor proteins are influenced by the force experienced by these proteins. This translates to the modulation of downstream signalling both the activation status and intensity of signalling.

As it is evident that integrin centred mechanical signalling culminates with transcriptional signature changes, the molecular foundation of pluripotency state maintenance and transition, being acquainted with the knowledge on their function in mESC pluripotency is warranted. That, sensing laminin as the polarization and naïve state exit initiation cue is through integrin-based adhesion, adds weight to the above reasoning.

1.3.5 Molecular organization of integrin adhesions in mESCs

Integrin-based adhesions are organized into Nascent adhesion (NA), Focal complexes (FC) and Focal adhesion (FA). The nomenclature is based on length, lifetime, and the adaptor protein composition, and only FA score high on all three counts lending them the capability to drive signalling cascades. Such competent FAs are identified by the presence of four key adaptor proteins: Focal adhesion kinase (FAK), Paxillin, Vinculin and Zyxin.

FAK is a non-receptor tyrosine kinase and one of the earliest to engage with integrins, with Paxillin being the other. The exact sequence of events is yet to be clarified in mESCs, but

both Paxillin and FAK promote the membrane localization of the other. Through their scaffolding function coupled with enzymatic activity, FAK and Paxillin, recruit other adaptor proteins and set in motion biochemical signalling cascades. One example is the Rho-GTPase signalling-based actin monomer assembly into filamentous actin (F-actin), initiated by the active/phosphorylated form of Paxillin (pPaxillin). Besides, pPaxillin sequesters vinculin, which transmits forces by binding to actin. Upon force propagation, Zyxin mobilizes to actin filaments through its interaction with the actin polymerization factor VASP thereby reinforcing actin bundle thickness and further consolidates actin linkage to focal adhesions.

Besides the molecular composition, another key attribute of focal adhesion regulates its mechano-sensing and mechano-transduction function, and it is the spatial organization of the aforementioned four proteins. Competent focal adhesions are organized into the following three distinct layers (1) Integrin signalling layer in which FAK and Paxillin reside (2) Force transduction layer marked by Vinculin and (3) Actin regulatory layer identified by Zyxin. The vertical spacing should also allow for a minimum 50nm separation between the integrin signalling layer and proximal end of actin binding. This is measured by the distance between VASP and FAK proteins. This is to provide room for the necessary conformational changes and substrate binding of various proteins upon force application. Any disorganization would, therefore, compromise the efficient force transmission and subsequent signal transduction by FA.

A noteworthy offshoot effect of both FAK's and pPaxillin signalling is the initiation of ERK cascade. Although, such regulation was shown in other cell systems, the pathway being implicated in mESC pluripotency makes it relevant for FAK and pPaxillin to be looked into in the mESC context. Following suit with Vinculin and Zyxin has its merits as both the proteins associate with actin, the cytoskeletal element whose structural arrangement is shown to play critical role in mESC pluripotency.

1.3.6 Attenuated focal adhesion function in naïve mESCs

Minimal cell spreading, as seen in naïve mESCs, is ascribed to weak substrate interaction. Besides high membrane tension, another causative factor for this phenomenon could be the reduced focal adhesion strength and signalling, as has been attested by two studies mESCs.

The work by Taleahmad et al [229] compared integrin signalling in 2i-grown homogeneous naïve population and Serum+LIF-grown mixed cultures. Through shotgun proteomic approach, they reported lower FAK phosphorylation and subsequent signalling in 2i conditions compared to Serum+LIF conditions. To prove that these changes were adhesion driven and not a consequence of culturing media, when integrins were artificially stimulated through Mn^{2+}, increased focal adhesion signalling were observed eventually translating to reduced naïve transcription factor expression for cells maintained in 2i conditions.

These attenuated focal adhesion mechano-responses were found to be due to the alterations in protein conformation and the structural organization of 3 layers, as shown in work of Xia et al [230]. In this study performed with Serum+LIF media, through super resolution microscopy, it was found that the macromolecular arrays of mature focal adhesions are conserved in mESCs. However, the three hierarchical layers are compressed with separation between actin and integrin signalling plane reduced to ~30nm, significantly less than the 50nm threshold required for force transmission. Additionally, vinculin was observed to be aligned anti parallelly to actin filaments. This compressed nanodomain organization coupled with orientation changes of vinculin, presented in Figure.10, renders focal adhesions in active in terms of force relay and signalling initiation.

It must be pointed out that in the earlier study, the typical vinculin arrangement was observed only for cells maintained on Laminin substrates. When cultured on Fibronectin or Gelatin (denatured collagen), only the compression of three layers was observed. This further emphasizes that the choice of ECM protein is critical as it determines the basal levels of integrin activation thereby affecting the comparisons, when drawn between naïve and differentiated states.

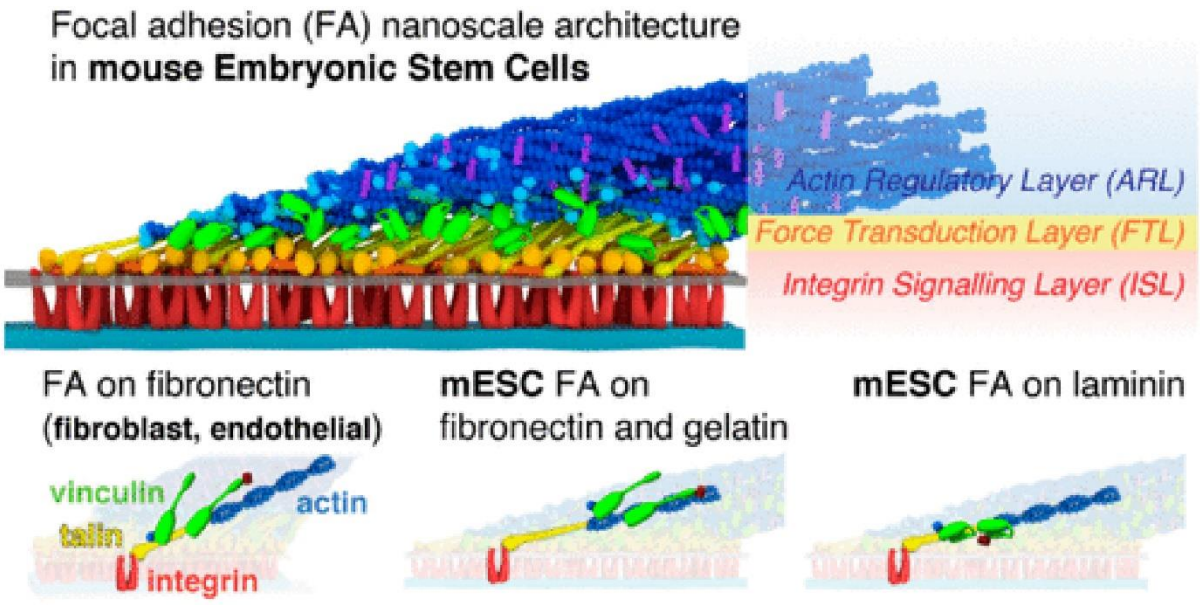

Figure.10: Schematic representation of various layers of integrin adhesions and the structurally compromised organization for mESCs. Picture adapted from Xia S *et al*., 2019 *Acs Biomater Engg*

There is a dearth of studies focusing on Paxillin expression levels and signalling activity in mESCs. Its requirement is however attested by the work of Wade R et al [231], which showed increased cell spreading and FAK activity in mESCs with forced expression of Paxillin. In the same study, knockout of Paxillin was shown to delay mESc spreading.

Finally, recent work from Zhang and colleagues [232] elucidated the molecular cause of reduced actin bundle reinforcement in naïve mESCs. Zyxin, the actin polymerization promoter, was found to be expressed in low levels in mESCs and, once subjected to differentiation, show a concomitant increase. Another molecular insight uncovered in this study is the negative regulation of Oct4 by Zyxin, highlighting the central role of focal adhesion-based mechanical signalling in pluripotency dissolution.

A well-characterized mechano-response involving integrin adhesions is the exertion of forces, termed traction forces, by the cells onto the underlying matrix. This is the coordinated result of actin fibre reinforcement and the contractile action of myosin motors driving actin rearward flow [233], occurring on integrin adhesion sites as anchorage points. They serve as a measure of cell-matrix interaction and with increasing traction forces, focal adhesions were shown to become more prominent in other cell systems.

Since the focal adhesions in mESCs are functionally incompetent, it is expected to reflect an exertion of low traction forces, as has been reported in Chowdhury et al. 2010 and Zhang S et al. 2023, studies referred to in an earlier [215, 232]. The maintenance of pluripotency is accompanied by low traction forces whereas pluripotency dissolution conditions displayed increased tractions. Once again it has to be pointed out that the traction force measurements in these studies were measured for single cells and correspond to discrete time points. Also, there is no report on the temporal profiles of traction forces in mESC pluripotency dissolution.

Apart from the actin-myosin contractile action, an alternative mode of mechanically stimulating integrins is through stretching the substrate to which cells adhere. Two studies employed this technique with mESCs. The first by Horiuchi R and colleagues [234] reported an attenuation in the decrease of *Nanog* when subjected to uniaxial cyclic stretching in LIF depleted conditions. In the second work by Verstreken C.M et al [235], although an initial increase of naïve pluripotency markers *Nanog*, *Klf4* and *Esrrb* was observed, at 6 hours post stretching with 2i removal, the changes were not statistically significant and the differences disappeared by 12 hours. Only when subjected to differentiation in serum media, an overall increase in pPaxillin and pERK levels with changes in nuclear aspect ratio, a morphological marker for nucleus under tensile stress, was reported. The authors hence concluded that, mESCs become mechanoresponsive only after naïve state exit. The commonality in both the studies is the higher *Nanog* expression upon stretching, while it was sustained in the first study, in the second it was acute. The inconsistencies in the results can be attributed to the following reasons (i) Use of different strain rates (10% in the first vs 35% in the second study), (ii) Different time periods for which stretching was performed (2 days in the first vs maximum of 12 hours for the second) and (iii) the use of different media.

Two key limitations exist for those works. The first is the use of PDMS as a substrate whose stiffness is in the megapascal range. Secondly, the experiments were conducted only after allowing the cells to spread. The transient phase between mESC attachment as rounded cells and initiation of cell spreading might be of regulatory importance to mechanical signalling and could not be addressed. Moreover, the differentiation protocol was performed in serum media, which adds further complexity to matrix mechano-sensing besides supplying a heterogeneous starting population.

Despite these shortcomings, the two studies have pointed in the next direction to focus on. The discussion has so far pertained to the region around the cell-matrix interface, be it the matrix, focal adhesions, E-cadherin, β-catenin and the cell cortex. As it has been reiterated several times, pluripotency state identity and transition are commissioned by the changes in transcriptional activity, which occurs in the nucleus. Therefore, for the mechanical signalling to influence transcriptional signature, the nuclear space has to be integrated into the force relay. The increase in nuclear aspect ratio upon stretching reported in Verstreken C.M et al [235] confirms the incorporation of nucleus into mechano-transduction events in mESCs.

On that account, outlining the characteristic traits of nucleus and the changes associated with force transmission is necessary to better evaluate our current understanding of mechanical regulation of naïve pluripotency and its dissolution. This is tackled in the next section following the digest of this section.

Section summary

- Installing, conserving, and terminating pluripotency are instructed by mechanical cues.
- Naïve mESCs have high membrane tension due to strong membrane-cortex tethering.
- Naïve mESCs have inward curving short actin filaments.
- Cell spreading driven by decrease in membrane tension is obligatory for naïve state exit.
- Upon differentiation, mESCs present reinforced actin fibres.
- Naïve mESC colonies grow as compact domes due to 3D-SAC and cadherin expression.
- Compressive forces borne out of dome shape promote *Oct4*, *Nanog* expression.
- Naïve state exit is initiated *in vivo* by integrin-based laminin mechano-sensing.
- Substrate stiffness determines pluripotency status *in vitro*.
- PAA gels are best suited to subject mESCs to physiologically relevant stiffnesses.
- Focal adhesion mechano-chemical functions are attenuated in naïve mESCs.
- mESC nucleus is integrated into the mechanical signalling relay.

Section 4: Mechanobiology of mESC nucleus

Nucleus, the organelle that houses the genome, is the terminus for all transcriptional activity. Given that the protein demographic changes in this subcellular region is on what state transition hinges upon, the importance of reviewing nucleus, specifically in the context of mechanical signalling in pluripotency cannot be overstated. Before moving that direction, a cautionary note. As mentioned earlier, a multitude of changes ranging from transcriptional rewiring, epigenetic landscape remodelling and chromatin organization occur in the nuclear space during pluripotency exit. Rather than being lost in that microcosm heeding to these details, the subsequent discussion considers nucleus as a single entity and first deals with the characteristic differences of naïve and primed nuclei. Later the focus is shifted onto the tractable changes, occurring between distinct states of pluripotency, in nuclear morphology and in the constituents of peri-nuclear space. A mere mention of the factors driving those changes is done. Like in earlier sections, as and when necessary, knowledge from other systems is solicited for comparison.

A striking feature of naïve mESCs is the high nuclear occupancy [94], which is attributed to the genomic confirmation. mESCs require both the pluripotency and differentiation genes to be at transcriptional disposal, the former for naïve maintenance and the latter to execute differentiation program upon induction. To facilitate this, the naïve genome is markedly hypomethylated [236]. Among the annotations present, rather than employing constitutive repression markers such as histone trimethylation at lysine 9, mESCs chromatin is deposited with facultative repressors like trimethylation at lysine 27 [237]. These modifications make naïve state chromatin more open [238, 239] thus requiring larger space to be accommodated. The peculiar actin organization further exaggerates the relative nuclear to cytoplasmic volume, as the cytoskeletal element is concentrated in and around the cell cortex.

In the primed state, due to the large-scale shutdown of pluripotency genes and due to their predisposition to a specific lineage, a significantly smaller portion of the genome exists in open chromatin confirmation. This is confirmed by the reports stating increased promoter hypermethylation and rearrangement of enhancer chromatin in EpiSCs [240, 241]. This, coupled with the reorganization of the actin cytoskeleton into radially oriented bundles, manifests as a lower nuclear to cytoplasmic volumetric ratio.

Such actin fibre alignment serves another key function in mechano-transduction. Their physical linkage to the nucleus mediates force transmission and brings about morphological changes both global and localized. The increase in nuclear aspect ratio upon stretching, discussed in the earlier sub-sectuibs is an example of large-scale nuclear shape change. The localized changes are observed in cells in the formative state, and it is the reduced corrugation with the nuclear membrane becoming taut [242]. This is in contrast to the higher wrinkling frequency observed in naïve and primed nuclei in the same work.

Interestingly the nuclear perimeter remains conserved between naïve and transitioning nuclei but increased in primed counterparts. In the same work, the transition nuclei were shown to exhibit an interesting material property termed auxeticity. Unlike elastic materials, which increase cross sectional area upon compression, auxetic materials show an area reduction along with stiffening [243]. The auxetic nature of transition nuclei was shown to be driven in part by chromatin decondensation that accompanies naive state exit [242].

The nuclear wrinkles in general correspond to regions bound to heterochromatin [244]. This arrangement ensures that euchromatin is localized either to the nuclear interior or close to nuclear pores, the channel through which transcription factors reach the nuclear region, thereby making euchromatin readily available for genetic information flow. This offers another explanation for the taut nuclear structure in transition cells and, nuclear ridges in naïve and primed cells. As transitioning cells need to have the coding regions of both formative genes and lineage specific genes open, there is less heterochromatin and thus less wrinkles. Once the cells proceed to primed state, due to their predisposition to one of three lineages, the regions corresponding to other two fates are condensed, in addition to the formative genes. This explains the increase in corrugations in primed state.

The nuclear boundary is a double-layered lipid membrane, and the binding of heterochromatin occurs on the interior side (Figure.11). It is mediated by a family of proteins named Lamins which also function to provide structural integrity thereby determining nuclear size, shape, and stiffness [245]. It has two subtypes, Lamin-A/C and Lamin-B [246]. Additionally, Lamins interact with the transmembrane SUN domain proteins, which are components of the linker of nucleo- and cytoskeleton (LINC) complexes [247]. The cytoplasmic component of LINC complex is the KASH domain proteins and binds to the cytoskeletal elements such as filamentous actin (F-actin) [248].

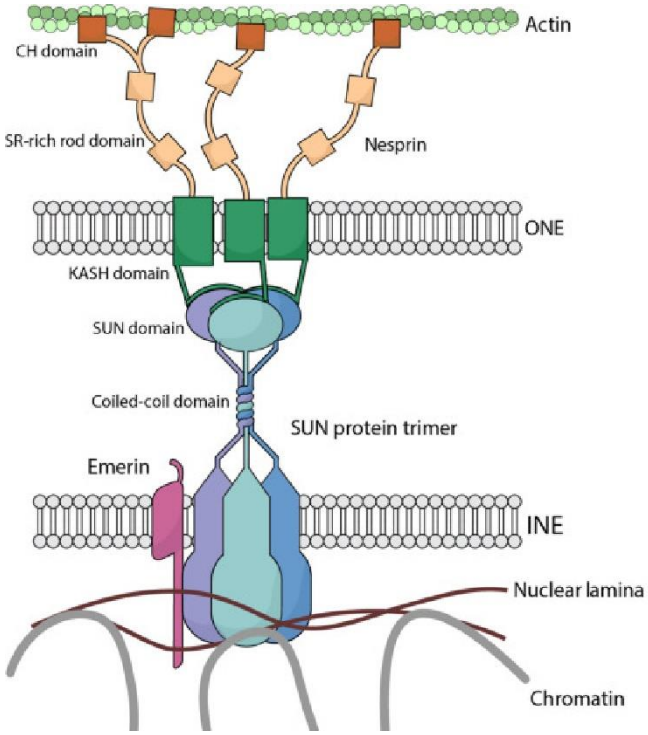

Figure.11: Schematic representation of the molecular organization around the peri-nuclear space. Picture adapted from Li EW, McKee-Muir OC and Gilbert PG *et al*., Chapter 4 – Myogenesis in Development and Disease, 2018 *Curr Top Dev Biol*.

LINC complex association with F-actin ensures the forces generated at integrin adhesion sites are transmitted to nuclear periphery. By anchoring LINC complexes to the nucleus, Lamins ensure the forces are translated to conformational changes in the genome, driving gene expression changes.

By forming a regulatory axis for mechano-transduction, LINC complexes and Lamins are adept at bringing about transcriptional changes, the molecular foundations for pluripotency dissolution. This merits the review of their role in mESCs. However, studies in this direction have been far and few, yielding conflicting results. Therefore, the following susections could be considered a compendium of works about Lamins and LINC complex in mESCs.

In the work of Khatau SB et al [249], Lamin depletion was shown to delay the differentiation onset in mESCs. It was found that the timing of differentiation commitment is signified by the formation of perinuclear actin cap on the apical side of the cell. Although not shown in mouse model, the positioning and stabilization of perinuclear actin cap was found to be dependent on LINC complex organization. In another study, Lamins were reported to determine the lineage outcome of mESC differentiation, with cells dedicated to visceral

endoderm upon Lamin depletion and fated to neuronal lineages in wildtype background [250]. This study also posited the dispensability of Lamins for pluripotency maintenance as Lamin haplo-insufficient cells didn't present significant differences in the expression levels of core pluripotency factors and Rex1. For both these works, the starting population was obtained from Serum+LIF cultures and the differentiation protocol was based on 3D embryoid body formation.

However, in the study Kim Y et al [251], lamins were deemed dispensable for murine pluripotency as the self-renewal and differentiation potential was found to be not compromised in a mESC cell line depleted of all lamin subtypes. More recent work from Wang and colleagues [252] reported the contrary as lamin A/C depletion was found to alter the chromatin organization and, as a result, the expression heterogeneity in *Oct4* expression along with the colonies growing with flat morphology. Furthermore, lamin A/C deficiency was observed to prime mESCs for cardiac mesoderm fate. Both these studies were performed on fibroblast feeders and in Serum+LIF media.

The usage of suboptimal media and differentiation protocol are major limitations of the four studies mentioned above. This along with the factual inconsistencies make the role of lamins in mESC pluripotency, yet to be clearly established.

Only two studies have been performed on the role of LINC complex with murine pluripotency and both focused on the regulation of differentiation. The first one by Smith ER and colleagues [253] played with the levels of the KASH domain protein Nesprin-1 and reported an increase in the propensity of mESC differentiation. Moreover, electron microscopy measurements suggested the undifferentiated mESC nucleus to be wider. The earlier mentioned nuclear wrinkling was attributed to low expression of Nesprin-1 as its increased expression in the differentiated cells yielded less frequency of irregularities. Additional observation includes the lack of apparent change in nuclear pore density. In the other study, David BG et al [254], mESC line with dominant negative KASH (DN-KASH), impaired in actin binding, was generated. Because of the abrogation of actin cytoskeletal anchorage to nuclear membrane, high expression levels of the pluripotency factors were maintained even in differentiated conditions. Other notable result, observed only for the cells differentiated on glass surfaces, is the formation of prominent actin stress fibres with their

ends highlighted by the focal adhesion protein Talin for cells. Like in earlier studies, these works were performed with Serum+LIF media.

Another significant consequence of force application to nucleus, as shown in the seminal works by Pere Roca-Cusachs' group, is the widening of nuclear pores, which affects the shuttling kinetics of transcription factors and, thereby, their subcellular localization [255, 256]. Due to this property, they are referred to as mechanosensitive proteins and one of the classical examples is YAP. That DN-KASH impairs YAP nuclear sequestration further underscores the mechano-regulation of YAP intracellular transport [256].

The relevance of YAP to murine pluripotency is already recognized in earlier discussion as it is the effector protein to translate positional cues and segregate ICM, the founder population for pluripotent epiblast. Importantly, YAP's role, albeit in other cell systems, in regulating proliferation, organ size and differentiation is well documented [257, 258]. These three factors influencing pluripotency progression *in vivo* present a valid argument to be informed on the function of YAP in mESCs. Like in the case of Lamins and LINC complex, the body of work on YAP in murine pluripotency primarily dealt with the effect on differentiation and the key ones are discussed next.

In Chung et al, YAP was reported to be an obligatory factor for permitting mESC differentiation but is dispensable for self-renewal [259]. Neither YAP's transcriptional co-activator TEAD nor its homologue Taz were found to compensate the loss of differentiation incurred with YAP depletion. Their role is similarly dispensable like YAP when it comes to self-renewal. Importantly, differentiation induction is accompanied by nuclear sequestration of YAP. Antithetical to this work, Tamm C et al [260] showed the absolute necessity of YAP to drive proliferation in serum media as LIF based self-renewal is observed to operate through YAP-TEAD pathway. Completing the contradiction, YAP-TEAD were reported to be downregulated upon differentiation induction. Both these studies are performed with serum media and employed shRNA-based YAP downregulation. One explanation to accommodate these discrepancies is that the studies used cell lines derived from different strains.

The recent work by Meyer and colleagues [261] cleared the confusion on the role of YAP in murine pluripotency. Employing optogenetic control of YAP subcellular localization, this study reports that the decision making between self-renewal and differentiation is

determined by both YAP concentration and pulsing frequency. The three important conclusions of this investigation are: (i) In naïve state, YAP induces *Oct4* and *Nanog* expression and displays steady state nuclear expression with low frequency of pulsing. (ii) Upon differentiation induction, the pulsing frequency of YAP increases and both *Oct4*, *Nanog* are repressed but with different IC50 levels. (iii) Finally, in the intermediate regime where *Nanog* is repressed but *Oct4* is maintained, differentiation lineage is specified by YAP dose with low levels inducing mesoderm. Another technically impressive result is the real time demonstration of transcriptional burst at Oct4 promoter, during differentiation, in response to YAP knockout. This work presented the case for YAP to be incorporated into the pluripotency transcriptional logic and is merited by the choice of media used: 2i+LIF. It has however only focused on single cells and insights into mESC colonies is lacking. Moreover, the comparison of naïve state YAP dynamics with differentiated state does not necessarily inform if and to what extent changes occur during naïve to primed state transition.

A certain degree of cell death is a normal occurrence when mESCs are subjected to differentiation. This is owed to the *Myc* based competitive elimination of early differentiating cells and serves to synchronize pluripotency exit both *in vitro* and *in vivo* [262]. YAP's involvement in regulating such programmed cell death was revealed by Leblanc L et al [263]. In this work, YAP through its activation of anti-apoptotic genes was found to augment the survival of differentiating cells further corroborating YAP's requirement in ensuring successful differentiation.

With this background knowledge, we are thoroughly informed on the current understanding of mechanical regulation of murine pluripotency. More importantly, the knowledge gaps that need attention have been alluded to. Of them, identifying the critical ones which form the basis of the current research will be performed in the next section. Before moving onto those, a concise synopsis of this section lies below.

Section summary

- Nuclear morphology serves as a yardstick for intracellular force relay.
- Force transmission to nucleus changes chromatin organization.
- Nucleus integration into mechano-transduction is mediated by Lamin and LINC complex.
- The influence of Lamins on murine pluripotency is yet to be clearly established.
- Compromised LINC complex function, attenuates force relay and preserves pluripotency.
- Force application drives nuclear sequestration of YAP.
- YAP dynamics and not just absolute levels dictate if mESCs divide or differentiate.
- Upon differentiation induction, YAP downregulates *Oct4* and *Nanog*.
- YAP improves the survival fitness of differentiating mESCs.

Chapter 2: Objectives of the study

Pluripotency progression beginning with naïve state exit is a dynamic process characterized by sequential molecular, morphological, and mechanical changes, driven *in vivo* by integrin-based laminin sensing. More importantly, although naïve identity is the property of each pre-implantation epiblast cell, naïve state exit occurs in a collective and synchronized fashion to match both morphological and developmental demands. The inability to study this short-lived phenomenon within the embryonic context was overcame through the establishment of pluripotent cell lines, fabrication of defined culture media and standardization of protocols. With this fillip, in the last decade, our understanding on the mechanical regulation of pluripotency, in both single cells and colonies, has taken giant strides. Despite the burgeoning growth, the field is yet to address the inadequacies and in some case the inconsistencies of the existing knowledge. In the last two sections of chapter.1, every discussion on a seminal study is followed by a footnote pointing out such knowledge gaps. Among those, a compilation of the significant ones that lay the premise for this thesis work is provided below, followed by the outlining of the current study's precise objectives.

- Earlier studies either cultured cells on plastic/glass surfaces or on hydrogels functionalized with collagen or fibronectin. A PAA gel substrate offering laminin as the sole matrix adhesion molecule and its compatibility to perform long term experiments was not tested.
- Distinct pluripotent states are annotated by specific transcription factor expression. The temporal changes in their levels are based on population-level statistics, data obtained from averaging several colonies. Whether individual colonies recapitulate those variations is unknown.
- Among the mechano-responses listed earlier, the ones involving cell-matrix interaction such as traction forces were only measured at distinct time points. Their evolution with pluripotency progression, and whether they execute a regulatory function on pluripotency dissolution is not known.
- There is no report on how the pluripotency dissolution dynamics is affected when mechano-transduction along the integrin-actin-nucleus axis is interfered with.
- Morphometric measurements serve as a proxy for the extent of force relayed to nucleus, which in turn influences transcription factor localization. However, the relationship between nuclear shapes, transcription factor localization and expression, and pluripotency dissolution is not established.

- Mechanically, mESCs require membrane tension decrease, promoted by GSK3β's inhibition of β-catenin, to initiate naïve state exit. Transcriptionally, the event to begin naïve identity loss, in single cells, is the ERK mediated degradation of Klf4 transcription factor. Which among the two events is obligatory for pluripotency dissolution, that too in colonies, thereby pointing out the dominant regulator for long-term pluripotency maintenance, is yet to be elucidated.

To answer these questions, the aim of this thesis is to study the role of cell-matrix force transmission in naïve to primed pluripotency transition in mouse embryonic stem cells.

To this end, this study employed the well characterized Rex1::GFPd2 cell line in which pluripotency dissolution is synonymous with gradual loss of fluorescence signal. Given this main objective, the specific aims of this study are as follows.

Aims of the study:

1. To fabricate a laminin coated PAA gel substrate that is compatible with simultaneously measuring mechano-responses while performing long-term differentiation protocol.
2. To validate the system through transcriptional expression profiles of bonafide markers and test if the patterns recapitulate those reported in both *in vitro* and *in vivo* studies.
3. To measure and thereby track the evolution of cell-matrix interaction during the course of pluripotency dissolution/Rex1-GFP fluorescence decay. The mechano-responses of interest are categorized into those measured at discrete time points such as focal adhesion, actin organization, and those monitored continuously as in traction forces.
4. To interfere with mechano-transduction and observe the effect on the temporal progression of Rex1-GFP signal.
5. To perform morphometric analysis of nucleus at discrete time points and test the correlation between nuclear shape and the expression levels of various pluripotency factors and the well-known mechano-transducer YAP.
6. To identify which among the mechanical and molecular triggers of naïve state exit function as the gatekeeper for long-term pluripotency maintenance.
7. To evaluate if mechano-responses are capable of forecasting pluripotency status *in vitro*.

Chapter 3: Methods and Materials

3.1 Media preparation

N2B27 defined basal medium contained 1:1 Neurobasal and DMEM/F-12 medium (Sigma-Aldrich D6421), Neurobasal medium (Life technologies 21103-049), 2.2 mM L-Glutamine (Thermo Fisher – 25030081), 0.5x B27 (Invitrogen – 17504044), 50 mM β-Mercaptoethanol (Thermo Fisher - 31350010), 12.5 $ng.mL^{-1}$ Insulin zinc (Sigma-Aldrich I9278), 0.1% Sodium bicarbonate (volume/volume) (Thermo Fisher – 25080094) and 0.5% N2 (volume/volume). N2 was prepared in-house with the composition given below.

200x N2 was made using 8.791 $mg.mL^{-1}$ Apotransferrin (Sigma-Aldrich T1147), 1.688 $mg.mL^{-1}$ Putrescine (Sigma-Aldrich P5780-5G), 3 µM Sodium Selenite (Sigma-Aldrich S5261), and 2.08 $µg.mL^{-1}$ Progesterone (Sigma-Aldrich P8783-1G). All the above components were dissolved in DMEM/F-12 (Sigma-Aldrich D6421). Fresh batch of N2 was prepared every 6 months and was batch tested as mentioned in Mulas *et al*., 2019 *Development* [79].

Chiron (Sigma-Aldrich SML1046) and PD0325901 (Sigma-Aldrich PZ0162) are the two small molecule inhibitors purchased as lyophilized powders and stored at -20^0C as 10mM aliquots in 100% DMSO (Sigma-Aldrich, cat. no. D8418). Both the inhibitors were added to N2B27 base media to have a final concentration of 3 µM for Chiron and 1 µM for PD0325901. Throughout this thesis, the N2B27 media with 2 inhibitors (N2B27+2i) is referred to as '2i'. This media mixture was stored at 4^0C and was used within one week.

For the retroviral transfection protocol, cells were cultured in Serum media supplemented with LIF (Millipore, cat.no. ESF1106) at 1000 units/ml. The composition of Serum media is as follows: Glasgow Eagle's Minimal Essential Medium (Sigma Aldrich, cat.no. G5154) 10% Foetal bovine serum (), L-glutamine, 1% v/v non-essential amino acids (Sigma Aldrich, cat.no. M7145), 1% v/v sodium pyruvate (ThermoFisher cat.no. 21103049) and 10 mM β-mercaptoethanol (Gibco, cat.no. 31350-010)

3.2 Cell culture

Rex1-GFP mESCs were cultured in accordance with Mulas *et al*., 2019 *Development*. The passaging protocol was performed once every two days and is as follows.

Cells were treated with accutase for 5 minutes at room temperature followed by neutralization using 8 times its volume with BSA fraction V (1.5% v/v in DMEM/F-12). Cell density was estimated using Neubauer chamber and is given by the formula,

$$Cell\ density = average\ cell\ count\ X\ 10^4 cells/ml$$

Based on the obtained cell density, the volume required for seeding cells at 15,000 cells.cm^{-2} was procured and the cell suspension was centrifuged for 3.5 minutes at 0.4 rcf at room temperature. The supernatant was vacuum aspirated, and the pellet was resuspended in 2i media with thorough mixing, later proceeding to plate on Nunc plates coated with Laminin-111 at 10µg/ml (in 1X-sterile PBS) for a minimum of 2 hours at 37^0 C. For the passage before the use of cells for experiment, cells were cultured only in 2i without LIF.

3.3 Cells cryopreservation

Before cryopreservation, cells were grown for 2 days in 2i media supplemented with LIF. The cell passaging protocol was performed as described with the following change. Upon vacuum aspirating the accutase neutralizing serum media, the pellet was resuspended in 2i media with 10% FBS (volume/volume) to obtain a cell density of 10^6 cells/ml. This cell suspension was mixed with DMSO (10% volume/volume in the final solution) and aliquoted into cryotubes which were frozen overnight at -80^0 C in an isopropanol bath (Mr. Frosty). On the next day, the cryotubes were placed in liquid nitrogen for long term storage.

3.4 Cell transfection

Retroviral particles for the generation of DN-KASH and Delta-PP lines were generated in HEK293T cells expressing retroviral packaging plasmids (gift from N. Montserrat) and transfected using Lipofectamine™ 3000 Transfection Reagent (Invitrogen). Two days post the transfection, the viral titer was collected from HEK293T cultures and was used to infect overnight the Rex1-GFP mESCs cultured in Serum+LIF for a day. After the overnight infection, the media with viral titer was replaced the next day to Serum+LIF and the mESC

cultures were grown to 80% confluency. The cultures were later expanded for cryopreservation and selection.

3.5 Selection of transfected cell lines

To select for the cells with stable integration of viral DNA into the genome, the culture was subjected to treatment of 400 µg/ml of Geneticin (Fischer scientific, cat.no. 10204773) after a day of growth in 2i+LIF. The Geneticin treatment was performed for 6 days with cells passaged once every 3 days. Throughout the selection protocol, cultures were maintained in 2i+LIF media without any cells being discarded while passaging. On the 7th day, the cultures were used for cryopreservation and selection for doxycycline-based induction.

To select the cells with high inducible expression of DN-KASH or DelPP with the mCherry fluorescent tag, cultures were grown for two days in 2i+LIF media with a treatment of 1µg/ml doxycycline (Sigma Aldrich, cat.no. D9891) for last 16 hours (overnight treatment). Following the cell passage protocol, a cell suspension was obtained and was subjected to fluorescence assisted cells sorting (FACS) selecting for cells with high Rex1-GFP and DN-KASH/DelPP-mCherry fluorescence levels. The FACS sorted cells were expanded by culturing in Serum+LIF for 3 days and were later cryopreserved.

3.6 Preparation of polyacrylamide gels for sulfo-SANPAH or NHS-Irgacure functionalization

Polyacrylamide gels were prepared as described previously [Perez-Gonzalez C *et al*., 2019 *Nat Phys*]. Cover glasses of No.1 thickness (Superior Marienfeld) were used as top coverslips and were treated with 20% v/v Surfasil (Fischer Scientific, cat.no. 11541094) in Chloroform for 2 hours at room temperature followed by quick wash with 100% methanol and air-drying. Glass bottom MatTek dishes (No.0) were activated with a solution of acetic acid (Sigma Aldrich, cat.no. A6283), 3-(Trimethoxysilyl) propyl methacrylate (Sigma Aldrich, cat.no. M6154), and 96% ethanol (1:1:14 in volume ratio) for 20 min at room temperature. The dishes were then quickly washed twice with 96% ethanol and air-dried. Different concentrations of acrylamide and bis-acrylamide were mixed to produce gels of different rigidity and mixed with fluorescent carboxylated 200 nm beads (Invitrogen), Ammonium persulfate APS (Sigma-Aldrich A3678), and tetramethylethylenedi-amine (Sigma-Aldrich T9281). The composition of hydrogel mix corresponding to different stiffness is given in

Table.4. The solution was placed on the silanized glass surface and covered with surfasil treated coverslip, letting the gel to polymerize for 50 minutes. The coverslip was then removed, and gels were washed twice with 1X-PBS and stored in 1X-PBS until functionalization.

For immunofluorescence samples, non-fluorescent carboxylated latex beads were used during gel preparation at a volumetric composition of 0.0125%. The remaining volume was replaced with 1x-PBS.

Stiffness	Acrylamide	Bis-acrylamide	Beads	APS	TEMED
1.5 kPa	5 %(w/v)	0.04 %(w/v)	0.04 %(v/v)	0.05 %(v/v)	0.05 %(v/v)
5 kPa	7.46 %(w/v)	0.044 %(w/v)	0.04 %(v/v)	0.05 %(v/v)	0.05 %(v/v)
15 kPa	7.5 %(w/v)	0.16 %(w/v)	0.04 %(v/v)	0.05 %(v/v)	0.05 %(v/v)

Table.4 Polyacrylamide gel composition for sulfo-SANPAH based protein functionalization. A 500 µl solution in 1x-PBS with the specified proportions of the different components was prepared. The reagents used were Acrylamide (BioRad cat.no. 1610140), Bis-acrylamide (BioRad, cat. No. 1610142), 0.2µm carboxylate modified polystyrene beads, Ammonium persulfate (APS, Sigma, cat.no. A3678, stock prepared at 10% in ultrapure water) and Tetramethylethylenediamine (TEMED, Sigma cat. no. T9281).

3.7 sulfo-SANPAH based polyacrylamide gel functionalization

Polymerized gels were coated with Sulfo-SANPAH (Invitrogen, cat. no. 22589) by applying 2mg/ml solution in ultrapure water and irradiated for 7.5 minutes with ultraviolet light (365 nm) (Blak Ray XX-15L UV bench lamp). Following the UV exposure, gels were washed twice with 10mM HEPES (Gibco, cat. no. H0887) and one wash with 1X-PBS in sterile conditions under cell culture hood. Finally, gels were incubated overnight at 4° C with 100µg/ml Laminin-2020 (Sigma-Aldrich, cat.no.114956-81-9) in 1X-PBS.

3.8 NHS-Irgacure based polyacrylamide gel functionalization

A mixture of 50 mM HEPES, 0.002 % (w/v) Bis-acrylamide, 0.05 % (w/v) Irgacure (Advanced Biomatrix, cat.no. 5200) and 0.2 mg/ml N-hydroxysuccinimide acrylate (Sigma Aldrich, cat.no. A8060) was prepared in ultrapure water. After vacuum aspiration of PBS, this solution is applied to the surface of polymerized gels and irradiated for 5 minutes with ultraviolet light (365 nm) (Blak Ray XX-15L UV bench lamp). Following the UV exposure, gels were washed once for 5 minutes with 0.25 M HEPES at pH 6.0 (Gibco, cat. no. H0887) and followed by one wash for 5 minutes with 1X-PBS in sterile conditions under cell culture

hood. Finally, gels were incubated overnight at 4° C with 100µg/ml Laminin-2020 (Sigma-Aldrich, cat.no.114956-81-9) in 1X-PBS.

3.9 StemBond hydrogel preparation and functionalization

Polyacrylamide gels were prepared as described previously [Labouesse, C., Tan, B.X., Agley, C.C. *et al*., 2021 *Nat Comm*]. Cover glasses of No.1 thickness (Superior Marienfeld) were used as top coverslips and were treated with 20% v/v Surfasil (Fischer Scientific, cat.no. 11541094) in Chloroform for 2 hours at room temperature followed by quick wash with 100% methanol and air-drying. Glass bottom MatTek dishes (No.0) were activated with a solution of acetic acid (Sigma Aldrich, cat.no. A6283), 3-(Trimethoxysilyl) propyl methacrylate (Sigma Aldrich, cat.no. M6154), and 96% ethanol (1:1:14 in volume ratio) for 20 min at room temperature. The dishes were then quickly washed twice with 96% ethanol and air-dried. Different concentrations of acrylamide, bis-acrylamide and 2-(prop-2-enoylamino) hexanoic acid) (6-AHA) were mixed to produce gels of different rigidity and mixed with fluorescent carboxylated 200 nm beads (Invitrogen), Ammonium persulfate APS (Sigma-Aldrich A3678), and tetramethylethylenedi-amine (Sigma-Aldrich T9281). The composition of hydrogel mix corresponding to different stiffness is given in Table.5. The solution was placed on the silanized glass surface and covered with surfasil treated coverslip, letting the gel to polymerize for 15 minutes at room temperature. The coverslip was then removed, and gels were washed twice with 100% methanol (Honeywell Research Chemicals, cat.no. 32213) and stored in 1X-PBS until functionalization.

Stiffness	Acrylamide	Bis-acrylamide	6-AHA	APS	TEMED
0.75 kPa	2.55 %(w/v)	0.11 %(w/v)	0.048 M	0.1 %(w/v)	0.5 %(w/v)
160 kPa	15.99 %(w/v)	0.6 %(w/v)	0.048 M	0.1 %(w/v)	0.5 %(w/v)

Table.5 Polyacrylamide gel composition in volume/volume proportions. A 500 µl solution in ultrapure water with the specified proportions of the different components was prepared. The reagents used were Acrylamide (BioRad cat.no. 1610140), Bis-acrylamide (BioRad, cat. No. 1610142), 2-(prop-2-enoylamino) hexanoic acid) 6-AHA (Tokoy Chemical, cat.no. A1896), Ammonium persulfate (APS, Sigma, cat.no. A3678, stock prepared at 10% in ultrapure water) and Tetramethylethylenediamine (TEMED, Sigma cat. no. T9281).

Polymerized hydrogels were quickly washed twice quickly with 1X-PBS followed by activation for 30-minutes with MES buffer (pH 6.1) containing 0.2 M EDAC-HCl (1-Ethyl-3-(3′-dimethylaminopropyl) carbodiimide, HCl) and 0.5 M NHS-acrylate (N-

hydroxysuccinimide acrylate) (Sigma Aldrich, cat.no. A8060). Post activation, the gels are rinsed twice quickly with ice-cold 60% methanol (v/v in 1X-PBS) followed by a quick wash with 50 mM HEPES (pH 8.5). Finally, gels were incubated overnight at 4° C with 100µg/ml Laminin-2020 (Sigma-Aldrich, cat.no.114956-81-9) in 50 mM HEPES (pH 8.5).

After protein coating, gels were blocked with freshly prepared 0.5 M ethanolamine (Sigma Aldrich, cat.no. 411000) in 50 mM HEPES (pH 8.5) under sterile conditions followed by two quick washes with 50 mM HEPES (pH 8.5) and one wash with 1X-PBS. Gels are stored in 1X-PBS until use.

3.10 PDMS preparation

Dowsil CY52-276 part-A and –B were vigourously mixed, at 4°C, in required weight ratios (1:1 for 3kPa and 9:10 for 12kPa). The mixture was degassed in vacuum chamber for at least 20 minutes while being maintained in ice. 100-120 µl of this degassed mixture was applied on 35mm glass bottom mattek dishes (No.0) and spun for 90 seconds with an acceleration of 100 and maximum rotational speed of 400 rpm. The spin coated PDMS substrates were cured overnight at 65°C.

3.11 Bead incorporation and functionalization of PDMS

Cured PDMS was treated for 3 minutes at room temperature with 5% v/v APTES (3-aminopropyltriethosiloxane) diluted in absolute ethanol. This surface etched PDMS was rinsed 3 times with absolute ethanol with 1-2 minute wait between each wash followed by a one-time rinse with ultrapure water. Then, the PDMS surface was incubated for 10 minutes at room temperature with 0.2µm carboxylate modified fluorescent polystyrene beads diluted in Borate buffer. To prevent aggregation, beads were sonicated prior to dilution and filtered through 0.45µm sterile filter. Finally, the PDMS substrates were washed 3 times (quickly) with ultrapure water and stored in the same at 4°C until used.

Beads incorporated PDMS plates were UV sterilized in cell culture hood followed by a quick wash with 1X-PBS solution. After vacuum aspirating PBS buffer, PDMS substrates were coated with 10 µg/ml of Laminin-2020 (Sigma-Aldrich, cat.no.114956-81-9), in 1X-PBS, for at least 1 hour at 37°C.

3.12 Experimental sample preparation

The protein-coated gels were sterilized with 15 min UV treatment at room temperature and equilibrated with 2i media at 37°C for 30 minutes. mESCs were seeded as single cells at 12 x 10^3 cells.cm^{-2} and grown for 2 days.

For timelapse microscopy, immediately before the start of acquisition, the samples were quickly washed with N2B27 media and changed to required media as per experimental condition in volumes that could be sustained for 48hr-60hr of imaging. All these steps were performed under sterile conditions in cell culture hood.

For immunofluorescence samples, the samples were quickly washed with N2B27 media and changed to required media as per experimental condition and was replenished every day. All these steps were performed under sterile conditions in cell culture hood.

For experiments pertaining to naïve state exit on glass substrates, glass bottom mattek dishes (No.0) were used and coated with 10µg/ml Laminin-111 (Sigma-Aldrich L2020) in 1X-PBS for 2 hours at 37°C. Upon protein coating, the surfaces were sterilized with 15 min UV treatment at room temperature following which mESCs were seeded as single cells at 12 x 10^3 cells.cm^{-2} and grown for 2 days.

For experiments involving DN-KASH and DelPP cell lines, treatment condition for each genotype was provided with 1µg/ml of doxycycline in N2B27 media from the start of experiment. For control conditions, equivalent proportion of sterile ultrapure water was added to the media.

3.13 Immunofluorescence

Cells were fixed with 4% formaldehyde for 10 minutes at room temperature followed by 3 washes with 1X PBS. Cells were then permeabilized with 0.1% Triton-X (in PBS) for 20 minutes followed by a 10-minute wash with 2% w/v BSA (in PBS). Blocking was performed with 2% w/v BSA + 2% v/v FBS in 1X-PBS for 30 minutes at room temperature. Cells were then incubated overnight at 4°C with the primary antibody. Secondary antibodies and Phalloidin-atto 488 (Sigma-Aldrich, Cat# 49409, when used) were added for 2 hours at dilutions 1:300 and 1:1000, respectively. Hoechst was used to label nuclei at 1:5000 concentration for 20 minutes at room temperature in blocking buffer. Finally, cells were

washed with blocking buffer 4 times (1-quick and three 10 minute) and stored in 1X/PBS. All the samples were imaged the following day.

The primary antibodies used, and their respective dilutions are: Rabbit Phospho-Paxillin 1:100 (Tyr118) (Cell Signaling, Cat# 69363), mouse anti-YAP1 (63.7) 1:100 (Santa Cruz, Cat# sc-101199), rat Nanog 1:200 (Thermo Fischer eBioMLC-51, Cat# 14-5761-80), goat KLF4 1:400 (R&D, Cat# AF3158), goat Otx2 1:300 (R&D, Cat# AF1979), rabbit Sox1 1:200 (Cell Signaling, Cat#4194), mouse E-cadherin 1:200 (Invitrogen, Cat#131700)

The secondary antibodies used are: goat anti-mouse Alexa Fluor − 488 (Cat# A-11029), −555 (Cat# A-21424), −647(Cat# A-21236), goat anti-rabbit Alexa Fluor −555 (Cat# A-21429), donkey anti Rabbit −488 (Cat# A-21206), −647 (Cat# A-31573), donkey anti-rat Alexa Fluor −488 (Cat# A-11006), −555 (Cat# A-21434), −647(Cat# A-21247), donkey anti-goat Alexa-Fluor −488(Cat# A-11055), -555(Cat# A-32816),−647(Cat# A-21447), and donkey anti-mouse Alexa-Flour −488(Cat# A-21202), −647(Cat# A-31571) all at 1:300 concentration (ThermoFisher).

3.14 Image acquisition

Immunofluorescence images were taken in a Nikon TiE inverted microscope with a spinning disk confocal unit (CSU-WD, Yokogawa) and a Zyla sCMOS camera (Andor), using 60x objective (plan apo; NA, 1.2; water immersion) at a resolution of 2,048 x 2,048 pixels (pixel size = 0.1083 µm). The laser power was maintained at 30% with an exposure time of 400 ms for Hoechst and Phalloidin channels, and 500 ms for proteins stained with antibodies. A z-step of 0.5 µm for the focal adhesion stainings and 1 µm for the rest of the samples was used for the acquisitions.

Time-lapse epifluorescence images pertaining to blebbistatin treatment and DN-KASH vs DelPP experiments, were taken on an automated inverted microscope (Nikon Eclipse Ti) using MetaMorph/NIS Elements imaging software and 40x objective (S-plan fluor, Ph2; NA, 0.75) at a resolution of 2,048 x 2,048 pixels (pixel size = 0.16125 µm). An exposure time of 50 ms for phase contrast imaging and 500 ms for the fluorescent channels was used with the sample illuminated for once every 2 hours. The microscope was equipped with a temperature box maintaining 37^{o}C in the microscope (Life Imaging Services) and a chamber maintaining CO_2 and humidity (Life Imaging services) was used.

Rest of the time-lapse confocal images were taken in a Nikon TiE inverted microscope with a spinning disk confocal unit (CSU-WD, Yokogawa) and a Zyla sCMOS camera (Andor), using 40x objective (S-plan fluor, Ph2; NA, 0.75) at a resolution of 2,048 x 2,048 pixels (pixel size = 0.1083 µm). An exposure time of 50 ms for phase contrast imaging and 200 ms for the fluorescent channels was used with the sample illuminated for once every 2 hours. For live imaging the laser power for fluorescent channels was kept at 15%. The microscope was equipped with a temperature box maintaining 37^{o}C in the microscope (Life Imaging Services) and a chamber maintaining CO_2 and humidity (Life Imaging services) was used. The open-source Micromanager was used to carry out multidimensional acquisitions with a custom-made script allowing beads channel to be imaged with a z-step of 0.5 µm and, the phase-contrast and GFP channel to be imaged with a z-step of 2 µm.

To reduce the phototoxicity and improve signal to noise ratio during time lapse imaging acquisition, media without phenol red was utilized. For traction force measurements, the relaxed state of PAA gel was obtained after detaching colonies by incubating with 10x-trypsin for 30 minutes. The z-step, laser power and exposure time were the same used while imaging the samples with colonies.

3.15 Traction force measurements

Maximum projections of the confocal stacks of fluorescent beads for both the deformed (by the cells) and relaxed (trypsinized) state were obtained through ImageJ. From those, the displacements of the beads were computed with homemade iterative 2D PIV software with an overlap of 0.75 and a window size of 32 X 32 pixels. Tractions were then computed from the deformations of the gel by solving the elastostatic equation in the Fourier space.

For the blebbistatin experiments, since the acquisition was performed in epifluorescence microscopy, no image preprocessing was performed before using them as inputs for the matlab code. The rest of the parameters remained the same for displacement calculation and traction force inference.

To measure the traction forces exerted by the colonies, through the phase-contrast images, the colony boundary for each time point is outlined. By using the colony boundaries as inputs for the custom-made MATLAB code, the areal mean of the stresses within the colony region was calculated.

3.16 Colony area measurements and normalization

The colony boundaries were outlined manually on phase-contrast image, in ImageJ using the freehand selection tool and the corresponding area was calculated. For a given colony, normalization is performed with the area at the start of experiment using the formula below.

$$(Normalized\ area)_t = \frac{(Colony\ area)_t}{(Colony\ area)_{0hr}}\ x\ 100$$

3.17 Rex1-GFP signal measurements and normalization

For a given colony, the boundary at each time point were outlined manually, using phase-contrast image, in ImageJ using the freehand selection tool. The integrated density of fluorescence signal within this Region of Interest (ROI) was divided by the colony area to obtain the areal mean of signal intensity which will be from now on referred to as mean intensity. The ROI was expanded by 20 pixels and through the XOR function between the original ROI and the expanded one, a background RIM is obtained. The mean intensity in this background rim is obtained as mentioned above. Using these two quantities the (background) corrected mean intensity is obtained based on the formula given below.

$$Corrected\ mean\ intensity = Mean\ intensity\ of\ ROI - Mean\ intensity\ of\ background\ rim$$

An example for measuring mean intensity through this pipeline is given below (Figure.12). When the above formula yields a negative value, the corrected mean intensity is zero.

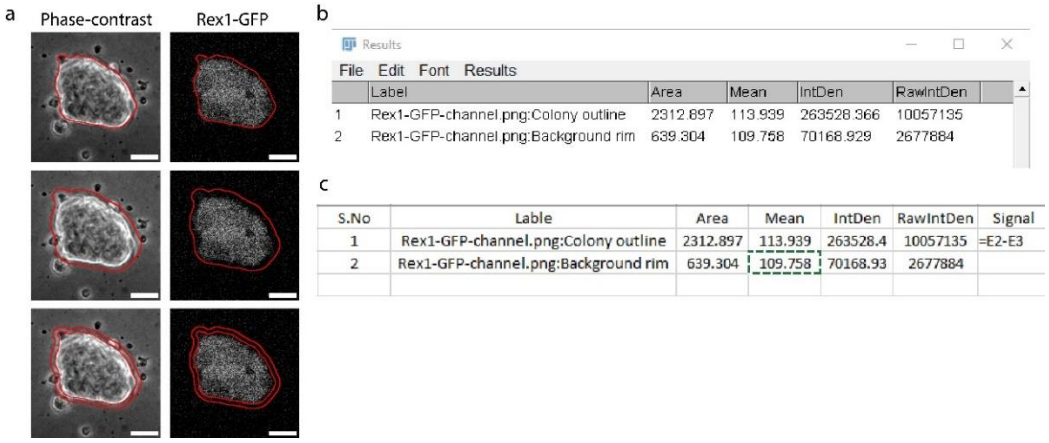

Figure.12: Pipeline for Rex1-GFP signal measurement: a. Representative phase-contrast and fluorescent images of mESCs overlaid with colony outline (top panel), enlarged colony outline (middle panel) and background rim (bottom panel), b. Measurement of Rex1-GFP signal measurement in ImageJ, c. Measurement of Rex1-GFP signal by subtracting mean intensity in background rim from mean intensity within colony outline. Scale bar is 20 µm.

Once the mean intensities are calculated for each time point, they are normalized as per the formula below.

$$(Normalized\ fluorescence)_t = \frac{(Corrected\ mean\ intensity)_t}{(Highest\ mean\ intensity)_{Start-End\ of\ experiment}}\ x\ 100$$

3.18 Decay constant measurements

An exponential fit using the normalized intensities was performed between the highest value and the normalized mean intensities corresponding to subsequent time points. The formula is given below. The exponential fit was performed in MATLAB.

$$(Normalized\ mean\ intensity)_t = 100\ e^{-\lambda t}$$

The final time point until which the exponential fit was performed is determined based on following criteria.

1. If the mean intensity declines to zero within the time frame of imaging, the instance after which the mean intensity becomes zero for the first time is considered to be naïve state exit.
2. If the mean intensity doesn't become zero, the exponential fitting is performed until the time point which the colony signal is monitored.

3.19 Measurement of pPaxillin length

The fluorescence channel corresponding to pPaxillin immunostaining was contrast adjusted and a median filter with 0.5-pixel radius was applied to improve the signal to noise ratio while preserving edge features. Later, the image was binarized and the individual focal adhesion ROIs were obtained using the following sequence of commands: Edit>Selection>Create-Selection>Add to ROI Manager>Split. The Feret length for each ROI was measured through the in-built ImageJ function and taken as the length for that particular focal adhesion. For the final data plotting, the average of all focal adhesion Feret lengths of a given colony is calculated and taken as a single data point.

3.20 Blebbistatin treatment

The para-nitro derivative of blebbistatin was chosen to perform myosin inhibition experiments owing to its non-phototoxic and non-cytotoxic effects. The drug was purchased as lyophilized powder (Motorpharma, cat.no. 1621326-32-6) and dissolved in 100% DMSO (Sigma-Aldrich, cat. no. D8418) to prepare a stock solution of 10mM concentration that is stored at -20^0 C.

For experiments involving blebbistatin treatment, para-nitro blebbistatin was added to N2B27 media to arrive at final concentrations of 1, 2 and 10µM. As a control, DMSO was added to media at the same volumetric proportions used for 10µM para-nitro blebbistatin. Both the DMSO-control and para-nitro blebbistatin containing media were briefly warmed at 37^0 C to ensure homogenization before adding to the experimental samples. As mentioned in earlier section of experimental sample preparation, addition of final media is always preceded by a quick wash with N2B27 under sterile conditions. For time lapse microscopy, sufficient media to be sustained for 48hr-60hr of imaging was provided. For immunofluorescence experiments, media was replenished every day.

3.21 Single inhibitor treatment

For single inhibitor treatments, the samples were provided with one of the following four media concoctions: (1) N2B27 + 2i (or simply 2i), (2) N2B27 + 3 µM for Chiron (N2B27 + Chir), (3) N2B27 + 1 µM for PD0325901 (N2B27+PD) and (4) N2B27. The media of choice was added to the samples after a quick wash with N2B27 under sterile conditions. For time lapse microscopy, sufficient media to be sustained for 48hr-60hr of imaging was provided. For immunofluorescence experiments, media was replenished every day.

3.22 Transcription factor nuclear signal measurement and data normalization

Hoechst channel was used to manually delimit the nuclear region and calculate the mean intensity of fluorescence signal. A region within the vicinity of the colony, devoid of cells and colonies, was used to calculate the mean intensity of background. The corrected mean intensity for each nucleus was obtained using earlier formula. The signal corresponding to a colony was obtained by averaging the corrected mean intensities of all the nuclei. The pooled colony data for 2i-0hr (control) in each independent experiment was averaged and was used to

normalize the corrected mean intensity of each colony as per formula below. Only basal plane nuclei are considered for this analysis.

$$Normalized\ value = {Corrected\ mean\ intensity}/{average\ (control\ colonies'corrected\ mean\ intensities)}$$

3.23 Nuclear aspect ratio measurements and data normalization

Hoechst channel was used to manually delimit the nuclear region and an ellipse was fit to the ROI using the ImageJ in built function. The ratio of major axis to minor axis was calculated and considered as the aspect ratio of the given nucleus. The signal corresponding to a colony was obtained by averaging the aspect ratios of all the nuclei. Only basal plane nuclei are considered for this analysis.

3.24 Resolving Edge and Interior regions for time lapse imaging measurements

Using the colony outlines drawn on the phase contrast images, a concentric region eroded through eucledian distance map to 80% of the original ROI radius was obtained. The region contained within it is labelled interior and the region in the remaining 20% of the rim is termed edge. The areal mean of traction stresses within these Interior and Edge regions was calculated as described above by solving the elastostatic equations and using fourier space to transform bead displacements into forces.

For Rex1-GFP fluorescence measurements, the colony outline for each time point was dilated through eucledian distance map to additional 10% radius. Then, mean intensity of fluorescence signal within the rim between this expanded ROI and the initial colony ROI was measure and taken as background. Using this background intensity, the corrected mean intensity of Interior and Edge regions at given time point t was calculated based on following formulae.

$$(Corrected\ mean\ intensity)_{Edge,t} = (Mean\ intensity\ of\ Edge\ ROI)_t - (Background\ intensity\ )_t$$

$$(Corrected\ mean\ intensity)_{interior\ ,t} = (Mean\ intensity\ of\ Interior\ ROI)_t - (Background\ intensity)_{\ t}$$

The corrected mean intensities of each region for each time point were normalized to the corrected mean intensity of overall colony at time point 0hr (the start of the experiment) as per below formula.

$$(Normalized\ intensity)_t = {(Corrected\ mean\ intensity)_t}/{(Corrected\ mean\ intensity\ of\ colony)_{0hr}}$$

The earlier described method for exponential fitting was followed to obtain the decay constants for each region.

3.25 Resolving Edge and Interior regions for measurements in immunofluorescence imaging

A cell with at least one side free of cell-cell adhesion is designated as edge cell and the conglomerate of all these edge cells is taken as the edge region. The rest of colony is considered the interior region. The corrected mean intensities of all edge cells are averaged and taken as edge signal of the particular colony. Similar approach is followed to obtain the interior signal of the colony. The edge and the interior signals for a given colony are normalized by the average of corrected mean intensities of all colonies pertaining to 2i-0hr (control). The formula is given below. Only basal plane nuclei are considered for this analysis. An example of edge and interior region separation in an immunofluorescence image through this pipeline is given in Figure.13 below.

$$Normalized\ value = {Corrected\ mean\ intensity}/{average\ (control\ colonies'corrected\ mean\ intensities)}$$

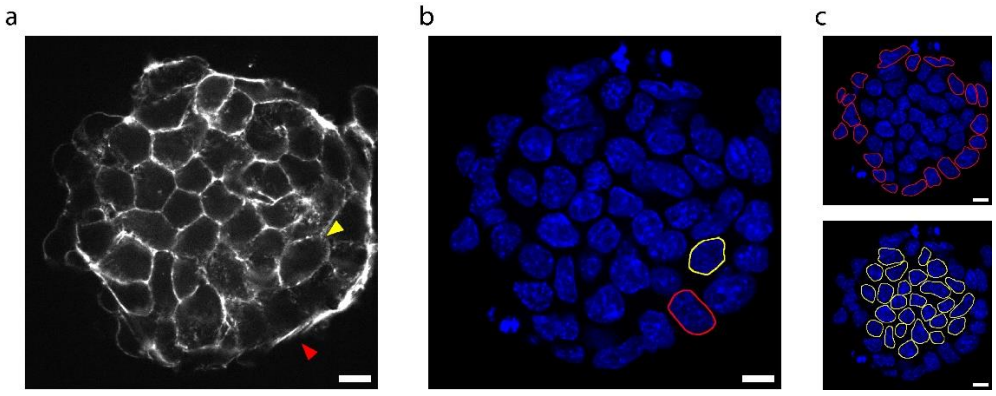

Figure.13: Pipeline for resolving edge and interior regions in immunofluorescence images: a. Representative images of actin staining with red arrowhead pointing to an edge cell and yellow arrowhead indicating interior cell, b. Representative images of nuclear staining overlaid with ROI for edge nuclei (red) and interior nuclei (yellow), c. Nuclei of edge region overlaid with respective ROIs (top) and nuclei of interior region overlaid with respective ROIs (bottom). Scale bar is 10 µm.

3.26 Measurement of YAP nuclear to cytoplasmic ratio

Using the Hoechst signal, the nuclear boundaries were delimited. For each nuclear ROI, an expansion by 5 pixels through eucledian distance map was performed. The mean intensity of fluorescence signal within the rim between this expanded ROI and the initial nuclear ROI was measured and taken as cytoplasmic signal. Later, the initial nuclear ROI was eroded by pixels through eucledian distance map by 5 pixels and the mean intensity of fluorescence signal within the rim between this eroded ROI and initial nuclear ROI was measured and taken as nuclear signal. The nuclear to cytoplasmic ratio (N/C ratio) is obtained for a given nucleus based on the following formula. An example for measuring N/C ratio of a nucleus through this pipeline is given in the Figure.14 below. The N/C ratios of all the nuclei in a colony are averaged and considered as colony signal, turned into single data point for plotting.

$$N/C\ ratio = (Nuclear\ signal - background) / (Cytoplasmic\ signal - background)$$

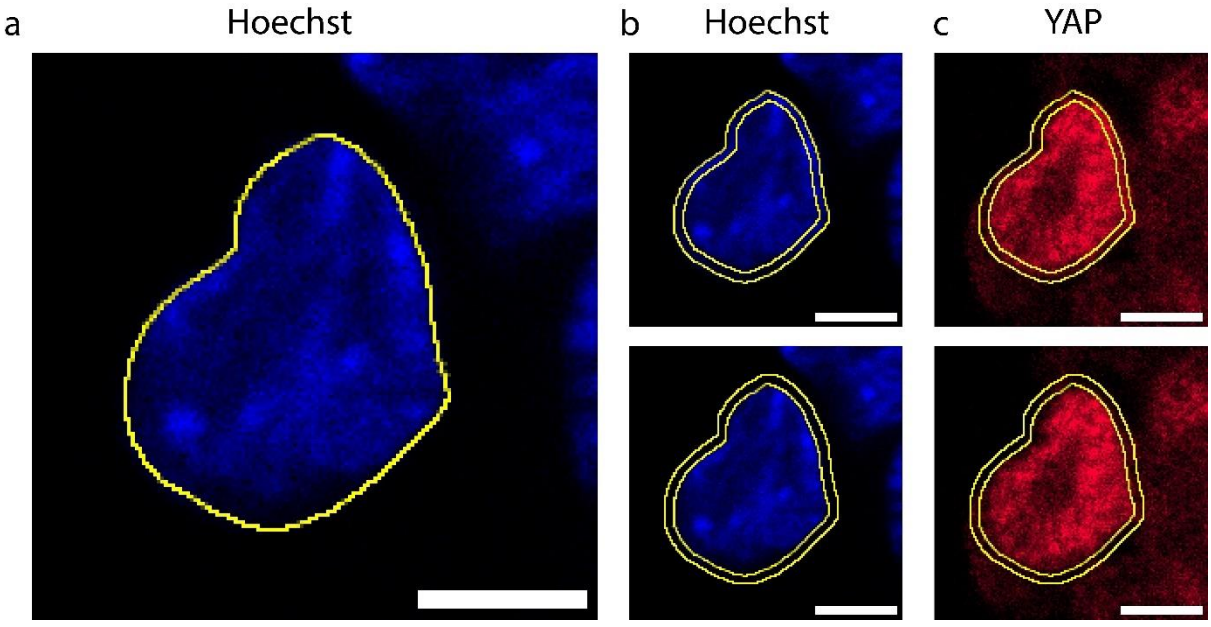

Figure.14: Pipeline for measuring Nuclear to Cytoplasmic ratio of YAP: a. Representative nucleus overlaid with outline ROI. The same nucleus overlaid with the ROI corresponding to nuclear rim (top panel b and c) and cytoplasmic rim (bottom panel b and c). Scale bar is 5 µm.

The same guidelines mentioned in pervious section were followed to resolve edge and interior nuclei of a colony. The average of N/C ratios of all the edge nuclei in a given colony are considered edge signal. Similar approach is followed for obtaining interior signal.

3.27 Statistical analysis

Statistical analysis was performed using GraphPad Prism software (GraphPad, version 9). Statistical significance was determined by the specific tests indicated in the corresponding Figure legends. Non-parametric tests were performed when both original and log-10 transformed datasets were not normally distributed where appropriate. All experiments presented in the manuscript were repeated in at least 3 independent experiments.

Chapter 4: Results

4.1 sulfo-SANPAH gels are amenable for mESC differentiation protocol

The first step of the investigation aimed at identifying the platform best suited to study cell-ECM interaction during naïve pluripotency exit in mESCs. For this, the following hydrogel setups were fabricated: PAA gels with Sulfo-SANPAH functionalization, PAA gels with NHS-Irgacure functionalization, StemBond hydrogels (PAA gels with acrylamidohexanoic acid as protein linker), and PDMS. These 4 were subjected to standard differentiation protocol in N2B27 for 3 days with cells initially maintained in 2i for 2 days. The hydrogel steups were evaluated on the following four criteria.

1. Stable mESC attachment to the matrix over a long-term (a minimum of 5 days)
2. Maintenance of characteristic 3D dome morphology of mESCs when cultured in 2i media.
3. Provision of wide range of substrate stiffness.
4. Reliability in traction force measurements.

Among the four hydrogels variations, sulfo-SANPAH PAA gels fared better in above four aspects and was therefore selected as a platform for further experiments. The specific reasoning for discarding each of the other three matrices are summarized below.

4.1.1 NHS-Irgacure hydrogels

Protein attachment to PAA gels through NHS-Irgacure protocol occurs through a two-step process. First, upon illumination with ultraviolet (UV) light, Irgacure decomposes into free radicals that promote the covalent binding of NHS to the polymerized gel. Later, the ECM protein of choice is coupled to NHS through ester-amine reaction.

mESCs seeded on PAA gels functionalized with NHS-Irgacure protocol could not maintain stable attachment. The poor adherence was signified by colonies remained rounded throughout the experiment. Also, cells were observed to detach 24 hours after seeding in 2i media and the proportion increased when the samples were subjected to N2B27 differentiation protocol (Figure.15). Thus, the set-up compromises on throughput. Moreover, increased cell death occured in all phases of sample maintenance, be it during the 2-day culture in 2i media or while subjecting the colonies to differentiation with two inhibitor withdrawal. As the cell attachment to the matrix isn't strong, the plausible cause of increased cell death might be anoikis. The low throughput in terms of cell attachment was further exacerbated by phototoxicity when the cells were subjected to timelapse microscopy.

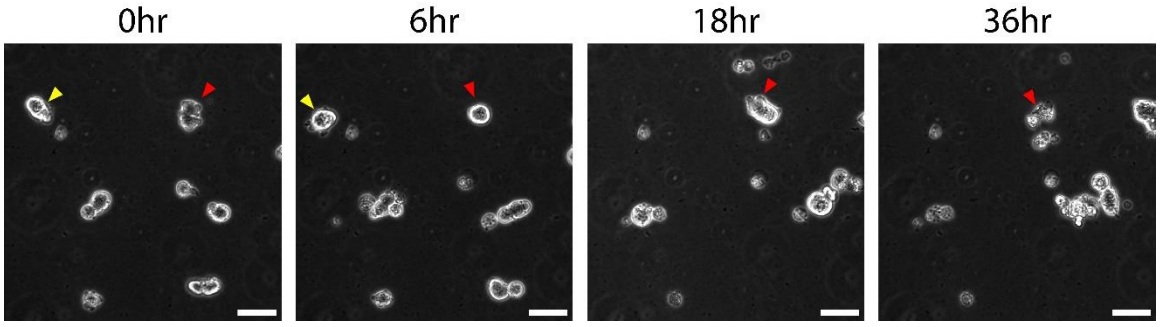

Figure.15: Representative phase contrast images of mESC colonies grown on NHS-Irgacure PAA gels. Yellow arrowheads indicate detaching colonies. Red arrowhead indicates dying colonies. Scale bar is 20µm.

4.1.2 StemBond hydrogels

Protein coating to StemBond hydrogels occurs in a two-step process. First, the carboxyl group of the acrylic acid linker molecule are activated by the carbodiimide compound EDC. This facilitates the binding of NHS forming an NHS ester which later couples to the protein through ester-amine reaction

On StemBond hydrogels, mESCs maintained stable matrix attachment. However, on the stiff substrates, colonies presented spread morphology even when maintained in 2i media (Figure). Importantly, the in-house MATLAB code for traction force quantification requires the fluorescent beads to be localized only on the top layer of the hydrogel. It is achieved by using 1X-PBS as the solvent for hydrogel mixture. However, when the StemBond hydrogel composition was adjusted accordingly by replacing ultrapure water with 1X-PBS, the bead localization to the top layer wasn't optimal. The beads localized at all depths of the gel leading to high fluorescence signal impeding faithful measurement of displacements and from thereon traction calculation (Figure.16).

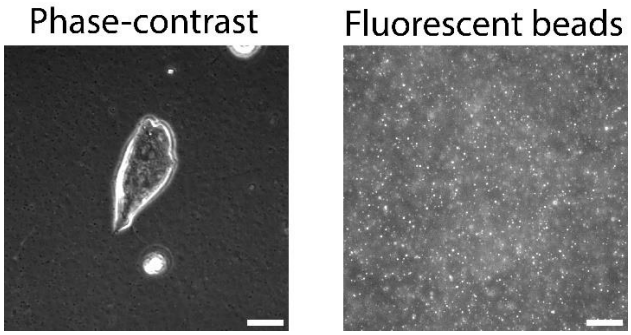

Figure.16: Representative phase-contract image of mESC colonies grown on StemBond hydrogels showing spread morphology. Representaive image of bead channel showing suboptimal bead distribution. Scale bar is 20µm.

The suboptimal distribution of fluorescent beads affects the quantification of mechano-responses and further downstream mechano-transduction. Other drawbacks of StemBond hydrogels include the limited range of substrate stiffnesses modulation.

4.1.3 PDMS

Like in StemBond hydrogels, mESCs on PDMS maintained long-term attachment to the matrix. However, the cell spreading couldn't be avoided even when cultured in 2i media and was similar to that observed on tissue culture plastic (Figure.17). This observation has also been reported in other studies [Labouesse C et al 2021 *Nat Comm*]. The effect of PDMS wasn't restricted to morphology as in the same study mESCs grown on PDMS in naïve conditions were shown to have high expression of post-implantation/formative markers such as *Fgf5*. As part of the preliminary experiments when labelling for the post-implantation marker *Otx2* was performed, colonies grown on PDMS in 2i for 2 days were observed to express high levels of *Otx2* with no further change in the expression levels when subjected to differentiation in N2B27 (Figure). Moreover, in the same set of preliminary experiments, when traction force microscopy imaging was performed a flare up of traction force bursts were observed even in the region devoid of cells (Figure). Such high background noise makes mechano-response quantification measurement unreliable. Other reason for discarding PDMS is the lack of multiple stiffness options.

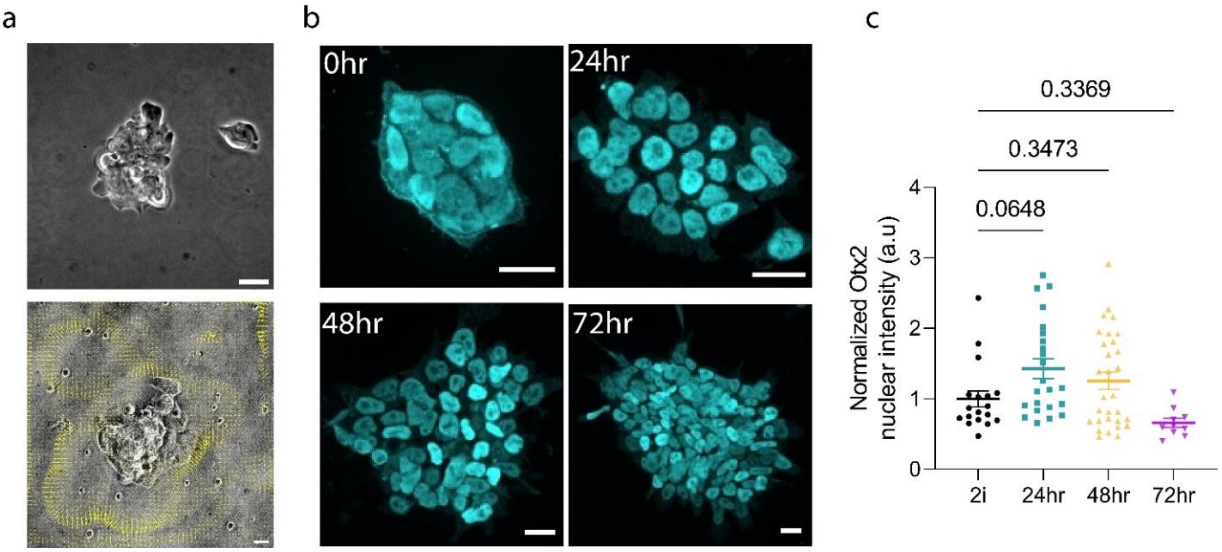

Figure.17: a. Representative phase contrast images of mESC colonies grown on PDMS showing spread colonies (top panel) and overlaid with traction PIVs showing high background tractions in regions without cells, b. Representative immunofluorescence images of mESC colonies grown on PDMS and stained for *Otx2* and c. Corresponding quantification of normalized fluorescence intensity of *Otx2* as a function of time. Data from 2 independent experiments (n = 18/20/30/10 for 2i/N2B27-24hr/N2B27-48hr/N2B27-72hr colonies). Scale bar is 20 µm.

4.1.4 sulfo-SANPAH PAA gels are ideally suited to study cell-matrix interaction of mESCs

Protein binding to PAA gels through sulfo-SANPAH protocol occurs in a two-step process. First the photoactivation of nitrophenyl azide in sulfo-SANPAH leads to its covalent binding to PAA gels. Later through ester-amine reaction, the protein is tethered to the gel.

On PAA gels functionalized with sulfo-SANPAH, mESCs had stable attachment with the formation of typical compact 3D domes when cultured for 2 days in 2i media (Figure.18). In fact, this peculiar morphology was perpetuated for additional 3 days when culturing in 2i media was continued (Figure.18). Only when the cells were subjected to N2B27 differentiation was the colony spreading observed (Figure.18). With both cell death and colony detachment being minimal during the 5 days of experimental protocol and the provision of wide range of matrix stiffness, further weight was added for the selection of this set up. Additionally, this system was found compatible for performing traction force microscopy owing to the localization of beads only to the top layer of gels. Importantly, the traction forces measurements were deemed reliable as little to no background noise was observed when computing tractions (Figure.18). Other advantage offered by this platform over PDMS is the higher fluorescent bead density (Figure.18) offering increased spatial resolution for traction force measurements. Hence, because of all the above reasons, PAA gels with sulfo-SANPAH functionalized were identified to be best suited for this study.

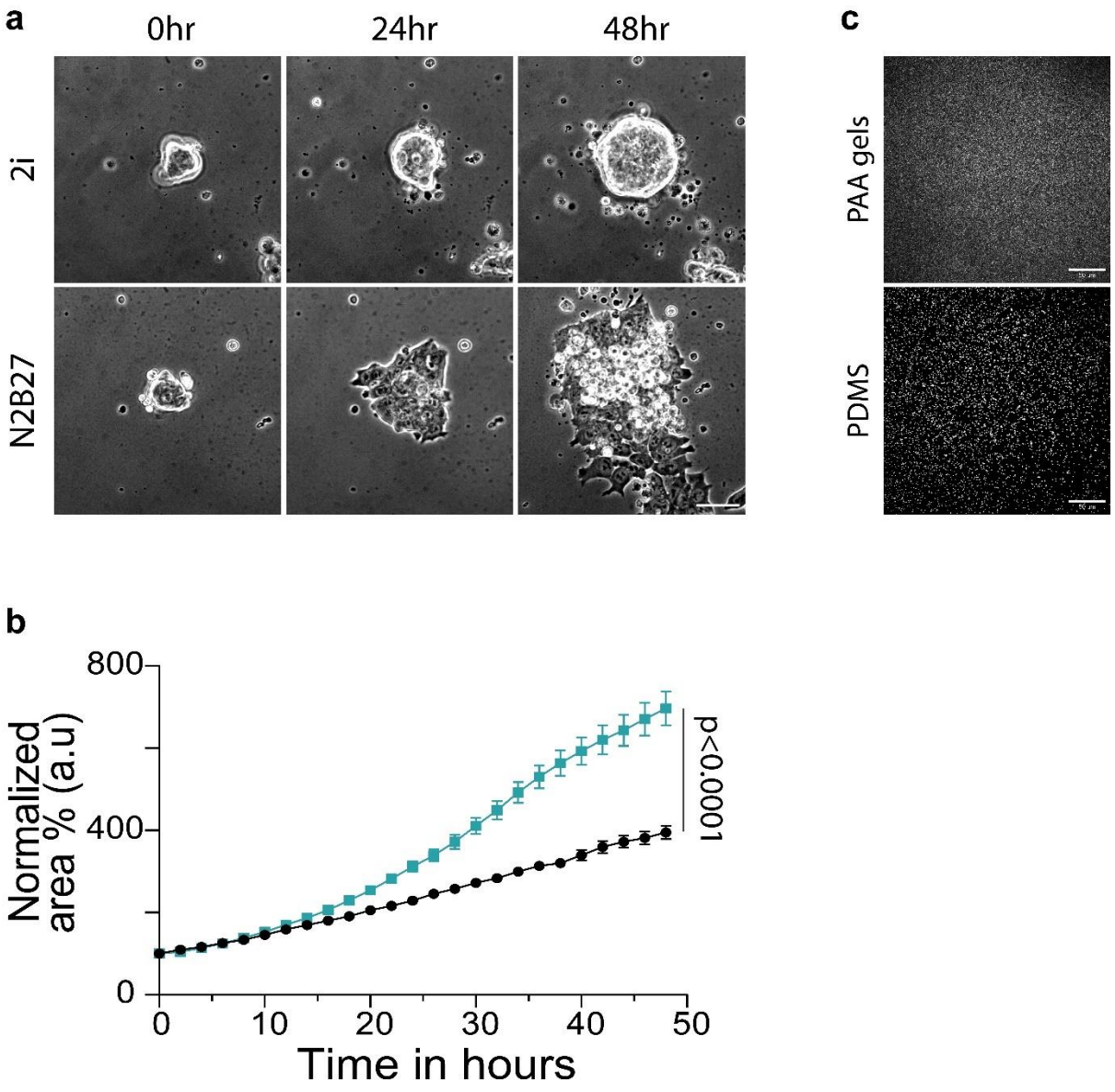

Figure.19: a. Phase contrast images of mESC colonies in 2i medium (left) or N2b27 medium (right) seeded on 5 kPa polyacrylamide gels and imaged as a function of time. Scale bar is 50 µm. b. Corresponding quantification of colony areas normalized to initial value. Data from 3 independent experiments (n = 72/91 colonies for 2i/N2B27). The effect of media change is significant (p<0.0001, student's t-test without Welsch correction, for last time point). c. Representative images of fluorescent bead distribution in sulfo-SANPAH gels (top) and PDMS (bottom). Scale bar is 50 µm.

With the hydrogel set up identified, the system validation was performed next. From now on the set up will be referred to as sulfo-SANPAH gels.

4.2 System recapitulates putative transcriptional changes of mESC pluripotency dissolution

More than the compliancy for experimental interventions, the key justification for using a hydrogel platform is when the molecular changes, associated with pluripotency loss in our case, are reproduced. Therefore, the expression profiles of three bonafide transcription factors were probed. These are: *Klf4*, *Nanog* and *Otx2*. For each of these three factors, the rationale for their selection and a comparison between what has been reported in literature to what was observed in the current system is summarized below.

As discussed earlier in the introduction, *Klf4* is the naïve state specifier ejected from the nuclear space first when mESCs are subjected to differentiation in N2B27. The decrease in *Klf4* levels is reported to occur within 24 hours post the withdrawal of two inhibitors. When the levels of *Klf4* were examined through immunofluorescence, the same was observed with all the mESC nulcei in the colony depleted of *Klf4* expression at the 24-hour time point (Figure). The lack of *Klf4* expression persisted in the later time points (48 and 72 hours). All these observations were also confirmed by quantifying nuclear intensity (Figure). Importantly, these changes in *Klf4* expression levels were observed only upon the two-inhibitor withdrawal. When culturing in 2i media was continued for 3 days instead of changing to N2B27, high *Klf4* expression was maintained (Figure.19).

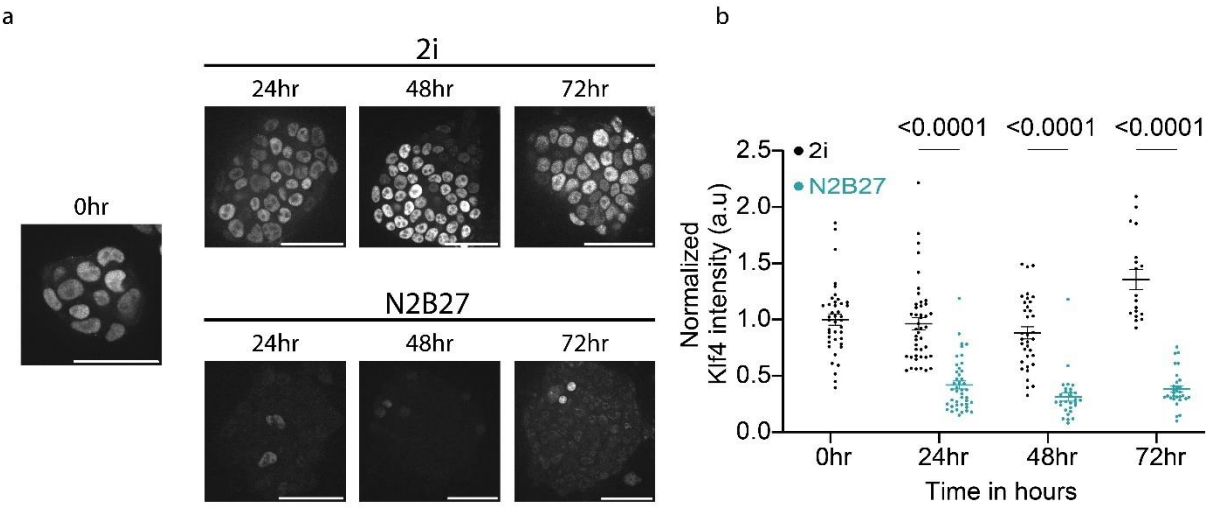

Figure.19: a. Representative images of mESC colonies immunostained for Klf4 in 2i (top)/N2B27 (bottom). Scale bar is 50 µm. b. Corresponding quantification of Klf4 nuclear intensity (normalized to average of 2i in corresponding experiment). Data from 3 independent experiments (n = 41/44/43/35/29/18/30 for 2i-0hr/2i-24hr/N2B27-24hr/2i-48hr/N2B27-48hr/2i-72hr/N2B27-72hr). The effect of media change is significant (Two-way ANOVA without repeated measures).

The post-implantation factor *Otx2* is expressed at basal levels in naïve state and upon pluripotency priming, its levels increase. In line with these reports, mESC colonies presented *Otx2*+ve cells after two days of culturing in 2i. However, the withdrawal of two inhibitors augmented *Otx2* levels with the expression being highest after 48 hours of differentiation in N2B27 (Figure). These changes were brought about by only media change as mESCs continued to be cultured in 2i media retained basal expression levels as observed at the start of experiment. All these observations were corroborated by quantification of *Otx2* nuclear intensity (Figure).

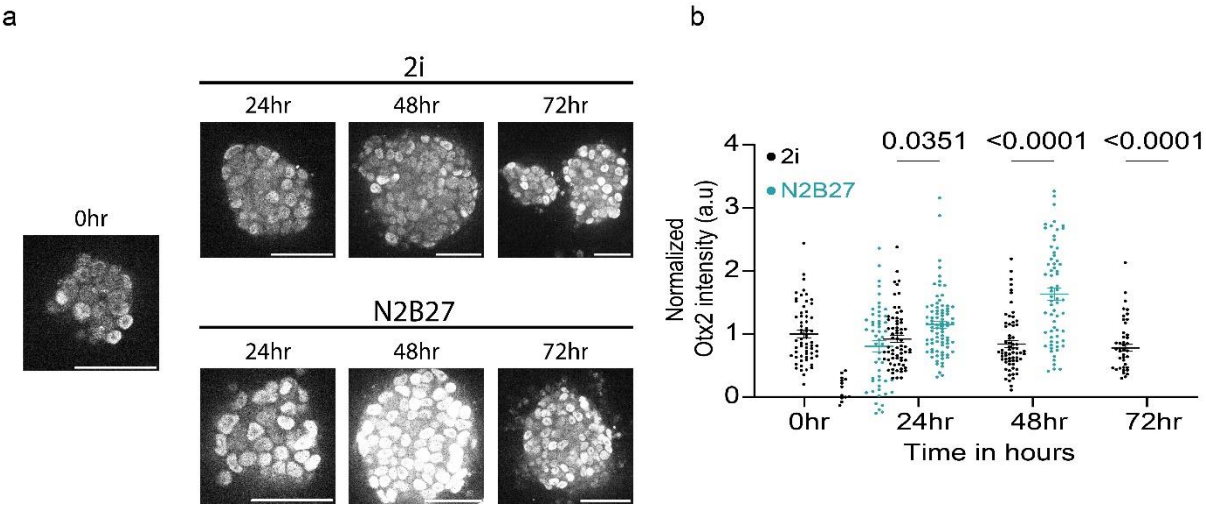

Figure.20: a. Representative images of mESC colonies immunostained for Otx2 in 2i (top)/N2B27 (bottom). Scale bar is 50 µm. b. Corresponding quantification of Otx2 nuclear intensity (normalized to average of 2i in corresponding experiment). Data from 3 independent experiments (n = 62/67/82/65/66/54/52 colonies for 2i-0hr/2i-24hr/N2B27-24hr/2i-48hr/N2B27-48hr/2i-72hr/N2B27-72hr). The effect of media change and time is significant (Two-way ANOVA without repeated measures).

It is established that the general pluripotency factor *Nanog* is expressed at highest levels in naïve state and upon commitment to pluripotency priming, it is downregulated. The expression patterns in the system confirmed the same, with mESC colonies being fortified with *Nanog* when maintained in 2i and, low and heterogeneous expression when differentiated in N2B27 (Figure.21). These conclusions were drawn based on the quantifications of nuclear signal.

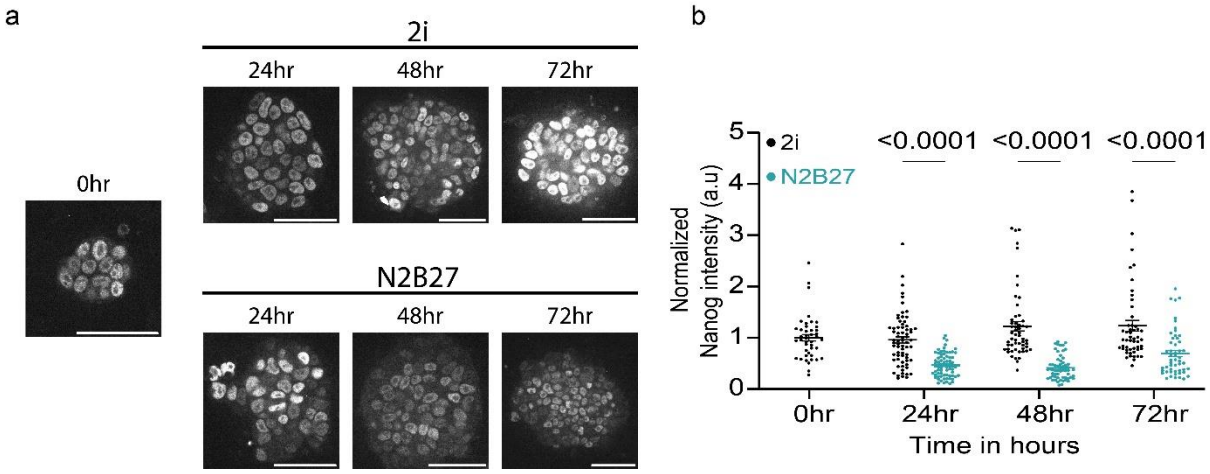

Figure.21: a. Representative images of mESC colonies immunostained for Nanog in 2i (top)/N2B27 (bottom). Scale bar is 50 µm. b. Corresponding quantification of Nanog nuclear intensity (normalized to average of 2i in corresponding experiment). Data from 3 independent experiments (n = 43/69/74/55/60/52/52 colonies for 2i-0hr/2i-24hr/N2B27-24hr/2i-48hr/N2B27-48hr/2i-72hr/N2B27-72hr). The effect of media change and time is significant (Two-way ANOVA without repeated measures)

A combined reason for the selection of *Nanog* and *Otx2*, is the functional antagonism between the two and pluripotency priming ensues when the stoichiometry is in favour of *Otx2*. When the dual expression of *Nanog* and *Otx2* was viewed in this lens, the immunostaining patterns suggested a reciprocal expression (Figure.22). The same was confirmed when a negative correlation between the expression of the two transcription factors was observed (Figure), meaning high *Otx2* levels corresponded to low *Nanog* levels with the contrapositive also being true.

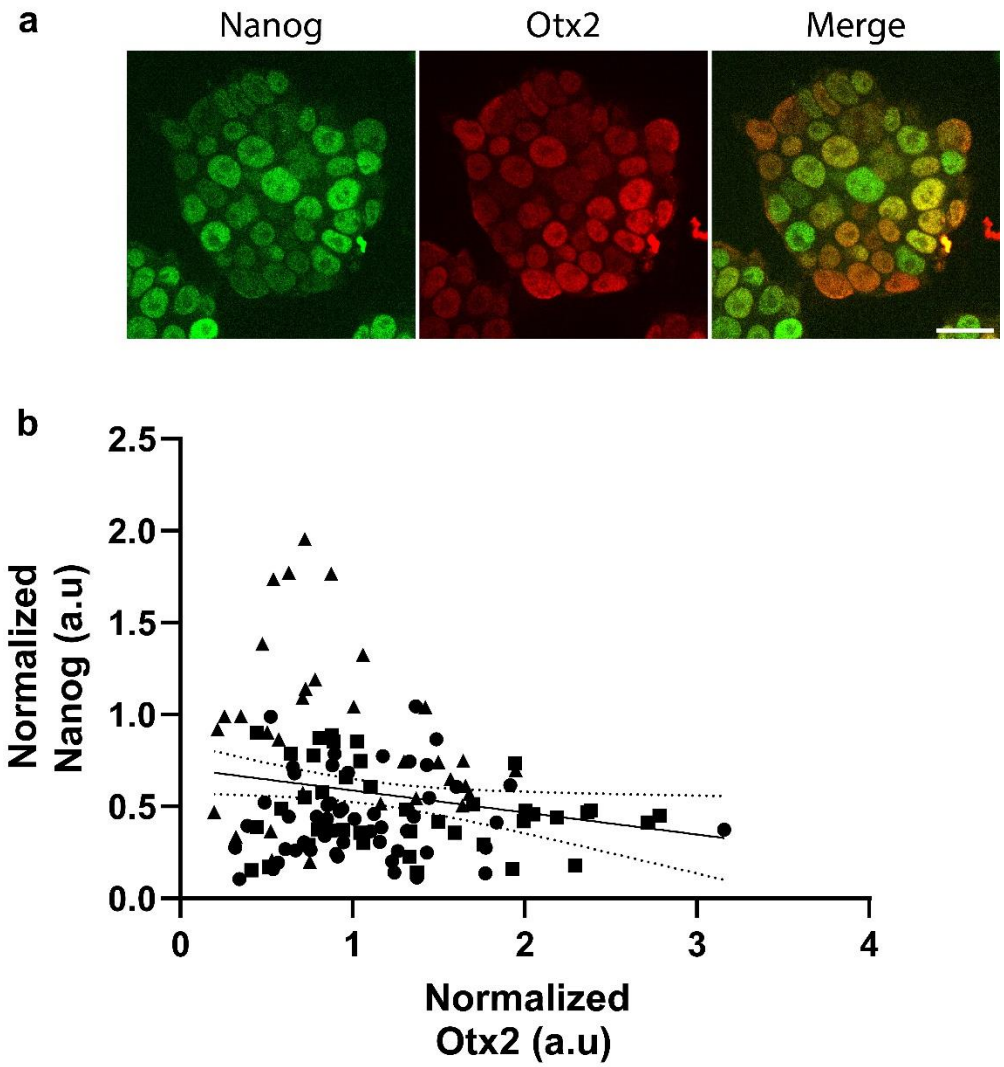

Figure.22: a. Representative image of mESC colony immunostained for Nanog (left), Otx2 (middle) and their merge (right). Scale bar is 50 µm. b. Quantification of correlation between Nanog and Otx2 expression. Data from 2 experiments (n = 126 colonies). Correlation is statistically significant (R^2 = 0.03776, p = 0.0292)

4.3 Rex1-GFP fluorescence intensity profiles gradual pluripotency dissolution

The molecular annotations mentioned in the introdcution were performed at discrete time points. However, it needs to be verified if those changes translate to gradual dissolution of pluripotency in the current set-up. To check the same, employing the Rex1-GFP cell line, the fluorescence intensity of the mESC colonies was monitored in naïve state maintenance and differentiating conditions.

It was observed that, upon the withdrawal of 2i, the Rex1-GFP fluorescent signal of the colonies progressed in two phases. As evident from the quantification (Figure.23), an initial period of a marginal increase in fluorescent signal was followed by a monotonic decrease in the fluorescence intensity after 48 hours of differentiation in N2B27, resembling that of the background (Figure.23). The decline in Rex1-GFP intensity was gradual mirroring the steady transition towards primed pluripotency. These fluorescence signal changes were only observed for mESC colonies submitted to N2B27. Cells cultured in 2i media preserved the Rex1-GFP intensity (Figure.23).

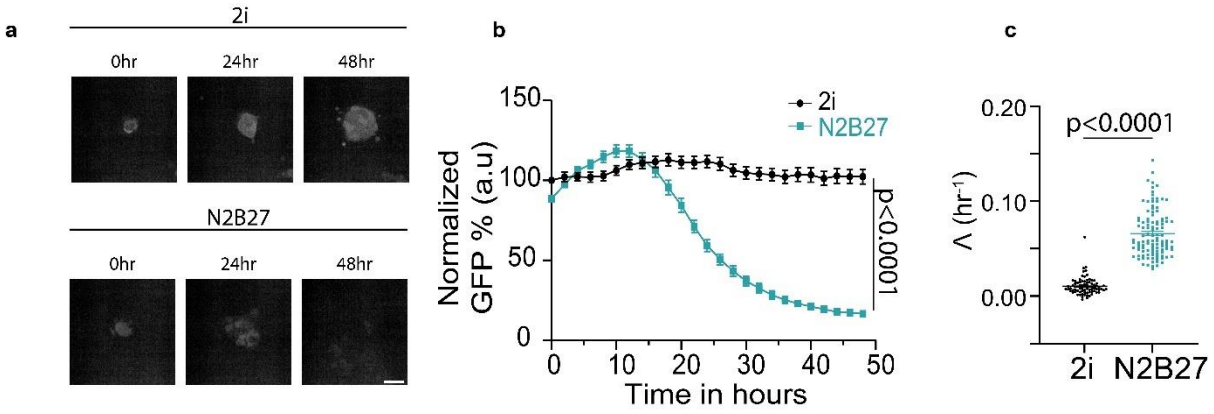

Figure.23: a. Rex1-GFP signal of mESC colonies in 2i medium (top) or N2b27 medium (bottom) as a function of time. Scale bar is 50 µm. b. Corresponding quantification of normalized Rex1-GFP mean intensity (Integrated fluorescence intensity averaged over colony area with initial time point value taken to be 100%). 3 independent experiments (n = 83/105 colonies for 2i/N2B27). The effect of media change is significant (p<0.0001, Welsch's t-test, for last time point). c. Decay constants obtained from exponential fitting of Rex1-GFP decay trajectories. 3 independent experiments (n = 71/110 colonies for 2i/N2B27) The effect of media change is significant (p<0.0001, Kolmogorov Smirnov test).

To measure the temporal progression of Rex1-GFP signal, the fluorescence intensity profiles were fit through an exponential function and the decay constants obtained were found to be significantly higher for the N2B27 differentiated colonies (Figure.23). The decay constant values of 2i condition being close to zero further suggests negligible changes in fluorescence intensity under naïve state maintenance.

With the Rex1-GFP signal progression certifying the experimental set up, the efforts were directed at quantifying mechano-responses accompanying pluripotency dissolution.

4.4 Pluripotency dissolution is associated with increasing cell-ECM interaction

Naïve state exit and further pluripotency transition in single cells was earlier reported to lead to cell spreading and an increase in contact area with the underlying substrate. To check if this is conserved in the current system, the changes in colony area were quantified as a function of time and a gradual increase was observed for colonies in either condition – naïve maintenance with 2i media or differentiation with 2i withdrawal. Importantly, in comparison to the increase in area for colonies in 2i, the areal growth in N2B27 condition was much steeper (Figure) with the normalized areas at the end of experiment being significantly higher (>2-fold). More notably, colonies in 2i media grew as hemispheres with the typical 3D dome morphology, while in N2B27 cells appeared more spread (Figure.24).

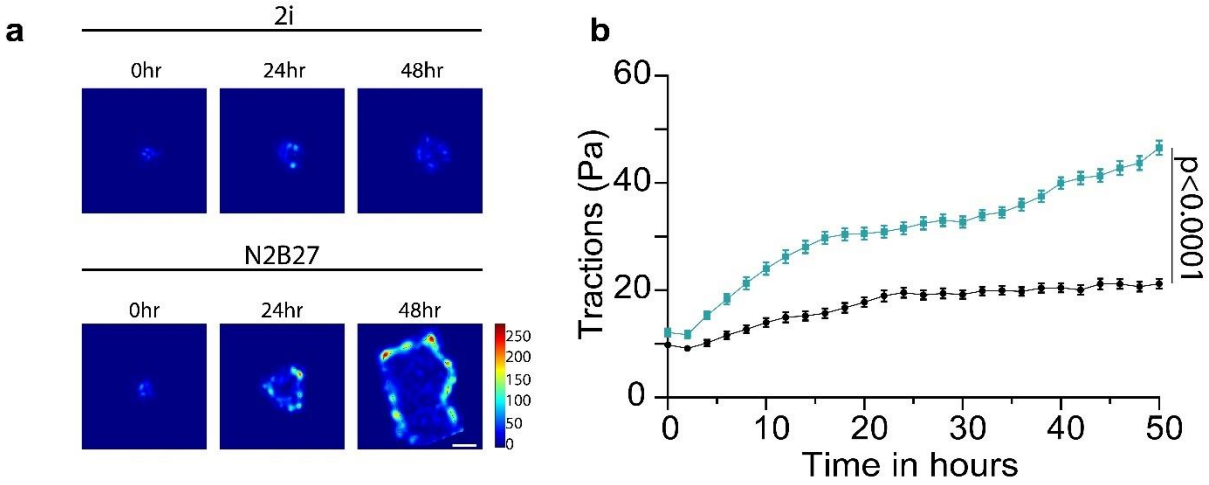

Figure.24: a. Traction forces exerted by mESC colonies in 2i medium (top) or N2b27 medium (bottom) as a function of time. Scale bar is 50 µm. b. Corresponding quantification of tTraction forces averaged over colony area. Data from 3 independent experiments (n = 72/91 colonies for 2i/N2B27). The effect of media change is significant (p<0.0001, Welsch's t-test, for last time point)

Cell-matrix adhesion is mediated by integrins. Since an increase in colony area was observed post naïve state exit and as integrin-based adhesions are known to regulate cell spreading [266], the focal adhesion signature was profiled. Through immunofluorescence, phosphorylation of Paxiilin (p-Pax) at Tyrosine 118 (Y118) was labelled. This post-translational modification of Paxillin enables signalling activity of focal adhesions and cell spreading [267,268]. suggesting a gradual increase in focal adhesion length (Figure.25) as pluripotency faded. Another key distinction between colonies whose naïve identity is preserved and colonies undergoing differentiation, is that in the latter, focal adhesion density within the colony interior is more prominent (Figure.25).

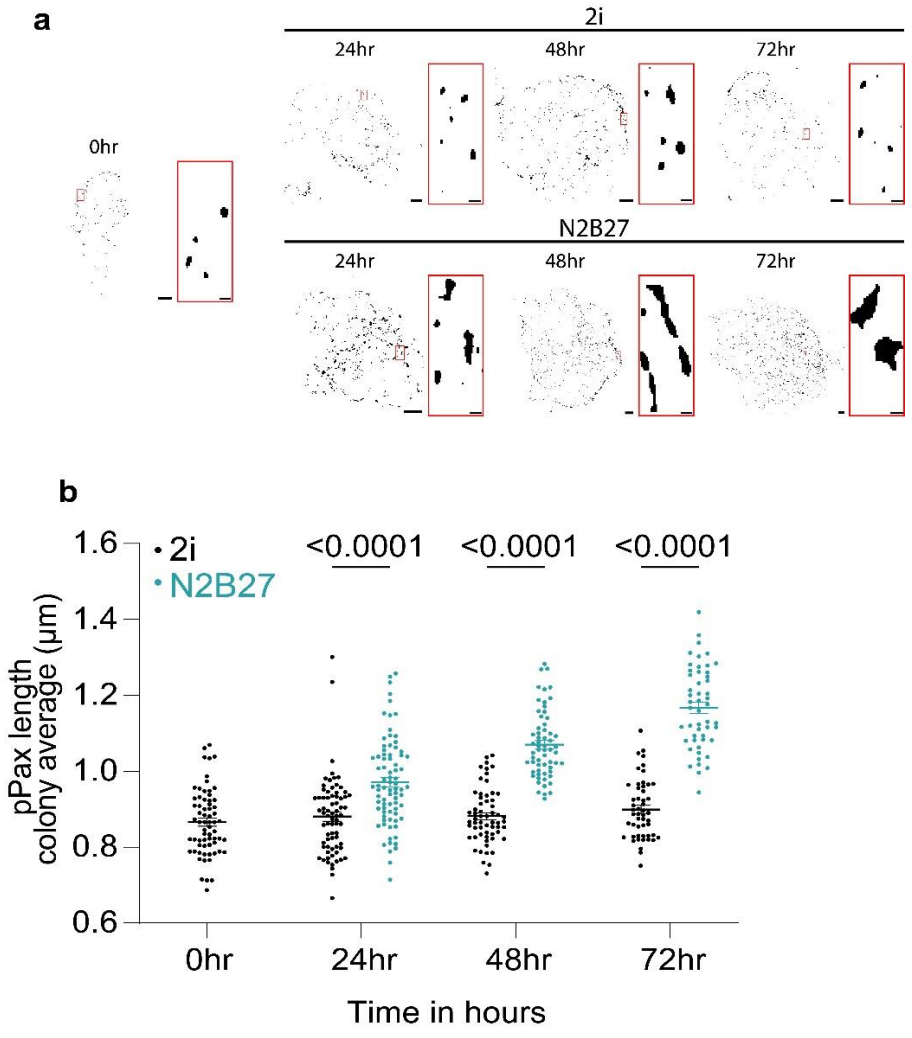

Figure.25: a. Representative images of phospho-paxillin staining as a function of time with respective zoomed insets (in red-bordered rectangles) to the right of each image. Top panel, 2i medium, bottom panel, N2B27 medium. Scale bar is 10 µm (main images) and 1um (insets). b. Quantification of the length of phospho-paxillin adhesions. Data is from 3 independent experiments (n = 66/72/80/60/61/51/51 colonies for 2i-0hr/2i-24hr/N2B27-24hr/2i-48hr/N2B27-48hr/2i-72hr/N2B27-72hr). The effect of media change and time is significant (Two-way ANOVA without repeated measures).

The increase in focal adhesion length suggests elevated signalling activity and as discussed earlier leads to polymerization of actin. To confirm if such organizational changes in the cytoskeleton are symptomatic of pluripotency loss in the current system, F-actin in the basal cell layer was visualized through Phalloidin staining. A marked difference in the cytoskeletal network arrangement was observed between the colonies with naïve state sustenance and their differentiated counterparts. For the ones maintained in 2i, actin was primarily concentrated at the cortex, with the organization in the cell interior having a mesh-like morphology (Figure.26). In contrast, for those undergoing pluripotency loss, cytoskeletal changes constituted progressive actin reinforcement into prominent stress fibres with directionality in alignment.

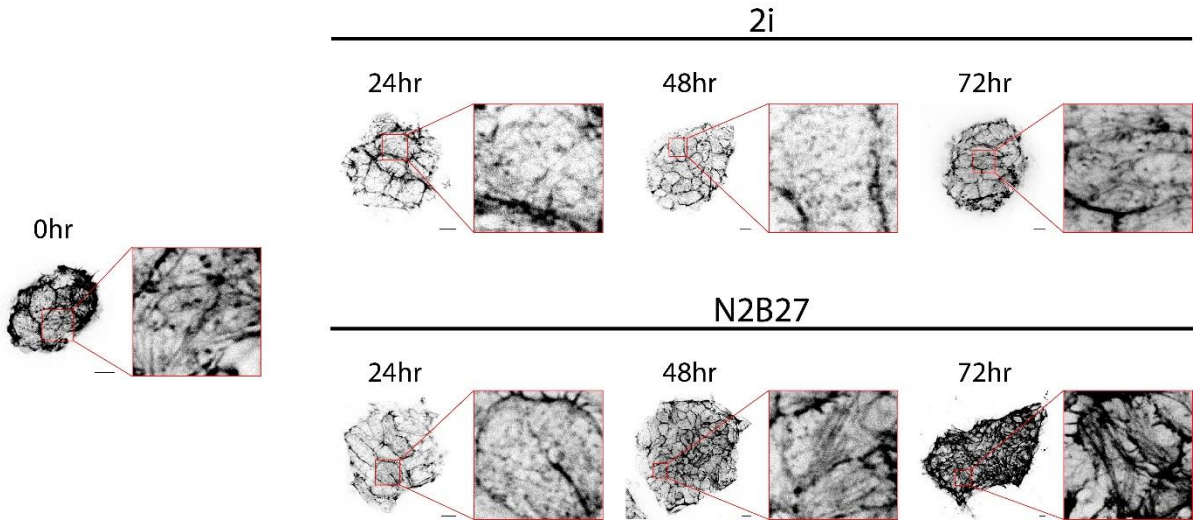

Figure.26: Representative images of Phalloidin staining for actin visualization, with respective zoomed insets (in red-bordered rectangles) to the right of each time point image. Top panel correspond to 2i and bottom panel correspond to N2B27

As actin filaments are anchored to focal adhesions, cells exert traction forces onto the substrate because of actin polymerization. They are another measure of cell-matrix interaction. In light of this information and given that differences exist between 2i- and N2B27-grown mESC colonies for both focal adhesion length and actin organization, traction force microscopy was performed simultaneously with the monitoring of Rex1-GFP fluorescence intensity. Although traction forces were found to be monotonically increasing in both conditions, the values were significantly higher when mESCs were differentiated in N2B27 (Figure). A concomitant dwindling of Rex1-GFP fluorescence signal (Figure) suggests that pluripotency dissolution is associated with ever-increasing traction forces.

The consistent increase in colony area, focal adhesion length and traction forces imply that interaction with the matrix increases for mESCs as they exit pluripotency.

In addition to the organizational changes in actin cytoskeleton, cells require the contractile activity of myosin motors to exert traction forces. Moreover, myosin motor function is integral for mechanical signal relay to nucleus thereby influencing transcriptional signature, the foundation for pluripotency state transition. Also, the magnitude of forces relayed into the cell interior depends on the extent of integrin engagement which is shown to be influenced by the matrix stiffness perceived by the cells. Therefore, matrix stiffness and myosin motor activity are the two key hotspots which could be targeted to influence the levels of mechano-transduction. The next topic deals with the results of experimental efforts in this direction.

4.5 Interference with mechano-transduction alters pluripotency decay kinetics

4.5.1 Cell contractility inhibition delays naïve state exit

To investigate the impact of attenuated cell-ECM force transmission, mESCs colonies were treated with different concentrations blebbistatin, a nonmuscle myosin IIA inhibitor [271]. The treatment was sustained for the entire differentiation period in N2B27 with combined monitoring of Rex1-GFP fluorescence signal and hydrogel stress profile. Traction forces progressively decreased as blebbistatin concentration increased (Figure.27). For the higher concentration (10μM), the traction forces were similar to background levels. This reduction in traction forces is consistent with what has been reported in the literature about myosin inhibition [309, 310] and, therefore, confirms the working of drug treatment in the system.

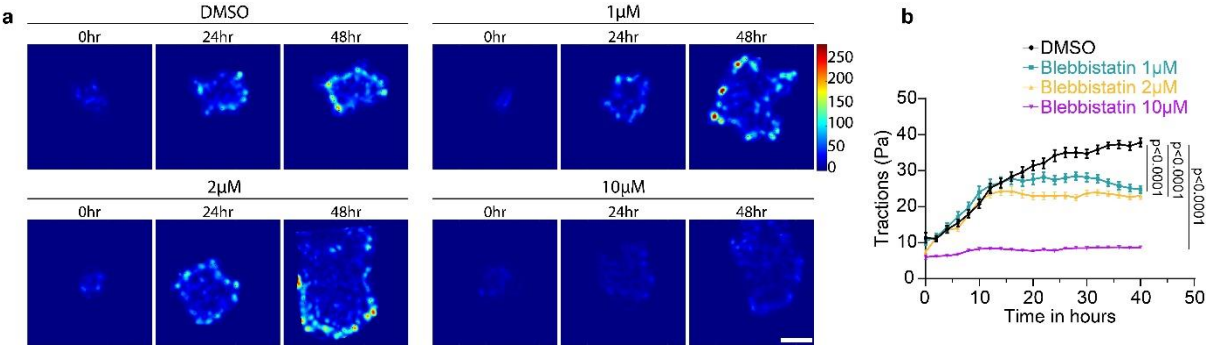

Figure.27: a. Representative heat maps of tractions exerted by mESC colonies in DMSO or different concentrations of blebbistatin. Scale bar is 20 μm. b. Corresponding quantification of traction forces averaged over colony area. Data from 3 independent experiments (n = 58/59/40/38 for DMSO/1μM-/2μM-/10μM-

Blebbistatin treatments). The effect of media change is significant (p<0.0001, one-way ANOVA with DMSO, for last time point).

Mirroring the traction force profiles, myosin inhibition had a profound effect on the Rex1-GFP signal with prolonged maintenance of fluorescence as blebbistatin concentration increased (Figure.28). The slowing down of pluripotency dissolution with blebbistatin treatment was also confirmed by a statistically significant decrease in decay constant values (Figure.28), showing a blebbistatin dose-dependent decrease in the decay constant of REX1-GFP signal.

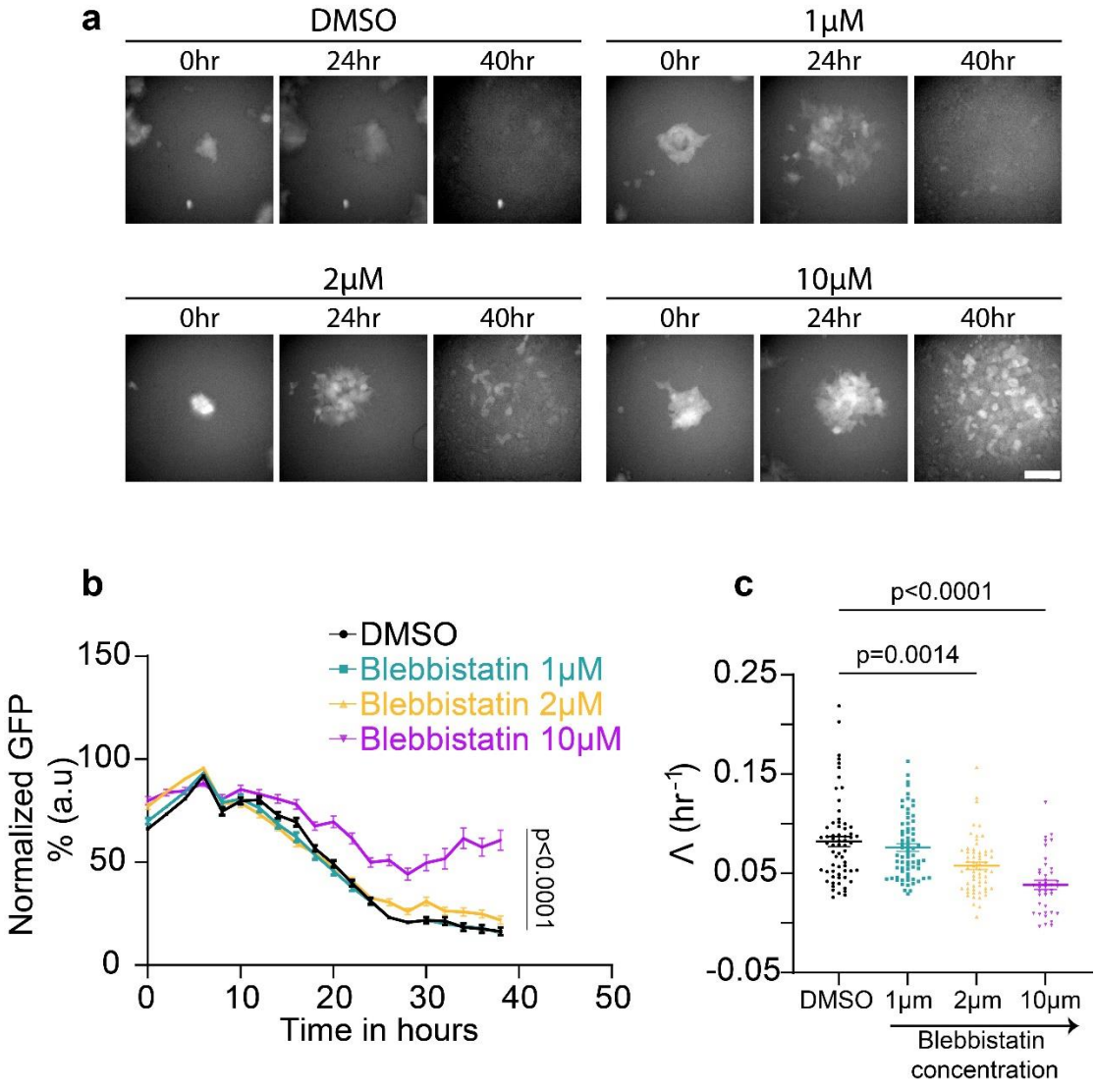

Figure.28: a. Rex1-GFP signal of mESC colonies in DMSO/1μM-/2μM-/10μM-Blebbistatin treatments as a function of time. Scale bar is 40 μm. b. Corresponding quantification of normalized Rex1-GFP mean intensity (Integrated fluorescence intensity averaged over colony area with maximum value taken to be 100%). 3 independent experiments (n = 65/70/61/40 for DMSO/1μM-/2μM-/10μM-Blebbistatin treatments). The effect of media change is significant (p<0.0001, Kruskal-wallis test with DMSO, for last time point). c. Decay constants obtained from exponential fitting of Rex1-GFP decay trajectories. 3 independent experiments (n = 65/70/61/40 for DMSO/1μM-/2μM-/10μM-Blebbistatin treatments). The effect of media change is significant (Kruskal-wallis test).

Besides force transmission to the matrix, myosin motor activity is required for permitting mitotic completion [269, 270] with its inhibition compromising cell division [271]. To assess if the observed effects of blebbistatin are because of impaired cell division, the change in colony area was measured. The rationale being, increase in cell count through mitosis contributes to an increase in colony area, the measure of colony spreading. It was found that colony area was lowered only for the highest concentration of blebbistatin. In fact, for both other concentrations employed, colony area was higher when compared to control condition (Figure.29). Therefore, the attenuated force transmission and accompanying delay in pluripotency dissolution upon blebbistatin treatment might be predominantly attributed to compromised mechanical function.

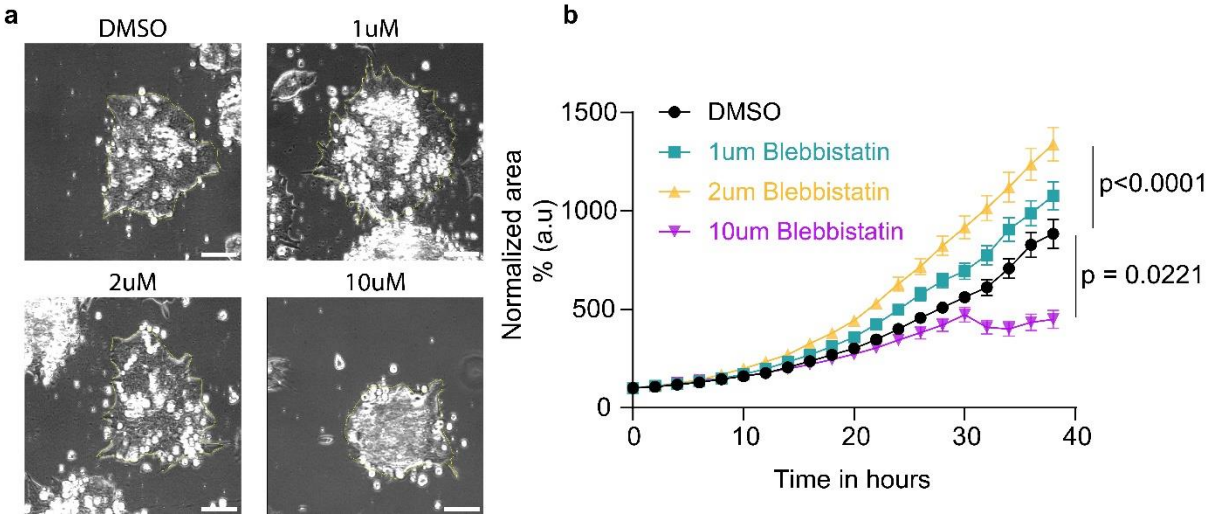

Figure.29: a. Representative phase contrast images of mESC colonies grown in indicated concentrations of blebbistatin for 48 hours. Colony borders are demarcated in yellow ROI. Scale bar is 50 µm. b. Quantification of colony area (normalized to initial value) as a function of time for mESC colonies grown in mentioned media. Data from 3 experiments (n=70/75/66/39 for DMSO/1µM-/2µM-/10µM-Blebbistatin treatments). Effect of media is statistically significant for the comparison between DMSO and 2µM-Blebbistatin, and, DMSO and 10µM-Blebbistatin. (Kruskal-wallis test, comparisons with respect to DMSO).

4.5.2 Substrate stiffness determines the rate of pluripotency dissolution

As a second approach to modulate cell-ECM interactions and mechanosensing, we modulated substrate stiffness. The tracking of naïve state exit was performed on PAA gels of 1.5kPa and 15kPa stiffness, in addition to the 5kPa we used for the rest of the experiments. A small yet measurable difference in Rex1-GFP signal progression with slower kinetics on soft substrate was observed and was confirmed by the lower decay constant values (Figure.30). The traction profiles were consistent with earlier observations as the conditions leading to quicker naïve state exit had higher forces transmitted to the matrix (Figure.30)

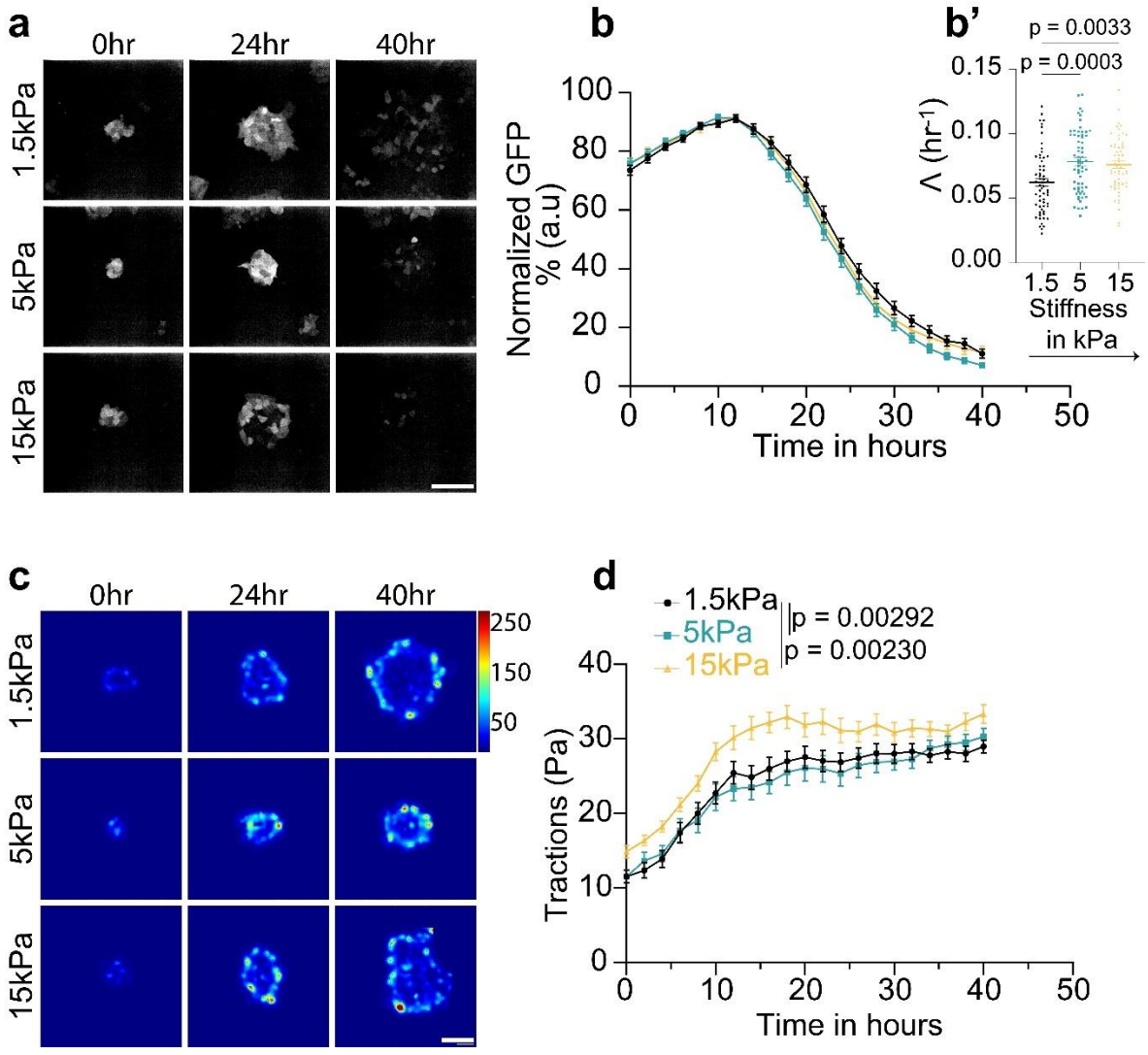

Figure.30: a. Representative images of Rex1-GFP signal of mESC colonies grown in mentioned stiffness conditions. Scale bar is 50 µm. b. Corresponding quantification of normalized Rex1-GFP mean intensity (Integrated fluorescence intensity averaged over colony area with maximum value taken to be 100%). 3 independent experiments (n = 61/64/57 for 1.5kPa/5kPa/15kPa). c. Decay constants λ obtained from exponential fitting of Rex1-GFP decay trajectories. 3 independent experiments. (n = 61/64/57 for 1.5kPa/5kPa/15kPa). The effect of stiffness is significant (One-way Anova Kruskal-wallis test, comparisons with respect to 1.5kPa)

When the evolution of traction forces and Rex1-GFP signal are taken together, both the above experiments are suggestive of pluripotency dissolution rate being proportional to the extent of force transmitted to the ECM.

The conclusions drawn so far are based on data pertaining to whole colony averages. A notable observation that was hitherto given little attention is the differences in the force and fluorescence profiles within distinct regions of a colony. This is discussed next.

4.6 Regional differences are heightened with pluripotency dissolution

4.6.1 Higher mechano-transduction at colony edge

When subjected to N2B27 differentiation, traction forces appeared to be predominantly concentrated at colony edges with the beginning of naïve identity loss and the same was confirmed by the quantification (Figure.31). For the differentiating colonies, traction forces in the exterior were found to be both increasing and always higher than the tractions from either region of mESC colonies grown in 2i (Figure.31).

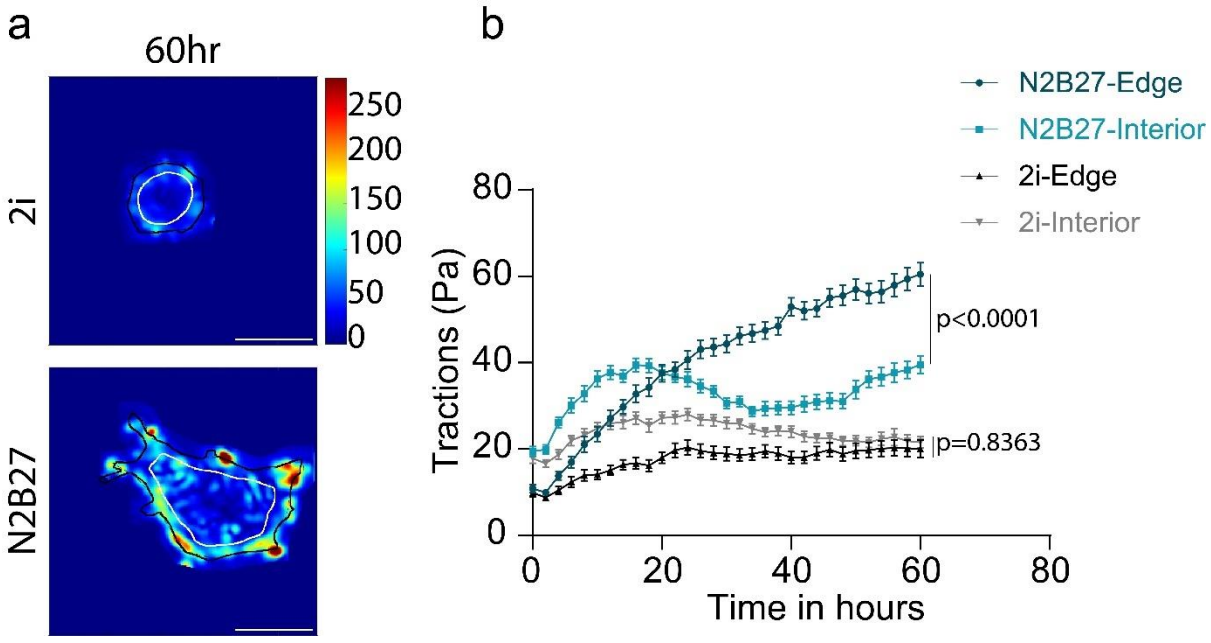

Figure.31: a. Representative traction heat maps of mESC colonies grown for 60 hours in mentioned media. The region between black and white outlines corresponds to edge, region within white outline is interior. Scale bar is 25 µm. b. Corresponding quantification of traction forces, as a function of time for edge and interior regions of mESC colonies grown in mentioned media. Data from 3 independent experiments (n = 48/62 colonies for 2i/N2B27). The effect of Edge vs Interior is significant only for N2B27 (Two-way ANOVA with repeated measures for last time point).

4.6.2 Rex1-GFP signal is lowered at the edges of the colony

Importantly, the Rex1-GFP signal was found to be significantly lower at the edge, in all time points, when compared to the interior and this holds true for colonies in both media conditions, 2i and N2B27 (Figure.32). Indeed, the fluorescence intensity of the colony edge resembled that of an isolated single cell with data supporting the same.

The distinction between edges of 2i-colonies and N2B27-colonies was revealed when the temporal profiles of the Rex1-GFP signal are considered. When in 2i, the fluorescence intensity of the colony edge was observed to increase with time whereas in N2B27, the signal extinguished. Concomitant with the rise in Rex1-GFP signal of their edges, naïve colonies' differences in traction forces between the two regions were ironed out. On the other hand, for colonies exiting pluripotency the traction force differences became starker with time (fig.32). Given these disparities, the fluorescence signal progression was compared between the two regions in differentiating colonies with an expectation of quicker naïve state exit at the edge. The measured decay constants were not significantly different during the differentiation condition, whereas for colonies maintained in 2i, the edge region had measurably higher decay constants.

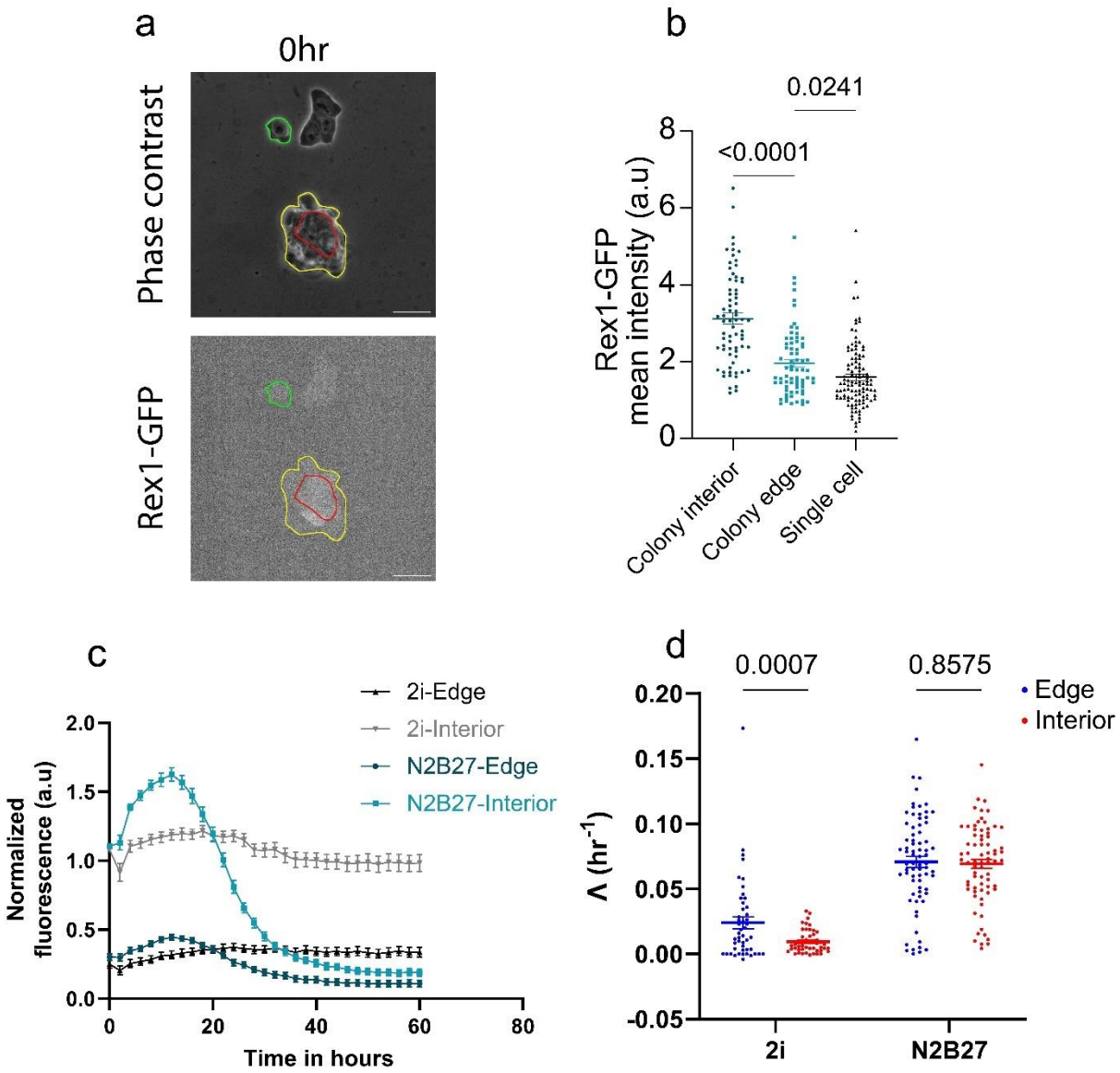

Figure.32: a. Representative phase-contrast image (top) and Confocal fluorescence image of green channel (bottom) for mESCs immediately after media change to N2B27. The region between the yellow and red outlines corresponds to colony edge, region within red outline is interior. Green outline corresponds to a single cell. Scale bar is 25µm. b. Comparison of Rex1-GFP mean-intensity between colony edge, colony interior and single cells, immediately after change of media to N2B27. Data from 3 experiments (n = 39/39/62 colonies for Colony-edge/Colony-interior/Single-cell). Only comparison between Colony-edge and Colony-interior are significantly different (One way ANOVA with respect to colony-edge). C. Quantification of Rex1-GFP intensity, as a function of time, resolved into edge and interior regions for mESC colonies grown in N2B27. Data from 3 independent experiments (n = 48/73 colonies for2i/N2B27). d. Quantificaiton of decay constants resolved into edge and interior regions for colonies grown in N2B27. Data from 3 independent experiments (n = 48/73 colonies for 2i/N2B27). Comparison between the regions is statistically significant for only 2i condition (Two-Way ANOVA with repeated measures)

The defining facet of colony edge is the reduction in cell-cell contact. This coupled with the increase in cell-matrix interaction has been shown to increase mechano-transduction and associated responses in edge cells, as was observed for traction forces. The conservation of this pattern needs to be verified and to this end, the spatial distribution of mechano-transduction markers was performed. Those results are discussed next.

4.6.3 Edge regions have higher nuclear localization of YAP

As a first attempt to check the consistency of regionalized differences for mechano-responses, the expression levels of YAP were measured. As discussed in the introduction, YAP is a well-established mechano-transducer [246,279] and pluripotency regulator [284]. Upon measuring the relative proportions of the subcellular distribution, YAP was found to be localized more in the nucleus for the edge cells in both media conditions and for all time points. An increase in YAP nuclear levels at colony edge was observed only in differentiation conditions (Figure.33). It is to be mentioned that no consistent pattern was observed when the whole colony averages of YAP nuclear to cytoplasmic ratio are compared between the two media conditions (Figure.33).

Importantly, this YAP localization pattern highlighted that mechanical signal relay changes the molecular signature of mESC nuclei. With this input, whether similar differences exist for the bonafide pluripotency markers was checked next.

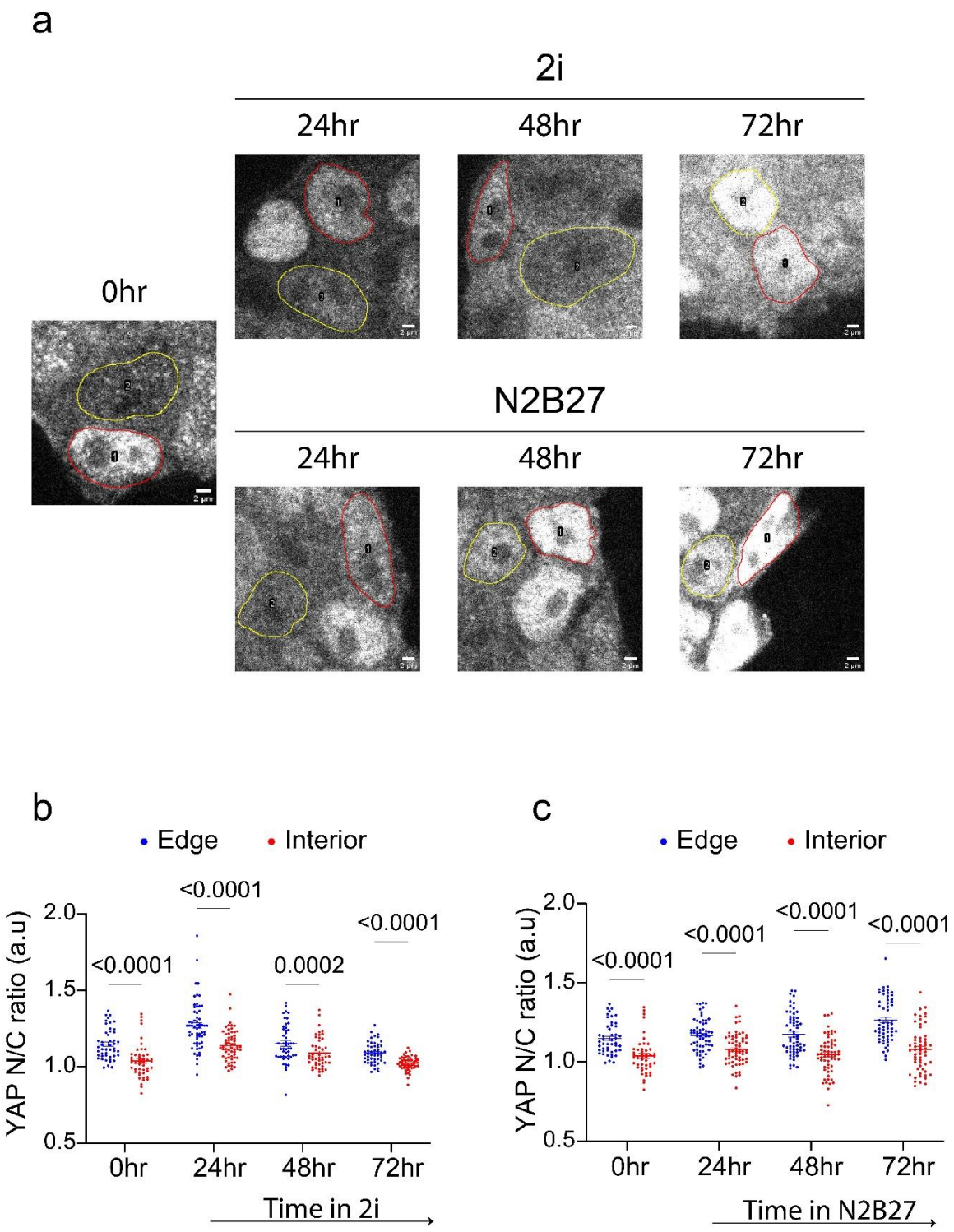

Figure.33: a. Representative fluorescence images of mESC colonies grown in 2i/N2B27 for mentioned time. Nuclear boundaries are demarcated with outlines, red corresponds to edge cell and yellow corresponds to interior cell. Scale bar is 2µm. b. Quantification of YAP nuclear to cytoplasmic ratio, resolved for edge and interior, and averaged for entire colony of mESC colonies grown in 2i for mentioned time. Data from 3 experiments (n = 47/61/49/51 colonies for 2i-0hr/2i-24hr/2i-48hr/2i-72hr). The Effect of Edge vs Interior is significant for all time points (Two-way ANOVA with repeated measures). C. Quantification of YAP nuclear to cytoplasmic ratio, resolved for edge and interior, and averaged for entire colony for mESC colonies grown in N2B27 for mentioned time. Data from 3 experiments (n = 47/62/62/57 colonies for 2i-0hr/N2B27-24hr/N2B27-48hr/N2B27-72hr). The effect of Edge vs Interior is significant for all time points (Two-way ANOVA with repeated measures).

4.6.4 Reduced naïve transcriptional signature and increased priming at colony edge

Along with higher mechano-transduction activity, cells at the colony edge presented lower Rex1-GFP signal. As the fluorescence readout is a marker of naïve pluripotency, we next tested if a similar profile exists for other naïve state transcriptional regulators.

For the absolute naïve state specifier Klf4, we observed similar levels between the edge and interior regions at all time points for both media conditions (fig.34).

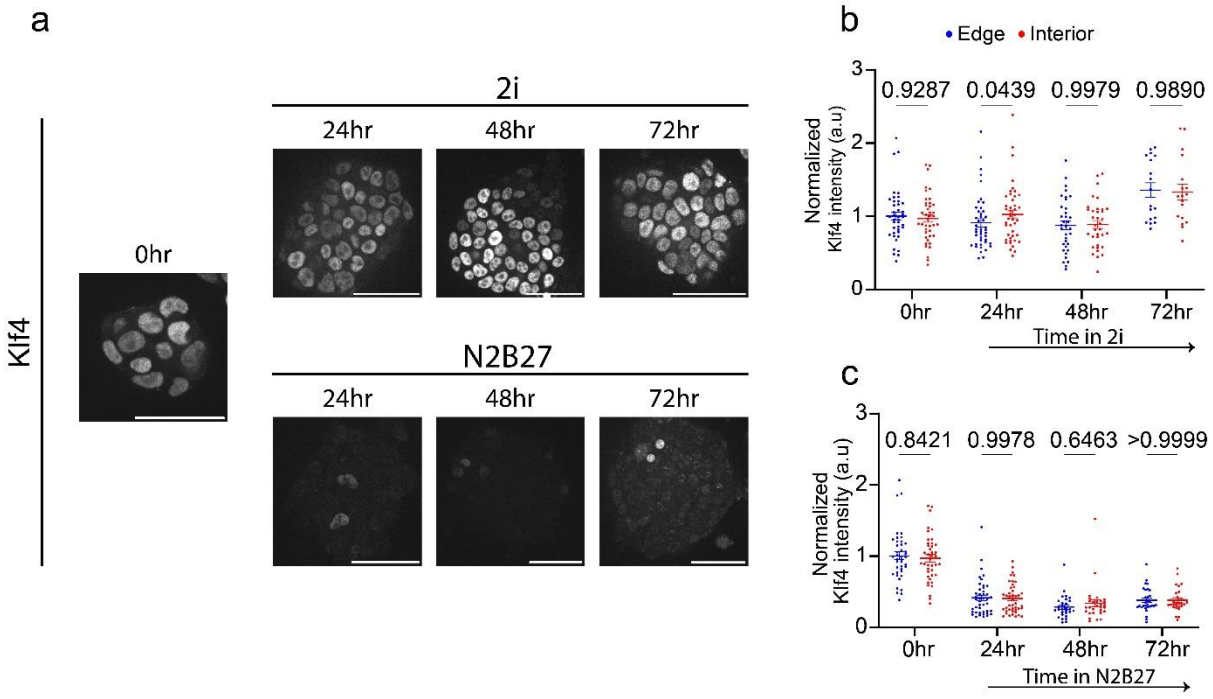

Figure.34: a. Representative images of mESC colonies immunostained for Klf4 in 2i (top)/N2B27 (bottom). Scale bar is 50 µm. b. Corresponding quantification of Klf4 nuclear intensity in 2i, colony edge vs Interior (n = 41/44/35/18/ for 2i-0hr/2i-24hr/2i-48hr/2i-72hr). 3 independent experiments. The effect of Edge vs Interior is not significant (Two-way ANOVA with repeated measures). c. Corresponding quantification of Klf4 nuclear intensity in N2B27, colony edge vs Interior(41/43/29/30 for 2i-0hr/N2B27-24hr/N2B27-48hr/N2B27-72hr). 3 independent experiments. The effect of Edge vs Interior is not significant (Two-way ANOVA with repeated measures)

For the other naïve state specifier Nanog, a clear distinction between the interior and edge regions was identified. Specifically, expression levels were lower in edge cells, indicating a more differentiated state (fig.35). The difference between regions was consistent across time points and media conditions (2i and N2B27) with high statistical significance.

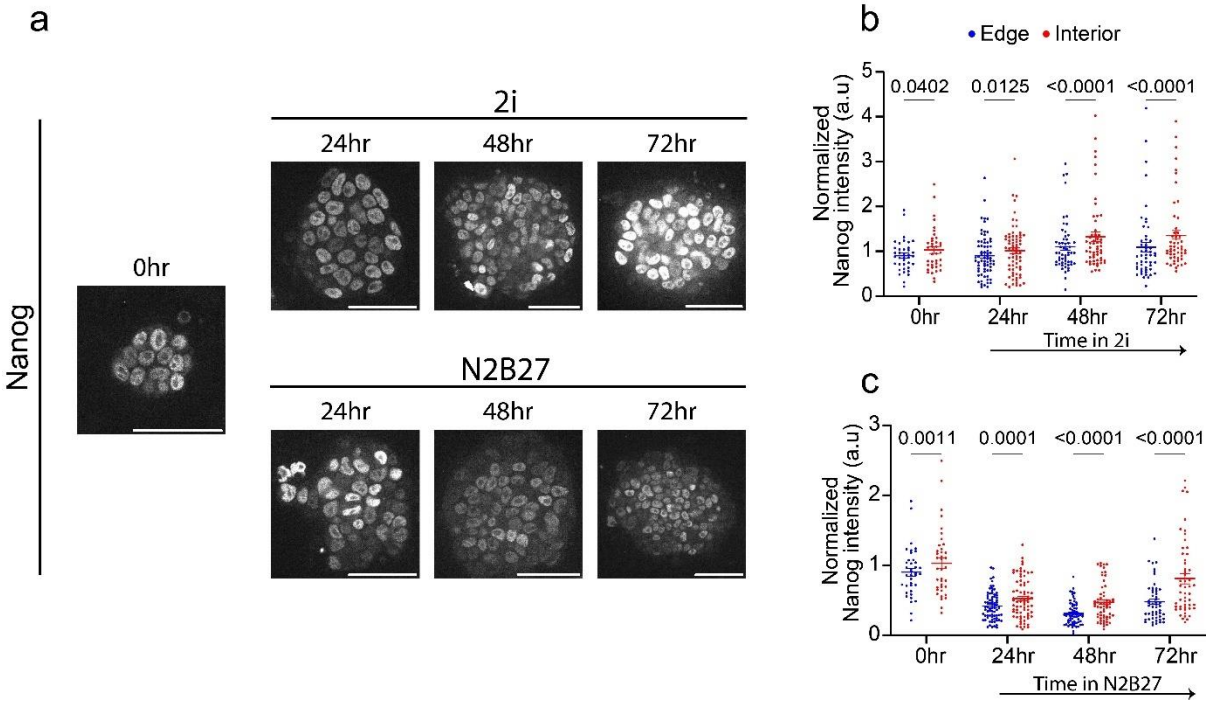

Figure.35: a. Representative images of mESC colonies immunostained for Nanog in 2i (top)/N2B27 (bottom). Scale bar is 50 µm. b. Corresponding quantification of Nanog nuclear intensity in 2i, colony edge vs Interior. 3 independent experiments. (n = 38/69/55/52 colonies for 2i-0hr/2i-24hr/2i-48hr/2i-72hr) The effect of Edge vs Interior and Time is significant (Two-way ANOVA with repeated measures). C. Corresponding quantification of Nanog nuclear in N2B27, colony edge vs Interior. 3 independent experiments (n = 38/74/60/52 colonies for 2i-0hr/N2B27-24hr/N2B27-48hr/N2B27-72hr). The effect of Edge vs Interior and Time is significant (Two-way ANOVA with repeated measures)

The disparity between edge and interior was maintained for post-implantation factor Otx2. However, in this case, Otx2 expression was higher for the edge cells (fig.36), again pointing to a more differentiated state. All the comparisons were statistically significant.

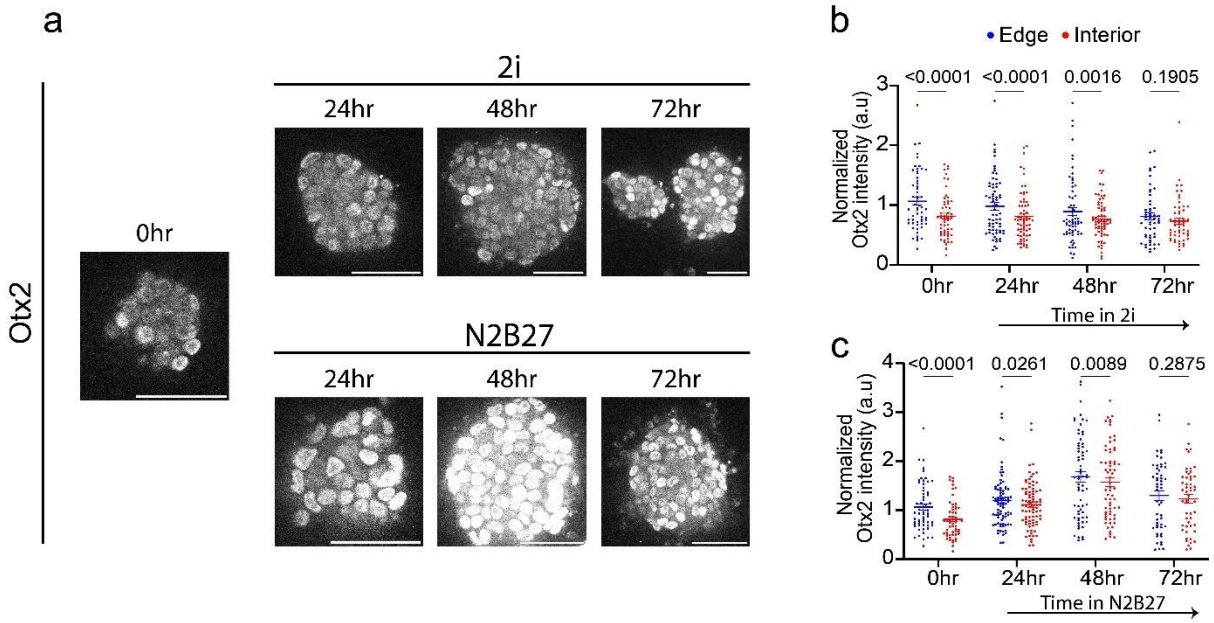

Figure.36: a. Representative images of mESC colonies immunostained for Otx2 in 2i (top)/N2B27 (bottom). Scale bar is 50 µm. b. Corresponding quantification of Otx2 nuclear intensity in 2i, colony edge vs Interior. 3 independent experiments (n = 57/67/65/54 colonies for 2i-0hr/2i-24hr/2i-48hr/2i-72hr). The effect of Edge vs Interior is significant for all except 2i-72hr, the effect of time is not significant (Two-way ANOVA with repeated measures). C. Corresponding quantification of Otx2 nuclear intensity in N2B27, colony edge vs Interior. 3 independent experiments (n = 57/83/66/52 colonies for 2i-0hr/N2B27-24hr/N2B27-48hr/N2B27-72hr). The effect of Edge vs Interior is significant for all except N2B27-72hr (Two-way ANOVA with repeated measures)

When taken together edge cells have lower naïve and higher formative factors. This attribute was observed even when naïve state is maintained and becomes more prominent with time after the commencement of pluripotency dissolution.

Differences in nuclear mechanotransduction is reported to alter the import/export of transcriptional regulators [255,256]. Whether this explains the disparity in transcription factor expression between in edge and interior regions was tested next.

4.6.5 Nuclear aspect ratio progressively increases at colony edge with pluripotency loss

Force transmission to the nucleus induces shape deformation leading to morphological asymmetry and as a measure of this parameter, nuclear aspect ratio was quantified. A more circular nucleus is indicated by an aspect ratio (AR) value of 1, and a value greater than 1 indicates a more elongated nucleus; the higher the value, the more elongated. Across the different time points in both media conditions, the aspect ratio of edge cells was always found to be higher than that of the interior (fig.37). Furthermore, the aspect ratios of edge cells showed a progressive increase when the colonies are differentiating (fig.37).

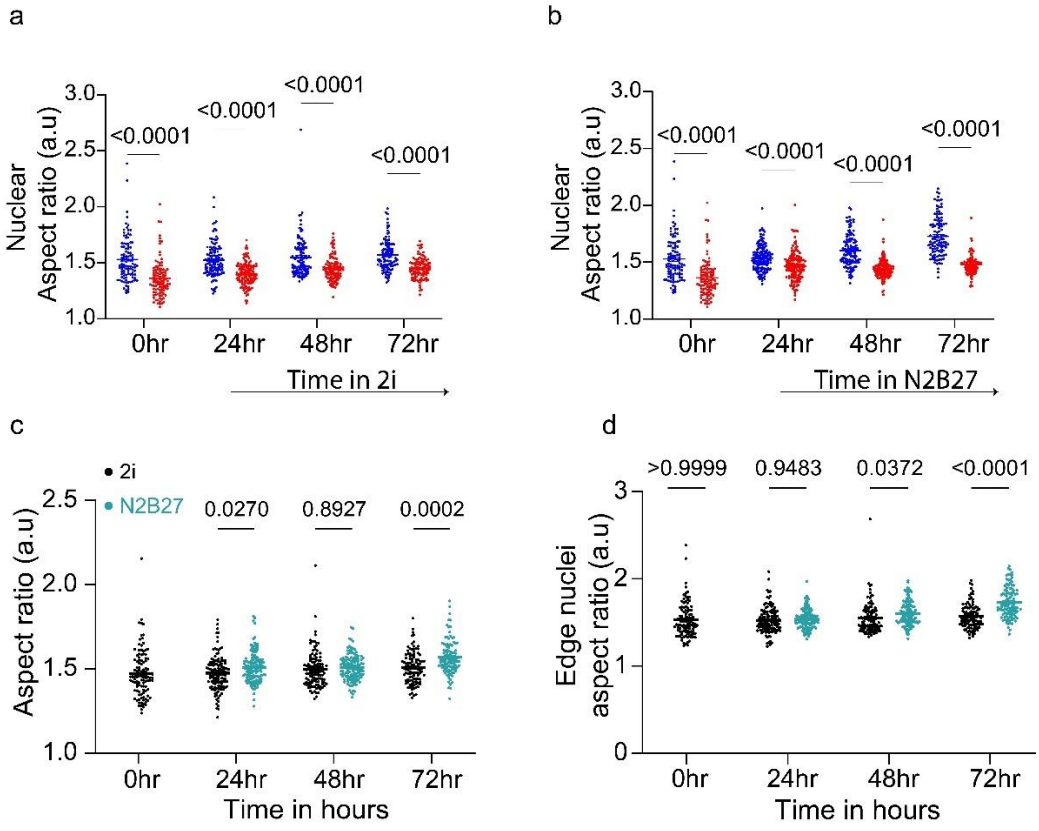

Figure.37: a. Quantification of nuclear aspect ratios, resolved for edge and interior, and averaged for entire colony for mESC colonies grown in 2i for mentioned time. Data from 6 experiments (n = 103/127/114/104 colonies for 2i-0hr/2i-24hr/2i-48hr/2i-72hr). Effect of Edge vs Interior is significant for all time points (Two-way ANOVA with repeated measures). b. Quantification of nuclear aspect ratios, resolved for edge and interior, and averaged for entire colony for mESC colonies grown in N2B27 for mentioned time. Data from 6 experiments (n = 103/145/128/108 colonies for 2i-0hr/ N2B27-24hr/N2B27-48hr/N2B27-72hr). The effect of Edge vs Interior is significant for all time points (Two-way ANOVA with repeated measures). c. Quantification of nuclear aspect ratios, averaged for entire mESC colonies. Data from 6 independent experiments (n = 103/127/114/104/145/128/108 colonies for 2i-0hr/2i-24hr/2i-48hr/2i-72hr/N2B27-24hr/N2B27-48hr/N2B27-72hr). The effect of media change is significant for only the comparison between 2i-72hr and N2B27-72hr (Two-way ANOVA without repeated measures) d. Quantification of edge cell nuclear aspect ratios, averaged for entire mESC colonies. Data from 6 independent experiments (n = 103/127/114/104/145/128/108 colonies for 2i-0hr/2i-24hr/2i-48hr/2i-72hr/N2B27-24hr/N2B27-48hr/N2B27-72hr). The effect of media change is significant for comparisons between 2i and N2B27 at 48hr and 72hr time points (Two-way ANOVA with repeated measures)

Of note, no consistent differences between the nuclear aspect ratios of naïve and differentiating conditions was observed when the whole colony averaged were compared (Figure.37). Despite this, the fidelity of aspect ratios as an indicator of mechanical signal relay was confirmed when the nuclear AR was quantified for blebbistatin-treated cells. Compared with control samples (DMSO treated cells), nuclei of blebbistatin-treated cells presented consistently lower aspect ratios (Figure) highlighting the attenuated force transmission (Figure.37).

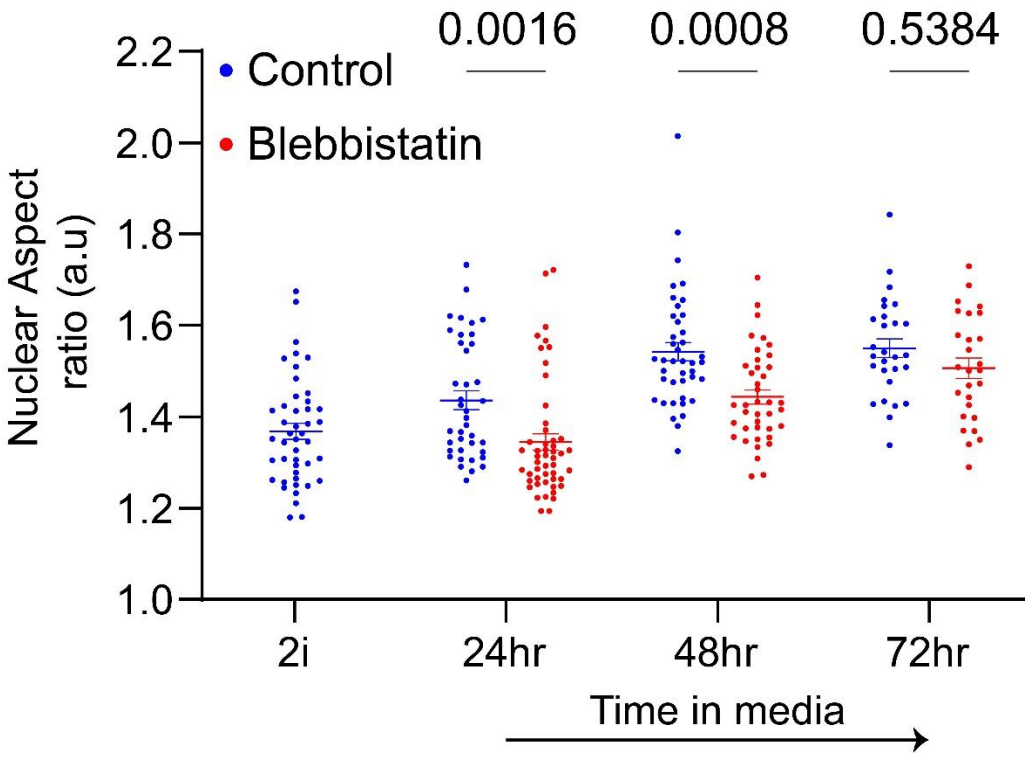

Figure.38: Quantification of Nuclear aspect ratio averaged over colony for mESC colonies grown in mentioned media. Data from 3 independent experiments (n = 45/39/50/41/40/28/27 colonies for 2i-0hr/N2B27+DMSO-24hr/N2B27+ 10µM-Blebbistatin –24hr/N2B27+DMSO-48hr/N2B27+48hr- 10µM-Blebbistatin/ N2B27+DMSO-72hr/N2B27+10µM-Blebbistatin-72hr). The effect of media change is statistically significant (Two-way ANOVA without repeated measurements)

The mechano-responses at the edge coupled with the transcriptional profiles, Rex1-GFP signal and nuclear shapes demonstrate that force transmission to the nucleus is at play to regulate pluripotency exit. To test this, Rex1-GFP cell lines with differences in nucleus-cytoskeleton linkage affinity were subjected to differentiation. The next sub-section discusses those results.

4.7 Disruption of Nucleus-Cytoskeleton linkage mildly affects pluripotency exit kinetics

Forces are transmitted to the cell nucleus through actomyosin contractility. Actin is directly bound to the nucleus through the LINC complexes. This function is executed by the KASH domain protein Nesprin. The earlier experiments dealing with interference in mechano-transduction either attenuated force transmission (blebbistatin treatment) or modulated it (seeding on multiple stiffness). Whether the pluripotency dissolution rate is affected when mechanical signal transmission to the nucleus is disrupted needs elucidation. We therefore used a dominant negative KASH, from here on DN-KASH, construct that disrupts actin-nesprin 1,2 interactions [REF]. The expression of DN-KASH was placed under the inducible control by doxycycline, which when supplemented in the media triggers the expression of DN-KASH, thereby abrogating the actin tethering to the nucleus [272,273]. As a control, a truncated form of the DN-KASH construct (ΔPP) that abolishes the dominant negative effect was used [272,273].

The Rex1-GFP signal progression in these two cell lines was monitored with doxycycline provision and two inhibitor withdrawal. The fluorescence intensity profiles indicated the delay of pluripotency dissolution only upon the induction of DN-KASH (Figure.39). The decay constants confirmed the same, as the values corresponding to doxycycline induction of DN-KASH were markedly lower (Figure). Of note these differences were small yet significant and were observed only when the pluripotency exit protocol was performed on glass substrates. On PAA gels, pluripotency dissolution kinetics remained unaffected irrespective of actin-nucleus coupling status (Figure.39). The minimal effect on force transmission upon DN-KASH induction was affirmed by nuclear shape measurements for which changes were not detectable (Figure.39).

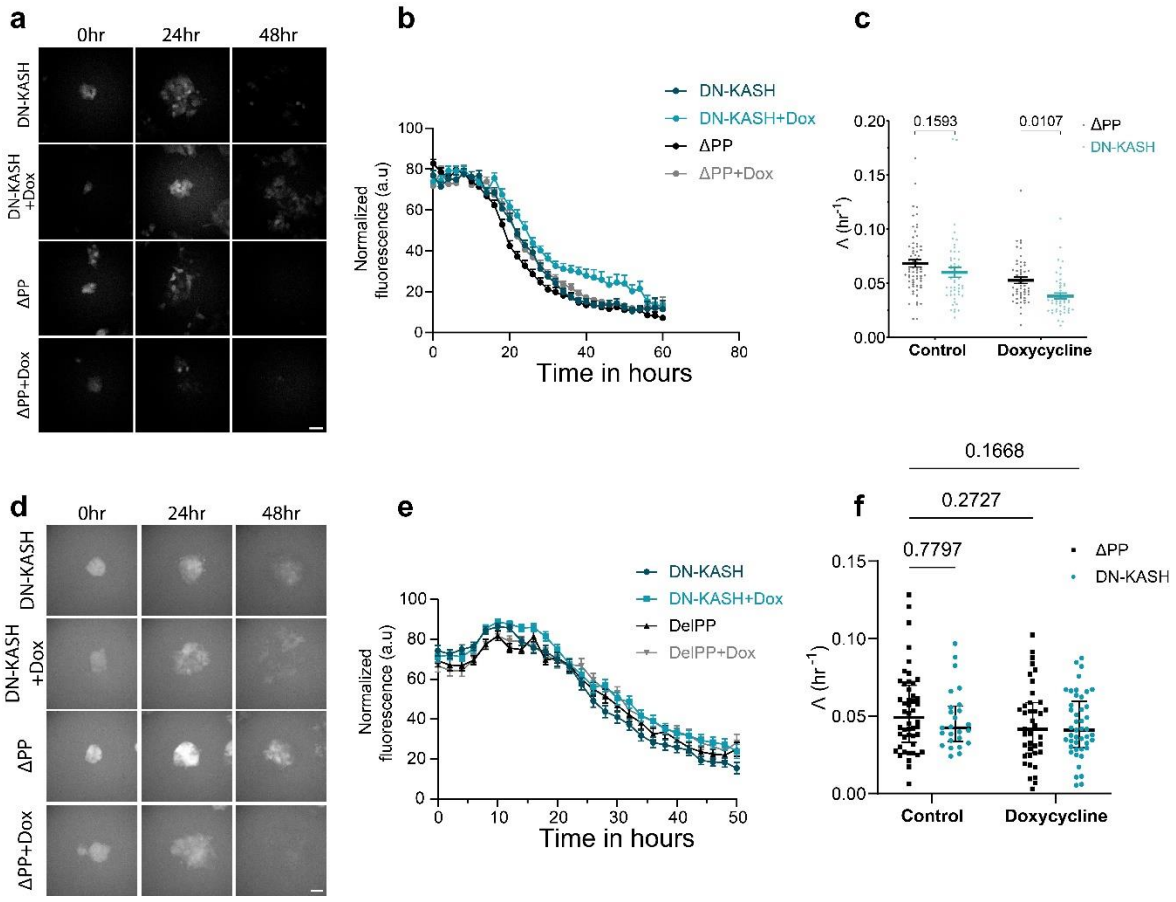

Figure.39: a. Representative fluorescence images of mESC colonies of DN-KASH/DelPP genetic background grown for mentioned time points in N2B27 on glass substrates. Scale bar is 50 µm Doxycycline treatment corresponds to induction and was added at 0hr (along with N2B27). b. Corresponding quantification of normalized Rex1-GFP intensity, as a function of time for each genetic background. Data from 3 independent experiments (n = 50/48/70/54 colonies for DN-KASH/DN-KASH+Doxycycline/ΔPP/ΔPP+Doxycycline). c. Quantification of decay constants for corresponding to Rex1-GFP quantificaiton in (m). Data from 3 independent experiments (n = 50/48/70/54 colonies for DN-KASH/DN-KASH+Doxycycline/ΔPP/ΔPP+Doxycycline). The effect of genetic background is significant only in Doxycycline induced conditions (Two-way AOVA without repeated measurements). d. Representative fluorescence images of mESC colonies of DN-KASH/ΔPP genetic background grown for mentioned time points in N2B27 on 5kPa polyacrylamide gels coated with Laminin. Scale bar is 50 µm. Doxycycline treatment corresponds to induction and was added at 0hr (along with N2B27). e. Corresponding quantification of normalized Rex1-GFP intensity, as a function of time for each genetic background. Data from 3 independent experiments (n = 25/48/45/39 colonies for DN-KASH/DN-KASH+Doxycycline/ΔPP/ΔPP+Doxycycline). f. Quantification of decay constants for corresponding to Rex1-GFP quantificaiton in d). Data from 3 independent experiments (n = 25/48/45/39 colonies for DN-KASH/DN-KASH+Doxycycline/ΔPP/ΔPP+Doxycycline). The effect of genetic background is significant only in Doxycycline induced conditions (Two-way AOVA without repeated measurements)

Force relay to nucleus has already been shown to alter the subcellular concentrations of transcription factors, example YAP, but in other systems [255,256]. To verify if this is recapitulated and can be applied to pluripotency factors, correlation analysis between nuclear shape and protein expression levels was performed and those results are dealt next.

4.8 Nuclear aspect ratio's prediction of protein expression is weak

From traction forces to transcription factor profiles, colony edge displayed striking differences that were preserved across conditions. Besides, with relatively greater cell-matrix interaction, the edge cells are best positioned making their nuclei the yardstick to assess mechano-transduction activity. To confirm this, the relative nuclear levels of YAP were compared with the aspect ratio. A positive correlation that is weak yet significant was observed (Figure.40) and given that aspect ratio stands as a measure of nuclear deformation, the result is consistent with what has been reported [256].

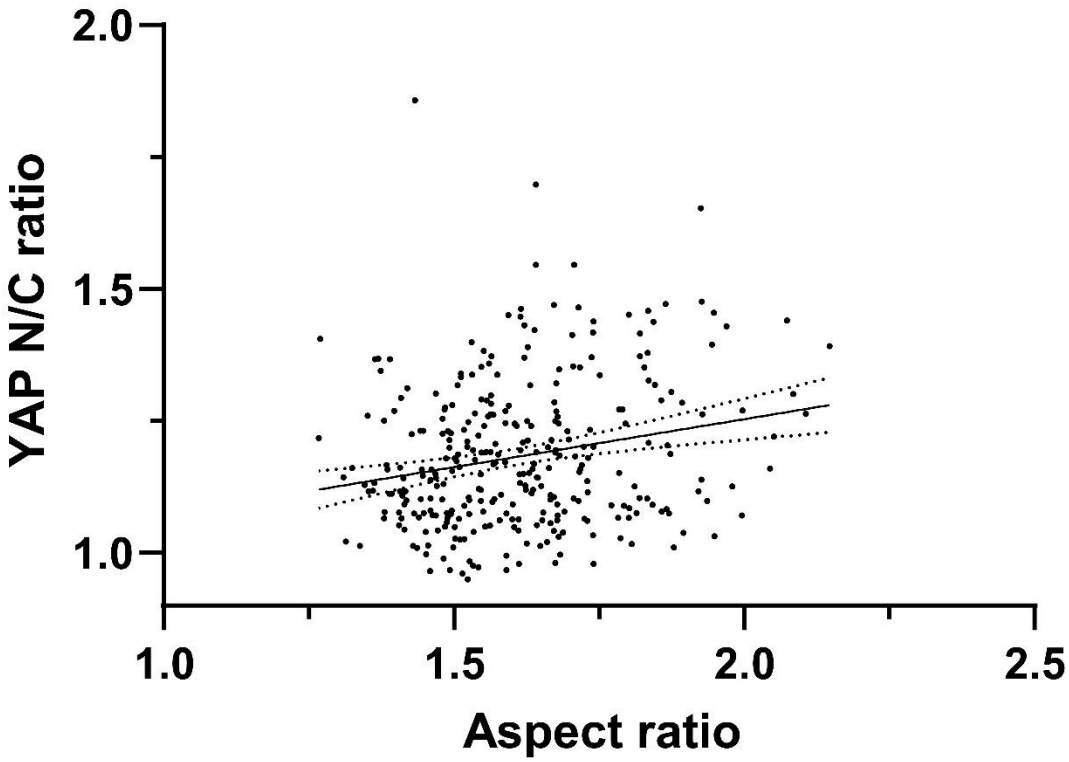

Figure.40: Correlation analysis between YAP Nucelar to cytoplasmic ratio and nuclear aspect ratio for edge cells. Each data point represent averaged value of an mESC colony. Data from 3 independent experiments (n = 315 mESC colonies). The comparison was found to be statistically significant. (Pearson correlation analysis: $R^2 = 0.04578$, $p < 0.0001$)

With this justification the focus was shifted to *Nanog* and *Otx2*. The reasons for the selection these two pluripotency factors are twofold. Firstly, regional differences in expression profiles were consistently maintained for both. Secondly, their regulation of transcriptional activity on Rex1 promoter, which in the current system translates to GFP signal, is well documented. In other words, *Nanog and Otx2* expression levels are the molecular origins for Rex1-GFP intensity which in turn was found to be inversely proportional to levels of mechano-transduction that can be deduced from nuclear shape. Given this background information, whether the temporal expression patterns of *Nanog* and *Otx2* are reflected by nuclear morphometrics was tested.

For *Nanog*, a negative correlation with the nuclear aspect ratio was observed (Figure.41) and although it is weak, the analysis was found to be statistically significant. For *Otx2*, the correlation was neither strong nor significant (Figure.41).

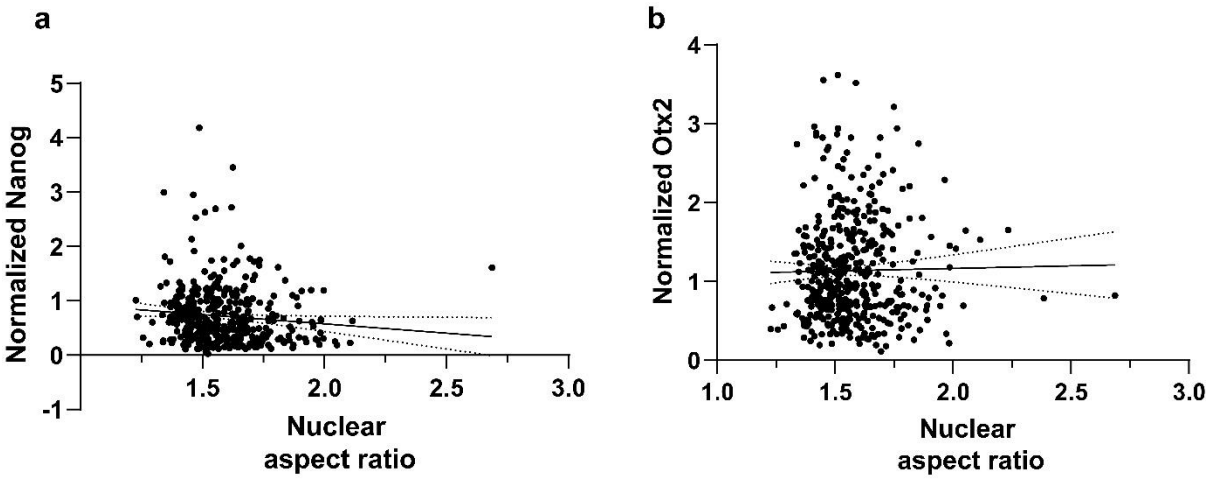

Figure.41: a. Correlation analysis between Nanog expression and nuclear aspect ratio of edge cells. Each data point represents averaged value of an mESC colony. Data from 3 independent experiments (n = 400 mESC colonies). The comparison was found to be statistically significant. (Pearson correlation analysis: R^2 = 0.01153, p = 0.0318). b. Correlation analysis between Otx2 expression and nuclear aspect ratio of edge cells. Each data point represents averaged value of an mESC colony. Data from 3 independent experiments (n = 444 mESC colonies). The comparison was not statistically significant. (Pearson correlation analysis: R^2 = 0.0002654, p = 0.7321)

Consistent with these results were the measurements of *Nanog* and *Otx2* expression levels upon blebbistatin treatment. Although the nuclei displayed lower deformation as confirmed by smaller aspect ratio values, no changes in expression levels of the two proteins was observed when compared with the control samples (Figure.42).

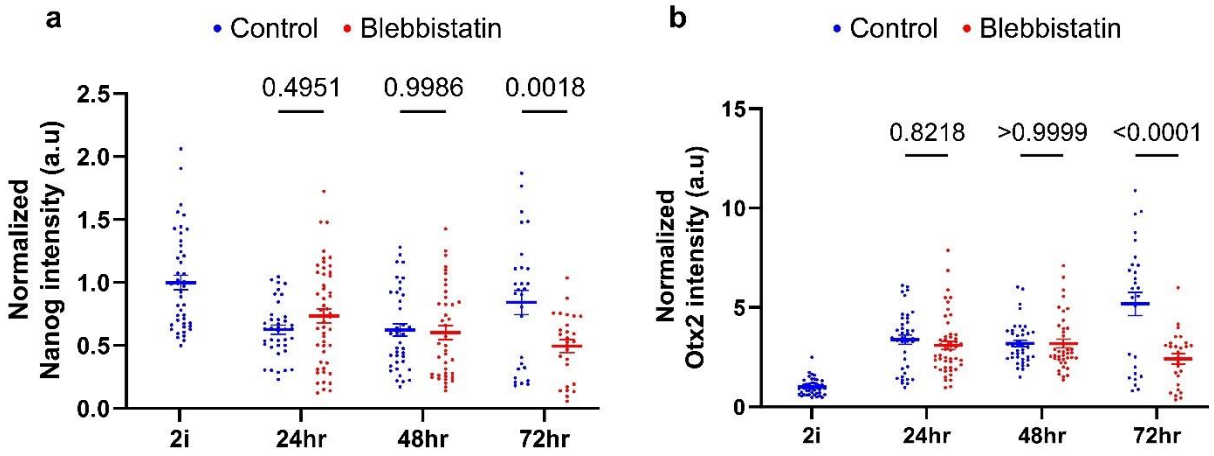

Figure.42: a. Quantification of Nanog nuclear intensity averaged over colony for mESC colonies grown in mentioned media. Data from 3 independent experiments (n = 45/39/50/41/40/28/27 colonies for 2i-0hr/N2B27+DMSO-24hr/N2B27+ 10µM-Blebbistatin –24hr/N2B27+DMSO-48hr/N2B27+48hr- 10µM-Blebbistatin/ N2B27+DMSO-72hr/N2B27+10µM-Blebbistatin-72hr). The effect of media change is statistically significant (Two-way ANOVA without repeated measurements). b. Quantification of Otx2 nuclear intensity averaged over colony for mESC colonies grown in mentioned media. Data from 3 independent experiments (n = 45/39/50/41/40/28/27 colonies for 2i-0hr/N2B27+DMSO-24hr/N2B27+ 10µM-Blebbistatin –24hr/N2B27+DMSO-48hr/N2B27+48hr- 10µM-Blebbistatin/ N2B27+DMSO-72hr/N2B27+10µM-Blebbistatin-72hr). The effect of media change is statistically significant (Two-way ANOVA without repeated measurements)

All in all, despite the reliability to infer mechano-transduction, nuclear aspect ratio could only weakly predict the protein expression changes and hence falls short in accounting for pluripotency dissolution.

In order to adequately explain naïve state exit, attention was given to the understand the biochemical logistics of pluripotency dissolution and how they police mechanical signalling. The experimental efforts in this direction and the corresponding results are detailed next.

4.9 Preserving β-catenin signalling is minimally sufficient to safeguard naïve identity

The initiator of naïve state exit in single cells was identified to be the nuclear export of Klf4 that is triggered by ERK signalling [132]. This is countered by the small molecular inhibitor PD0325901, from here on PD, which prevents ERK phosphorylation. The second inhibitor CHIR99021, from now on Chir, inhibits the kinase activity of GSK3β thereby withholding β-catenin phosphorylation and subsequent degradation. The mechanical implications of maintaining β-catenin expression acquire greater prominence in colonies given that it stabilizes cadherin adhesion [274, 275] and promotes Ezrin phosphorylation thereby conferring high membrane tension to the cells [190]. Mechanical signalling is reported to activate both ERK pathway and β-catenin degradation [142, 276] highlighting their close association with mechano-transduction. To evaluate which among the two molecular events exerts a dominant control in determining naïve pluripotency exit, the Rex1-GFP signal was monitored with the removal of only one of the two inhibitors.

The media conditions are mentioned as N2B27+Chir (for PD removal and hence ERK activation) and N2B27+PD (for Chir removal and hence β-catenin degrading). Fluorescence intensities in 2i and N2B27 media were measured for reference. In contrast to what has been reported earlier, ERK activation alone didn't lead to naïve state exit as no decline in Rex1-GFP signal was observed even after culturing for ~2 days in N2B27+Chir (ERK activation alone) (Figure.43). The gradual loss of fluorescence signal in N2B27+PD (ERK inhibition) asserts the same (Figure.43).

Interestingly, the progression of Rex1-GFP signal upon β-catenin preservation was highly similar to what was observed for 2i media. Moreover, the decay constants for both the conditions were not measurably different (Figure.43). Whereas, the fluorescence dwindled in both the standard differentiation condition (N2B27) and ERK-only inhibition (N2B27+PD), though at a slower rate in the latter.

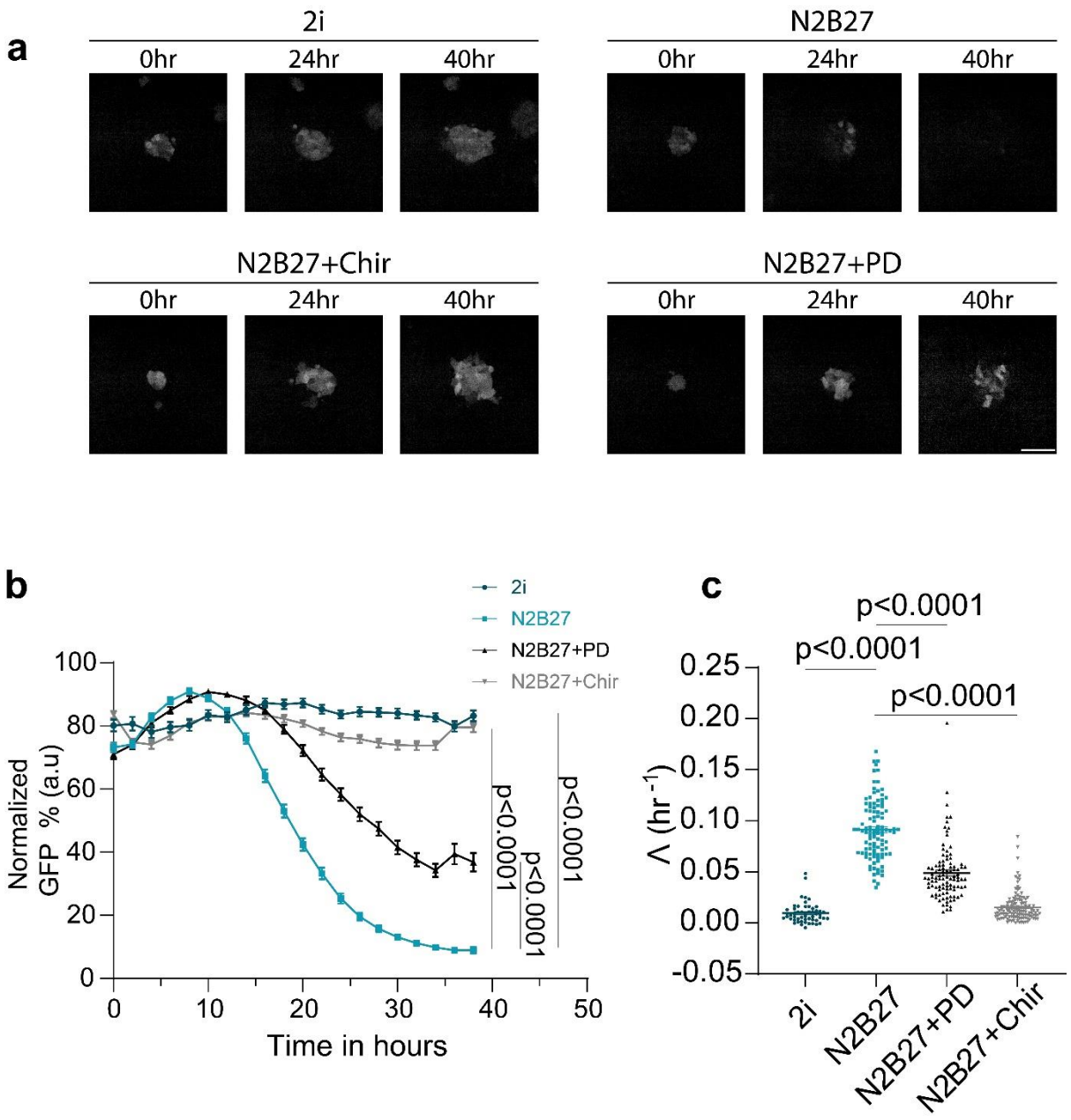

Figure 43: a. Representative images of Rex1-GFP signal of mESC colonies in 2i/N2B27/N2B27+PD/N2B27+Chiron as a function of time. Scale bar is 40 µm. b. Corresponding quantification of normalized Rex1-GFP mean intensity (Integrated fluorescence intensity averaged over colony area with maximum value taken to be 100%). 3 independent experiments (n = 53/106/101/129 for 2i/N2B27/N2B27+PD/N2B27+Chiron). The effect of media change is significant (p<0.0001, Kruskal-wallis test, comparisons with N2B27, for last time point). c. Decay constants obtained from exponential fitting of Rex1-GFP decay trajectories. 3 independent experiments (n = 53/106/101/129 for 2i/N2B27/N2B27+PD/N2B27+Chiron). The effect of media change is significant (Kruskal-wallis test, comparisons with N2B27)

Importantly, these fluorescence profiles suggest that for pluripotency dissolution in colonies the weakening of cell adhesions mediated by β-catenin degradation is obligatory. Substantiating the same, mESC colonies were observed to have high naïve factor expression (Figure.44 and Figure.45) and lower levels of post-implantation factor (Figure.46). Moreover, the molecular annotation of pluripotency priming which is increased Otx2 levels was observed in N2B27+PD with high degree of similarity to standard differentiation condition (N2B27) (Figure.45).

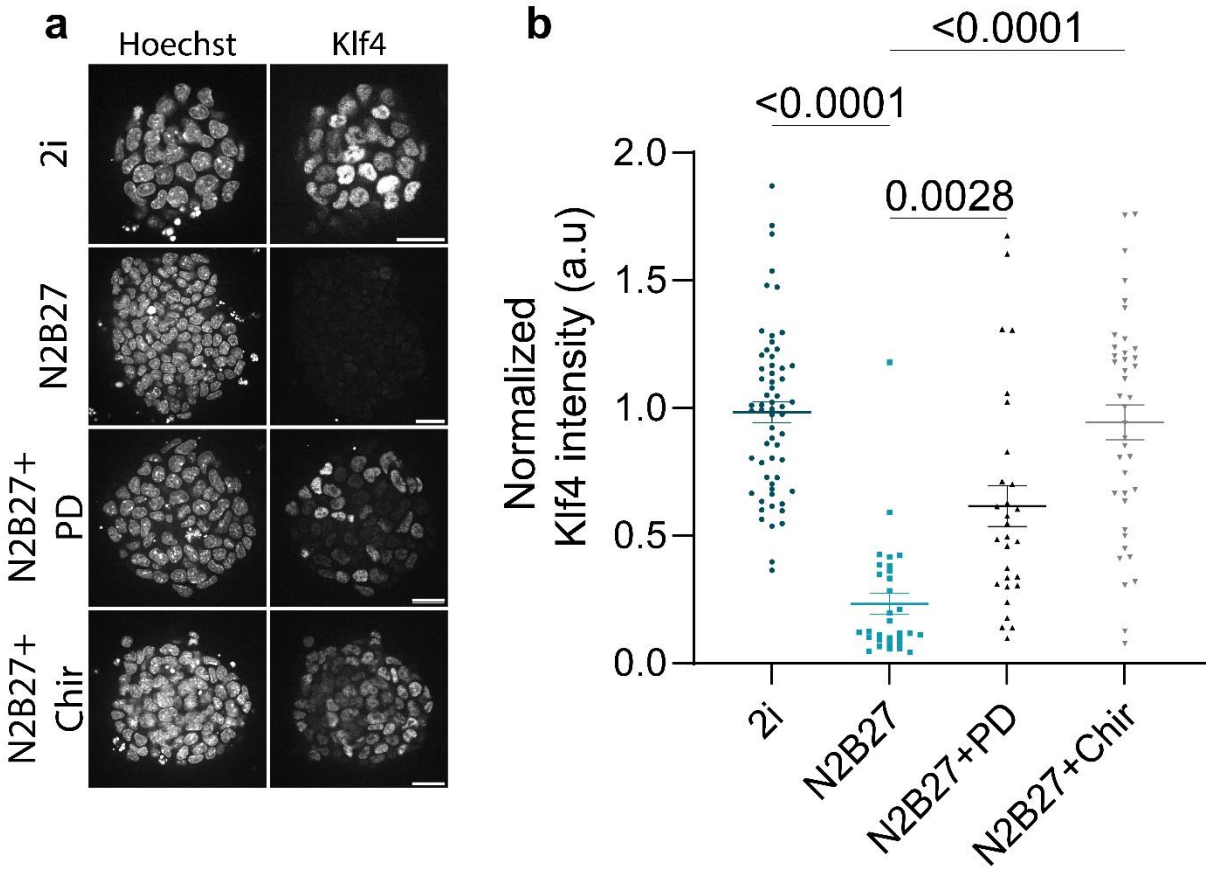

Figure.44: a. Representative immunofluorescence images of Klf4 after 48-hour culture on 5kPa polyacrylamide gels in 2i/N2B27/N2B27+PD/N2B27+Chiron media. Scale bar is 25µm. b. Corresponding quantification of normalized nuclear intensity averaged over colony. Data from 3 independent experiments (n = 61/31/29/40 for 2i/N2B27/N2B27+PD/N2B27+Chiron). The effect of media change is significant (One-way ANOVA).

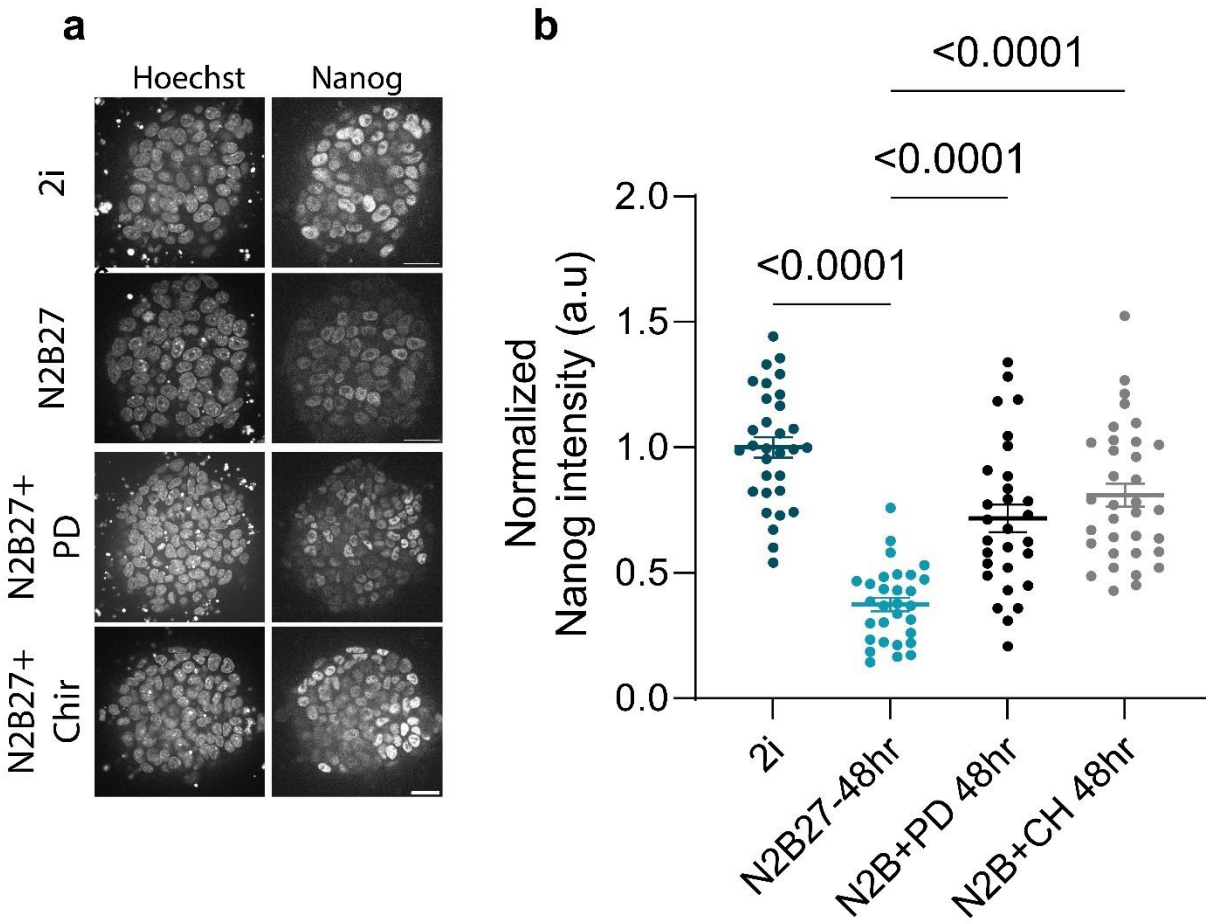

Figure.45: a. Representative immunofluorescence images of Nanog after 48-hour culture on 5kPa polyacrylamide gels in 2i/N2B27/N2B27+PD/N2B27+Chiron media. Scale bar is 25µm. b. Corresponding quantification of normalized nuclear intensity of Nanog, averaged over colony. Data from 3 independent experiments (n =35/30/29/34 for 2i/N2B27/N2B27+PD/N2B27+Chiron). The effect of media change is significant (One-way ANOVA).

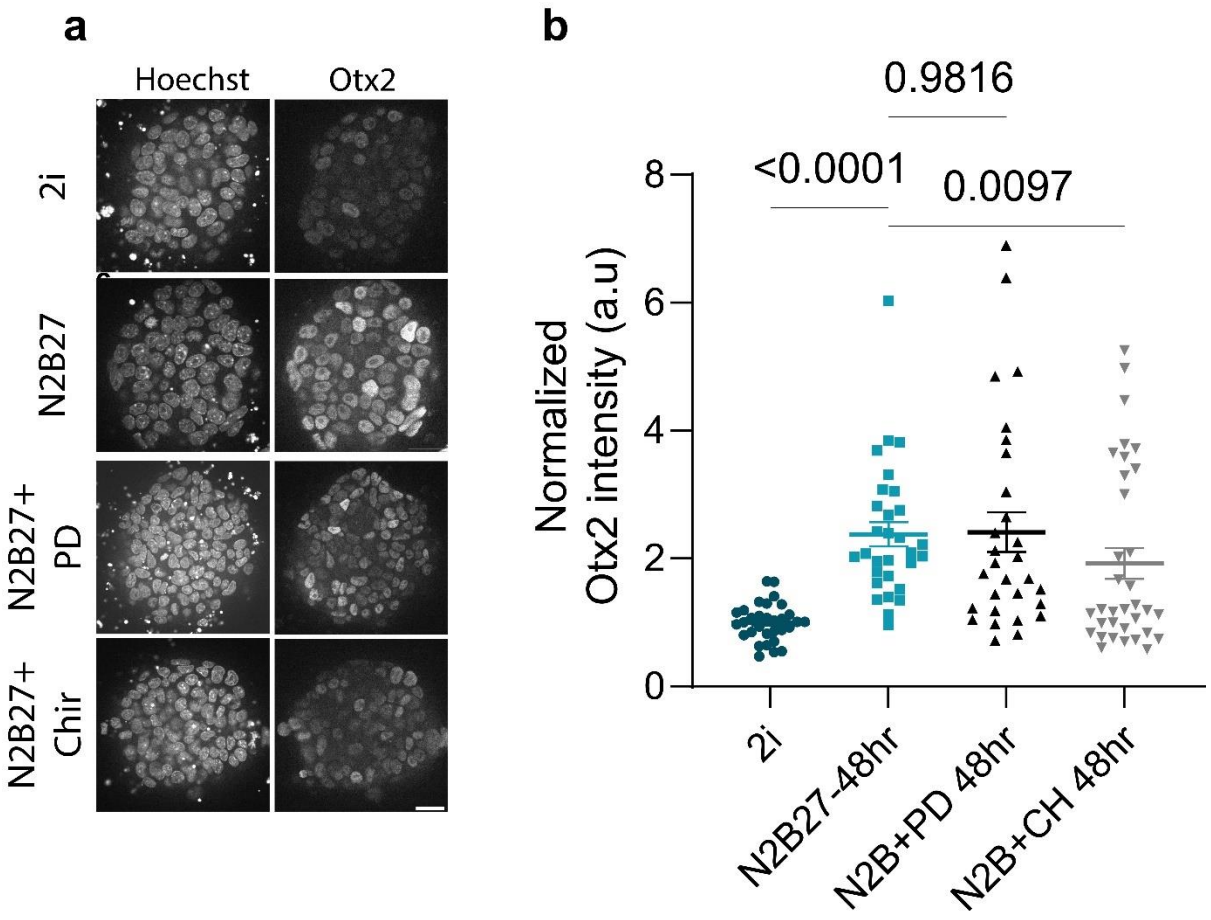

Figure.46: a. Representative immunofluorescence images of Otx2 after 48-hour culture on 5kPa polyacrylamide gels in 2i/N2B27/N2B27+PD/N2B27+Chiron media. Scale bar is 25µm. b. Corresponding quantification of normalized nuclear intensity of Otx2, averaged over colony. Data from 3 independent experiments (n =35/30/29/34 for 2i/N2B27/N2B27+PD/N2B27+Chiron). The effect of media change is significant (One-way ANOVA).

Taken together all these results establish that sustenance of β-catenin signalling is minimally sufficient to ensure long term preservation of naïve pluripotency.

To verify that the above-mentioned traits are driven by mechanical signalling, the putative mechano-responses were measured, and those results are discussed below.

4.10 Cell-cell adhesion strengthening by β-catenin lowers cell-matrix interaction

Cadherin junctions' role in regulating pluripotency is well documented [75,195]. Its influence in modulating mechano-transduction is also well understood, although it was elucidated in other cell systems [194]. Despite these implications, the regulation of mechanoreponses in mESC colonies by cadherins was hitherto investigated. Given that β-catenin stabilises cadherins [274,275], the single inhibitor experiments stand to answer this and to do so, the real-time monitoring of two parameters was performed: colony morphology and traction forces.

The spreading of colony, earlier identified as a marker for pluripotency exit, is found to be mediated, in other systems, by progressive weakening of cell adhesion [194]. In case of mESC colonies, spreading is measured as area growth. Since insulating β-catenin from GSK3β's mediated degradation conserved naïve pluripotency, the temporal progression of area for colonies in N2B27+Chir was measured and compared with values in other media combinations. While the colony areas increased consistently for all, the growth rate for N2B27+Chir was not as steep as it was for N2B27 and N2B27+PD, the two media conditions in which pluripotency dissolution occurred (Figure.45). In fact, the area growth of N2B27+Chir was closer to 2i, whose naïve maintenance is implacable. Moreover, colonies in 2i and N2B27+Chir propagated as 3D compact domes while for NB27 and N2B27+PD, cell spreading was observed (Figure.45)

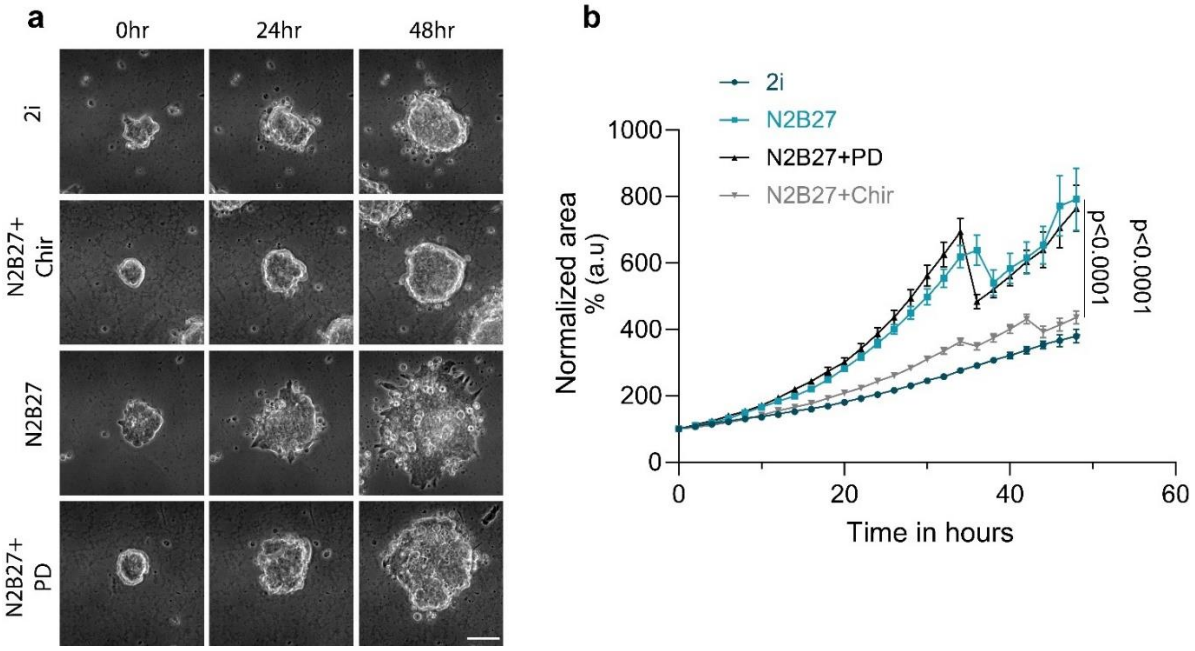

Figure.45: a. Representative Phase contrast images of mESC colonies in 2i/N2B27/N2B27+PD/N2B27+Chiron. Scale bar is 50 µm. b. Corresponding quantification of colony area. Data from 3 independent experiments (n = 56/108/103/134 for 2i/N2B27/N2B27+PD/N2B27+Chiron). The effect of media change is significant (p<0.0001, Kruskal-wallis test, comparisons with N2B27, for last time point).

Overall, the colony morphology had a striking resemblance for conditions with similar pluripotency outcomes: compact, highly spherical and 3D for 2i and N2B27+Chir, pronounced spreading with height reduction and shape asymmetry for N2B27 and N2B27+PD.

To check if these differences in the structural organization of colonies translate to changes in mechanoresponses, traction forces were measured. In line with what has been observed in earlier experiments, in media concoctions leading to pluripotency dissolution, colonies exerted higher traction forces, while for the ones upholding naïve identity, significantly lower tractions were recorded (Figure).

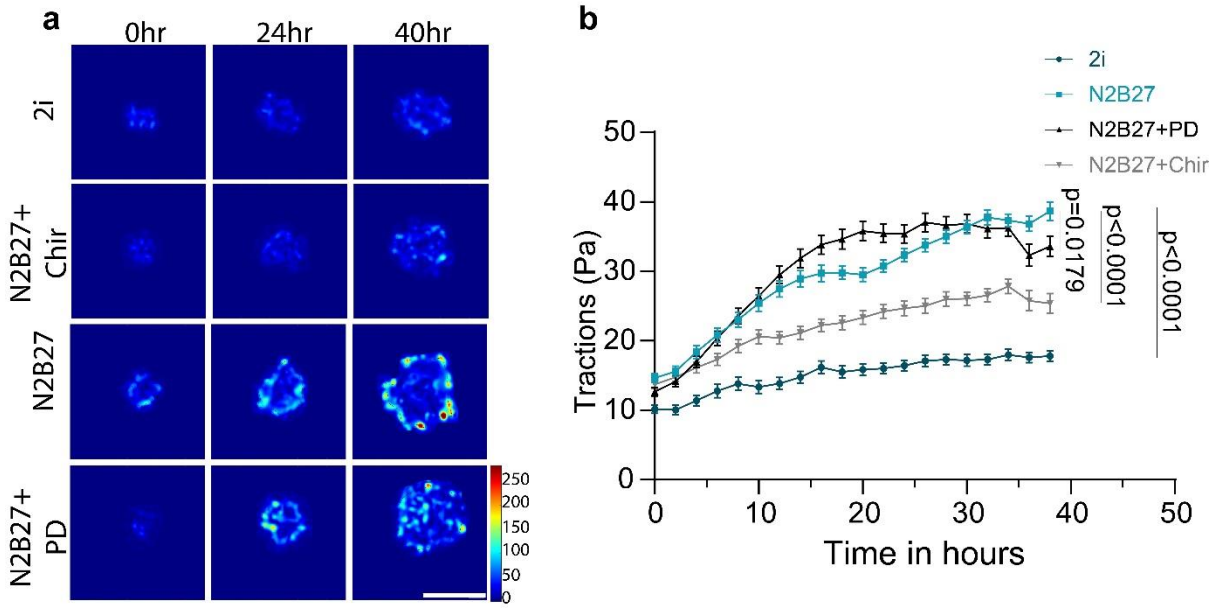

Figure.46: a. Representative heat maps of tractions exerted by mESC colonies in 2i/N2B27/N2B27+PD/N2B27+Chiron. Scale bar is 20 µm. b. Corresponding quantification of traction forces averaged over colony area. Data from 3 independent experiments (n = 29/72/75/74 for 2i/N2B27/N2B27+PD/N2B27+Chiron). The effect of media change is significant (p<0.0001, Kruskal-wallis test, comparisons with N2B27, for last time point).

Hence, β-catenin preservation downregulates cell-matrix interaction by augmenting cell-cell adhesion strength. Whether these changes are reflected in nuclear shape were investigated next.

4.11 Stronger cell-cell adhesion reduces nuclear deformation.

To assess if the difference in cell-matrix interaction is translated to nuclear deformation, the nuclear aspect ratios in all four media conditions was measured. Mirroring the levels of cell-matrix interaction, colonies in N2B27 and N2B27+PD were observed to have higher aspect ratio whereas in conditions of naïve state preservation, 2i and N2B27+Chir, values were significantly lower (Figure).

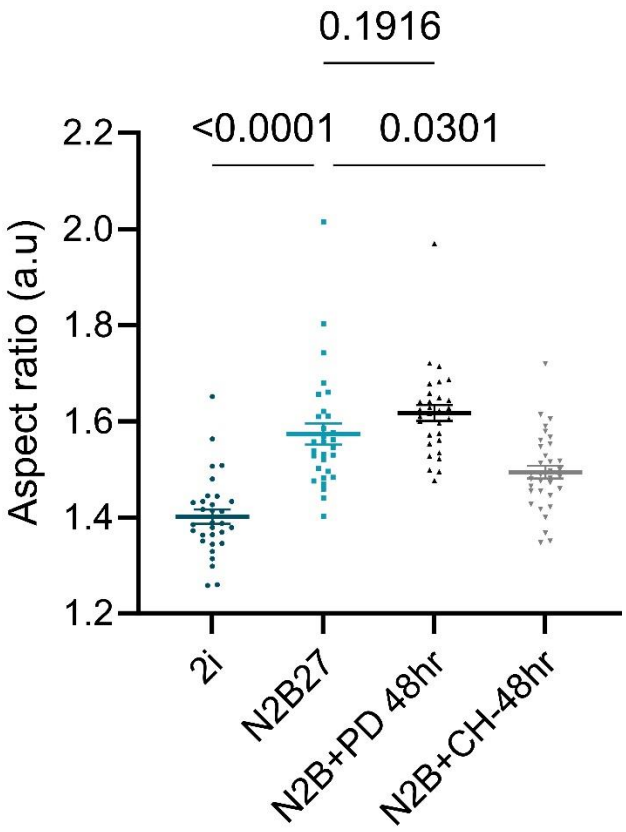

Figure.47: Quantification of Nuclear aspect ratio averaged over colony for mESC colonies grown in mentioned media for 48 hours. Data from 3 experiments (n=35/30/29/34 colonies for 2i/N2B27/N2B27+PD/N2B27+Chiron). The effect of media change is not signficant only for the comparison between N2B27 and N2B27+PD (One way ANOVA)

The mechanotransduction was earlier observed to be primarily concentrated at the edge of the colonies in standard differentiation conditions. A clear distinction between the edge and the interior regions was also identified for the expression of pluripotency factors and for the mechano-sensitive protein YAP. How the additional biochemical cues encountered by the colonies in single inhibitor experiments affect the force, fluorescence and transcription factor profiles was assessed with the corresponding results detailed in the next sub-section.

4.12 Regional differences are conserved in line with colony´s pluripotency status

The compact colonies in N2B27+Chir media were characterized by higher expression of naïve factor *Nanog* and lower expression of *Otx2* compared to the differentiated counterparts in N2B27 and N2B27+PD. Both *Nanog* and *Otx2* exhibited consistent regional differences in expression in earlier experiments. Hence, the regional status of these proteins was compared in single inhibitor conditions. Additionally, although the naïve state specifier *Klf4* was not differentially expressed between regions, if its regional profiles change upon treatment with one of the two inhibitors, it was also investigated.

For *Klf4*, no significant differences were observed between the edge and interior regions in any of the media conditions (Figure.48), consistent with our previous findings. For *Otx2*, a small yet statistically significant difference was observed only for colonies grown in N2B27+PD and control N2B27 (Figure.48). For *Nanog*, a striking disparity between the two regions was observed in all the non-2i conditions with the colony edge consistently expressing lower levels (Figure.48).

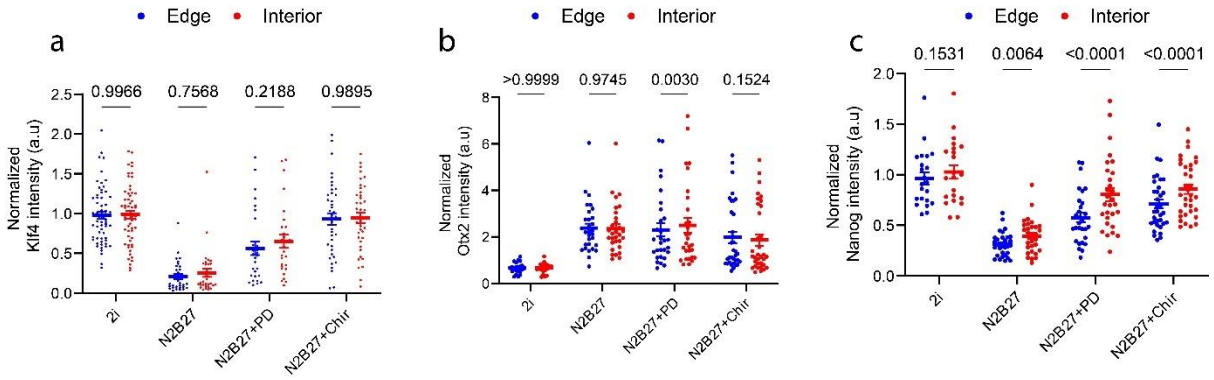

Figure.48: Quantification of normalized nuclear intensity of Klf4 averaged over colony resolved as Edge vs Interior for mESC colonies grown for 48 hours in mentioned media. Data from 3 independent experiments (n = 61/31/29/40 for 2i/N2B27/N2B27+PD/N2B27+Chiron). The effect of edge vs interior is not signficant for any of the comparisons (two-way ANOVA, repeated measures). b. **Quantification of normalized nuclear intensity of Otx2 averaged over colony resolved as Edge vs Interior for mESC colonies grown for 48 hours in mentioned media. Data from 3 independent experiments (n =35/30/29/34 for 2i/N2B27/N2B27+PD/N2B27+Chiron). The effect of edge vs interior is significant only for N2B27+PD (two-way ANOVA, repeated measures)**. **Quantification of normalized nuclear intensity of Nanog averaged over colony resolved as Edge vs Interior for mESC colonies grown for 48 hours in mentioned media. Data from 3 independent experiments (n =35/30/29/34 for 2i/N2B27/N2B27+PD/N2B27+Chiron). The effect of edge vs interior is significant for all conditions except 2i (two-way ANOVA, repeated measures).**

Next, the nuclear localization of YAP was compared and resembling earlier results, colony edge always expressed higher nuclear to cytoplasmic ratio than the interior. However, no differences were observed between the four media conditions when the values corresponding to colony edge were compared. Moreover, the only difference observed was for the measurements of interior regions and was only significant for comparison between 2i and N2B27 (Figure.49).

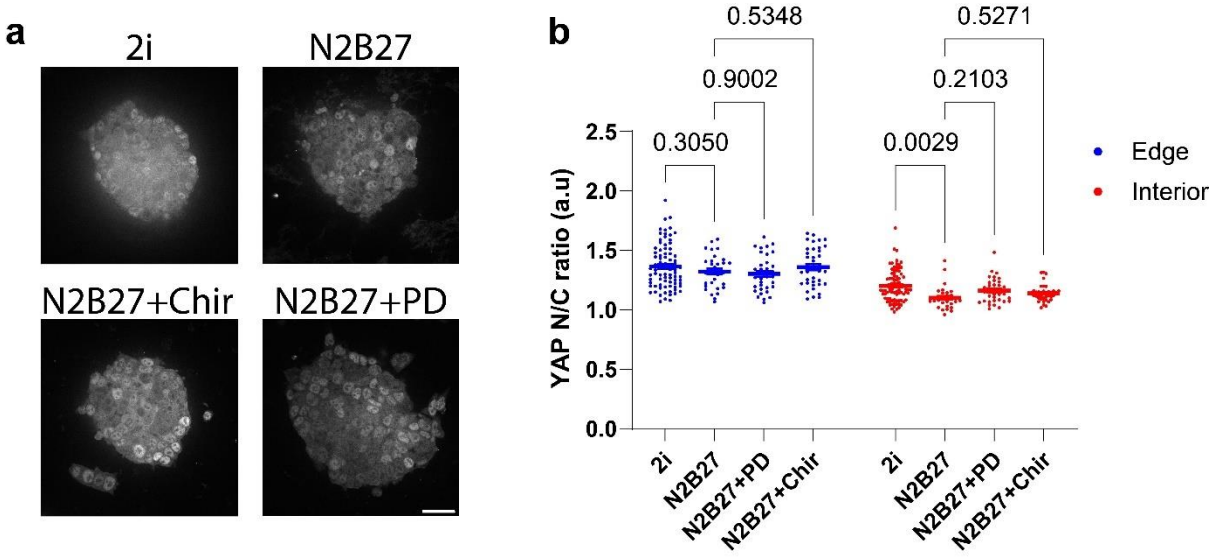

Figure.49: a. Quantification of Nuclear aspect ratio averaged over colony for mESC colonies grown in mentioned media for 48 hours. Data from 3 experiments (n=35/30/29/34 for 2i/N2B27/N2B27+PD/N2B27+Chiron). The effect of media change is not signficant only for the comparison between N2B27 and N2B27+PD (One way ANOVA) b. **Representative immunofluorescence images of YAP after 48 hours culture in mentioned media. 2i/N2B27/N2B27+PD/N2B27+Chiron. Scale bar is 20 µm. Data from 3 independent experiments (n = 61/31/29/40 for 2i/N2B27/N2B27+PD/N2B27+Chiron). Only The comparison between 2i-interior and N2B27-interior are statistically significant. (Two-way ANOVA with repeated measures).**

As *Nanog*'s transcriptional activity determines Rex1-GFP signal, given its low expression at colony edges in both the single inhibitor conditions, how the fluorescence intensity between the two regions is affected with the addition of one of the inhibitors was next tested. In accordance with earlier results, Rex1-GFP intensity at the edge of the colonies was always lower irrespective of the media. However, with Chiron addition, a steady growth was observed whereas for colonies in PD, the fluorescence signal at edge diminished with time (Figure.50).

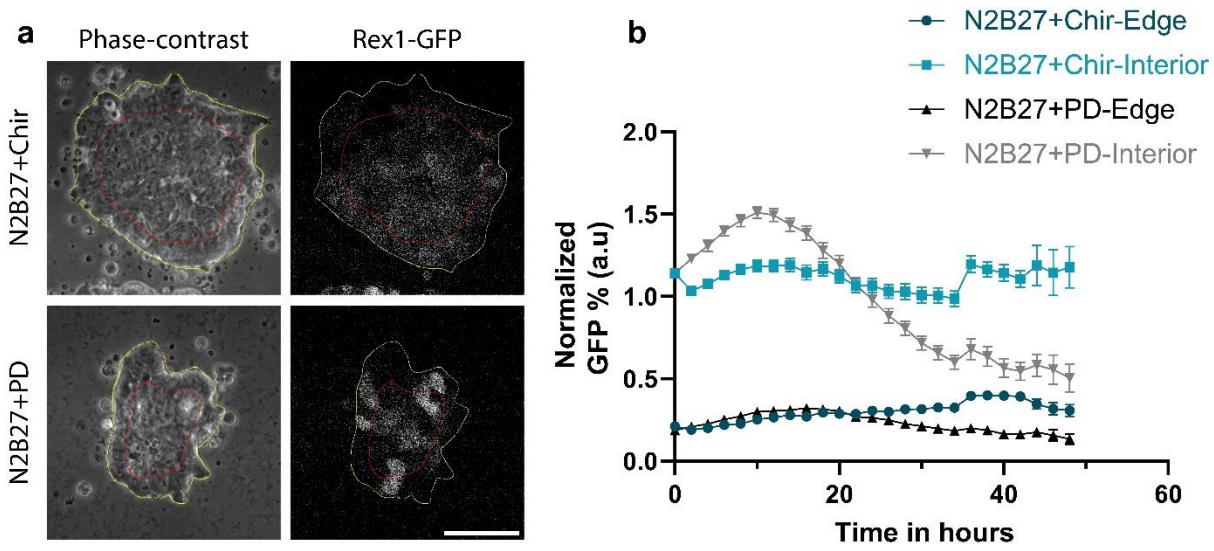

Figure.50: a. Representative phase-contrast and fluorescent images of mESC colonies grown for 48 hours in N2B27+Chir (top) or N2B27+PD (bottom). The region between the yellow and red outlines corresponds to colony edge, region within red outline is interior. b. Quantification of Rex1-GFP intensity, as a function of time, resolved into edge and interior regions for mESC colonies grown in N2B27. Data from 3 independent experiments (n = 70/79 colonies for N2B27+PD/N2B27+Chiron).

Despite the lack of significant alteration in YAP expression patterns between the media combinations, colony edges displayed higher nuclear localization. As this suggests upregulated mechano-transduction, whether it is also recapitulated for traction force measurements was verified. No significant differences were observed for the regional differences in traction forces for mESC colonies cultured in either media.

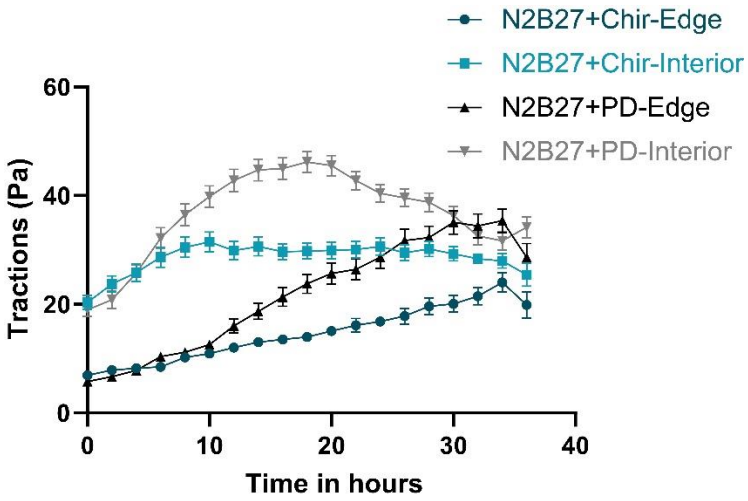

Figure.51: . Quantification of traction forces, as a function of time, resolved into edge and interior regions for mESC colonies grown in N2B27. Data from 3 independent experiments (n = 70/79 colonies for N2B27+PD/N2B27+Chiron).

Taken together, the regional differences pertaining to: traction forces, transcription factor expression patterns and Rex1-GFP fluorescence signal are intimately linked to pluripotency status. Importantly, the measurements were highly similar between the 2i and N2B27+Chir. Given this, it can be posited that β-catenin preservation is minimally sufficient to preserve naïve state and is accompanied by lowering of cell-matrix interaction.

Chapter 5: Discussion

In mouse embryo, exit from naïve state pluripotency marks the unwavering commitment of epiblast tissue to germ layer specification, thereby laying foundation for organismal development. It is initiated by the deposition of extra-cellular matrix (ECM) rich in laminin. Owing to their insolubility and structural organization, ECM proteins such as laminin confer mechanical properties to the matrix and are therefore perceived as mechano-chemical cues by the cells via the adhesion molecules integrins. Laminin being heavily localized at the basal plane serves as a polarization cue and drives the morphological transition of epiblast [24]. Concomitantly pluripotency dissolution occurs gradually with dynamic changes in transcription factor expression. Importantly, the pluripotent state and shape are shown to be interdependent [23].

This intimate linking between fate and form serves as a quality control to ensure robustness during embryonic development. While this synchrony being borne out by integrin-mediated cell-ECM interaction is acknowledged, the accompanying cellular mechano-responses and their evolution are yet to be elucidated. Moreover, how the mechanical signal induction precipitates to the nuclear space to alter transcriptional signature and thus regulate pluripotency dissolution needs to be delineated. The current thesis aimed at addressing these knowledge gaps. However, studying pluripotency progression in the *in vivo* context is fraught with technical challenges. Therefore, this work employed ab *in vitro* models, culturing on laminin coated PAA gels a (mESC) line with a fluorescent reporter whose signal intensity marks the pluripotency status.

To ensure a homogeneously naïve population for each experiment, the cells were maintained in a defined serum-free media N2B27 supplemented with the two inhibitors (2i), one for MEK/ERK signalling and the other for GSK3β mediated β-catenin degradation. In 2i media, mESCs perpetuate with high fluorescent signal and upon the two inhibitors withdrawal the fluorescent signal gradually declines marking the exit from naïve state and further pluripotency dissolution.

With this information, the study began by identifying the platform compatible with long-term mESC culturing and simultaneous measurements of mechano-responses. Among the hydrogel set ups tested, polyacrylamide (PAA) gels functionalized with sulfo-SANPAH maintained stable attachment. Additionally, the colonies retained the 3D dome morphology when cultured in 2i on PAA gels, unlike on PDMS where high colony spreading was observed.

One possible explanation for the loss of 3D morphology on PDMS is the stiffness mismatch between the surface and bulk material. Throughout their preparation, PDMS gels are exposed to oxygen, and it has been reported to alter surface chemistry creating a thin and rigid silica layer [277, 278]. This plausibly leads to the increased spreading observed on PDMS given that substrate stiffness dictating morphology is well documented in several other cell systems [279-283]. Moreover, coating PDMS with charged molecules such as ECM proteins is reported to alter the elastic modulus [284], adding further complexity. Another decisive factor for the selection of sulfo-SANPAH gels is the optimal distribution of fiduciary markers to monitor the hydrogel stress offering greater spatial resolution compared to PDMS.

As part of the system validation, expression levels of bonafide transcription factors were quantified and the changes occurring upon pluripotency dissolution were in line with what has been reported [45]. The decrease of *Nanog* and *Klf4* coincided with elevated levels of post-implantation factor *Otx2*. Interestingly *Otx2* expression was already detected before the colonies were subjected to differentiation. *Otx2* is reported to antagonize the self-renewal and promote the commitment to differentiation [73]. It is countered by *Nanog* which promotes self-renewal [285] and this functional antagonism was recapitulated in the reciprocal expression patterns of *Nanog* and *Otx2*. When continued to be cultured in 2i, colonies are fortified with *Nanog* expression, while differentiation induction elevates *Otx2* levels. Hence, even before the biochemical induction with the two-inhibitor withdrawal, the cells already exist in a metastable state. Within the colony, the standout feature of basal layer of cells is their adhesion to the matrix through integrins. Given this information, the metastable state of basal cells suggests the pro-differentiation activity of integrin-based mechano-sensing which is further compounded by biochemical environment. This could be proven by comparing the expression levels of *Nanog* and *Otx2* between the basal plane and the regions dominated by cell-cell adhesion.

Next, the temporal progression of Rex1-GFP signal was monitored in both naïve state sustenance and pluripotency dissolving media conditions. The fluorescent signal gradually declined upon two inhibitor withdrawal and was preserved in 2i media. As the transcriptional activity on Rex1 promoter depends on naïve factor expression and considering the downregulation of *Nanog* expression in N2B27, this result is consistent with earlier observations. Whether differences in Rex1-GFP signal exist between the different layers of

colony needs to be verified. If such variation in fluorescent signal does exist, it further substantiates the earlier mentioned differentiation promotion by integrins independently of the biochemical cues.

The cell spreading observed upon naïve state exit in single mESCs was also observed for the colonies as signified by the progressive increase in colony area. In case of single cells this is attributed to the reduction of membrane cortex attachment driven by lowering of phosphorylated Ezrin (pEzrin) [190]. It needs to be tested whether colony spreading is facilitated by the same mechanism and to do so immunofluorescence staining of pEzrin at different time points during pluripotency dissolution would suffice.

The colony area was also observed to increase for colonies maintained in naïve culture conditions in which membrane cortex attachment and pEzrin levels are known to be not compromised. This could however be explained when the focal adhesion profiles of naïve and differentiated cells are viewed in light of the molecular clutch model.

As per this model, each focal adhesion (clutch) has a characteristic binding and unbinding rate, with the latter being influenced by the clutch's force-bearing capacity. If the build-up of force generated by myosin contraction on actin filaments is greater than the force endurance of clutch, the components of focal adhesion disengage without further growth in adhesion size. If the force transmitted to the clutch is below the threshold, the engagement is persisted during which time other focal adhesion can bind to actin filaments. This leads to load distribution resulting in integrin clustering that is considered as growth in focal adhesion length and stability.

In naïve cells as the focal adhesions are functionally attenuated, their load-bearing capacity might be lowered. This leads to greater propensity of focal adhesion disengagement reducing the incidence of integrin clustering and adhesion length consolidation. Whereas, with differentiation, the force endurance of integrin adhesions is enhanced which culminates with increase in length and stability of focal adhesions. Given that increased focal adhesion stability is shown to permit persistent cell spreading [286,287], the molecular clutch model therefore explains the prodigious colony spreading in N2B27 and stunted area growth while naïve maintenance.

As actin arrangement as supracellular cortex is required for the compact morphology in naïve state, the change in actin cytoskeletal organization explains the loss of 3D dome shape in colonies subjected to differentiation. The heavy membrane localization in naïve conditions attest the strong membrane cortex attachment aiding in the maintenance of the peculiar morphology. Whereas actin being redirected from the cortex into fibres spanning the cell length leads to decrease in membrane tension and might further contribute to colony spreading.

The peculiar 3D dome morphology is shown to promote, through compressive forces, the expression of *Nanog* while colony spreading downregulates its levels [191]. If such mechanical logic occurs for other transcription factors, specifically the post-implantation factor *Otx2* needs to be investigated. The progressive increase in its expression as mESC colonies spread suggests that *Otx2* levels might be regulated by the same intra-colony forces with the effect being opposite to that of *Nanog*; High compressive forces and low *Otx2.*

The differences in the integrin force bearing capacity and actin cytoskeletal arrangement also explains the traction profiles in the two media conditions. The force build-up from the acto-myosin contractility, when transmitted to the engaged integrins are exerted as traction forces onto the underlying matrix. The competence and other attributes of focal adhesions coupled with observed actin organization thus explain the consistent increase in traction forces upon differentiation induction.

A key detail of the mESC focal adhesion is the organization of the three force transduction layers. In naïve state the focal adhesion apparatus is compressed with anti-parallel organization of vinculin thus impeding the force transmission. The instructive cue that brings about the change in the stacking of the three-force transduction layer needs to be identified. Also, the vinculin misorientation was reported only for naïve mESCs grown on laminin coated substrates. Whether vinculin's directionality is corrected during differentiation and if not, why such typical alignment exists only on laminin coated substrates is worth studying. Since vinculin's directionality in mESCs is dependent on ECM protein identity, it is of interest to investigate if mESC mechano-responses, their evolution and pluripotency dissolution kinetics are influenced by the protein tethered to the matrix.

Till date, force transmission to matrix is considered as a regulator of only mESC self-renewal [215]. Whether it exerts similar influence on pluripotency dissolution wasn't established. The results from blebbistatin treatments and multi-stiffness experiments suggest that traction force exertion indeed does regulate pluripotency dissolution kinetics. Conditions with lower force transmission exhibiting slower Rex1-GFP signal decay attest the same.

While in the current system the traction force-based deformation happens to an inert polymer, in the embryonic context they are transmitted to basement membrane (BM), which incurs structural changes. Changes in BM organization is reported to guide morphogenesis in other tissues [288,289]. Whether the epiblast tissue exerts forces onto BM and lead to such morphological consequence in the mouse embryo is not known. Mole and colleagues [290] recently implicated the force transmission apparatus in such sculpting activity. In this work, it was reported that integrin activation is required for the epiblast to form rosette structures which enables lumen formation and commitment to pluripotency priming. Therefore, epiblast, via integrins, exerting forces onto BM to facilitate this shape change is not a far-fetched idea but needs experimental validation.

In addition to attenuating force transmission, blebbistatin treatment is notorious for stalling mitotic cell division [291]. For pluripotency dissolution, mitosis assumes greater prominence as cell division completion, marked by cytoplasmic abscission, is shown to be obligatory for naïve state exit [292]. However, at the concentrations of blebbistatin employed in this study, no defect in cell cycle progression was observed. In fact, monitored cells undergoing at least two rounds of cell division confirm no replication crisis. Therefore, the observed slowdown of Rex1-GFP signal decay and thereby the pluripotency dissolution is due to attenuated traction force generation.

Pluripotency dissolution was also characterized by regional differences in cell-matrix interaction. The traction forces and focal adhesions were quantifiably higher at the edge of the colony compared to the interior region. These mechano-responses were accompanied by a lower Rex1-GFP signal at the edge prior to the withdrawal of the two inhibitors. The fluorescence intensity of the edge was more similar to isolated single cells. Importantly, the regional differences in mechano-responses and fluorescence signal existed for the naïve colonies and with time they were reconciled. Only in the differentiation conditions did the disparity between the two regions grow.

An earlier work from the group of Pere Roca-Cusachs [256] reported similar mechano-response pattern: higher traction forces at the edge. In the same work, the regions with high cell-matrix interaction were reported to have increased nuclear localization of the mechano-transducer protein YAP. Mirroring the same, the relative nuclear concentration at the edge was higher for mESC colonies. This was the case irrespective of the media condition. However, similar to the other mechano-responses the difference between the edge and the interior region for YAP nuclear localization became starker with time for differentiating colonies.

When the YAP nuclear localization of only edge cells is compared between the two media conditions, no significant differences were observed. This lack of dissimilarity between the naïve state maintaining and pluripotency losing colonies may be explained when the functional role of YAP in mESCs is considered. At any state of the pluripotency, mESCs are choosing between self-renewal and differentiation, both of which are driven by YAP. It has been recently shown that the road taken by mESCs is determined by the frequency of YAP activation pulses [261]. Cyclic nuclear sequestration and expulsion of YAP favours proliferation while persistent nuclear localization enables differentiation. Importantly, the frequency of the pulses was of the order of minutes and the YAP immunofluorescence analysis in the present study was performed after every 24 hours. These time resolutions vary by at least two orders of magnitude and therefore it is possible that the differences are evened out in the current system. It is to be pointed out that the YAP pulsing frequency in the work by Meyer and colleagues [261] was varied through optogenetic control.

In the work from Pere Roca-Cusachs' group cited above, YAP nuclear translocation was shown to be driven by force application mediated nuclear deformation [265]. The recent work suggests that the same is applicable for single mESCs as increase in intracellular tension was shown to cause YAP sequestration and nuclear shape changes [293]. Since, high YAP nuclear localization was observed at the edge of the colonies, whether it is reflected in nuclear morphology in the current system was tested. Mimicking YAP expression pattern, the nuclear aspect ratio, a measure of nuclear deformation, was found to be significantly higher for edge region across all conditions and time points. Once again, the differences between the two regions became more striking when the colonies are subjected to differentiation. Moreover, when the aspect ratios of only the edge cells are considered, the values steadily increased for differentiation colonies and were significantly higher than their naïve counterparts.

Importantly, when the YAP nuclear to cytoplasmic ratio was compared with nuclear aspect ratio for edge cells, a weak yet statistically significant positive correlation was observed. Since higher aspect ratio result from higher force applied on to the nucleus, the correlation suggests that force application to nucleus in the current system aids in YAP sequestration. All in all, this implies that mESC nuclei respond to mechano-transduction by changing their transcriptional signature.

The reasons for not considering nuclei of interior cells are twofold. First, mechano-transduction and nuclear deformation was relatively lower in the interior of colony. Second, interior cells possess cadherin mediated cell-cell adhesion whose inhibition of YAP nuclear sequestration via HIPPO pathway is well documented [257]. Also, cadherin is implicated in mechanical signalling. Furthermore, in the current system the individual contributions of focal adhesions and cell-cell adhesions to mechano-transduction cannot be uncoupled. Because of these additional layers of complexity, the shape and transcriptional signature of interior nuclei do not stand as the true reflection of cell matrix interaction and hence omitted from analysis.

In spite of no measurable difference in nuclear localization signal, YAP might be serving different functions in the edge cells of naïve and primed colonies. It is highly possible that under naïve maintenance YAP promotes self-renewal and in N2B27, it actively contributes to pluripotency dissolution. This can be confirmed if differences exist in YAP pulsing frequencies which can be retrieved from measuring nuclear to cytoplasmic shuttling rates. Whether such pulsing frequency differences exist and if mechanical signalling further amplifies it to bias the decision making between self-renewal and differentiation is worth looking into. The pursuit of this topic for investigation is supported by the regional differences in YAP and nuclear aspect ratio prior to biochemical differentiation.

The low GFP signal of the colony edge at the start of the experiment suggests that a certain degree of differentiation occurs prior to the two-inhibitor withdrawal. Since the fluorescence is a readout of the strength of naïve transcriptional program, if the pluripotency markers exhibit such regional differences was tested. Only for *Otx2* and *Nanog* was a consistent difference between the two regions observed, with *Otx2* significantly higher at the edge and *Nanog* significantly lower. This pattern of pluripotency factor expression validates the early start of differentiation induction at colony edge. The state of pluripotency for edge

cells might be more formative than primed and this is supported by two observations. When maintained in 2i, the edge cells seems to remain in this metastable state confirmed by lower *Nanog* expression and Rex1-GFP signal compared to interior cells. In N2B27, both the naïve pluripotency factor levels and Rex1-GFP signal continued to dwindle with concomitant consolidation of *Otx2* expression.

To infer if *Otx2* and *Nanog* expression in the edge cells is under similar mechanical control as YAP, their levels were compared with nuclear aspect ratio. For *Nanog*, a weak yet statistically significant negative correlation was observed suggesting that force application to the nucleus might contribute to *Nanog's* downregulation. For *Otx2* no correlation was observed. Since *Klf4* expression wasn't dependent on cell position within the colony and its downregulation occurred uniformly with 2i removal, the same analysis wasn't performed for *Klf4*.

Force application to the nucleus affecting the intracellular localization is well established [294]. It occurs through either retention mechanism [141, 295] or by altering the diffusion rates in and out of nucleus via the nuclear pore complexes (NPCs) [255, 297]. In the first scenario, force application enhances the binding affinity to a molecular target in the nucleus or cytoplasm and thus sequestered in a particular subcellular space. The second mechanism is thoroughly explained in the recent work, Andreu I and Granero-Moya I et al [255]. In this study, the authors show that two factors determine intracellular transport rates, protein's molecular weight (MW) and its affinity to nuclear transport receptors: importins and exportins. Shuttling through NPC occurs through passive diffusion or facilitated diffusion. Although force application was found to affect both modes of transport, the additional influence of molecular weight was stronger for passive diffusion. Using this information and considering the individual attributes of the three pluripotency factors, a plausible explanation for their mechano-sensitivity or lack of it is given below.

Klf4 has high molecular weight (~53kDa) [297] and due to this higher size, *Klf4* relies on facilitated transport through Exportin-1 (XPO1) [132]. However, to become the cargo of XPO1, *Klf4* is to be phosphorylated by ERK. Once excluded from nucleus, *Klf4* is degraded and in N2B27 it is not replenished with additional synthesis. Therefore, *Klf4* is predominantly under biochemical regulation and might hence be non-responsive to nuclear force application as is supported by lack of regional differences in its expression.

Among the three pluripotency factors employed in this study, *Otx2* has the lowest molecular weight (~35 kDa) [298], a size range in which passive diffusion is the primary mode of intracellular shuttling [299]. In Andreu I and Granero-Moya I et al, force application to the nucleus was found to equally affect the influx and efflux rates of passively diffusive proteins leading to no discernible changes in nuclear localization signal [255]. Similar effect could be at play for *Otx2*, rendering its nuclear transport non mechano-sensitive and this is also supported by no change in *Otx2* expression with blebbistatin treatment despite the lowered nuclear aspect ratio. Importantly, there is no consensus on the nuclear importer of *Otx2*. Although *Otx2* association with the transport protein, Transpotin-2 is reported [300], the conclusions were based on yeast two hybrid assay, an experimental technique that yields spurious interactions and high false positive rates [301, 302]. Moreover, Transportin-2 nuclear import capabilities are documented for other proteins [303, 304], but it remains to be validated for *Otx2*. Hence, the possible mode of nuclear import being passive diffusion makes *Otx2* expression non-responsive to nuclear force in mESCs.

Nanog is a 40kDa protein, and its molecular weight falls in the mechano-sensitive regime reported in Andreu I and Granero-Moya I et al [255]. In the same work, the mechano-sensitive protein shuttling was shown to be mediated by importins and they likely take part in *Nanog's* transport as importin knockdown was shown to lower *Nanog* levels [305]. Moreover, *Nanog* expression is shown to be transcriptionally inhibited by YAP [261], whose nuclear entry is shown to be mediated by force application. These three attributes might therefore be conferring the mechano-sensitivity to *Nanog* in the current system.

A recent study alludes to such shuttling kinetics-based mechano-sensitivity of *Nanog,* but in zebrafish embryo [306]. In this work, it is identified that *Nanog* nuclear localization requires NPC size maturation and the levels increased as tissue assumed a 3D morphology. Furthermore, NPC size was found to be dependent on its composition. For mESCs NPC composition was found to change when subjected to differentiation [307, 308]. It would be interesting to check if this gives rise to size changes of NPC complex to influence the intracellular transport rates and, thereby, the mechano-sensitivity of key transcription factors.

Higher mechanical signalling at the edge leads to increased nuclear aspect ratio and differentiation can, eventually promote transcriptional changes. This suggest that nucleus is

integrated into mechano-transduction and its regulatory role on mESC priming needs to be identified. To do so, the nucleus-actin connection was abrogated through DN-KASH induction and its effect on pluripotency dissolution kinetics was analysed.

Attenuating force transmission through DN-KASH expression delayed pluripotency dissolution as confirmed by slower decay kinetics of Rex1-GFP signal. However, the effect was minimal and observed only when the differentiation is performed on glass. When the colonies are subjected to differentiation on gels, DN-KASH induction didn't lead to significant change in pluripotency dissolution rate. This could be due to differences in mechanical properties of the two substrates.

The stiffness of glass is in the megapascal to gigapascal range, which is at least 3 orders of magnitude higher than the PAA gels employed in the study. As higher stiffness leads to higher force transmission to the nucleus, the force differential between control and DN-KASH induced conditions would be significantly higher for glass compared to gels. This might be the underlying cause for the delay in pluripotency dissolution on glass and no apparent change on gels with DN-KASH expression. Moreover, the DN-KASH induction couldn't be sustained throughout the experiment and persisted for a period of 16-24 hours. Therefore, the force transmission to nucleus is compromised only transiently in the experiment and thus the small changes in dissolution kinetics even on glass. This is also confirmed by no measurable difference in the nuclear aspect ratios between the DN-KASH induced and control colonies after 48 hours of differentiation in N2B27 media.

Nuclear deformation was highest at the edge and the edge of the colonies was more similar to single cells. Hence it needs to be seen whether DN-KASH induction yields significantly slower pluripotency dissolution in single cells on PAA gels and if the effect is much more profound on glass. Also, the difference in force transmission between PAA gels and glass can be substantiated by comparing the aspect ratios on the two substrates during various time points of differentiation.

The composition of culturing media affecting cell-matrix interaction is appreciated in case of mESCs. The standout example is the striking morphological differences in Serum+LIF media and 2i media: flat 2D colonies and compact 3D domes respectively. A change in morphology implies change in cell-matrix force transmission. Also, pluripotency dissolution is

not free from biochemical influence as naïve state exit is initiated with the withdrawal of ERK and GSK3α/β inhibitors: PD and Chir respectively. To check how biochemical regulation of naïve pluripotency influences cell-matrix force transmission, mESC differentiation was performed with the selected removal of only one inhibitor.

It was observed that preserving β-catenin signalling by Chir was minimally sufficient to safeguard naïve pluripotency. This was attested by the sustenance of high Rex1-GFP signal and naïve pluripotency factor expression. Importantly the mechanical signature of mESC colonies with Chir treatment mirrored that of naïve colonies cultured in 2i media: lower traction forces, decreased colony spreading and smaller nuclear aspect ratio. Moreover, the evolution of mechano-responses and Rex1-GFP signal between the edge and interior regions of the colonies were similar between 2i and N2B27+Chir media conditions. Hence, in every facet, be it molecular or mechanical, mESC colonies with Chir treatment recapitulated the naïve signature of 2i colonies.

On the other hand, inhibiting ERK activation by PD could only delay pluripotency dissolution. The mechano-responses and transcription factor expression with PD treatment were strikingly similar with the profiles observed for colonies differentiated in N2B27. Additionally, the regional differences in traction forces and Rex1-GFP signal were similar between N2B27 and N2B27+PD media conditions. Therefore, it can be stated that ERK inhibition alone cannot preserve naïve state pluripotency in mESC colonies.

The above results are in contradiction to what was earlier reported. In the work Dhaliwal N et al it was identified that naïve state exit is initiated by *Klf4* phosphorylation for which ERK activation is required [132]. The authors reported that by solely inhibiting MEK/ERK pathway through PD, *Klf4* expression is sustained, and naïve pluripotency is secured. This inconsistency will be reconciled when the key differences in the experimental details are considered. In the current thesis naïve pluripotency exit was performed in defined N2B27 media for mESC colonies. Whereas, in Dhaliwal N et al, differentiation was initiated in serum media and single cells. The two studies vary in the cell number, media type and substrate coating, and the individual contributions of these three differences are detailed below.

The cadherin-mediated cell junctions in mESC colonies imparts additional regulatory control over *Klf4* expression and enhances its stability. Intercellular junction formation

engages cadherin which is shown to promote the JAK/STAT pathway [311-313]. In mESCs, JAK/STAT cascade drives the expression of the *Klf4* [314-316]. This ensures that *Klf4* is constantly replenished in colonies as opposed to single cells. In fact, in Dhaliwal N et al, *Klf4* expression was observed to be reinitiated 24 hours after 2i withdrawal at which point mESCs were forming colonies, despite a complete loss of *Klf4* signal by 6 hours in single cells. Such expression pattern is also not consistent with what has been observed in physiological conditions. During mouse embryonic development, once epiblast loses *Klf4* expression, it remains as such until lineage specification [77].

Unlike N2B27, serum media is not devoid of differentiation promoting factors and is also shown to induce an acute activation of MEK/ERK pathway [317, 318]. Since Erk activation promotes *Klf4* degradation, the rapid downregulation of *Klf4* in Dhaliwal N et al [132] can be thought of as the exacerbating effect by serum media.

While *Klf4* nuclear exit to be the initiator of naïve state exit is not being challenged, the process being solely under control of MEK/ERK pathway as reported in Dhaliwal N et al might only be specific for single cells. This is supported by following observations in the current work: high *Klf4* expression for mESC colonies treated with Chir and decrease in *Klf4* levels despite MEK/ERK inhibition by PD. This above information however still does not offer complete explanation as to why preserving β-catenin through Chir inhibition of GSK3β safeguards naïve pluripotency while MEK/ERK inhibition by PD does not. This might be clarified by considering the fine details of how PD functions and by looking into the mechanical and molecular implications of β-catenin signalling in mESCs.

ERK activation during pluripotency dissolution in mESCs primarily occurs through the autocrine secretion of fibroblast growth factor (Fgf) [319]. Upon binding to its receptor, Fgf initiates the Ras-Raf pathway and the downstream effector of this cascade, MEK, promotes Erk nuclear translocation through its phosphorylation action. The small molecule inhibitor PD0325901 (PD) prevents ERK phosphorylation by targeting the kinase activity of MEK [320].

Through such indirect inhibition, PD impedes ERK nuclear entry, thereby averting the phosphorylation, nuclear exit, and subsequent degradation of *Klf4*. Having said that, alternative routes of ERK activation that are MEK-independent exist [320-323] and the ones relevant to mESCs are the PI3K/Akt pathway and integrin β1/FAK pathway.

Insulin is a putative activator of PI3K/Akt pathway and its presence in the N2B27 media might be alleviating the PD mediated inhibition of ERK phosphorylation. This is supported by a reduction in phosphor-ERK levels upon insulin receptor knockout in mouse induced pluripotent stem cells [324]. Moreover, the laminin receptor in mESCs is integrin β1 [325-327], which is implicated in ERK activation through focal adhesion kinase activation. Since in the current system, mESCs adhere to the hydrogel through integrin-based adhesion and present prominent focal adhesions, the integrin β1/FAK pathway based ERK phosphorylation seems plausible. Hence, through these two mechanisms, ERK activation might be bypassed in mESCs despite the provision of PD.

Phosphorylation is not the only post-translational modification to drive *Klf4* nuclear exit and subsequent degradation as mentioned in Dhaliwal et al [132]. In the follow-up study from the same group, ubiquitination of *Klf4* was also found to drive its nuclear export and degradation [328]. Taken together, it is highly likely that the lowered expression of *Klf4* despite MEK inhibition is contrived by the bypassing of ERK inactivation by PD and non-phosphorylation mediated *Klf4* degradation.

In addition to the above mechanisms, *Klf4* stability is also determined by β-catenin transcriptional activity. This might further explain the *Klf4* expression pattern in the two single inhibitor conditions.

Nuclear localization of β-catenin promotes the expression of the core pluripotency triad: *Oct4, Sox2* and *Nanog*, and the naïve state specifiers: *Esrrb, Tcfp2l1* [329-332]. *Klf4* interacts with both these categories of proteins, and it was shown to increase its half-life (>24 hours) [329, 333]. This is also supported by enhanced *Klf4* expression in mESCs treated with Chir, which preserves β-catenin through GSK3β inhibition [334]. Besides such stabilization, the transcription of *Klf4* might also be promoted by β-catenin as it upregulates Stat3 [335], the effector of JAK/STAT pathway which drives the expression of all naïve pluripotency factors. For these reasons, *Klf4* expression might be sustained with Chir treatment.

With Chir removal, GSK3β activation ensues leading to degradation of β-catenin. This leads to the downregulation of both the general pluripotency factors and naïve state specifiers. The decrease in their expression levels initiates differentiation and is shown to coincide with a dramatic reduction in *Klf4* half-life (<2 hours) [328]. Such low stability might

not be compensated by non-canonical means of *Klf4* production such as cadherin mediated JAK/STAT pathway. This could be another contributing factor for reduction in *Klf4* expression for mESCs treated with PD despite the presence of cell-cell adhesion. In this way, β-catenin signalling has a profound effect on the stability of pluripotency transcriptional network and might therefore be a dominant regulator of naïve state pluripotency maintenance and dissolution.

The above-mentioned molecular logic adequately explains the transcriptional signature observed in the single inhibitor experiment. However, it falls short in accounting for the notable similarity in cell-ECM interaction between 2i and N2B27+Chir conditions. For this, the mechanical implication of β-catenin preservation needs to be considered.

Besides its transcriptional function, β-catenin exerts control over mESC structural organization. It binds to the cytoplasmic tail of cadherins and is shown to strengthen cell-cell adhesion albeit in other cell systems [274,275]. Such strong intercellular adhesion is shown to impede cell/colony spreading, which in turn reduces cell-matrix interaction and traction force exertion [216]. Apart from the cell-cell adhesion stabilization, β-catenin also operates through promoting the membrane cortex attachment through Ezrin phosphorylation. This sequesters majority of the F-actin to the plasma membrane due to which cells acquire high membrane tension which is non-permissive for cell spreading. Also, F-actin being heavily localized at the cortex implies the force transmitted by the myosin motor activity to integrins is lowered and might be causing the reduction in traction forces. The impaired force transmission could also be the reason for reduced nuclear deformation as suggested by lower nuclear aspect ratio.

In the two conditions where pluripotency dissolution occurred: N2B27 and N2B27+PD, the media composition doesn't preserve β-catenin, be it cytoplasmic or nuclear. If the cell-cell adhesion strengthening and/or membrane cortex tethering functions are compromised, it is expected to result in increased colony spreading, traction force exertion and nuclear deformation. Since all these were observed in N2B27 and N2B27+PD, it is highly probable that the above explanation holds true as to how membrane associated β-catenin influences cell-matrix interaction and nuclear force transmission. To confirm if indeed this is the mechanism of action, measuring the expression levels of phosphorylated Ezrin through immunofluorescence would suffice. To check if the regulation is through stabilization of

cadherin junction, immunofluorescence staining of E-cadherin phosphorylated at serine residues – 840/-842/-848 could be performed. The rationale being phosphorylation at any of these three sites is reported to promote binding affinity to β-catenin thereby increasing cadherin junction stability [336]. Generating dominant negative cadherin mutants with mentioned serine residues converted to alanine is an alternative way of confirming cell adhesion strengthening and thereby pluripotency preservation by β-catenin.

The membrane activity of β-catenin might be of greater significance than its transcriptional activity, as nuclear translocation of β-catenin is also implicated in differentiation of both mouse and human ESCs [337]. Besides, nuclear β-catenin is shown to drive epithelial to mesenchymal transition (EMT) [338, 339], the morphological transformation that accompanies pluripotency loss in mESCs [61, 62]. To confirm this, mESCs could be treated with low dose of lithium chloride (LiCl) which has been shown to promote the translocation of membrane bound β-catenin to the nucleus [340-342]. LiCl treatment could be performed for mESCs cultured in N2B27 or N2B27+PD and is expected to not alter the high cell-ECM force transmission observed in these conditions. Non rescue of Rex1-GFP signal decay and naïve pluripotency factor loss further validates that membrane activity of β-catenin is indispensable for naïve pluripotency maintenance.

Overall, through a comprehensive molecular characterization and mechano-response quantification, this thesis highlights the importance of cell-ECM force transmission for pluripotency dissolution in mESCs. *In vivo*, pluripotency loss is followed by gastrulation. As it occurs in the implanted embryos, elucidating post-gastrulation development and its regulation by cell-ECM interaction remains a challenge. Given the attributes of sulfo-SANPAH gels presented in this work and the availability of gastrulation inducing media, it now becomes experimentally viable to open and to delineate the governing mechanical principles of this developmental ‘black box’.

Chapter 6: Conclusions

In view of the results presented in the thesis, the following conclusions are drawn:

1. Polyacrylamide gels functionalized with sulfo-SANPAH protocol are ideally suited to study cell-matrix interaction during mESC pluripotency dissolution.
2. The temporal changes of transcriptional factor expression associated with pluripotency dissolution are recapitulated for mESC colonies cultured on sulfo-SANPAH gels.
3. Gradual pluripotency dissolution for mESC colonies on sulfo-SANPAH gels is attested by progressive decline in Rex1-GFP fluorescence signal.
4. Cell-matrix interaction evolves with pluripotency dissolution as signified by an increase in colony area, focal adhesion length and traction forces of differentiating colonies.
5. Interferences with cell-matrix force transmission alters the kinetics of pluripotency dissolution.
6. The edge of the colonies exhibits a less naive signature and a higher mechanotransduction profile, which is further amplified when colonies are subjected to N2B27 differentiation.
7. Shape changes confirm the integration of the nucleus into the mechanotransduction that accompanies pluripotency dissolution in mESC colonies.
8. Abrogating nuclear and actin cytoskeleton linkage mildly slows down the pluripotency dissolution.
9. Regional differences in the expression of YAP and Nanog are correlated with Nuclear shape changes
10. Regional differences in Otx2 expression cannot be adequately explained by nuclear shape changes.
11. β-catenin signalling is minimally sufficient to safeguard naive state pluripotency in mESC colonies.
12. The transcriptional and mechanical signature of mESC colonies upon β-catenin preservation mimic those of absolute naive colonies grown in 2i media.
13. Cell-matrix force transmission forecasts the evolution of pluripotency status in mESC colonies.

Chapter 7: Bibliography

1. Frum T, Murphy TM, Ralston A. HIPPO signaling resolves embryonic cell fate conflicts during establishment of pluripotency in vivo. Elife. 2018 Dec 11;7:e42298. doi: 10.7554/eLife.42298. PMID: 30526858; PMCID: PMC6289571.
2. Carter AM, Enders AC, Pijnenborg R. The role of invasive trophoblast in implantation and placentation of primates. Philos Trans R Soc Lond B Biol Sci. 2015 Mar 5;370(1663):20140070. doi: 10.1098/rstb.2014.0070. PMID: 25602074; PMCID: PMC4305171.
3. Silva JF, Serakides R. Intrauterine trophoblast migration: A comparative view of humans and rodents. Cell Adh Migr. 2016 Mar 3;10(1-2):88-110. doi: 10.1080/19336918.2015.1120397. Epub 2016 Jan 8. PMID: 26743330; PMCID: PMC4853047.
4. Boiani M, Schöler HR. Regulatory networks in embryo-derived pluripotent stem cells. Nat Rev Mol Cell Biol. 2005 Nov;6(11):872-84. doi: 10.1038/nrm1744. PMID: 16227977.
5. Bedzhov I, Graham SJ, Leung CY, Zernicka-Goetz M. Developmental plasticity, cell fate specification and morphogenesis in the early mouse embryo. Philos Trans R Soc Lond B Biol Sci. 2014 Dec 5;369(1657):20130538. doi: 10.1098/rstb.2013.0538. Erratum in: Philos Trans R Soc Lond B Biol Sci. 2015 Feb 5;370(1661):20140339. PMID: 25349447; PMCID: PMC4216461.
6. Bessonnard S, De Mot L, Gonze D, Barriol M, Dennis C, Goldbeter A, Dupont G, Chazaud C. Gata6, Nanog and Erk signaling control cell fate in the inner cell mass through a tristable regulatory network. Development. 2014 Oct;141(19):3637-48. doi: 10.1242/dev.109678. Epub 2014 Sep 10. PMID: 25209243.
7. Wu J, Yamauchi T, Izpisua Belmonte JC. An overview of mammalian pluripotency. Development. 2016 May 15;143(10):1644-8. doi: 10.1242/dev.132928. PMID: 27190034.
8. Hermitte S, Chazaud C. Primitive endoderm differentiation: from specification to epithelium formation. Philos Trans R Soc Lond B Biol Sci. 2014 Dec 5;369(1657):20130537. doi: 10.1098/rstb.2013.0537. PMID: 25349446; PMCID: PMC4216460.
9. Gardner RL, Beddington RS. Multi-lineage 'stem' cells in the mammalian embryo. J Cell Sci Suppl. 1988;10:11-27. doi: 10.1242/jcs.1988.supplement_10.2. PMID: 3077932.
10. Boroviak T, Loos R, Bertone P, Smith A, Nichols J. The ability of inner-cell-mass cells to self-renew as embryonic stem cells is acquired following epiblast specification. Nat Cell Biol. 2014 Jun;16(6):516-28. doi: 10.1038/ncb2965. Epub 2014 May 25. PMID: 24859004; PMCID: PMC4878656.
11. Nichols J, Smith A. Pluripotency in the embryo and in culture. Cold Spring Harb Perspect Biol. 2012 Aug 1;4(8):a008128. doi: 10.1101/cshperspect.a008128. PMID: 22855723; PMCID: PMC3405859.
12. Li M, Liu GH, Izpisua Belmonte JC. Navigating the epigenetic landscape of pluripotent stem cells. Nat Rev Mol Cell Biol. 2012 Jul 23;13(8):524-35. doi: 10.1038/nrm3393. PMID: 22820889.
13. Pierce GB, Arechaga J, Muro C, Wells RS. Differentiation of ICM cells into trophectoderm. Am J Pathol. 1988 Aug;132(2):356-64. PMID: 3400778; PMCID: PMC1880734.

14. Niwa H, Toyooka Y, Shimosato D, Strumpf D, Takahashi K, Yagi R, Rossant J. Interaction between Oct3/4 and Cdx2 determines trophectoderm differentiation. Cell. 2005 Dec 2;123(5):917-29. doi: 10.1016/j.cell.2005.08.040. PMID: 16325584.
15. Strumpf D, Mao CA, Yamanaka Y, Ralston A, Chawengsaksophak K, Beck F, Rossant J. Cdx2 is required for correct cell fate specification and differentiation of trophectoderm in the mouse blastocyst. Development. 2005 May;132(9):2093-102. doi: 10.1242/dev.01801. Epub 2005 Mar 23. PMID: 15788452.
16. Guo G, Huss M, Tong GQ, Wang C, Li Sun L, Clarke ND, Robson P. Resolution of cell fate decisions revealed by single-cell gene expression analysis from zygote to blastocyst. Dev Cell. 2010 Apr 20;18(4):675-85. doi: 10.1016/j.devcel.2010.02.012. PMID: 20412781.
17. Ohnishi Y, Huber W, Tsumura A, Kang M, Xenopoulos P, Kurimoto K, Oleś AK, Araúzo-Bravo MJ, Saitou M, Hadjantonakis AK, Hiiragi T. Cell-to-cell expression variability followed by signal reinforcement progressively segregates early mouse lineages. Nat Cell Biol. 2014 Jan;16(1):27-37. doi: 10.1038/ncb2881. Epub 2013 Dec 1. PMID: 24292013; PMCID: PMC4062977.
18. Nishioka N, Inoue K, Adachi K, Kiyonari H, Ota M, Ralston A, Yabuta N, Hirahara S, Stephenson RO, Ogonuki N, Makita R, Kurihara H, Morin-Kensicki EM, Nojima H, Rossant J, Nakao K, Niwa H, Sasaki H. The Hippo signaling pathway components Lats and Yap pattern Tead4 activity to distinguish mouse trophectoderm from inner cell mass. Dev Cell. 2009 Mar;16(3):398-410. doi: 10.1016/j.devcel.2009.02.003. PMID: 19289085.
19. Yanagida A, Corujo-Simon E, Revell CK, Sahu P, Stirparo GG, Aspalter IM, Winkel AK, Peters R, De Belly H, Cassani DAD, Achouri S, Blumenfeld R, Franze K, Hannezo E, Paluch EK, Nichols J, Chalut KJ. Cell surface fluctuations regulate early embryonic lineage sorting. Cell. 2022 Mar 31;185(7):1258. doi: 10.1016/j.cell.2022.03.015. Erratum for: Cell. 2022 Mar 3;185(5):777-793.e20. PMID: 35364033; PMCID: PMC8970287.
20. Ryan AQ, Chan CJ, Graner F, Hiiragi T. Lumen Expansion Facilitates Epiblast-Primitive Endoderm Fate Specification during Mouse Blastocyst Formation. Dev Cell. 2019 Dec 16;51(6):684-697.e4. doi: 10.1016/j.devcel.2019.10.011. Epub 2019 Nov 14. PMID: 31735667; PMCID: PMC6912163.
21. Carey FJ, Linney EA, Pedersen RA. Allocation of epiblast cells to germ layer derivatives during mouse gastrulation as studied with a retroviral vector. Dev Genet. 1995;17(1):29-37. doi: 10.1002/dvg.1020170105. PMID: 7554493.
22. Hamidi S, Nakaya Y, Nagai H, Alev C, Kasukawa T, Chhabra S, Lee R, Niwa H, Warmflash A, Shibata T, Sheng G. Mesenchymal-epithelial transition regulates initiation of pluripotency exit before gastrulation. Development. 2020 Feb 3;147(3):dev184960. doi: 10.1242/dev.184960. PMID: 32014865.
23. Shahbazi MN, Scialdone A, Skorupska N, Weberling A, Recher G, Zhu M, Jedrusik A, Devito LG, Noli L, Macaulay IC, Buecker C, Khalaf Y, Ilic D, Voet T, Marioni JC, Zernicka-Goetz M. Pluripotent state transitions coordinate morphogenesis in mouse and human embryos. Nature. 2017 Dec 14;552(7684):239-243. doi: 10.1038/nature24675. Epub 2017 Nov 29. Erratum in: Nature. 2018 Feb 28;555(7694):126. PMID: 29186120; PMCID: PMC5768241.

24. Bedzhov I, Zernicka-Goetz M. Self-organizing properties of mouse pluripotent cells initiate morphogenesis upon implantation. Cell. 2014 Feb 27;156(5):1032-44. doi: 10.1016/j.cell.2014.01.023. Epub 2014 Feb 13. PMID: 24529478; PMCID: PMC3991392.
25. Christodoulou N, Weberling A, Strathdee D, Anderson KI, Timpson P, Zernicka-Goetz M. Morphogenesis of extra-embryonic tissues directs the remodelling of the mouse embryo at implantation. Nat Commun. 2019 Aug 7;10(1):3557. doi: 10.1038/s41467-019-11482-5. PMID: 31391456; PMCID: PMC6686005.
26. Kyprianou C, Christodoulou N, Hamilton RS, Nahaboo W, Boomgaard DS, Amadei G, Migeotte I, Zernicka-Goetz M. Basement membrane remodelling regulates mouse embryogenesis. Nature. 2020 Jun;582(7811):253-258. doi: 10.1038/s41586-020-2264-2. Epub 2020 May 6. PMID: 32523119; PMCID: PMC7308173.
27. Kim YS, Fan R, Kremer L, Kuempel-Rink N, Mildner K, Zeuschner D, Hekking L, Stehling M, Bedzhov I. Deciphering epiblast lumenogenesis reveals proamniotic cavity control of embryo growth and patterning. Sci Adv. 2021 Mar 10;7(11):eabe1640. doi: 10.1126/sciadv.abe1640. PMID: 33692105; PMCID: PMC7946377.
28. Chan CJ, Costanzo M, Ruiz-Herrero T, Mönke G, Petrie RJ, Bergert M, Diz-Muñoz A, Mahadevan L, Hiiragi T. Hydraulic control of mammalian embryo size and cell fate. Nature. 2019 Jul;571(7763):112-116. doi: 10.1038/s41586-019-1309-x. Epub 2019 Jun 12. PMID: 31189957.
29. Latorre E, Kale S, Casares L, Gómez-González M, Uroz M, Valon L, Nair RV, Garreta E, Montserrat N, Del Campo A, Ladoux B, Arroyo M, Trepat X. Addendum: Active superelasticity in three-dimensional epithelia of controlled shape. Nature. 2021 Apr;592(7856):E30. doi: 10.1038/s41586-021-03281-0. Erratum for: Nature. 2018 Nov;563(7730):203-208. PMID: 33846613.
30. Chen Q, Zhang Y, Elad D, Jaffa AJ, Cao Y, Ye X, Duan E. Navigating the site for embryo implantation: biomechanical and molecular regulation of intrauterine embryo distribution. Mol Aspects Med. 2013 Oct;34(5):1024-42. doi: 10.1016/j.mam.2012.07.017. Epub 2012 Aug 14. Erratum in: Mol Aspects Med. 2013 Dec;34(6):1257. PMID: 22921800.
31. Hiramatsu R, Matsuoka T, Kimura-Yoshida C, Han SW, Mochida K, Adachi T, Takayama S, Matsuo I. External mechanical cues trigger the establishment of the anterior-posterior axis in early mouse embryos. Dev Cell. 2013 Oct 28;27(2):131-144. doi: 10.1016/j.devcel.2013.09.026. PMID: 24176640.
32. Zhang S, Kong S, Wang B, Cheng X, Chen Y, Wu W, Wang Q, Shi J, Zhang Y, Wang S, Lu J, Lydon JP, DeMayo F, Pear WS, Han H, Lin H, Li L, Wang H, Wang YL, Li B, Chen Q, Duan E, Wang H. Uterine Rbpj is required for embryonic-uterine orientation and decidual remodeling via Notch pathway-independent and -dependent mechanisms. Cell Res. 2014 Aug;24(8):925-42. doi: 10.1038/cr.2014.82. Epub 2014 Jun 27. PMID: 24971735; PMCID: PMC4123295.
33. Brons IG, Smithers LE, Trotter MW, Rugg-Gunn P, Sun B, Chuva de Sousa Lopes SM, Howlett SK, Clarkson A, Ahrlund-Richter L, Pedersen RA, Vallier L. Derivation of pluripotent epiblast stem cells from mammalian embryos. Nature. 2007 Jul 12;448(7150):191-5. doi: 10.1038/nature05950. Epub 2007 Jun 27. PMID: 17597762.
34. Leitch HG, McEwen KR, Turp A, Encheva V, Carroll T, Grabole N, Mansfield W, Nashun B, Knezovich JG, Smith A, Surani MA, Hajkova P. Naive pluripotency is

associated with global DNA hypomethylation. Nat Struct Mol Biol. 2013 Mar;20(3):311-6. doi: 10.1038/nsmb.2510. Epub 2013 Feb 17. PMID: 23416945; PMCID: PMC3591483.
35. Marks H, Kalkan T, Menafra R, Denissov S, Jones K, Hofemeister H, Nichols J, Kranz A, Stewart AF, Smith A, Stunnenberg HG. The transcriptional and epigenomic foundations of ground state pluripotency. Cell. 2012 Apr 27;149(3):590-604. doi: 10.1016/j.cell.2012.03.026. PMID: 22541430; PMCID: PMC3398752.
36. Nichols J, Smith A. Naive and primed pluripotent states. Cell Stem Cell. 2009 Jun 5;4(6):487-92. doi: 10.1016/j.stem.2009.05.015. PMID: 19497275.
37. Tesar PJ, Chenoweth JG, Brook FA, Davies TJ, Evans EP, Mack DL, Gardner RL, McKay RD. New cell lines from mouse epiblast share defining features with human embryonic stem cells. Nature. 2007 Jul 12;448(7150):196-9. doi: 10.1038/nature05972. Epub 2007 Jun 27. PMID: 17597760.
38. Weinberger L, Ayyash M, Novershtern N, Hanna JH. Dynamic stem cell states: naive to primed pluripotency in rodents and humans. Nat Rev Mol Cell Biol. 2016 Mar;17(3):155-69. doi: 10.1038/nrm.2015.28. Epub 2016 Feb 10. PMID: 26860365.
39. Morgani S, Nichols J, Hadjantonakis AK. The many faces of Pluripotency: in vitro adaptations of a continuum of in vivo states. BMC Dev Biol. 2017 Jun 13;17(1):7. doi: 10.1186/s12861-017-0150-4. PMID: 28610558; PMCID: PMC5470286.
40. Smith A. Formative pluripotency: the executive phase in a developmental continuum. Development. 2017 Feb 1;144(3):365-373. doi: 10.1242/dev.142679. PMID: 28143843; PMCID: PMC5430734.
41. Beddington RS, Robertson EJ. Axis development and early asymmetry in mammals. Cell. 1999 Jan 22;96(2):195-209. doi: 10.1016/s0092-8674(00)80560-7. PMID: 9988215.
42. Sheng G. Epiblast morphogenesis before gastrulation. Dev Biol. 2015 May 1;401(1):17-24. doi: 10.1016/j.ydbio.2014.10.003. Epub 2014 Oct 19. PMID: 25446532.
43. Arnold SJ, Robertson EJ. Making a commitment: cell lineage allocation and axis patterning in the early mouse embryo. Nat Rev Mol Cell Biol. 2009 Feb;10(2):91-103. doi: 10.1038/nrm2618. Epub 2009 Jan 8. PMID: 19129791.
44. Lawson KA, Meneses JJ, Pedersen RA. Clonal analysis of epiblast fate during germ layer formation in the mouse embryo. Development. 1991 Nov;113(3):891-911. doi: 10.1242/dev.113.3.891. PMID: 1821858.
45. Kalkan T, Smith A. Mapping the route from naive pluripotency to lineage specification. Philos Trans R Soc Lond B Biol Sci. 2014 Dec 5;369(1657):20130540. doi: 10.1098/rstb.2013.0540. PMID: 25349449; PMCID: PMC4216463.
46. Hackett JA, Surani MA. Regulatory principles of pluripotency: from the ground state up. Cell Stem Cell. 2014 Oct 2;15(4):416-430. doi: 10.1016/j.stem.2014.09.015. PMID: 25280218.
47. Boroviak T, Nichols J. Primate embryogenesis predicts the hallmarks of human naïve pluripotency. Development. 2017 Jan 15;144(2):175-186. doi: 10.1242/dev.145177. PMID: 28096211; PMCID: PMC5430762.
48. Soufi A, Dalton S. Cycling through developmental decisions: how cell cycle dynamics control pluripotency, differentiation and reprogramming. Development. 2016 Dec

1;143(23):4301-4311. doi: 10.1242/dev.142075. PMID: 27899507; PMCID: PMC5201050.
49. Dalton S. Linking the Cell Cycle to Cell Fate Decisions. Trends Cell Biol. 2015 Oct;25(10):592-600. doi: 10.1016/j.tcb.2015.07.007. PMID: 26410405; PMCID: PMC4584407.
50. Li M, Izpisua Belmonte JC. Deconstructing the pluripotency gene regulatory network. Nat Cell Biol. 2018 Apr;20(4):382-392. doi: 10.1038/s41556-018-0067-6. Epub 2018 Mar 28. PMID: 29593328; PMCID: PMC6620196.
51. Loh KM, Lim B. A precarious balance: pluripotency factors as lineage specifiers. Cell Stem Cell. 2011 Apr 8;8(4):363-9. doi: 10.1016/j.stem.2011.03.013. PMID: 21474100.
52. Chew JL, Loh YH, Zhang W, Chen X, Tam WL, Yeap LS, Li P, Ang YS, Lim B, Robson P, Ng HH. Reciprocal transcriptional regulation of Pou5f1 and Sox2 via the Oct4/Sox2 complex in embryonic stem cells. Mol Cell Biol. 2005 Jul;25(14):6031-46. doi: 10.1128/MCB.25.14.6031-6046.2005. PMID: 15988017; PMCID: PMC1168830.
53. Chambers I, Colby D, Robertson M, Nichols J, Lee S, Tweedie S, Smith A. Functional expression cloning of Nanog, a pluripotency sustaining factor in embryonic stem cells. Cell. 2003 May 30;113(5):643-55. doi: 10.1016/s0092-8674(03)00392-1. PMID: 12787505.
54. Barral A, Rollan I, Sanchez-Iranzo H, Jawaid W, Badia-Careaga C, Menchero S, Gomez MJ, Torroja C, Sanchez-Cabo F, Göttgens B, Manzanares M, Sainz de Aja J. *Nanog* regulates *Pou3f1* expression at the exit from pluripotency during gastrulation. Biol Open. 2019 Dec 2;8(11):bio046367. doi: 10.1242/bio.046367. PMID: 31791948; PMCID: PMC6899006.
55. Hart AH, Hartley L, Ibrahim M, Robb L. Identification, cloning and expression analysis of the pluripotency promoting Nanog genes in mouse and human. Dev Dyn. 2004 May;230(1):187-98. doi: 10.1002/dvdy.20034. PMID: 15108323.
56. Mullin NP, Yates A, Rowe AJ, Nijmeijer B, Colby D, Barlow PN, Walkinshaw MD, Chambers I. The pluripotency rheostat Nanog functions as a dimer. Biochem J. 2008 Apr 15;411(2):227-31. doi: 10.1042/BJ20080134. PMID: 18290762.
57. Ehnes DD, Hussein AM, Ware CB, Mathieu J, Ruohola-Baker H. Combinatorial metabolism drives the naive to primed pluripotent chromatin landscape. Exp Cell Res. 2020 Apr 15;389(2):111913. doi: 10.1016/j.yexcr.2020.111913. Epub 2020 Feb 19. PMID: 32084392.
58. Plath K, Mlynarczyk-Evans S, Nusinow DA, Panning B. Xist RNA and the mechanism of X chromosome inactivation. Annu Rev Genet. 2002;36:233-78. doi: 10.1146/annurev.genet.36.042902.092433. Epub 2002 Jun 11. PMID: 12429693.
59. Disteche CM. Dosage compensation of the sex chromosomes and autosomes. Semin Cell Dev Biol. 2016 Aug;56:9-18. doi: 10.1016/j.semcdb.2016.04.013. Epub 2016 Apr 22. PMID: 27112542; PMCID: PMC4955796.
60. Morey C, Avner P. The demoiselle of X-inactivation: 50 years old and as trendy and mesmerising as ever. PLoS Genet. 2011 Jul;7(7):e1002212. doi: 10.1371/journal.pgen.1002212. Epub 2011 Jul 21. PMID: 21811421; PMCID: PMC3141017.
61. Hamidi S, Nakaya Y, Nagai H, Alev C, Kasukawa T, Chhabra S, Lee R, Niwa H, Warmflash A, Shibata T, Sheng G. Mesenchymal-epithelial transition regulates

initiation of pluripotency exit before gastrulation. Development. 2020 Feb 3;147(3):dev184960. doi: 10.1242/dev.184960. PMID: 32014865
62. Ferrer-Vaquer A, Viotti M, Hadjantonakis AK. Transitions between epithelial and mesenchymal states and the morphogenesis of the early mouse embryo. Cell Adh Migr. 2010 Jul-Sep;4(3):447-57. doi: 10.4161/cam.4.3.10771. Epub 2010 Jul 30. PMID: 20200481; PMCID: PMC2958623
63. Choi HW, Joo JY, Hong YJ, Kim JS, Song H, Lee JW, Wu G, Schöler HR, Do JT. Distinct Enhancer Activity of Oct4 in Naive and Primed Mouse Pluripotency. Stem Cell Reports. 2016 Nov 8;7(5):911-926. doi: 10.1016/j.stemcr.2016.09.012. Epub 2016 Oct 27. PMID: 28157483; PMCID: PMC5106531.
64. Kim EJY, Sorokin L, Hiiragi T. ECM-integrin signalling instructs cellular position sensing to pattern the early mouse embryo. Development. 2022 Jan 1;149(1):dev200140. doi: 10.1242/dev.200140. Epub 2022 Jan 13. PMID: 34908109; PMCID: PMC8881741.
65. Aksoy I, Jauch R, Chen J, Dyla M, Divakar U, Bogu GK, Teo R, Leng Ng CK, Herath W, Lili S, Hutchins AP, Robson P, Kolatkar PR, Stanton LW. Oct4 switches partnering from Sox2 to Sox17 to reinterpret the enhancer code and specify endoderm. EMBO J. 2013 Apr 3;32(7):938-53. doi: 10.1038/emboj.2013.31. Epub 2013 Mar 8. PMID: 23474895; PMCID: PMC3616284.
66. Cui L, Johkura K, Yue F, Ogiwara N, Okouchi Y, Asanuma K, Sasaki K. Spatial distribution and initial changes of SSEA-1 and other cell adhesion-related molecules on mouse embryonic stem cells before and during differentiation. J Histochem Cytochem. 2004 Nov;52(11):1447-57. doi: 10.1369/jhc.3A6241.2004. PMID: 15505339; PMCID: PMC3957812.
67. Shakiba N, White CA, Lipsitz YY, Yachie-Kinoshita A, Tonge PD, Hussein SMI, Puri MC, Elbaz J, Morrissey-Scoot J, Li M, Munoz J, Benevento M, Rogers IM, Hanna JH, Heck AJR, Wollscheid B, Nagy A, Zandstra PW. CD24 tracks divergent pluripotent states in mouse and human cells. Nat Commun. 2015 Jun 16;6:7329. doi: 10.1038/ncomms8329. PMID: 26076835; PMCID: PMC4490408.
68. George EL, Georges-Labouesse EN, Patel-King RS, Rayburn H, Hynes RO. Defects in mesoderm, neural tube and vascular development in mouse embryos lacking fibronectin. Development. 1993 Dec;119(4):1079-91. doi: 10.1242/dev.119.4.1079. PMID: 8306876.
69. Niwa H, Ogawa K, Shimosato D, Adachi K. A parallel circuit of LIF signalling pathways maintains pluripotency of mouse ES cells. Nature. 2009 Jul 2;460(7251):118-22. doi: 10.1038/nature08113. PMID: 19571885.
70. Martello G, Bertone P, Smith A. Identification of the missing pluripotency mediator downstream of leukaemia inhibitory factor. EMBO J. 2013 Oct 2;32(19):2561-74. doi: 10.1038/emboj.2013.177. Epub 2013 Aug 13. PMID: 23942233; PMCID: PMC3791366.
71. Ye S, Li P, Tong C, Ying QL. Embryonic stem cell self-renewal pathways converge on the transcription factor Tfcp2l1. EMBO J. 2013 Oct 2;32(19):2548-60. doi: 10.1038/emboj.2013.175. Epub 2013 Aug 13. PMID: 23942238; PMCID: PMC3791365.
72. Boroviak T, Loos R, Lombard P, Okahara J, Behr R, Sasaki E, Nichols J, Smith A, Bertone P. Lineage-Specific Profiling Delineates the Emergence and Progression of

Naive Pluripotency in Mammalian Embryogenesis. Dev Cell. 2015 Nov 9;35(3):366-82. doi: 10.1016/j.devcel.2015.10.011. PMID: 26555056; PMCID: PMC4643313.
73. Acampora D, Omodei D, Petrosino G, Garofalo A, Savarese M, Nigro V, Di Giovannantonio LG, Mercadante V, Simeone A. Loss of the Otx2-Binding Site in the Nanog Promoter Affects the Integrity of Embryonic Stem Cell Subtypes and Specification of Inner Cell Mass-Derived Epiblast. Cell Rep. 2016 Jun 21;15(12):2651-64. doi: 10.1016/j.celrep.2016.05.041. Epub 2016 Jun 9. PMID: 27292645.
74. Kalkan T, Olova N, Roode M, Mulas C, Lee HJ, Nett I, Marks H, Walker R, Stunnenberg HG, Lilley KS, Nichols J, Reik W, Bertone P, Smith A. Tracking the embryonic stem cell transition from ground state pluripotency. Development. 2017 Apr 1;144(7):1221-1234. doi: 10.1242/dev.142711. Epub 2017 Feb 7. PMID: 28174249; PMCID: PMC5399622.
75. Acampora D, Di Giovannantonio LG, Simeone A. Otx2 is an intrinsic determinant of the embryonic stem cell state and is required for transition to a stable epiblast stem cell condition. Development. 2013 Jan 1;140(1):43-55. doi: 10.1242/dev.085290. Epub 2012 Nov 15. PMID: 23154415.
76. Kunath T, Saba-El-Leil MK, Almousailleakh M, Wray J, Meloche S, Smith A. FGF stimulation of the Erk1/2 signalling cascade triggers transition of pluripotent embryonic stem cells from self-renewal to lineage commitment. Development. 2007 Aug;134(16):2895-902. doi: 10.1242/dev.02880. PMID: 17660198.
77. Neagu A, van Genderen E, Escudero I, Verwegen L, Kurek D, Lehmann J, Stel J, Dirks RAM, van Mierlo G, Maas A, Eleveld C, Ge Y, den Dekker AT, Brouwer RWW, van IJcken WFJ, Modic M, Drukker M, Jansen JH, Rivron NC, Baart EB, Marks H, Ten Berge D. In vitro capture and characterization of embryonic rosette-stage pluripotency between naive and primed states. Nat Cell Biol. 2020 May;22(5):534-545. doi: 10.1038/s41556-020-0508-x. Epub 2020 May 4. PMID: 32367046.
78. Mead RA. Embryonic diapause in vertebrates. J Exp Zool. 1993 Sep 1;266(6):629-41. doi: 10.1002/jez.1402660611. PMID: 8371102.
79. Mulas C, Kalkan T, von Meyenn F, Leitch HG, Nichols J, Smith A. Defined conditions for propagation and manipulation of mouse embryonic stem cells. Development. 2019 Mar 26;146(6):dev173146. doi: 10.1242/dev.173146. Erratum in: Development. 2019 Apr 11;146(7): PMID: 30914406; PMCID: PMC6451320.
80. Rugg-Gunn P. Derivation and Culture of Epiblast Stem Cell (EpiSC) Lines. Cold Spring Harb Protoc. 2017 Jan 3;2017(1). doi: 10.1101/pdb.prot093971. PMID: 28049783.
81. McGrath J, Solter D. Nuclear transplantation in the mouse embryo by microsurgery and cell fusion. Science. 1983 Jun 17;220(4603):1300-2. doi: 10.1126/science.6857250. PMID: 6857250.
82. Takahashi K, Tanabe K, Ohnuki M, Narita M, Ichisaka T, Tomoda K, Yamanaka S. Induction of pluripotent stem cells from adult human fibroblasts by defined factors. Cell. 2007 Nov 30;131(5):861-72. doi: 10.1016/j.cell.2007.11.019. PMID: 18035408.
83. Leitch HG, Blair K, Mansfield W, Ayetey H, Humphreys P, Nichols J, Surani MA, Smith A. Embryonic germ cells from mice and rats exhibit properties consistent with a generic pluripotent ground state. Development. 2010 Jul;137(14):2279-87. doi: 10.1242/dev.050427. Epub 2010 Jun 2. PMID: 20519324; PMCID: PMC2889601.

84. Matsui Y, Zsebo K, Hogan BL. Derivation of pluripotential embryonic stem cells from murine primordial germ cells in culture. Cell. 1992 Sep 4;70(5):841-7. doi: 10.1016/0092-8674(92)90317-6. PMID: 1381289.
85. Kanatsu-Shinohara M, Inoue K, Lee J, Yoshimoto M, Ogonuki N, Miki H, Baba S, Kato T, Kazuki Y, Toyokuni S, Toyoshima M, Niwa O, Oshimura M, Heike T, Nakahata T, Ishino F, Ogura A, Shinohara T. Generation of pluripotent stem cells from neonatal mouse testis. Cell. 2004 Dec 29;119(7):1001-12. doi: 10.1016/j.cell.2004.11.011. PMID: 15620358.
86. Ko K, Tapia N, Wu G, Kim JB, Bravo MJ, Sasse P, Glaser T, Ruau D, Han DW, Greber B, Hausdörfer K, Sebastiano V, Stehling M, Fleischmann BK, Brüstle O, Zenke M, Schöler HR. Induction of pluripotency in adult unipotent germline stem cells. Cell Stem Cell. 2009 Jul 2;5(1):87-96. doi: 10.1016/j.stem.2009.05.025. PMID: 19570517.
87. Hayashi K, Ohta H, Kurimoto K, Aramaki S, Saitou M. Reconstitution of the mouse germ cell specification pathway in culture by pluripotent stem cells. Cell. 2011 Aug 19;146(4):519-32. doi: 10.1016/j.cell.2011.06.052. Epub 2011 Aug 4. PMID: 21820164.
88. Buecker C, Srinivasan R, Wu Z, Calo E, Acampora D, Faial T, Simeone A, Tan M, Swigut T, Wysocka J. Reorganization of enhancer patterns in transition from naive to primed pluripotency. Cell Stem Cell. 2014 Jun 5;14(6):838-53. doi: 10.1016/j.stem.2014.04.003. PMID: 24905168; PMCID: PMC4491504.
89. Hanna J, Saha K, Pando B, van Zon J, Lengner CJ, Creyghton MP, van Oudenaarden A, Jaenisch R. Direct cell reprogramming is a stochastic process amenable to acceleration. Nature. 2009 Dec 3;462(7273):595-601. doi: 10.1038/nature08592. Epub 2009 Nov 8. PMID: 19898493; PMCID: PMC2789972.
90. Guo G, Yang J, Nichols J, Hall JS, Eyres I, Mansfield W, Smith A. Klf4 reverts developmentally programmed restriction of ground state pluripotency. Development. 2009 Apr;136(7):1063-9. doi: 10.1242/dev.030957. Epub 2009 Feb 18. PMID: 19224983; PMCID: PMC2685927.
91. Bao S, Tang F, Li X, Hayashi K, Gillich A, Lao K, Surani MA. Epigenetic reversion of post-implantation epiblast to pluripotent embryonic stem cells. Nature. 2009 Oct 29;461(7268):1292-5. doi: 10.1038/nature08534. PMID: 19816418; PMCID: PMC3863718.
92. Najm FJ, Chenoweth JG, Anderson PD, Nadeau JH, Redline RW, McKay RD, Tesar PJ. Isolation of epiblast stem cells from preimplantation mouse embryos. Cell Stem Cell. 2011 Mar 4;8(3):318-25. doi: 10.1016/j.stem.2011.01.016. PMID: 21362571; PMCID: PMC3073125.
93. Theunissen TW, Powell BE, Wang H, Mitalipova M, Faddah DA, Reddy J, Fan ZP, Maetzel D, Ganz K, Shi L, Lungjangwa T, Imsoonthornruksa S, Stelzer Y, Rangarajan S, D'Alessio A, Zhang J, Gao Q, Dawlaty MM, Young RA, Gray NS, Jaenisch R. Systematic identification of culture conditions for induction and maintenance of naive human pluripotency. Cell Stem Cell. 2014 Oct 2;15(4):471-487. doi: 10.1016/j.stem.2014.07.002. Epub 2014 Jul 24. Erratum in: Cell Stem Cell. 2014 Oct 2;15(4):523. Erratum in: Cell Stem Cell. 2014 Oct 2;15(4):524-526. PMID: 25090446; PMCID: PMC4184977.

94. Evans MJ, Kaufman MH. Establishment in culture of pluripotential cells from mouse embryos. Nature. 1981 Jul 9;292(5819):154-6. doi: 10.1038/292154a0. PMID: 7242681.
95. Meng GL, Zur Nieden NI, Liu SY, Cormier JT, Kallos MS, Rancourt DE. Properties of murine embryonic stem cells maintained on human foreskin fibroblasts without LIF. Mol Reprod Dev. 2008 Apr;75(4):614-22. doi: 10.1002/mrd.20790. PMID: 17886269.
96. Lee KH. Conditions and techniques for mouse embryonic stem cell derivation and culture. Pluripotent Stem Cells. 2013. pp. 85–115.
97. Hilbert L, Sato Y, Kuznetsova K, Bianucci T, Kimura H, Jülicher F, Honigmann A, Zaburdaev V, Vastenhouw NL. Transcription organizes euchromatin via microphase separation. Nat Commun. 2021 Mar 1;12(1):1360. doi: 10.1038/s41467-021-21589-3. Erratum in: Nat Commun. 2021 Jul 6;12(1):4240. PMID: 33649325; PMCID: PMC7921102.
98. Pettinato G, Wen X, Zhang N. Engineering Strategies for the Formation of Embryoid Bodies from Human Pluripotent Stem Cells. Stem Cells Dev. 2015 Jul 15;24(14):1595-609. doi: 10.1089/scd.2014.0427. Epub 2015 Jun 2. PMID: 25900308; PMCID: PMC4499791.
99. McKee C, Chaudhry GR. Advances and challenges in stem cell culture. Colloids Surf B Biointerfaces. 2017 Nov 1;159:62-77. doi: 10.1016/j.colsurfb.2017.07.051. Epub 2017 Jul 27. PMID: 28780462.
100. Tsuji Y, Yoshimura N, Aoki H, Sharov AA, Ko MS, Motohashi T, Kunisada T. Maintenance of undifferentiated mouse embryonic stem cells in suspension by the serum- and feeder-free defined culture condition. Dev Dyn. 2008 Aug;237(8):2129-38. doi: 10.1002/dvdy.21617. Erratum in: Dev Dyn. 2009 Feb;238(2):501. Tsuji, Yukiiko [corrected to Tsuji, Yukiko]. PMID: 18624284; PMCID: PMC2559871.
101. Tamm C, Pijuan Galitó S, Annerén C. A comparative study of protocols for mouse embryonic stem cell culturing. PLoS One. 2013 Dec 10;8(12):e81156. doi: 10.1371/journal.pone.0081156. PMID: 24339907; PMCID: PMC3858223.
102. Pettinato G, Wen X, Zhang N. Formation of well-defined embryoid bodies from dissociated human induced pluripotent stem cells using microfabricated cell-repellent microwell arrays. Sci Rep. 2014 Dec 10;4:7402. doi: 10.1038/srep07402. PMID: 25492588; PMCID: PMC4261164.
103. Wu J, Rostami MR, Cadavid Olaya DP, Tzanakakis ES. Oxygen transport and stem cell aggregation in stirred-suspension bioreactor cultures. PLoS One. 2014 Jul 17;9(7):e102486. doi: 10.1371/journal.pone.0102486. PMID: 25032842; PMCID: PMC4102498.
104. Badylak SF, Freytes DO, Gilbert TW. Extracellular matrix as a biological scaffold material: Structure and function. Acta Biomater. 2009 Jan;5(1):1-13. doi: 10.1016/j.actbio.2008.09.013. Epub 2008 Oct 2. PMID: 18938117.
105. Hollister SJ. Porous scaffold design for tissue engineering. Nat Mater. 2005 Jul;4(7):518-24. doi: 10.1038/nmat1421. Erratum in: Nat Mater. 2006 Jul;5(7):590. PMID: 16003400.
106. Caliari SR, Burdick JA. A practical guide to hydrogels for cell culture. Nat Methods. 2016 Apr 28;13(5):405-14. doi: 10.1038/nmeth.3839. PMID: 27123816; PMCID: PMC5800304.

107. Serban MA, Scott A, Prestwich GD. Use of hyaluronan-derived hydrogels for three-dimensional cell culture and tumor xenografts. Curr Protoc Cell Biol. 2008 Sep;Chapter 10:Unit 10.14. doi: 10.1002/0471143030.cb1014s40. PMID: 18819087; PMCID: PMC3319462.
108. Solchaga LA, Tognana E, Penick K, Baskaran H, Goldberg VM, Caplan AI, Welter JF. A rapid seeding technique for the assembly of large cell/scaffold composite constructs. Tissue Eng. 2006 Jul;12(7):1851-63. doi: 10.1089/ten.2006.12.1851. PMID: 16889515; PMCID: PMC1858629.
109. Baiguera S, Urbani L, Del Gaudio C. Tissue engineered scaffolds for an effective healing and regeneration: reviewing orthotopic studies. Biomed Res Int. 2014;2014:398069. doi: 10.1155/2014/398069. Epub 2014 Aug 27. PMID: 25250319; PMCID: PMC4163448.
110. Woods T, Gratzer PF. Effectiveness of three extraction techniques in the development of a decellularized bone-anterior cruciate ligament-bone graft. Biomaterials. 2005 Dec;26(35):7339-49. doi: 10.1016/j.biomaterials.2005.05.066. PMID: 16023194.
111. Li X, Sun Q, Li Q, Kawazoe N, Chen G. Functional Hydrogels With Tunable Structures and Properties for Tissue Engineering Applications. Front Chem. 2018 Oct 22;6:499. doi: 10.3389/fchem.2018.00499. PMID: 30406081; PMCID: PMC6204355.
112. Labouesse C, Tan BX, Agley CC, Hofer M, Winkel AK, Stirparo GG, Stuart HT, Verstreken CM, Mulas C, Mansfield W, Bertone P, Franze K, Silva JCR, Chalut KJ. StemBond hydrogels control the mechanical microenvironment for pluripotent stem cells. Nat Commun. 2021 Oct 21;12(1):6132. doi: 10.1038/s41467-021-26236-5. PMID: 34675200; PMCID: PMC8531294.
113. Li P, Wang S, Zhan L, He X, Chi G, Lv S, Xu Z, Xia Y, Teng S, Li L, Li Y. Efficient feeder cells preparation system for large-scale preparation and application of induced pluripotent stem cells. Sci Rep. 2017 Sep 25;7(1):12266. doi: 10.1038/s41598-017-10428-5. PMID: 28947775; PMCID: PMC5612988.
114. Namba M, Fukushima F, Kimoto T. Effects of feeder layers made of human, mouse, hamster, and rat cells on the cloning efficiency of transformed human cells. In Vitro. 1982 May;18(5):469-75. doi: 10.1007/BF02796475. PMID: 6749654.
115. Yang K, Lee J, Cho SW. Engineering biomaterials for feeder-free maintenance of human pluripotent stem cells. Int J Stem Cells. 2012 May;5(1):1-5. doi: 10.15283/ijsc.2012.5.1.1. PMID: 24298348; PMCID: PMC3840981.
116. Chen G, Xu X, Zhang L, Fu Y, Wang M, Gu H, Xie X. Blocking autocrine VEGF signaling by sunitinib, an anti-cancer drug, promotes embryonic stem cell self-renewal and somatic cell reprogramming. Cell Res. 2014 Sep;24(9):1121-36. doi: 10.1038/cr.2014.112. Epub 2014 Aug 22. PMID: 25145356; PMCID: PMC4152737.
117. Blancas AA, Chen CS, Stolberg S, McCloskey KE. Adhesive forces in embryonic stem cell cultures. Cell Adh Migr. 2011 Nov-Dec;5(6):472-9. doi: 10.4161/cam.5.6.18270. PMID: 22274712; PMCID: PMC3277780.
118. Godwin S, Ward D, Pedone E, Homer M, Fletcher AG, Marucci L. An extended model for culture-dependent heterogenous gene expression and proliferation dynamics in mouse embryonic stem cells. NPJ Syst Biol Appl. 2017 Aug 3;3:19. doi: 10.1038/s41540-017-0020-5. PMID: 28794899; PMCID: PMC5543144.

119. Mannello F, Tonti GA. Concise review: no breakthroughs for human mesenchymal and embryonic stem cell culture: conditioned medium, feeder layer, or feeder-free; medium with fetal calf serum, human serum, or enriched plasma; serum-free, serum replacement nonconditioned medium, or ad hoc formula? All that glitters is not gold! Stem Cells. 2007 Jul;25(7):1603-9. doi: 10.1634/stemcells.2007-0127. Epub 2007 Mar 29. PMID: 17395775.
120. Nichols J, Ying QL. Derivation and propagation of embryonic stem cells in serum- and feeder-free culture. Methods Mol Biol. 2006;329:91-8. doi: 10.1385/1-59745-037-5:91. PMID: 16845986.
121. Cartwright P, McLean C, Sheppard A, Rivett D, Jones K, Dalton S. LIF/STAT3 controls ES cell self-renewal and pluripotency by a Myc-dependent mechanism. Development. 2005 Mar;132(5):885-96. doi: 10.1242/dev.01670. Epub 2005 Jan 26. PMID: 15673569.
122. Chambers I, Silva J, Colby D, Nichols J, Nijmeijer B, Robertson M, Vrana J, Jones K, Grotewold L, Smith A. Nanog safeguards pluripotency and mediates germline development. Nature. 2007 Dec 20;450(7173):1230-4. doi: 10.1038/nature06403. PMID: 18097409.
123. Toyooka Y, Shimosato D, Murakami K, Takahashi K, Niwa H. Identification and characterization of subpopulations in undifferentiated ES cell culture. Development. 2008 Mar;135(5):909-18. doi: 10.1242/dev.017400. PMID: 18263842.
124. Hayashi K, de Sousa Lopes SMC, Tang F, Lao K, Surani MA. Dynamic equilibrium and heterogeneity of mouse pluripotent stem cells with distinct functional and epigenetic states. Cell Stem Cell. 2008 Oct 9;3(4):391-401. doi: 10.1016/j.stem.2008.07.027. PMID: 18940731; PMCID: PMC3847852.
125. Wray J, Kalkan T, Smith AG. The ground state of pluripotency. Biochem Soc Trans. 2010 Aug;38(4):1027-32. doi: 10.1042/BST0381027. PMID: 20658998.
126. Ying QL, Wray J, Nichols J, Batlle-Morera L, Doble B, Woodgett J, Cohen P, Smith A. The ground state of embryonic stem cell self-renewal. Nature. 2008 May 22;453(7194):519-23. doi: 10.1038/nature06968. PMID: 18497825; PMCID: PMC5328678.
127. Hirai H, Karian P, Kikyo N. Regulation of embryonic stem cell self-renewal and pluripotency by leukaemia inhibitory factor. Biochem J. 2011 Aug 15;438(1):11-23. doi: 10.1042/BJ20102152. PMID: 21793804; PMCID: PMC3418323.
128. Donovan PJ, de Miguel MP. Turning germ cells into stem cells. Curr Opin Genet Dev. 2003 Oct;13(5):463-71. doi: 10.1016/j.gde.2003.08.010. PMID: 14550410.
129. Pieters T, van Roy F. Role of cell-cell adhesion complexes in embryonic stem cell biology. J Cell Sci. 2014 Jun 15;127(Pt 12):2603-13. doi: 10.1242/jcs.146720. PMID: 24931943.
130. Heurtier V, Owens N, Gonzalez I, Mueller F, Proux C, Mornico D, Clerc P, Dubois A, Navarro P. The molecular logic of Nanog-induced self-renewal in mouse embryonic stem cells. Nat Commun. 2019 Mar 7;10(1):1109. doi: 10.1038/s41467-019-09041-z. PMID: 30846691; PMCID: PMC6406003.
131. Young RA. Control of the embryonic stem cell state. Cell. 2011 Mar 18;144(6):940-54. doi: 10.1016/j.cell.2011.01.032. PMID: 21414485; PMCID: PMC3099475.

132. Dhaliwal NK, Miri K, Davidson S, Tamim El Jarkass H, Mitchell JA. KLF4 Nuclear Export Requires ERK Activation and Initiates Exit from Naive Pluripotency. Stem Cell Reports. 2018 Apr 10;10(4):1308-1323. doi: 10.1016/j.stemcr.2018.02.007. Epub 2018 Mar 8. PMID: 29526737; PMCID: PMC6000723.
133. del Valle I, Rudloff S, Carles A, Li Y, Liszewska E, Vogt R, Kemler R. E-cadherin is required for the proper activation of the Lifr/Gp130 signaling pathway in mouse embryonic stem cells. Development. 2013 Apr;140(8):1684-92. doi: 10.1242/dev.088690. Epub 2013 Mar 13. PMID: 23487312.
134. Chambers I, Tomlinson SR. The transcriptional foundation of pluripotency. Development. 2009 Jul;136(14):2311-22. doi: 10.1242/dev.024398. PMID: 19542351; PMCID: PMC2729344.
135. Faunes F, Hayward P, Descalzo SM, Chatterjee SS, Balayo T, Trott J, Christoforou A, Ferrer-Vaquer A, Hadjantonakis AK, Dasgupta R, Arias AM. A membrane-associated β-catenin/Oct4 complex correlates with ground-state pluripotency in mouse embryonic stem cells. Development. 2013 Mar;140(6):1171-83. doi: 10.1242/dev.085654. PMID: 23444350; PMCID: PMC3585656.
136. Kerr CL, Hill CM, Blumenthal PD, Gearhart JD. Expression of pluripotent stem cell markers in the human fetal testis. Stem Cells. 2008 Feb;26(2):412-21. doi: 10.1634/stemcells.2007-0605. Epub 2007 Nov 15. PMID: 18024420.
137. De Miguel, Maria & Kerr, Candace & López-Iglesias, Pilar & Alcaina, Yago. (2011). Techniques and Conditions for Embryonic Germ Cell Derivation and Culture. 10.13140/RG.2.1.2545.9688.
138. Luo M, Xia Y, Wang F, Zhang H, Su D, Su C, Yang C, Wu S, An S, Lin S, Fu L. PD0325901, an ERK inhibitor, enhances the efficacy of PD-1 inhibitor in non-small cell lung carcinoma. Acta Pharm Sin B. 2021 Oct;11(10):3120-3133. doi: 10.1016/j.apsb.2021.03.010. Epub 2021 Mar 9. PMID: 34729305; PMCID: PMC8546891.
139. Lee SY, Chae MK, Yoon JS, Kim CY. The Effect of CHIR 99021, a Glycogen Synthase Kinase-3β Inhibitor, on Transforming Growth Factor β-Induced Tenon Fibrosis. Invest Ophthalmol Vis Sci. 2021 Dec 1;62(15):25. doi: 10.1167/iovs.62.15.25. PMID: 34940783; PMCID: PMC8711002.
140. Fernandez-Sanchez ME, et al. Mechanical induction of the tumorigenic [bgr]-catenin pathway by tumour growth pressure. Nature. 2015;523:92–95.
141. Bastow ER, Lamb KJ, Lewthwaite JC, Osborne AC, Kavanagh E, Wheeler-Jones CP, Pitsillides AA. Selective activation of the MEK-ERK pathway is regulated by mechanical stimuli in forming joints and promotes pericellular matrix formation. J Biol Chem. 2005 Mar 25;280(12):11749-58. doi: 10.1074/jbc.M414495200. Epub 2005 Jan 12. PMID: 15647286.
142. Morgani SM, Brickman JM. LIF supports primitive endoderm expansion during pre-implantation development. Development. 2015 Oct 15;142(20):3488-99. doi: 10.1242/dev.125021. Epub 2015 Sep 22. PMID: 26395492.
143. Anderson KGV, Hamilton WB, Roske FV, Azad A, Knudsen TE, Canham MA, Forrester LM, Brickman JM. Insulin fine-tunes self-renewal pathways governing naive pluripotency and extra-embryonic endoderm. Nat Cell Biol. 2017 Oct;19(10):1164-1177. doi: 10.1038/ncb3617. Epub 2017 Sep 25. PMID: 28945231.

144. Chen Y, Blair K, Smith A. Robust self-renewal of rat embryonic stem cells requires fine-tuning of glycogen synthase kinase-3 inhibition. Stem Cell Reports. 2013 Aug 22;1(3):209-17. doi: 10.1016/j.stemcr.2013.07.003. PMID: 24319657; PMCID: PMC3849254.
145. Wongpaiboonwattana W, Stavridis MP. Neural differentiation of mouse embryonic stem cells in serum-free monolayer culture. J Vis Exp. 2015 May 14;(99):e52823. doi: 10.3791/52823. PMID: 26066640; PMCID: PMC4542683.
146. Zhang K, Li L, Huang C, Shen C, Tan F, Xia C, Liu P, Rossant J, Jing N. Distinct functions of BMP4 during different stages of mouse ES cell neural commitment. Development. 2010 Jul;137(13):2095-105. doi: 10.1242/dev.049494. Epub 2010 May 26. PMID: 20504958.
147. Hayashi Y, Furue MK, Tanaka S, Hirose M, Wakisaka N, Danno H, Ohnuma K, Oeda S, Aihara Y, Shiota K, Ogura A, Ishiura S, Asashima M. BMP4 induction of trophoblast from mouse embryonic stem cells in defined culture conditions on laminin. In Vitro Cell Dev Biol Anim. 2010 May;46(5):416-30. doi: 10.1007/s11626-009-9266-6. Epub 2009 Dec 24. PMID: 20033790; PMCID: PMC2862943.
148. Makoolati Z, Movahedin M, Forouzandeh-Moghadam M. In vitro germ cell differentiation from embryonic stem cells of mice: induction control by BMP4 signalling. Biosci Rep. 2016 Nov 8;36(6):e00407. doi: 10.1042/BSR20160348. PMID: 27694305; PMCID: PMC5100000.
149. Hayashi Y, Furue MK, Tanaka S, Hirose M, Wakisaka N, Danno H, Ohnuma K, Oeda S, Aihara Y, Shiota K, Ogura A, Ishiura S, Asashima M. BMP4 induction of trophoblast from mouse embryonic stem cells in defined culture conditions on laminin. In Vitro Cell Dev Biol Anim. 2010 May;46(5):416-30. doi: 10.1007/s11626-009-9266-6. Epub 2009 Dec 24. PMID: 20033790; PMCID: PMC2862943.
150. Festuccia N, Osorno R, Halbritter F, Karwacki-Neisius V, Navarro P, Colby D, Wong F, Yates A, Tomlinson SR, Chambers I. Esrrb is a direct Nanog target gene that can substitute for Nanog function in pluripotent cells. Cell Stem Cell. 2012 Oct 5;11(4):477-90. doi: 10.1016/j.stem.2012.08.002. PMID: 23040477; PMCID: PMC3473361.
151. Yeo JC, Jiang J, Tan ZY, Yim GR, Ng JH, Göke J, Kraus P, Liang H, Gonzales KA, Chong HC, Tan CP, Lim YS, Tan NS, Lufkin T, Ng HH. Klf2 is an essential factor that sustains ground state pluripotency. Cell Stem Cell. 2014 Jun 5;14(6):864-72. doi: 10.1016/j.stem.2014.04.015. PMID: 24905170.
152. Yu S, Zhou C, He J, Yao Z, Huang X, Rong B, Zhu H, Wang S, Chen S, Wang X, Cai B, Zhao G, Chen Y, Xiao L, Liu H, Qin Y, Guo J, Wu H, Zhang Z, Zhang M, Zhao X, Lan F, Wang Y, Chen J, Cao S, Pei D, Liu J. BMP4 drives primed to naïve transition through PGC-like state. Nat Commun. 2022 May 19;13(1):2756. doi: 10.1038/s41467-022-30325-4. PMID: 35589713; PMCID: PMC9120449.
153. Morikawa M, Koinuma D, Mizutani A, Kawasaki N, Holmborn K, Sundqvist A, Tsutsumi S, Watabe T, Aburatani H, Heldin CH, Miyazono K. BMP Sustains Embryonic Stem Cell Self-Renewal through Distinct Functions of Different Krüppel-like Factors. Stem Cell Reports. 2016 Jan 12;6(1):64-73. doi: 10.1016/j.stemcr.2015.12.004. PMID: 26771354; PMCID: PMC4719190.
154. Hussein SM, Duff EK, Sirard C. Smad4 and beta-catenin co-activators functionally interact with lymphoid-enhancing factor to regulate graded expression of

Msx2. J Biol Chem. 2003 Dec 5;278(49):48805-14. doi: 10.1074/jbc.M305472200. Epub 2003 Oct 9. PMID: 14551209.

155. Itoh F, Itoh S, Goumans MJ, Valdimarsdottir G, Iso T, Dotto GP, Hamamori Y, Kedes L, Kato M, ten Dijke Pt P. Synergy and antagonism between Notch and BMP receptor signaling pathways in endothelial cells. EMBO J. 2004 Feb 11;23(3):541-51. doi: 10.1038/sj.emboj.7600065. Epub 2004 Jan 22. PMID: 14739937; PMCID: PMC1271801.

156. Itoh F, Itoh S, Goumans MJ, Valdimarsdottir G, Iso T, Dotto GP, Hamamori Y, Kedes L, Kato M, ten Dijke Pt P. Synergy and antagonism between Notch and BMP receptor signaling pathways in endothelial cells. EMBO J. 2004 Feb 11;23(3):541-51. doi: 10.1038/sj.emboj.7600065. Epub 2004 Jan 22. PMID: 14739937; PMCID: PMC1271801.

157. Tsaytler P, Liu J, Blaess G, Schifferl D, Veenvliet JV, Wittler L, Timmermann B, Herrmann BG, Koch F. BMP4 triggers regulatory circuits specifying the cardiac mesoderm lineage. Development. 2023 May 15;150(10):dev201450. doi: 10.1242/dev.201450. Epub 2023 May 22. PMID: 37082965; PMCID: PMC10233716.

158. Gao Y, Yang L, Chen L, Wang X, Wu H, Ai Z, Du J, Liu Y, Shi X, Wu Y, Guo Z, Zhang Y. Vitamin C facilitates pluripotent stem cell maintenance by promoting pluripotency gene transcription. Biochimie. 2013 Nov;95(11):2107-13. doi: 10.1016/j.biochi.2013.08.001. Epub 2013 Aug 13. PMID: 23954801.

159. D'Aniello C, Habibi E, Cermola F, Paris D, Russo F, Fiorenzano A, Di Napoli G, Melck DJ, Cobellis G, Angelini C, Fico A, Blelloch R, Motta A, Stunnenberg HG, De Cesare D, Patriarca EJ, Minchiotti G. Vitamin C and l-Proline Antagonistic Effects Capture Alternative States in the Pluripotency Continuum. Stem Cell Reports. 2017 Jan 10;8(1):1-10. doi: 10.1016/j.stemcr.2016.11.011. Epub 2016 Dec 22. PMID: 28017658; PMCID: PMC5233408.

160. Perino MG, Yamanaka S, Riordon DR, Tarasova Y, Boheler KR. Ascorbic acid promotes cardiomyogenesis through SMAD1 signaling in differentiating mouse embryonic stem cells. PLoS One. 2017 Dec 12;12(12):e0188569. doi: 10.1371/journal.pone.0188569. PMID: 29232368; PMCID: PMC5726630.

161. Tovy A, Spiro A, McCarthy R, Shipony Z, Aylon Y, Allton K, Ainbinder E, Furth N, Tanay A, Barton M, Oren M. p53 is essential for DNA methylation homeostasis in naïve embryonic stem cells, and its loss promotes clonal heterogeneity. Genes Dev. 2017 May 15;31(10):959-972. doi: 10.1101/gad.299198.117. Epub 2017 Jun 12. Erratum in: Genes Dev. 2018 Oct 1;32(19-20):1358. PMID: 28607180; PMCID: PMC5495125.

162. Shimizu T, Ueda J, Ho JC, Iwasaki K, Poellinger L, Harada I, Sawada Y. Dual inhibition of Src and GSK3 maintains mouse embryonic stem cells, whose differentiation is mechanically regulated by Src signaling. Stem Cells. 2012 Jul;30(7):1394-404. doi: 10.1002/stem.1119. PMID: 22553165.

163. Zhang X, Li B, Li W, Ma L, Zheng D, Li L, Yang W, Chu M, Chen W, Mailman RB, Zhu J, Fan G, Archer TK, Wang Y. Transcriptional repression by the BRG1-SWI/SNF complex affects the pluripotency of human embryonic stem cells. Stem Cell Reports. 2014 Sep 9;3(3):460-74. doi: 10.1016/j.stemcr.2014.07.004. Epub 2014 Aug 14. PMID: 25241744; PMCID: PMC4266000.

164. Meyn MA 3rd, Smithgall TE. Chemical genetics identifies c-Src as an activator of primitive ectoderm formation in murine embryonic stem cells. Sci Signal. 2009 Oct 13;2(92):ra64. doi: 10.1126/scisignal.2000311. PMID: 19825829; PMCID: PMC2775445.
165. Tan BS, Kwek J, Wong CK, Saner NJ, Yap C, Felquer F, Morris MB, Gardner DK, Rathjen PD, Rathjen J. Src Family Kinases and p38 Mitogen-Activated Protein Kinases Regulate Pluripotent Cell Differentiation in Culture. PLoS One. 2016 Oct 10;11(10):e0163244. doi: 10.1371/journal.pone.0163244. PMID: 27723793; PMCID: PMC5056717.
166. Jain S, Wang X, Chang CC, Ibarra-Drendall C, Wang H, Zhang Q, Brady SW, Li P, Zhao H, Dobbs J, Kyrish M, Tkaczyk TS, Ambrose A, Sistrunk C, Arun BK, Richards-Kortum R, Jia W, Seewaldt VL, Yu D. Src Inhibition Blocks c-Myc Translation and Glucose Metabolism to Prevent the Development of Breast Cancer. Cancer Res. 2015 Nov 15;75(22):4863-75. doi: 10.1158/0008-5472.CAN-14-2345. Epub 2015 Sep 17. PMID: 26383165; PMCID: PMC4651709.
167. Hunt GC, Singh P, Schwarzbauer JE. Endogenous production of fibronectin is required for self-renewal of cultured mouse embryonic stem cells. Exp Cell Res. 2012 Sep 10;318(15):1820-31. doi: 10.1016/j.yexcr.2012.06.009. Epub 2012 Jun 16. PMID: 22710062; PMCID: PMC3582329.
168. Yuan Y, Park J, Tian Y, Choi J, Pasquariello R, Alexenko AP, Dai A, Behura SK, Roberts RM, Ezashi T. A six-inhibitor culture medium for improving naïve-type pluripotency of porcine pluripotent stem cells. Cell Death Discov. 2019 Jun 17;5:104. doi: 10.1038/s41420-019-0184-4. PMID: 31240131; PMCID: PMC6579764.
169. Pastor WA, Chen D, Liu W, Kim R, Sahakyan A, Lukianchikov A, Plath K, Jacobsen SE, Clark AT. Naive Human Pluripotent Cells Feature a Methylation Landscape Devoid of Blastocyst or Germline Memory. Cell Stem Cell. 2016 Mar 3;18(3):323-329. doi: 10.1016/j.stem.2016.01.019. Epub 2016 Feb 4. PMID: 26853856; PMCID: PMC4779431.
170. Dong C, Beltcheva M, Gontarz P, Zhang B, Popli P, Fischer LA, Khan SA, Park KM, Yoon EJ, Xing X, Kommagani R, Wang T, Solnica-Krezel L, Theunissen TW. Derivation of trophoblast stem cells from naïve human pluripotent stem cells. Elife. 2020 Feb 12;9:e52504. doi: 10.7554/eLife.52504. PMID: 32048992; PMCID: PMC7062471.
171. Cinkornpumin JK, Kwon SY, Guo Y, Hossain I, Sirois J, Russett CS, Tseng HW, Okae H, Arima T, Duchaine TF, Liu W, Pastor WA. Naive Human Embryonic Stem Cells Can Give Rise to Cells with a Trophoblast-like Transcriptome and Methylome. Stem Cell Reports. 2020 Jul 14;15(1):198-213. doi: 10.1016/j.stemcr.2020.06.003. Epub 2020 Jul 2. PMID: 32619492; PMCID: PMC7363941.
172. Festuccia N, Owens N, Chervova A, Dubois A, Navarro P. The combined action of Esrrb and Nr5a2 is essential for murine naïve pluripotency. Development. 2021 Sep 1;148(17):dev199604. doi: 10.1242/dev.199604. Epub 2021 Sep 10. PMID: 34397088; PMCID: PMC8451941.
173. Okamura E, Tam OH, Posfai E, Li L, Cockburn K, Lee CQE, Garner J, Rossant J. Esrrb function is required for proper primordial germ cell development in presomite

stage mouse embryos. Dev Biol. 2019 Nov 15;455(2):382-392. doi: 10.1016/j.ydbio.2019.07.008. Epub 2019 Jul 14. PMID: 31315026.

174. Yang SH, Kalkan T, Morissroe C, Marks H, Stunnenberg H, Smith A, Sharrocks AD. Otx2 and Oct4 drive early enhancer activation during embryonic stem cell transition from naive pluripotency. Cell Rep. 2014 Jun 26;7(6):1968-81. doi: 10.1016/j.celrep.2014.05.037. Epub 2014 Jun 12. PMID: 24931607; PMCID: PMC4074343.

175. Mulas C, Chia G, Jones KA, Hodgson AC, Stirparo GG, Nichols J. Oct4 regulates the embryonic axis and coordinates exit from pluripotency and germ layer specification in the mouse embryo. Development. 2018 Jun 18;145(12):dev159103. doi: 10.1242/dev.159103. PMID: 29915126; PMCID: PMC6031404.

176. Hart AH, Hartley L, Ibrahim M, Robb L. Identification, cloning and expression analysis of the pluripotency promoting Nanog genes in mouse and human. Dev Dyn. 2004 May;230(1):187-98. doi: 10.1002/dvdy.20034. PMID: 15108323.

177. Pelton TA, Sharma S, Schulz TC, Rathjen J, Rathjen PD. Transient pluripotent cell populations during primitive ectoderm formation: correlation of in vivo and in vitro pluripotent cell development. J Cell Sci. 2002 Jan 15;115(Pt 2):329-39. doi: 10.1242/jcs.115.2.329. PMID: 11839785.

178. Festuccia N, Halbritter F, Corsinotti A, Gagliardi A, Colby D, Tomlinson SR, Chambers I. Esrrb extinction triggers dismantling of naïve pluripotency and marks commitment to differentiation. EMBO J. 2018 Nov 2;37(21):e95476. doi: 10.15252/embj.201695476. Epub 2018 Oct 1. PMID: 30275266; PMCID: PMC6213284.

179. Silva J, Nichols J, Theunissen TW, Guo G, van Oosten AL, Barrandon O, Wray J, Yamanaka S, Chambers I, Smith A. Nanog is the gateway to the pluripotent ground state. Cell. 2009 Aug 21;138(4):722-37. doi: 10.1016/j.cell.2009.07.039. PMID: 19703398; PMCID: PMC3437554.

180. Masui S, Ohtsuka S, Yagi R, Takahashi K, Ko MS, Niwa H. Rex1/Zfp42 is dispensable for pluripotency in mouse ES cells. BMC Dev Biol. 2008 Apr 24;8:45. doi: 10.1186/1471-213X-8-45. PMID: 18433507; PMCID: PMC2386458.

181. Leeb M, Walker R, Mansfield B, Nichols J, Smith A, Wutz A. Germline potential of parthenogenetic haploid mouse embryonic stem cells. Development. 2012 Sep;139(18):3301-5. doi: 10.1242/dev.083675. PMID: 22912412; PMCID: PMC3424041.

182. Wray J, Kalkan T, Gomez-Lopez S, Eckardt D, Cook A, Kemler R, Smith A. Inhibition of glycogen synthase kinase-3 alleviates Tcf3 repression of the pluripotency network and increases embryonic stem cell resistance to differentiation. Nat Cell Biol. 2011 Jun 19;13(7):838-45. doi: 10.1038/ncb2267. Erratum in: Nat Cell Biol. 2012 May;14(5):555. PMID: 21685889; PMCID: PMC3160487.

183. Li X, Zhao X, Fang Y, Jiang X, Duong T, Fan C, Huang CC, Kain SR. Generation of destabilized green fluorescent protein as a transcription reporter. J Biol Chem. 1998 Dec 25;273(52):34970-5. doi: 10.1074/jbc.273.52.34970. PMID: 9857028.

184. Acampora D, Di Giovannantonio LG, Garofalo A, Nigro V, Omodei D, Lombardi A, Zhang J, Chambers I, Simeone A. Functional Antagonism between OTX2 and NANOG Specifies a Spectrum of Heterogeneous Identities in Embryonic Stem

Cells. Stem Cell Reports. 2017 Nov 14;9(5):1642-1659. doi: 10.1016/j.stemcr.2017.09.019. Epub 2017 Oct 19. PMID: 29056334; PMCID: PMC5935799.

185. Christine M. Ritter, Natascha Leijnse, Younes Farhangi Barooji, Joshua M. Brickman, Amin Doostmohammadi, Lene B. Oddershede bioRxiv 2022.09.21.508812; doi: https://doi.org/10.1101/2022.09.21.508812

186. Schwarz US, Gardel ML. United we stand: integrating the actin cytoskeleton and cell-matrix adhesions in cellular mechanotransduction. J Cell Sci. 2012 Jul 1;125(Pt 13):3051-60. doi: 10.1242/jcs.093716. Epub 2012 Jul 13. PMID: 22797913; PMCID: PMC3434863.

187. Mote RD, Yadav J, Singh SB, Tiwari M, V SL, Patil S, Subramanyam D. Pluripotency of embryonic stem cells lacking clathrin-mediated endocytosis cannot be rescued by restoring cellular stiffness. J Biol Chem. 2020 Dec 4;295(49):16888-16896. doi: 10.1074/jbc.AC120.014343. Epub 2020 Oct 21. PMID: 33087446; PMCID: PMC7864080.

188. Barooji YF, Hvid KG, Petitjean II, Brickman JM, Oddershede LB, Bendix PM. Changes in Cell Morphology and Actin Organization in Embryonic Stem Cells Cultured under Different Conditions. Cells. 2021 Oct 23;10(11):2859. doi: 10.3390/cells10112859. PMID: 34831083; PMCID: PMC8616278.

189. Bergert M, Lembo S, Sharma S, Russo L, Milovanović D, Gretarsson KH, Börmel M, Neveu PA, Hackett JA, Petsalaki E, Diz-Muñoz A. Cell Surface Mechanics Gate Embryonic Stem Cell Differentiation. Cell Stem Cell. 2021 Feb 4;28(2):209-216.e4. doi: 10.1016/j.stem.2020.10.017. Epub 2020 Nov 17. PMID: 33207217; PMCID: PMC7875094.

190. De Belly H, Stubb A, Yanagida A, Labouesse C, Jones PH, Paluch EK, Chalut KJ. Membrane Tension Gates ERK-Mediated Regulation of Pluripotent Cell Fate. Cell Stem Cell. 2021 Feb 4;28(2):273-284.e6. doi: 10.1016/j.stem.2020.10.018. Epub 2020 Nov 19. PMID: 33217323; PMCID: PMC7875115.

191. Du J, Fan Y, Guo Z, Wang Y, Zheng X, Huang C, Liang B, Gao L, Cao Y, Chen Y, Zhang X, Li L, Xu L, Wu C, Weitz DA, Feng X. Compression Generated by a 3D Supracellular Actomyosin Cortex Promotes Embryonic Stem Cell Colony Growth and Expression of Nanog and Oct4. Cell Syst. 2019 Aug 28;9(2):214-220.e5. doi: 10.1016/j.cels.2019.05.008. Epub 2019 Jul 3. PMID: 31279504.

192. Dietrich JE, Hiiragi T. Stochastic patterning in the mouse pre-implantation embryo. Development. 2007 Dec;134(23):4219-31. doi: 10.1242/dev.003798. Epub 2007 Oct 31. PMID: 17978007.

193. Närvä E, Stubb A, Guzmán C, Blomqvist M, Balboa D, Lerche M, Saari M, Otonkoski T, Ivaska J. A Strong Contractile Actin Fence and Large Adhesions Direct Human Pluripotent Colony Morphology and Adhesion. Stem Cell Reports. 2017 Jul 11;9(1):67-76. doi: 10.1016/j.stemcr.2017.05.021. Epub 2017 Jun 15. PMID: 28625538; PMCID: PMC5511101.

194. Pérez-González C, Alert R, Blanch-Mercader C, Gómez-González M, Kolodziej T, Bazellieres E, Casademunt J, Trepat X. Active wetting of epithelial tissues. Nat Phys. 2019 Jan;15(1):79-88. doi: 10.1038/s41567-018-0279-5. Epub 2018 Sep 24. PMID: 31537984; PMCID: PMC6753015.

195. Ohtsuka S, Nishikawa-Torikai S, Niwa H. E-cadherin promotes incorporation of mouse epiblast stem cells into normal development. PLoS One. 2012;7(9):e45220. doi: 10.1371/journal.pone.0045220. Epub 2012 Sep 18. PMID: 23028858; PMCID: PMC3445497.
196. Cao R, Yang ZS, Hu SL, Liang SJ, Zhang SM, Zhu SQ, Lu L, Long CH, Yao ST, Ma YJ, Liang XH. Molecular Mechanism of Mouse Uterine Smooth Muscle Regulation on Embryo Implantation. Int J Mol Sci. 2022 Oct 18;23(20):12494. doi: 10.3390/ijms232012494. PMID: 36293350; PMCID: PMC9604262.
197. Freund JB, Goetz JG, Hill KL, Vermot J. Fluid flows and forces in development: functions, features and biophysical principles. Development. 2012 Apr;139(7):1229-45. doi: 10.1242/dev.073593. Erratum in: Development. 2012 Aug;139(16):3063. PMID: 22395739; PMCID: PMC3294433.
198. Frantz C, Stewart KM, Weaver VM. The extracellular matrix at a glance. J Cell Sci. 2010 Dec 15;123(Pt 24):4195-200. doi: 10.1242/jcs.023820. PMID: 21123617; PMCID: PMC2995612.
199. Walma DAC, Yamada KM. The extracellular matrix in development. Development. 2020 May 28;147(10):dev175596. doi: 10.1242/dev.175596. PMID: 32467294; PMCID: PMC7272360.
200. Leivo I, Vaheri A, Timpl R, Wartiovaara J. Appearance and distribution of collagens and laminin in the early mouse embryo. Dev Biol. 1980 Apr;76(1):100-14. doi: 10.1016/0012-1606(80)90365-6. PMID: 6991310.
201. Pöschl E, Schlötzer-Schrehardt U, Brachvogel B, Saito K, Ninomiya Y, Mayer U. Collagen IV is essential for basement membrane stability but dispensable for initiation of its assembly during early development. Development. 2004 Apr;131(7):1619-28. doi: 10.1242/dev.01037. Epub 2004 Mar 3. PMID: 14998921.
202. Cosgrove D, Meehan DT, Grunkemeyer JA, Kornak JM, Sayers R, Hunter WJ, Samuelson GC. Collagen COL4A3 knockout: a mouse model for autosomal Alport syndrome. Genes Dev. 1996 Dec 1;10(23):2981-92. doi: 10.1101/gad.10.23.2981. PMID: 8956999.
203. Miner JH, Cunningham J, Sanes JR. Roles for laminin in embryogenesis: exencephaly, syndactyly, and placentopathy in mice lacking the laminin alpha5 chain. J Cell Biol. 1998 Dec 14;143(6):1713-23. doi: 10.1083/jcb.143.6.1713. PMID: 9852162; PMCID: PMC2132973.
204. Miner JH, Yurchenco PD. Laminin functions in tissue morphogenesis. Annu Rev Cell Dev Biol. 2004;20:255-84. doi: 10.1146/annurev.cellbio.20.010403.094555. PMID: 15473841.
205. Alpy F, Jivkov I, Sorokin L, Klein A, Arnold C, Huss Y, Kedinger M, Simon-Assmann P, Lefebvre O. Generation of a conditionally null allele of the laminin alpha1 gene. Genesis. 2005 Oct;43(2):59-70. doi: 10.1002/gene.20154. PMID: 16100707.
206. Murray P, Prewitz M, Hopp I, Wells N, Zhang H, Cooper A, Parry KL, Short R, Antoine DJ, Edgar D. The self-renewal of mouse embryonic stem cells is regulated by cell-substratum adhesion and cell spreading. Int J Biochem Cell Biol. 2013 Nov;45(11):2698-705. doi: 10.1016/j.biocel.2013.07.001. Epub 2013 Jul 17. PMID: 23871934; PMCID: PMC3898852.

207. Morin N, Sullivan R. Expression of fibronectin and a fibronectin-binding molecule during preimplantation development in the mouse. Hum Reprod. 1994 May;9(5):894-901. doi: 10.1093/oxfordjournals.humrep.a138613. PMID: 7929739.
208. Wartiovaara J, Leivo I, Vaheri A. Expression of the cell surface-associated glycoprotein, fibronectin, in the early mouse embryo. Dev Biol. 1979 Mar;69(1):247-57. doi: 10.1016/0012-1606(79)90289-6. PMID: 376373.
209. Barnum CE, Fey JL, Weiss SN, Barila G, Brown AG, Connizzo BK, Shetye SS, Elovitz MA, Soslowsky LJ. Tensile Mechanical Properties and Dynamic Collagen Fiber Re-Alignment of the Murine Cervix are Dramatically Altered Throughout Pregnancy. J Biomech Eng. 2017 Jun 1;139(6):0610081–7. doi: 10.1115/1.4036473. PMID: 28418563; PMCID: PMC6993786.
210. Nallasamy S, Yoshida K, Akins M, Myers K, Iozzo R, Mahendroo M. Steroid Hormones Are Key Modulators of Tissue Mechanical Function via Regulation of Collagen and Elastic Fibers. Endocrinology. 2017 Apr 1;158(4):950-962. doi: 10.1210/en.2016-1930. PMID: 28204185; PMCID: PMC5460796.
211. Chowdhury F, Na S, Li D, Poh YC, Tanaka TS, Wang F, Wang N. Material properties of the cell dictate stress-induced spreading and differentiation in embryonic stem cells. Nat Mater. 2010 Jan;9(1):82-8. doi: 10.1038/nmat2563. Epub 2009 Oct 18. PMID: 19838182; PMCID: PMC2833279.
212. Wang X, Zhang Z, Tao H, Liu J, Hopyan S, Sun Y. Characterizing Inner Pressure and Stiffness of Trophoblast and Inner Cell Mass of Blastocysts. Biophys J. 2018 Dec 18;115(12):2443-2450. doi: 10.1016/j.bpj.2018.11.008. Epub 2018 Nov 10. PMID: 30509858; PMCID: PMC6301984.
213. Engler AJ, Sen S, Sweeney HL, Discher DE. Matrix elasticity directs stem cell lineage specification. Cell. 2006 Aug 25;126(4):677-89. doi: 10.1016/j.cell.2006.06.044. PMID: 16923388.
214. Gilbert PM, Havenstrite KL, Magnusson KE, Sacco A, Leonardi NA, Kraft P, Nguyen NK, Thrun S, Lutolf MP, Blau HM. Substrate elasticity regulates skeletal muscle stem cell self-renewal in culture. Science. 2010 Aug 27;329(5995):1078-81. doi: 10.1126/science.1191035. Epub 2010 Jul 15. PMID: 20647425; PMCID: PMC2929271.
215. Chowdhury F, Li Y, Poh YC, Yokohama-Tamaki T, Wang N, Tanaka TS. Soft substrates promote homogeneous self-renewal of embryonic stem cells via downregulating cell-matrix tractions. PLoS One. 2010 Dec 13;5(12):e15655. doi: 10.1371/journal.pone.0015655. PMID: 21179449; PMCID: PMC3001487.
216. Kechagia Z, Sáez P, Gómez-González M, Canales B, Viswanadha S, Zamarbide M, Andreu I, Koorman T, Beedle AEM, Elosegui-Artola A, Derksen PWB, Trepat X, Arroyo M, Roca-Cusachs P. The laminin-keratin link shields the nucleus from mechanical deformation and signalling. Nat Mater. 2023 Nov;22(11):1409-1420. doi: 10.1038/s41563-023-01657-3. Epub 2023 Sep 14. PMID: 37709930; PMCID: PMC10627833.
217. Wang Y, Wang Z, Dong Y. Collagen-Based Biomaterials for Tissue Engineering. ACS Biomater Sci Eng. 2023 Mar 13;9(3):1132-1150. doi: 10.1021/acsbiomaterials.2c00730. Epub 2023 Feb 17. PMID: 36800415.

218. Kleinman HK, McGarvey ML, Hassell JR, Star VL, Cannon FB, Laurie GW, Martin GR. Basement membrane complexes with biological activity. Biochemistry. 1986 Jan 28;25(2):312-8. doi: 10.1021/bi00350a005. PMID: 2937447.
219. Zhu J. Bioactive modification of poly(ethylene glycol) hydrogels for tissue engineering. Biomaterials. 2010 Jun;31(17):4639-56. doi: 10.1016/j.biomaterials.2010.02.044. Epub 2010 Mar 19. PMID: 20303169; PMCID: PMC2907908.
220. Kandow CE, Georges PC, Janmey PA, Beningo KA. Polyacrylamide hydrogels for cell mechanics: steps toward optimization and alternative uses. Methods Cell Biol. 2007;83:29-46. doi: 10.1016/S0091-679X(07)83002-0. PMID: 17613303.
221. Tilghman RW, Cowan CR, Mih JD, Koryakina Y, Gioeli D, Slack-Davis JK, Blackman BR, Tschumperlin DJ, Parsons JT. Matrix rigidity regulates cancer cell growth and cellular phenotype. PLoS One. 2010 Sep 23;5(9):e12905. doi: 10.1371/journal.pone.0012905. PMID: 20886123; PMCID: PMC2944843.
222. Dupont S, Morsut L, Aragona M, Enzo E, Giulitti S, Cordenonsi M, Zanconato F, Le Digabel J, Forcato M, Bicciato S, Elvassore N, Piccolo S. Role of YAP/TAZ in mechanotransduction. Nature. 2011 Jun 8;474(7350):179-83. doi: 10.1038/nature10137. PMID: 21654799.
223. Wen JH, Vincent LG, Fuhrmann A, Choi YS, Hribar KC, Taylor-Weiner H, Chen S, Engler AJ. Interplay of matrix stiffness and protein tethering in stem cell differentiation. Nat Mater. 2014 Oct;13(10):979-87. doi: 10.1038/nmat4051. Epub 2014 Aug 10. PMID: 25108614; PMCID: PMC4172528.
224. Tsou YH, Khoneisser J, Huang PC, Xu X. Hydrogel as a bioactive material to regulate stem cell fate. Bioact Mater. 2016 May 12;1(1):39-55. doi: 10.1016/j.bioactmat.2016.05.001. PMID: 29744394; PMCID: PMC5883979.
225. Domura R, Sasaki R, Ishikawa Y, Okamoto M. Cellular Morphology-Mediated Proliferation and Drug Sensitivity of Breast Cancer Cells. J Funct Biomater. 2017 Jun 6;8(2):18. doi: 10.3390/jfb8020018. PMID: 28587314; PMCID: PMC5491999.
226. Martín C, Merino S, González-Domínguez JM, Rauti R, Ballerini L, Prato M, Vázquez E. Graphene Improves the Biocompatibility of Polyacrylamide Hydrogels: 3D Polymeric Scaffolds for Neuronal Growth. Sci Rep. 2017 Sep 8;7(1):10942. doi: 10.1038/s41598-017-11359-x. PMID: 28887551; PMCID: PMC5591295.
227. Kechagia JZ, Ivaska J, Roca-Cusachs P. Integrins as biomechanical sensors of the microenvironment. Nat Rev Mol Cell Biol. 2019 Aug;20(8):457-473. doi: 10.1038/s41580-019-0134-2. PMID: 31182865.
228. Ross TD, Coon BG, Yun S, Baeyens N, Tanaka K, Ouyang M, Schwartz MA. Integrins in mechanotransduction. Curr Opin Cell Biol. 2013 Oct;25(5):613-8. doi: 10.1016/j.ceb.2013.05.006. Epub 2013 Jun 21. PMID: 23797029; PMCID: PMC3757118.
229. Taleahmad S, Mirzaei M, Parker LM, Hassani SN, Mollamohammadi S, Sharifi-Zarchi A, Haynes PA, Baharvand H, Salekdeh GH. Proteome Analysis of Ground State Pluripotency. Sci Rep. 2015 Dec 16;5:17985. doi: 10.1038/srep17985. PMID: 26671762; PMCID: PMC4680864.
230. Xia S, Yim EKF, Kanchanawong P. Molecular Organization of Integrin-Based Adhesion Complexes in Mouse Embryonic Stem Cells. ACS Biomater Sci Eng. 2019

Aug 12;5(8):3828-3842. doi: 10.1021/acsbiomaterials.8b01124. Epub 2019 Jan 29. PMID: 33438423.

231. Wade R, Bohl J, Vande Pol S. Paxillin null embryonic stem cells are impaired in cell spreading and tyrosine phosphorylation of focal adhesion kinase. Oncogene. 2002 Jan 3;21(1):96-107. doi: 10.1038/sj.onc.1205013. PMID: 11791180.

232. Zhang S, Chong LH, Woon JYX, Chua TX, Cheruba E, Yip AK, Li HY, Chiam KH, Koh CG. Zyxin regulates embryonic stem cell fate by modulating mechanical and biochemical signaling interface. Commun Biol. 2023 Jan 18;6(1):62. doi: 10.1038/s42003-023-04421-0. PMID: 36653484; PMCID: PMC9849324.

233. Huttenlocher A, Horwitz AR. Integrins in cell migration. Cold Spring Harb Perspect Biol. 2011 Sep 1;3(9):a005074. doi: 10.1101/cshperspect.a005074. PMID: 21885598; PMCID: PMC3181029.

234. Horiuchi R, Akimoto T, Hong Z, Ushida T. Cyclic mechanical strain maintains Nanog expression through PI3K/Akt signaling in mouse embryonic stem cells. Exp Cell Res. 2012 Aug 15;318(14):1726-32. doi: 10.1016/j.yexcr.2012.05.021. Epub 2012 Jun 6. PMID: 22683858.

235. Verstreken CM, Labouesse C, Agley CC, Chalut KJ. Embryonic stem cells become mechanoresponsive upon exit from ground state of pluripotency. Open Biol. 2019 Jan 31;9(1):180203. doi: 10.1098/rsob.180203. PMID: 30958114; PMCID: PMC6367133.

236. Habibi E, Brinkman AB, Arand J, Kroeze LI, Kerstens HH, Matarese F, Lepikhov K, Gut M, Brun-Heath I, Hubner NC, Benedetti R, Altucci L, Jansen JH, Walter J, Gut IG, Marks H, Stunnenberg HG. Whole-genome bisulfite sequencing of two distinct interconvertible DNA methylomes of mouse embryonic stem cells. Cell Stem Cell. 2013 Sep 5;13(3):360-9. doi: 10.1016/j.stem.2013.06.002. Epub 2013 Jul 11. PMID: 23850244.

237. Tosolini M, Brochard V, Adenot P, Chebrout M, Grillo G, Navia V, Beaujean N, Francastel C, Bonnet-Garnier A, Jouneau A. Contrasting epigenetic states of heterochromatin in the different types of mouse pluripotent stem cells. Sci Rep. 2018 Apr 10;8(1):5776. doi: 10.1038/s41598-018-23822-4. PMID: 29636490; PMCID: PMC5893598.

238. Ahmed K, Dehghani H, Rugg-Gunn P, Fussner E, Rossant J, Bazett-Jones DP. Global chromatin architecture reflects pluripotency and lineage commitment in the early mouse embryo. PLoS One. 2010 May 7;5(5):e10531. doi: 10.1371/journal.pone.0010531. PMID: 20479880; PMCID: PMC2866533.

239. Meshorer E, Yellajoshula D, George E, Scambler PJ, Brown DT, Misteli T. Hyperdynamic plasticity of chromatin proteins in pluripotent embryonic stem cells. Dev Cell. 2006 Jan;10(1):105-16. doi: 10.1016/j.devcel.2005.10.017. Erratum in: Dev Cell. Jan 17;22(1):233-4. PMID: 16399082; PMCID: PMC1868458.

240. Kojima Y, Kaufman-Francis K, Studdert JB, Steiner KA, Power MD, Loebel DA, Jones V, Hor A, de Alencastro G, Logan GJ, Teber ET, Tam OH, Stutz MD, Alexander IE, Pickett HA, Tam PP. The transcriptional and functional properties of mouse epiblast stem cells resemble the anterior primitive streak. Cell Stem Cell. 2014 Jan 2;14(1):107-20. doi: 10.1016/j.stem.2013.09.014. Epub 2013 Oct 17. PMID: 24139757.

241. Veillard AC, Marks H, Bernardo AS, Jouneau L, Laloë D, Boulanger L, Kaan A, Brochard V, Tosolini M, Pedersen R, Stunnenberg H, Jouneau A. Stable methylation at promoters distinguishes epiblast stem cells from embryonic stem cells and the in vivo epiblasts. Stem Cells Dev. 2014 Sep 1;23(17):2014-29. doi: 10.1089/scd.2013.0639. Epub 2014 Jun 12. PMID: 24738887; PMCID: PMC4142781.
242. Pagliara S, Franze K, McClain CR, Wylde G, Fisher CL, Franklin RJM, Kabla AJ, Keyser UF, Chalut KJ. Auxetic nuclei in embryonic stem cells exiting pluripotency. Nat Mater. 2014 Jun;13(6):638-644. doi: 10.1038/nmat3943. Epub 2014 Apr 20. PMID: 24747782; PMCID: PMC4283157.
243. Evans, K.E. and Alderson, A. (2000), Auxetic Materials: Functional Materials and Structures from Lateral Thinking!. Adv. Mater., 12: 617-628. https://doi.org/10.1002/(SICI)1521-4095(200005)12:9<617::AID ADMA617>3.0.CO;2-3
244. Hoskins VE, Smith K, Reddy KL. The shifting shape of genomes: dynamics of heterochromatin interactions at the nuclear lamina. Curr Opin Genet Dev. 2021 Apr;67:163-173. doi: 10.1016/j.gde.2021.02.003. Epub 2021 Mar 25. PMID: 33774266; PMCID: PMC8489734.
245. Vahabikashi A, Adam SA, Medalia O, Goldman RD. Nuclear lamins: Structure and function in mechanobiology. APL Bioeng. 2022 Feb 1;6(1):011503. doi: 10.1063/5.0082656. PMID: 35146235; PMCID: PMC8810204.
246. Zuela N, Bar DZ, Gruenbaum Y. Lamins in development, tissue maintenance and stress. EMBO Rep. 2012 Dec;13(12):1070-8. doi: 10.1038/embor.2012.167. Epub 2012 Nov 13. PMID: 23146893; PMCID: PMC3512410.
247. Lee YL, Burke B. LINC complexes and nuclear positioning. Semin Cell Dev Biol. 2018 Oct;82:67-76. doi: 10.1016/j.semcdb.2017.11.008. Epub 2017 Nov 27. PMID: 29191370.
248. Chang W, Worman HJ, Gundersen GG. Accessorizing and anchoring the LINC complex for multifunctionality. J Cell Biol. 2015 Jan 5;208(1):11-22. doi: 10.1083/jcb.201409047. PMID: 25559183; PMCID: PMC4284225.
249. Khatau SB, Kusuma S, Hanjaya-Putra D, Mali P, Cheng L, Lee JS, Gerecht S, Wirtz D. The differential formation of the LINC-mediated perinuclear actin cap in pluripotent and somatic cells. PLoS One. 2012;7(5):e36689. doi: 10.1371/journal.pone.0036689. Epub 2012 May 4. PMID: 22574215; PMCID: PMC3344930.
250. Sehgal P, Chaturvedi P, Kumaran RI, Kumar S, Parnaik VK. Lamin A/C haploinsufficiency modulates the differentiation potential of mouse embryonic stem cells. PLoS One. 2013;8(2):e57891. doi: 10.1371/journal.pone.0057891. Epub 2013 Feb 25. PMID: 23451281; PMCID: PMC3581495.
251. Kim Y, Zheng X, Zheng Y. Proliferation and differentiation of mouse embryonic stem cells lacking all lamins. Cell Res. 2013 Dec;23(12):1420-3. doi: 10.1038/cr.2013.118. Epub 2013 Aug 27. PMID: 23979018; PMCID: PMC3847566.
252. Wang Y, Elsherbiny A, Kessler L, Cordero J, Shi H, Serke H, Lityagina O, Trogisch FA, Mohammadi MM, El-Battrawy I, Backs J, Wieland T, Heineke J, Dobreva G. Lamin A/C-dependent chromatin architecture safeguards naïve pluripotency to prevent aberrant cardiovascular cell fate and function. Nat Commun.

2022 Nov 4;13(1):6663. doi: 10.1038/s41467-022-34366-7. PMID: 36333314; PMCID: PMC9636150.

253. Smith ER, Zhang XY, Capo-Chichi CD, Chen X, Xu XX. Increased expression of Syne1/nesprin-1 facilitates nuclear envelope structure changes in embryonic stem cell differentiation. Dev Dyn. 2011 Oct;240(10):2245-55. doi: 10.1002/dvdy.22717. Epub 2011 Aug 23. PMID: 21932307; PMCID: PMC3290128.

254. David BG, Fujita H, Yasuda K, Okamoto K, Panina Y, Ichinose J, Sato O, Horie M, Ichimura T, Okada Y, Watanabe TM. Linking substrate and nucleus via actin cytoskeleton in pluripotency maintenance of mouse embryonic stem cells. Stem Cell Res. 2019 Dec;41:101614. doi: 10.1016/j.scr.2019.101614. Epub 2019 Oct 24. PMID: 31715427.

255. Andreu I, Granero-Moya I, Chahare NR, Clein K, Molina-Jordán M, Beedle AEM, Elosegui-Artola A, Abenza JF, Rossetti L, Trepat X, Raveh B, Roca-Cusachs P. Mechanical force application to the nucleus regulates nucleocytoplasmic transport. Nat Cell Biol. 2022 Jun;24(6):896-905. doi: 10.1038/s41556-022-00927-7. Epub 2022 Jun 9. PMID: 35681009; PMCID: PMC7614780.

256. Elosegui-Artola A, Andreu I, Beedle AEM, Lezamiz A, Uroz M, Kosmalska AJ, Oria R, Kechagia JZ, Rico-Lastres P, Le Roux AL, Shanahan CM, Trepat X, Navajas D, Garcia-Manyes S, Roca-Cusachs P. Force Triggers YAP Nuclear Entry by Regulating Transport across Nuclear Pores. Cell. 2017 Nov 30;171(6):1397-1410.e14. doi: 10.1016/j.cell.2017.10.008. Epub 2017 Oct 26. PMID: 29107331.

257. Yu FX, Zhao B, Guan KL. Hippo Pathway in Organ Size Control, Tissue Homeostasis, and Cancer. Cell. 2015 Nov 5;163(4):811-28. doi: 10.1016/j.cell.2015.10.044. PMID: 26544935; PMCID: PMC4638384.

258. Zhao B, Li L, Lei Q, Guan KL. The Hippo-YAP pathway in organ size control and tumorigenesis: an updated version. Genes Dev. 2010 May;24(9):862-74. doi: 10.1101/gad.1909210. PMID: 20439427; PMCID: PMC2861185.

259. Chung H, Lee BK, Uprety N, Shen W, Lee J, Kim J. Yap1 is dispensable for self-renewal but required for proper differentiation of mouse embryonic stem (ES) cells. EMBO Rep. 2016 Apr;17(4):519-29. doi: 10.15252/embr.201540933. Epub 2016 Feb 25. PMID: 26917425; PMCID: PMC4818770.

260. Tamm C, Böwer N, Annerén C. Regulation of mouse embryonic stem cell self-renewal by a Yes-YAP-TEAD2 signaling pathway downstream of LIF. J Cell Sci. 2011 Apr 1;124(Pt 7):1136-44. doi: 10.1242/jcs.075796. Epub 2011 Mar 8. PMID: 21385842.

261. Meyer K, Lammers NC, Bugaj LJ, Garcia HG, Weiner OD. Optogenetic control of YAP reveals a dynamic communication code for stem cell fate and proliferation. Nat Commun. 2023 Oct 30;14(1):6929. doi: 10.1038/s41467-023-42643-2. PMID: 37903793; PMCID: PMC10616176.

262. Díaz-Díaz C, Fernandez de Manuel L, Jimenez-Carretero D, Montoya MC, Clavería C, Torres M. Pluripotency Surveillance by Myc-Driven Competitive Elimination of Differentiating Cells. Dev Cell. 2017 Sep 25;42(6):585-599.e4. doi: 10.1016/j.devcel.2017.08.011. Epub 2017 Sep 14. PMID: 28919206.

263. LeBlanc L, Lee BK, Yu AC, Kim M, Kambhampati AV, Dupont SM, Seruggia D, Ryu BU, Orkin SH, Kim J. Yap1 safeguards mouse embryonic stem cells from

excessive apoptosis during differentiation. Elife. 2018 Dec 18;7:e40167. doi: 10.7554/eLife.40167. PMID: 30561326; PMCID: PMC6307859.
264. Shahbazi MN, Zernicka-Goetz M. Deconstructing and reconstructing the mouse and human early embryo. Nat Cell Biol. 2018 Aug;20(8):878-887. doi: 10.1038/s41556-018-0144-x. Epub 2018 Jul 23. PMID: 30038253.
265. Li EW, McKee-Muir OC and Gilbert PG et al., Chapter 4 – Myogenesis in Development and Disease, 2018 Curr Top Dev Biol
266. Price LS, Leng J, Schwartz MA, Bokoch GM. Activation of Rac and Cdc42 by integrins mediates cell spreading. Mol Biol Cell. 1998 Jul;9(7):1863-71. doi: 10.1091/mbc.9.7.1863. PMID: 9658176; PMCID: PMC25428.
267. Bellis SL, Perrotta JA, Curtis MS, Turner CE. Adhesion of fibroblasts to fibronectin stimulates both serine and tyrosine phosphorylation of paxillin. Biochem J. 1997 Jul 15;325 (Pt 2)(Pt 2):375-81. doi: 10.1042/bj3250375. PMID: 9230116; PMCID: PMC1218570.
268. Cai X, Li M, Vrana J, Schaller MD. Glycogen synthase kinase 3- and extracellular signal-regulated kinase-dependent phosphorylation of paxillin regulates cytoskeletal rearrangement. Mol Cell Biol. 2006 Apr;26(7):2857-68. doi: 10.1128/MCB.26.7.2857-2868.2006. PMID: 16537926; PMCID: PMC1430314.
269. Rosenblatt J, Cramer LP, Baum B, McGee KM. Myosin II-dependent cortical movement is required for centrosome separation and positioning during mitotic spindle assembly. Cell. 2004 Apr 30;117(3):361-72. doi: 10.1016/s0092-8674(04)00341-1. PMID: 15109496.
270. Gupta P, Martin R, Knölker HJ, Nihalani D, Kumar Sinha D. Myosin-1 inhibition by PClP affects membrane shape, cortical actin distribution and lipid droplet dynamics in early Zebrafish embryos. PLoS One. 2017 Jul 5;12(7):e0180301. doi: 10.1371/journal.pone.0180301. PMID: 28678859; PMCID: PMC5498032.
271. Straight AF, Cheung A, Limouze J, Chen I, Westwood NJ, Sellers JR, Mitchison TJ. Dissecting temporal and spatial control of cytokinesis with a myosin II Inhibitor. Science. 2003 Mar 14;299(5613):1743-7. doi: 10.1126/science.1081412. PMID: 12637748.
272. Zhang, Q., Narayanan, V., Mui, K.L., O'Bryan, C.S., Anderson, R.H., KC, B., Cabe, J.I., Denis, K.B., Antoku, S., Roux, K.J., et al. (2019). Mechanical Stabilization of the Glandular Acinus by Linker of Nucleoskeleton and Cytoskeleton Complex. Current Biology 29, 2826-2839.e4. 10.1016/j.cub.2019.07.021.
273. Sosa, B.A., Rothballer, A., Kutay, U., and Schwartz, T.U. (2012). LINC complexes form by binding of three KASH peptides to domain interfaces of trimeric SUN proteins. Cell *149*, 1035–1047. 10.1016/j.cell.2012.03.046.
274. Oas RG, Nanes BA, Esimai CC, Vincent PA, García AJ, Kowalczyk AP. p120-catenin and β-catenin differentially regulate cadherin adhesive function. Mol Biol Cell. 2013 Mar;24(6):704-14. doi: 10.1091/mbc.E12-06-0471. Epub 2013 Jan 16. PMID: 23325790; PMCID: PMC3596243
275. Lickert H, Bauer A, Kemler R, Stappert J. Casein kinase II phosphorylation of E-cadherin increases E-cadherin/beta-catenin interaction and strengthens cell-cell adhesion. J Biol Chem. 2000 Feb 18;275(7):5090-5. doi: 10.1074/jbc.275.7.5090. PMID: 10671552.

276. Fernández-Sánchez ME, Barbier S, Whitehead J, Béalle G, Michel A, Latorre-Ossa H, Rey C, Fouassier L, Claperon A, Brullé L, Girard E, Servant N, Rio-Frio T, Marie H, Lesieur S, Housset C, Gennisson JL, Tanter M, Ménager C, Fre S, Robine S, Farge E. Mechanical induction of the tumorigenic β-catenin pathway by tumour growth pressure. Nature. 2015 Jul 2;523(7558):92-5. doi: 10.1038/nature14329. Epub 2015 May 11. PMID: 25970250.
277. Adolfo del Campo, Aurora Nogales, Tiberio A. Ezquerra, Juan Rodríguez-Hernández,
278. Modification of poly(dimethylsiloxane) as a basis for surface wrinkle formation: Chemical and mechanical characterization, Polymer, Volume 98, 2016, Pages 327-335, ISSN 0032-3861
279. Mills KL, Zhu X, Takayama S, Thouless MD. The mechanical properties of a surface-modified layer on poly(dimethylsiloxane). J Mater Res. 2008 Jan 1;23(1):37-48. doi: 10.1557/JMR.2008.0029. PMID: 19779588; PMCID: PMC2749279.
280. Engler AJ, Richert L, Wong JY, Picart C, Discher DE. Surface probe measurements of the elasticity of sectioned tissue, thin gels and polyelectrolyte multilayer films: correlations between substrate stiffness and cell adhesion. *Surf Sci* 570: 142–154, 2004. doi: 10.1016/j.susc.2004.06.179.
281. Brown XQ, Ookawa K, Wong JY. Evaluation of polydimethylsiloxane scaffolds with physiologically-relevant elastic moduli: interplay of substrate mechanics and surface chemistry effects on vascular smooth muscle cell response. *Biomaterials* 26: 3123–3129, 2005. doi: 10.1016/j.biomaterials.2004.08.009.
282. Li Z, Dranoff JA, Chan EP, Uemura M, Sévigny J, Wells RG. Transforming growth factor-beta and substrate stiffness regulate portal fibroblast activation in culture. *Hepatology* 46: 1246–1256, 2007. doi: 10.1002/hep.21792
283. Qiu Y, Brown AC, Myers DR, Sakurai Y, Mannino RG, Tran R, Ahn B, Hardy ET, Kee MF, Kumar S, Bao G, Barker TH, Lam WA. Platelet mechanosensing of substrate stiffness during clot formation mediates adhesion, spreading, and activation. *Proc Natl Acad Sci USA* 111: 14430–14435, 2014. doi: 10.1073/pnas.1322917111.
284. Urbano RL, Furia C, Basehore S, Clyne AM. Stiff Substrates Increase Inflammation-Induced Endothelial Monolayer Tension and Permeability. *Biophys J* 113: 645–655, 2017. doi: 10.1016/j.bpj.2017.06.033.
285. Wang L, Sun B, Ziemer KS, Barabino GA, Carrier RL. Chemical and physical modifications to poly(dimethylsiloxane) surfaces affect adhesion of Caco-2 cells. J Biomed Mater Res A. 2010 Jun 15;93(4):1260-71. doi: 10.1002/jbm.a.32621. PMID: 19827104.
286. Heurtier V, Owens N, Gonzalez I, Mueller F, Proux C, Mornico D, Clerc P, Dubois A, Navarro P. The molecular logic of Nanog-induced self-renewal in mouse embryonic stem cells. Nat Commun. 2019 Mar 7;10(1):1109. doi: 10.1038/s41467-019-09041-z. PMID: 30846691; PMCID: PMC6406003.
287. Cavalcanti-Adam EA, Volberg T, Micoulet A, Kessler H, Geiger B, Spatz JP. Cell spreading and focal adhesion dynamics are regulated by spacing of integrin ligands. Biophys J. 2007 Apr 15;92(8):2964-74. doi: 10.1529/biophysj.106.089730. Epub 2007 Feb 2. PMID: 17277192; PMCID: PMC1831685.

288. Lemma ED, Jiang Z, Klein F, Landmann T, Weißenbruch K, Bertels S, Hippler M, Wehrle-Haller B, Bastmeyer M. Adaptation of cell spreading to varying fibronectin densities and topographies is facilitated by β1 integrins. Front Bioeng Biotechnol. 2022 Aug 10;10:964259. doi: 10.3389/fbioe.2022.964259. PMID: 36032704; PMCID: PMC9399860.
289. Töpfer U. Basement membrane dynamics and mechanics in tissue morphogenesis. Biol Open. 2023 Aug 15;12(8):bio059980. doi: 10.1242/bio.059980. Epub 2023 Aug 2. PMID: 37531197; PMCID: PMC10411871.
290. Tanner K. Regulation of the basement membrane by epithelia generated forces. Phys Biol. 2012 Dec;9(6):065003. doi: 10.1088/1478-3975/9/6/065003. Epub 2012 Nov 29. PMID: 23196920; PMCID: PMC3526973.
291. Molè MA, Weberling A, Fässler R, Campbell A, Fishel S, Zernicka-Goetz M. Integrin β1 coordinates survival and morphogenesis of the embryonic lineage upon implantation and pluripotency transition. Cell Rep. 2021 Mar 9;34(10):108834. doi: 10.1016/j.celrep.2021.108834. PMID: 33691117; PMCID: PMC7966855.
292. Kümper S, Mardakheh FK, McCarthy A, Yeo M, Stamp GW, Paul A, Worboys J, Sadok A, Jørgensen C, Guichard S, Marshall CJ. Rho-associated kinase (ROCK) function is essential for cell cycle progression, senescence and tumorigenesis. Elife. 2016 Jan 14;5:e12994. doi: 10.7554/eLife.12203. PMID: 26765561; PMCID: PMC4798951.
293. Chaigne A, Labouesse C, White IJ, Agnew M, Hannezo E, Chalut KJ, Paluch EK. Abscission Couples Cell Division to Embryonic Stem Cell Fate. Dev Cell. 2020 Oct 26;55(2):195-208.e5. doi: 10.1016/j.devcel.2020.09.001. Epub 2020 Sep 25. PMID: 32979313; PMCID: PMC7594744.
294. Bertels S, Jaggy M, Richter B, Keppler S, Weber K, Genthner E, Fischer AC, Thiel M, Wegener M, Greiner AM, Autenrieth TJ, Bastmeyer M. Geometrically defined environments direct cell division rate and subcellular YAP localization in single mouse embryonic stem cells. Sci Rep. 2021 Apr 29;11(1):9269. doi: 10.1038/s41598-021-88336-y. PMID: 33927254; PMCID: PMC8084931.
295. Kassianidou E, Kalita J, Lim RYH. The role of nucleocytoplasmic transport in mechanotransduction. Exp Cell Res. 2019 Apr 15;377(1-2):86-93. doi: 10.1016/j.yexcr.2019.02.009. Epub 2019 Feb 13. PMID: 30768931.
296. Zhao XH, Laschinger C, Arora P, Szászi K, Kapus A, McCulloch CA. Force activates smooth muscle alpha-actin promoter activity through the Rho signaling pathway. J Cell Sci. 2007 May 15;120(Pt 10):1801-9. doi: 10.1242/jcs.001586. Epub 2007 Apr 24. PMID: 17456553.
297. Jacchetti E, Nasehi R, Boeri L, Parodi V, Negro A, Albani D, Osellame R, Cerullo G, Matas JFR, Raimondi MT. The nuclear import of the transcription factor MyoD is reduced in mesenchymal stem cells grown in a 3D micro-engineered niche. Sci Rep. 2021 Feb 4;11(1):3021. doi: 10.1038/s41598-021-81920-2. PMID: 33542304; PMCID: PMC7862644.
298. Ghaleb AM, Yang VW. Krüppel-like factor 4 (KLF4): What we currently know. Gene. 2017 May 5;611:27-37. doi: 10.1016/j.gene.2017.02.025. Epub 2017 Feb 22. PMID: 28237823; PMCID: PMC5391259.
299. Park JW, Lee EJ, Moon E, Kim HL, Kim IB, Hodzic D, Kim N, Kweon HS, Kim JW. Orthodenticle homeobox 2 is transported to lysosomes by nuclear budding

vesicles. Nat Commun. 2023 Feb 27;14(1):1111. doi: 10.1038/s41467-023-36697-5. PMID: 36849521; PMCID: PMC9971051.
300. Shimozono S, Tsutsui H, Miyawaki A. Diffusion of large molecules into assembling nuclei revealed using an optical highlighting technique. Biophys J. 2009 Sep 2;97(5):1288-94. doi: 10.1016/j.bpj.2009.06.024. PMID: 19720016; PMCID: PMC2749756.
301. Luck K, Kim DK, Lambourne L, Spirohn K, Begg BE, Bian W, Brignall R, Cafarelli T, Campos-Laborie FJ, Charloteaux B, Choi D, Coté AG, Daley M, Deimling S, Desbuleux A, Dricot A, Gebbia M, Hardy MF, Kishore N, Knapp JJ, Kovács IA, Lemmens I, Mee MW, Mellor JC, Pollis C, Pons C, Richardson AD, Schlabach S, Teeking B, Yadav A, Babor M, Balcha D, Basha O, Bowman-Colin C, Chin SF, Choi SG, Colabella C, Coppin G, D'Amata C, De Ridder D, De Rouck S, Duran-Frigola M, Ennajdaoui H, Goebels F, Goehring L, Gopal A, Haddad G, Hatchi E, Helmy M, Jacob Y, Kassa Y, Landini S, Li R, van Lieshout N, MacWilliams A, Markey D, Paulson JN, Rangarajan S, Rasla J, Rayhan A, Rolland T, San-Miguel A, Shen Y, Sheykhkarimli D, Sheynkman GM, Simonovsky E, Taşan M, Tejeda A, Tropepe V, Twizere JC, Wang Y, Weatheritt RJ, Weile J, Xia Y, Yang X, Yeger-Lotem E, Zhong Q, Aloy P, Bader GD, De Las Rivas J, Gaudet S, Hao T, Rak J, Tavernier J, Hill DE, Vidal M, Roth FP, Calderwood MA. A reference map of the human binary protein interactome. Nature. 2020 Apr;580(7803):402-408. doi: 10.1038/s41586-020-2188-x. Epub 2020 Apr 8. PMID: 32296183; PMCID: PMC7169983.
302. Mehla J, Caufield JH, Sakhawalkar N, Uetz P. A Comparison of Two-Hybrid Approaches for Detecting Protein-Protein Interactions. Methods Enzymol. 2017;586:333-358. doi: 10.1016/bs.mie.2016.10.020. Epub 2017 Jan 5. PMID: 28137570; PMCID: PMC5737774.
303. Huang H, Jedynak BM, Bader JS. Where have all the interactions gone? Estimating the coverage of two-hybrid protein interaction maps. PLoS Comput Biol. 2007 Nov;3(11):e214. doi: 10.1371/journal.pcbi.0030214. Epub 2007 Sep 21. PMID: 18039026; PMCID: PMC2082503.
304. Güttinger S, Mühlhäusser P, Koller-Eichhorn R, Brennecke J, Kutay U. Transportin2 functions as importin and mediates nuclear import of HuR. Proc Natl Acad Sci U S A. 2004 Mar 2;101(9):2918-23. doi: 10.1073/pnas.0400342101. Epub 2004 Feb 23. PMID: 14981248; PMCID: PMC365720.
305. Twyffels L, Gueydan C, Kruys V. Transportin-1 and Transportin-2: protein nuclear import and beyond. FEBS Lett. 2014 May 21;588(10):1857-68. doi: 10.1016/j.febslet.2014.04.023. Epub 2014 Apr 26. PMID: 24780099.
306. Sangel P, Oka M, Yoneda Y. The role of Importin-βs in the maintenance and lineage commitment of mouse embryonic stem cells. FEBS Open Bio. 2014 Jan 6;4:112-20. doi: 10.1016/j.fob.2014.01.001. PMID: 24490135; PMCID: PMC3907685.
307. Shen W, Gong B, Xing C, Zhang L, Sun J, Chen Y, Yang C, Yan L, Chen L, Yao L, Li G, Deng H, Wu X, Meng A. Comprehensive maturity of nuclear pore complexes regulates zygotic genome activation. Cell. 2022 Dec 22;185(26):4954-4970.e20. doi: 10.1016/j.cell.2022.11.011. Epub 2022 Dec 8. PMID: 36493774.
308. D'Angelo MA, Gomez-Cavazos JS, Mei A, Lackner DH, Hetzer MW. A change in nuclear pore complex composition regulates cell differentiation. Dev Cell. 2012 Feb

14;22(2):446-58. doi: 10.1016/j.devcel.2011.11.021. Epub 2012 Jan 19. PMID: 22264802; PMCID: PMC3288503.

309. Lupu F, Alves A, Anderson K, Doye V, Lacy E. Nuclear pore composition regulates neural stem/progenitor cell differentiation in the mouse embryo. Dev Cell. 2008 Jun;14(6):831-42. doi: 10.1016/j.devcel.2008.03.011. PMID: 18539113; PMCID: PMC2495767.

310. Yip AK, Iwasaki K, Ursekar C, Machiyama H, Saxena M, Chen H, Harada I, Chiam KH, Sawada Y. Cellular response to substrate rigidity is governed by either stress or strain. Biophys J. 2013 Jan 8;104(1):19-29. doi: 10.1016/j.bpj.2012.11.3805. Epub 2013 Jan 8. PMID: 23332055; PMCID: PMC3540269.

311. Messi Z, Bornert A, Raynaud F, Verkhovsky AB. Traction Forces Control Cell-Edge Dynamics and Mediate Distance Sensitivity during Cell Polarization. Curr Biol. 2020 May 4;30(9):1762-1769.e5. doi: 10.1016/j.cub.2020.02.078. Epub 2020 Mar 26. PMID: 32220324.

312. Arulanandam R, Vultur A, Cao J, Carefoot E, Elliott BE, Truesdell PF, Larue L, Feracci H, Raptis L. Cadherin-cadherin engagement promotes cell survival via Rac1/Cdc42 and signal transducer and activator of transcription-3. Mol Cancer Res. 2009 Aug;7(8):1310-27. doi: 10.1158/1541-7786.MCR-08-0469. Epub 2009 Aug 11. PMID: 19671682.

313. Raptis L, Arulanandam R, Vultur A, Geletu M, Chevalier S, Feracci H. Beyond structure, to survival: activation of Stat3 by cadherin engagement. Biochem Cell Biol. 2009 Dec;87(6):835-43. doi: 10.1139/o09-061. PMID: 19935869.

314. McCrea PD, Maher MT, Gottardi CJ. Nuclear signaling from cadherin adhesion complexes. Curr Top Dev Biol. 2015;112:129-96. doi: 10.1016/bs.ctdb.2014.11.018. Epub 2015 Feb 12. PMID: 25733140; PMCID: PMC4410048.

315. Hall J, Guo G, Wray J, Eyres I, Nichols J, Grotewold L, Morfopoulou S, Humphreys P, Mansfield W, Walker R, Tomlinson S, Smith A. Oct4 and LIF/Stat3 additively induce Krüppel factors to sustain embryonic stem cell self-renewal. Cell Stem Cell. 2009 Dec 4;5(6):597-609. doi: 10.1016/j.stem.2009.11.003. PMID: 19951688.

316. Zhang P, Andrianakos R, Yang Y, Liu C, Lu W. Kruppel-like factor 4 (Klf4) prevents embryonic stem (ES) cell differentiation by regulating Nanog gene expression. J Biol Chem. 2010 Mar 19;285(12):9180-9. doi: 10.1074/jbc.M109.077958. Epub 2010 Jan 13. PMID: 20071344; PMCID: PMC2838337.

317. Xie L, Torigoe SE, Xiao J, Mai DH, Li L, Davis FP, Dong P, Marie-Nelly H, Grimm J, Lavis L, Darzacq X, Cattoglio C, Liu Z, Tjian R. A dynamic interplay of enhancer elements regulates *Klf4* expression in naïve pluripotency. Genes Dev. 2017 Sep 1;31(17):1795-1808. doi: 10.1101/gad.303321.117. PMID: 28982762; PMCID: PMC5666677.

318. Prusty D, Park BH, Davis KE, Farmer SR. Activation of MEK/ERK signaling promotes adipogenesis by enhancing peroxisome proliferator-activated receptor gamma (PPARgamma) and C/EBPalpha gene expression during the differentiation of 3T3-L1 preadipocytes. J Biol Chem. 2002 Nov 29;277(48):46226-32. doi: 10.1074/jbc.M207776200. Epub 2002 Sep 20. PMID: 12270934.

319. Wu L, Cai X, Dong H, Jing W, Huang Y, Yang X, Wu Y, Lin Y. Serum regulates adipogenesis of mesenchymal stem cells via MEK/ERK-dependent

PPARgamma expression and phosphorylation. J Cell Mol Med. 2010 Apr;14(4):922-32. doi: 10.1111/j.1582-4934.2009.00709.x. Epub 2009 Feb 20. PMID: 19243475; PMCID: PMC3823124.

320. Lanner F, Rossant J. The role of FGF/Erk signaling in pluripotent cells. Development. 2010 Oct;137(20):3351-60. doi: 10.1242/dev.050146. PMID: 20876656.

321. Weiss BD, Wolters PL, Plotkin SR, Widemann BC, Tonsgard JH, Blakeley J, Allen JC, Schorry E, Korf B, Robison NJ, Goldman S, Vinks AA, Emoto C, Fukuda T, Robinson CT, Cutter G, Edwards L, Dombi E, Ratner N, Packer R, Fisher MJ. NF106: A Neurofibromatosis Clinical Trials Consortium Phase II Trial of the MEK Inhibitor Mirdametinib (PD-0325901) in Adolescents and Adults With NF1-Related Plexiform Neurofibromas. J Clin Oncol. 2021 Mar 1;39(7):797-806. doi: 10.1200/JCO.20.02220. Epub 2021 Jan 28. PMID: 33507822; PMCID: PMC8078274.

322. Aksamitiene E, Kholodenko BN, Kolch W, Hoek JB, Kiyatkin A. PI3K/Akt-sensitive MEK-independent compensatory circuit of ERK activation in ER-positive PI3K-mutant T47D breast cancer cells. Cell Signal. 2010 Sep;22(9):1369-78. doi: 10.1016/j.cellsig.2010.05.006. Epub 2010 May 12. PMID: 20471474; PMCID: PMC2893265.

323. Grammer TC, Blenis J. Evidence for MEK-independent pathways regulating the prolonged activation of the ERK-MAP kinases. Oncogene. 1997 Apr 10;14(14):1635-42. doi: 10.1038/sj.onc.1201000. PMID: 9135064.

324. Saleem S, Li J, Yee SP, Fellows GF, Goodyer CG, Wang R. beta1 integrin/FAK/ERK signalling pathway is essential for human fetal islet cell differentiation and survival. J Pathol. 2009 Oct;219(2):182-92. doi: 10.1002/path.2577. PMID: 19544355.

325. Gupta MK, De Jesus DF, Kahraman S, Valdez IA, Shamsi F, Yi L, Swensen AC, Tseng YH, Qian WJ, Kulkarni RN. Insulin receptor-mediated signaling regulates pluripotency markers and lineage differentiation. Mol Metab. 2018 Dec;18:153-163. doi: 10.1016/j.molmet.2018.09.003. Epub 2018 Sep 19. PMID: 30316806; PMCID: PMC6308035.

326. Cooper HM, Tamura RN, Quaranta V. The major laminin receptor of mouse embryonic stem cells is a novel isoform of the alpha 6 beta 1 integrin. J Cell Biol. 1991 Nov;115(3):843-50. doi: 10.1083/jcb.115.3.843. PMID: 1833411; PMCID: PMC2289180.

327. Suh HN, Han HJ. Laminin regulates mouse embryonic stem cell migration: involvement of Epac1/Rap1 and Rac1/cdc42. Am J Physiol Cell Physiol. 2010 May;298(5):C1159-69. doi: 10.1152/ajpcell.00496.2009. Epub 2010 Jan 20. PMID: 20089929.

328. Cattavarayane S, Palovuori R, Tanjore Ramanathan J, Manninen A. α6β1- and αV-integrins are required for long-term self-renewal of murine embryonic stem cells in the absence of LIF. BMC Cell Biol. 2015 Feb 27;16:3. doi: 10.1186/s12860-015-0051-y. PMID: 25886986; PMCID: PMC4348401.

329. Dhaliwal NK, Abatti LE, Mitchell JA. KLF4 protein stability regulated by interaction with pluripotency transcription factors overrides transcriptional control. Genes Dev. 2019 Aug 1;33(15-16):1069-1082. doi: 10.1101/gad.324319.119. Epub 2019 Jun 20. PMID: 31221664; PMCID: PMC6672055.

330. Martello G, Sugimoto T, Diamanti E, Joshi A, Hannah R, Ohtsuka S, Göttgens B, Niwa H, Smith A. Esrrb is a pivotal target of the Gsk3/Tcf3 axis regulating embryonic stem cell self-renewal. Cell Stem Cell. 2012 Oct 5;11(4):491-504. doi: 10.1016/j.stem.2012.06.008. Erratum in: Cell Stem Cell. 2013 May 2;12(5):630. PMID: 23040478; PMCID: PMC3465555.
331. Pereira L, Yi F, Merrill BJ. Repression of Nanog gene transcription by Tcf3 limits embryonic stem cell self-renewal. Mol Cell Biol. 2006 Oct;26(20):7479-91. doi: 10.1128/MCB.00368-06. Epub 2006 Aug 7. PMID: 16894029; PMCID: PMC1636872.
332. Qiu D, Ye S, Ruiz B, Zhou X, Liu D, Zhang Q, Ying QL. Klf2 and Tfcp2l1, Two Wnt/β-Catenin Targets, Act Synergistically to Induce and Maintain Naive Pluripotency. Stem Cell Reports. 2015 Sep 8;5(3):314-22. doi: 10.1016/j.stemcr.2015.07.014. Epub 2015 Aug 28. PMID: 26321140; PMCID: PMC4618593.
333. Kelly KF, Ng DY, Jayakumaran G, Wood GA, Koide H, Doble BW. β-catenin enhances Oct-4 activity and reinforces pluripotency through a TCF-independent mechanism. Cell Stem Cell. 2011 Feb 4;8(2):214-27. doi: 10.1016/j.stem.2010.12.010. PMID: 21295277; PMCID: PMC3465368.
334. Xie L, Torigoe SE, Xiao J, Mai DH, Li L, Davis FP, Dong P, Marie-Nelly H, Grimm J, Lavis L, Darzacq X, Cattoglio C, Liu Z, Tjian R. A dynamic interplay of enhancer elements regulates Klf4 expression in naïve pluripotency. Genes Dev. 2017 Sep 1;31(17):1795-1808. doi: 10.1101/gad.303321.117. PMID: 28982762; PMCID: PMC5666677.
335. Ai Z, Shao J, Wu Y, Yu M, Du J, Shi X, Shi X, Zhang Y, Guo Z. CHIR99021 enhances Klf4 Expression through β-Catenin Signaling and miR-7a Regulation in J1 Mouse Embryonic Stem Cells. PLoS One. 2016 Mar 3;11(3):e0150936. doi: 10.1371/journal.pone.0150936. PMID: 26938105; PMCID: PMC4777400.
336. Hao J, Li TG, Qi X, Zhao DF, Zhao GQ. WNT/beta-catenin pathway up-regulates Stat3 and converges on LIF to prevent differentiation of mouse embryonic stem cells. Dev Biol. 2006 Feb 1;290(1):81-91. doi: 10.1016/j.ydbio.2005.11.011. Epub 2005 Dec 5. PMID: 16330017.
337. Choi HJ, Gross JC, Pokutta S, Weis WI. Interactions of plakoglobin and beta-catenin with desmosomal cadherins: basis of selective exclusion of alpha- and beta-catenin from desmosomes. J Biol Chem. 2009 Nov 13;284(46):31776-88. doi: 10.1074/jbc.M109.047928. Epub 2009 Sep 16. PMID: 19759396; PMCID: PMC2797248.
338. Kim H, Wu J, Ye S, Tai CI, Zhou X, Yan H, Li P, Pera M, Ying QL. Modulation of β-catenin function maintains mouse epiblast stem cell and human embryonic stem cell self-renewal. Nat Commun. 2013;4:2403. doi: 10.1038/ncomms3403. PMID: 23985566; PMCID: PMC4183150.
339. Kim WK, Kwon Y, Jang M, Park M, Kim J, Cho S, Jang DG, Lee WB, Jung SH, Choi HJ, Min BS, Il Kim T, Hong SP, Paik YK, Kim H. β-catenin activation down-regulates cell-cell junction-related genes and induces epithelial-to-mesenchymal transition in colorectal cancers. Sci Rep. 2019 Dec 5;9(1):18440. doi: 10.1038/s41598-019-54890-9. PMID: 31804558; PMCID: PMC6895046.
340. Sánchez-Tilló E, de Barrios O, Siles L, Cuatrecasas M, Castells A, Postigo A. β-catenin/TCF4 complex induces the epithelial-to-mesenchymal transition (EMT)-

activator ZEB1 to regulate tumor invasiveness. Proc Natl Acad Sci U S A. 2011 Nov 29;108(48):19204-9. doi: 10.1073/pnas.1108977108. Epub 2011 Nov 11. PMID: 22080605; PMCID: PMC3228467.

341. Xia MY, Zhao XY, Huang QL, Sun HY, Sun C, Yuan J, He C, Sun Y, Huang X, Kong W, Kong WJ. Activation of Wnt/β-catenin signaling by lithium chloride attenuates d-galactose-induced neurodegeneration in the auditory cortex of a rat model of aging. FEBS Open Bio. 2017 Apr 25;7(6):759-776. doi: 10.1002/2211-5463.12220. PMID: 28593132; PMCID: PMC5458451.

342. Du Y, Ling J, Wei X, Ning Y, Xie N, Gu H, Yang F. Wnt/β-catenin signaling participates in cementoblast/osteoblast differentiation of dental follicle cells. Connect Tissue Res. 2012;53(5):390-7. doi: 10.3109/03008207.2012.668980. Epub 2012 Mar 21. PMID: 22360497.

343. Déjardin T, Carollo PS, Sipieter F, Davidson PM, Seiler C, Cuvelier D, Cadot B, Sykes C, Gomes ER, Borghi N. Nesprins are mechanotransducers that discriminate epithelial-mesenchymal transition programs. J Cell Biol. 2020 Oct 5;219(10):e201908036. doi: 10.1083/jcb.201908036. PMID: 32790861; PMCID: PMC7659719.

344. Sozen B, Cornwall-Scoones J, Zernicka-Goetz M. The dynamics of morphogenesis in stem cell-based embryology: Novel insights for symmetry breaking. Dev Biol. 2021 Jun;474:82-90. doi: 10.1016/j.ydbio.2020.12.005. Epub 2020 Dec 15. PMID: 33333067; PMCID: PMC8259461.